



THE HONG KONG
POLYTECHNIC UNIVERSITY

香港理工大學

Pao Yue-kong Library

包玉剛圖書館

Copyright Undertaking

This thesis is protected by copyright, with all rights reserved.

By reading and using the thesis, the reader understands and agrees to the following terms:

1. The reader will abide by the rules and legal ordinances governing copyright regarding the use of the thesis.
2. The reader will use the thesis for the purpose of research or private study only and not for distribution or further reproduction or any other purpose.
3. The reader agrees to indemnify and hold the University harmless from and against any loss, damage, cost, liability or expenses arising from copyright infringement or unauthorized usage.

IMPORTANT

If you have reasons to believe that any materials in this thesis are deemed not suitable to be distributed in this form, or a copyright owner having difficulty with the material being included in our database, please contact lbsys@polyu.edu.hk providing details. The Library will look into your claim and consider taking remedial action upon receipt of the written requests.

**KERATIN COMPOSITE NANOFIBROUS
ANTI-TUMOR DRUG DELIVERY SYSTEM**

ZHANG JING

Ph.D

The Hong Kong Polytechnic University

2014

THE HONG KONG POLYTECHNIC UNIVERSITY

INSTITUTE OF TEXTILES AND CLOTHING

**KERATIN COMPOSITE NANOFIBROUS
ANTI-TUMOR DRUG DELIVERY SYSTEM**

ZHANG JING

A thesis submitted in partial fulfillment of the requirements for
the degree of Doctor of Philosophy

April 2014

CERTIFICATE OF ORIGINALITY

I hereby declare that this thesis is my own work and that, to the best of my knowledge and belief, it reproduces no material previously published or written, nor material that has been accepted for the award of any other degree or diploma, except where due acknowledgement has been made in the text.

_____ (Signed)

ZHANG JING (Name of student)

ABSTRACT

Tissue engineering is an emerging interdisciplinary field that applies the principles of biology and engineering to the development of viable substitutes that restore, maintain, or improve the function of human tissues and organs. The crucial step in the whole tissue engineering process is the selection of proper scaffolds. The present study is to investigate a keratin composite biocompatible material for scaffolds with certain functional purpose, e.g., biodegradable implant, drug delivery, anti-tumor therapy.

The present work started with transforming wool into the functional protein biomaterials. In order to achieve this objective, isoelectric precipitation process was introduced to produce the targeted bio-functional keratin polypeptides. Wool fibers were hydrolyzed and adjusted to predetermined pH values. The results suggested that keratin polypeptides with different amino acids compositions could be tailored from wool hydrolyzed solution. Keratin particles at nanometer-scale were collected successfully. The chemical structure of keratin polypeptides endured the same as the pristine wool and the crystal structure of keratin polypeptides became more amorphous.

Secondly, the prepared keratin polypeptides were applied into biofunctional tissue engineering scaffolds system. In order to achieve the keratin composite nanofibers, keratin polypeptides were blended with Poly (*L*-lactic acid) (PLLA) organic solution

with an “ethanol replacement” process and electrospun into nanofibers. The results indicated that the nanofibrous composite membrane possessed ultrafine and homogenous structure without keratin aggregation. The Fourier transform infrared spectrometry (FT-IR) revealed the existence of keratin in the composite fibers. The thermal property of the composite membrane was more stable than pure keratin. XRD spectra revealed a crystal transformation of keratin after the process of electrospinning. The biocompatibility was examined by seeding cells on the surface of the composite nanofibers. Compared to pure PLLA nanofibers, keratin/PLLA fibrous membrane showed an enhanced impact on cells viability and affinity.

Thirdly, in order to investigate both the chemical and physical change during the *in vitro* degradation process, the degradability of keratin/PLLA nanofibers was discussed through several aspects. The chemical change was mainly reflected by the loss of keratin from the nanofibers as a function of degradation time. The physical change was mainly indicated by the decrease of thermal-stability of keratin/PLLA nanofibers. The rate of degradation was positively related to the amount of keratin peptides added into the composite nanofibers comparing with pure PLLA nanofibers.

Fourthly, in order to explore the drug delivery profile of keratin/PLLA nanofibers as a controlled release scaffolds system, 5-fluorouracil (5-FU) was loaded into the nanofibers as a drug model. The results proved the controlled release effect of 5-FU/keratin/PLLA nanofibers and the release periods of 5-FU were prolonged to 120

hours. The X-ray diffraction (XRD) analysis revealed that 5-FU dispersed uniformly within the nanofibers at a molecular level and electro-charges interactions were observed between 5-FU and keratin. The chemical characterization indicated 5-FU kept its original chemical structure within the nanofibers.

Fifthly, in order to investigate the pH-sensitivity of 5-FU/keratin/PLLA nanofibers, two pH-valued environments, i.e. pH 6.0 and pH 7.4 were introduced. A full-factorial design with two factors at two-levels was employed to optimize fiber fabrication factors to achieve desirable controlled release performance of the composite nanofibers in different pH environments. The results indicated that electrospinning voltage of 15 KV and weight ratio of keratin at 10 wt. % can enhance the pH-sensitivity of 5-FU/keratin/PLLA nanofibers. HCT-116 cells line was utilized to examine the anti-tumor effect 5-FU/keratin/PLLA nanofibers. In 120 hours, 5-FU/keratin/PLLA significantly inhibited the proliferation rate of tumor cells comparing to 5-FU/PLLA ($p < 0.01$).

Finally, to address the issue of infection during antitumor operation, a regenerated antimicrobial peptide (AMP) Attacin2 was introduced into the above composite fibers. The results indicated that after adding the antimicrobial peptides into the membrane, the nanofibrous scaffolds demonstrated antibacterial function. Further, the antitumor effect could be observed by adding Attacin2 into the keratin/PLLA nanofibers, especially after 24 hours observation. The results verified the feasibility of combining

both chemical antitumor drugs and biological antimicrobial peptides together, suggesting the further direction of applying nanofibers in the realm of antitumor therapy.

In conclusion, the keratin composite nanofibrous anti-tumor drug delivery system including keratin/PLLA, 5-FU/keratin/PLLA, Attacin2/keratin/PLLA and Attacin2/5-FU/keratin/PLLA have been developed successfully by electrospinning technology. The composite controlled release system can be utilized for potential biomedical application, e.g., anti-tumor therapy.

LIST OF PUBLICATIONS

Referred Journal Papers

1. **Zhang J**, Li Y, Li J, Zhao Z, Liu X, Li Z, et al. Isolation and characterization of biofunctional keratin particles extracted from wool wastes. Powder Technology. 2013;246:356-62. Online.
DOI: 10.1016/j.powtec.2013.05.037.
2. **Zhang J**, Li Y, Li J, Zhao Z, Liu X, Zhang Y, et al. Generation of biofunctional and biodegradable electrospun nanofibers composed of poly (L-lactic acid) and wool isoelectric precipitate. Textile Research Journal. 2013. Online.
DOI: 10.1177/0040517513499438.
3. **Zhang J**, Li Y, Li J. pH-Responsive nano-fiber membrane based on PLLA and nano wool protein for controlled release of anti-tumor drugs. Journal of Controlled Release.2013;172:e41-e2.Online.
DOI: <http://dx.doi.org/10.1016/j.jconrel.2013.08.089>.
4. Li J, Liu X, **Zhang J**, Zhang Y, Han Y, Hu J, et al. Synthesis and characterization of wool keratin/hydroxyapatite nanocomposite. Journal of Biomedical Materials Research Part B-Applied Biomaterials. 2012;100B:896-902. Online.
DOI: 10.1002/jbm.b.32645.
5. Li J-S, Li Y, Liu X, **Zhang J**, Zhang Y. Strategy to introduce an hydroxyapatite-keratin nanocomposite into a fibrous membrane for bone tissue engineering. Journal of Materials Chemistry B. 2013;1:432-7. Online.

DOI: 10.1039/c2tb00460g.

6. Li JS, Li Y, Zhang Y, Liu X, Zhao Z, **Zhang J**, et al. Toxicity study of isolated polypeptide from wool hydrolysate. *Food and Chemical Toxicology*. 2013;57:338-45. Online.

DOI: 10.1016/j.fct.2013.03.047.

7. **Zhang J**, Li Y, Li J-S et al. Investigation of controlled release effect and anti-tumor activity of a 5-FU-loaded electrospun nanofibers composed of poly (*L*-lactic acid) and wool isoelectric precipitated. (Prepared).

Referred Conference Papers

1. **Zhang J**, Li Y, Li JS. Investigation on the Effects of Operational Factors on Controlled Release Performance of the Composite Electrospun Membrane. *Textile Bioengineering and Informatics Symposium Proceedings, 2012; Vols 1 and 2: 193-200.*
2. Li JS, Li Y, Zhao Z, Li G, **Zhang J**. Review on Drug Delivery of 5-Fluorouracil for Anti-Cancer Tissue Engineering. *Textile Bioengineering and Informatics Symposium Proceedings, 2012; Vols 1 and 2: 234-252.*

Patents

1. Li Yi, Li Jiashen, Hu Junyan, Arthur F.T. Mak, **Zhang Jing**. Electrospinning biopolymers and polypeptides nano-composite fibrous scaffolds for medical application.
2. Li Yi, Li Jiashen, Hu Junyan, Arthur F.T. Mak, **Zhang Jing**. Method for fabricating apatite/keratin composite scaffold for bone regeneration.

Awards

1. Year of 2013, Outstanding research seminar award, 1st runner-up. Title: review of wool-based materials for bio-functional applications. Conference and location: The Hong Kong Polytechnic University, Institute of Textiles and Clothing. The 7th ITC Research Student Seminar, The Hong Kong Polytechnic University.
2. Year of 2013, Outstanding research paper award. Title: Investigation on the effects of operational factors on controlled release performance of the composite electrospun membrane. Conference and location : The 5th International Symposium of Textile Bioengineering and Informatics, Shinshu University, Ueda, Japan.

ACKNOWLEDGEMENTS

First and for most, I would like to express my most sincere appreciations to my chief supervisor, Prof. Yi Li, the Institute of Textiles and Clothing, for giving me the opportunity to do this interesting and promising research. Without his constant guidance, insightful suggestions, encouragement, and patience, this research would not be completed. He taught me research methodology and how to develop the scientific evidence to prove or disprove a hypothesis. His enthusiasm on scientific pursuit and indefatigable dedication on academic research have always been a great inspiration for me.

I am also deeply grateful to my co-supervisors, Dr. Jiashen Li, the Institute of Textiles and Clothing, who brought me to this interesting research field and tried his best to help me solve the problem in the research. Dr. Li has been a friend and mentor. I have learned a lot from his scientific thought and lifestyle. Without his valuable guidance and constructive suggestions, completion of PhD study could not be possible.

I would also like to express my sincere thanks to my colleges collaborated with me in the past four years, Ms.Han Yanxia, Dr. Hu Junyan , Dr. Yao Lei, Dr.Zhao Zheng, Ms. Liu Xuan, Mr. Liu Xuqing, Dr.Li Gang, Mr.Li Zhi, Ms. Lin Xiaofen, Mr.Xie Maobing. I did enjoy my four year study in such a passionate team.

Finally, I want to express my appreciation towards my family, my parents, my grandparents, my aunt, my uncles and all my loved friends. The luckiest story in my life is to have you all in my life.

Life is a miraculous journey and it deserves to be cherished.

TABLE OF CONTENTS

| | |
|---|--------|
| CERTIFICATE OF ORIGINALITY | I |
| ABSTRACT | II |
| LIST OF PUBLICATIONS | VI |
| ACKNOWLEDGEMENTS | IX |
| TABLE OF CONTENTS | XI |
| LIST OF FIGURES | XVIII |
| LIST OF TABLES | XXV |
| LIST OF ABBREVIATIONS | XXVIII |
| CHAPTER 1 INTRODUCTION | 1 |
| 1.1 Background..... | 1 |
| 1.2 Objectives and significance..... | 2 |
| 1.3 Research methodology..... | 3 |
| 1.3.1 Nanofibers formation technology..... | 3 |
| 1.3.2 Characterization of nanofibers..... | 4 |
| 1.3.3 Drug loading and in vitro release properties..... | 4 |
| 1.3.4 Biological evaluation of nanofibers..... | 5 |
| 1.4 Outline of the thesis..... | 6 |
| CHAPTER 2 LITERATURE REVIEW | 12 |
| 2.1 Tissue engineering and scaffolds..... | 12 |
| 2.1.1 Tissue engineering..... | 12 |
| 2.1.2 Scaffolds..... | 15 |

| | |
|---|----|
| 2.2 Biomaterials..... | 17 |
| 2.2.1 Introduction about biomaterials..... | 17 |
| 2.2.2 Natural Biopolymers..... | 18 |
| 2.2.3 Wool Keratin..... | 21 |
| 2.2.4 Synthetic Biopolymers..... | 27 |
| 2.2.5 Poly(<i>L</i> -lactic acid) (PLLA)..... | 28 |
| 2.2.6 Degradability of Biopolymers..... | 30 |
| 2.3 Fabrication technology applied in tissue engineering..... | 32 |
| 2.3.1 Fabrication technology for nanofibers..... | 32 |
| 2.3.2 Electrospinning technology applied in tissue engineering..... | 36 |
| 2.4 Bio-functionalized electrospun nanofibers for tissue engineering..... | 39 |
| 2.4.1 Target drug loading and controlled-release from nanofibers..... | 39 |
| 2.4.2 pH-sensitive drug delivery system..... | 43 |
| 2.4.3 Synergistic effect between anti-tumor drugs and antimicrobial peptides...48 | |
| 2.5 Summary of the knowledge gaps..... | 49 |

CHAPTER 3 ISOLATION AND CHARACTERIZATION OF

BIOFUNCTIONAL KERATIN ISOELECTRIC PRECIPITATES.....52

| | |
|--|----|
| 3.1. Materials and Methods..... | 52 |
| 3.1.1 Materials..... | 52 |
| 3.1.2 Hydrolysis of raw wool fibers..... | 52 |
| 3.1.3 Isoelectric-point precipitation process of keratin polypeptides..... | 54 |
| 3.1.4 The crystal structure analysis by XRD measurement..... | 54 |

| | |
|--|----|
| 3.1.5 Surface morphology observation..... | 54 |
| 3.1.6 The thermal stability evaluation by TG-DSC measurement..... | 55 |
| 3.1.7 Chemical bonding evaluation by FT-IR measurement..... | 55 |
| 3.2 Results and discussion..... | 55 |
| 3.2.1 The characterizations of acidic hydrolysis peptides..... | 55 |
| 3.2.2 The characterizations of alkaline hydrolysis peptides..... | 64 |
| 3.2.3 The comparison between the acidic hydrolysis and alkaline hydrolysis.... | 72 |
| 3.3 Conclusion..... | 73 |

CHAPTER 4 INVESTIGATION ON KERATIN AND POLY(L-LACTIC ACID)

| | |
|---|-----------|
| BIOFUNCTIONAL ELECTROSPUN MEMBRANE..... | 75 |
| 4.1 Materials and Methods..... | 76 |
| 4.1.1 Materials..... | 76 |
| 4.1.2 Preparation of wool keratin precipitate..... | 76 |
| 4.1.3 Electrospinning the keratin/PLLA fibrous membrane..... | 76 |
| 4.1.4 Extraction of keratin from membrane..... | 77 |
| 4.1.5 Characterizations of the keratin composite nanofibrous membranes..... | 78 |
| 4.1.6 Cells culture on the keratin composite membranes..... | 79 |
| 4.2 Results and Discussion..... | 80 |
| 4.2.1 Morphology of keratin/PLLA membrane by SEM..... | 80 |
| 4.2.2 FT-IR spectrum of keratin/PLLA membrane..... | 85 |
| 4.2.3 TEM morphology of keratin/PLLA membrane..... | 86 |
| 4.2.4 XRD spectra of keratin/PLLA membrane..... | 87 |

| | |
|--|------------|
| 4.2.5 Thermal property of keratin/PLLA membrane..... | 89 |
| 4.2.6 Cells culture on keratin/PLLA nanofibrous membrane..... | 90 |
| 4.3 Conclusion..... | 93 |
| | |
| CHAPTER 5 DEGRADATION EVALUATION OF KERATIN AND POLY (L-LACTIC ACID) ELECTROSPUN NANOFIBROUS MEMBRANE..... | 94 |
| 5.1 Materials and methods..... | 94 |
| 5.1.1 Materials..... | 94 |
| 5.1.2 Preparation of keratin/PLLA electrospun nanofibers..... | 94 |
| 5.1.3 Methodology of degradability evaluation of keratin/PLLA nanofibrous membrane..... | 95 |
| 5.2 Results and discussion..... | 96 |
| 5.2.1 Morphology of keratin/PLLA electrospinning membrane..... | 96 |
| 5.2.2 Degradability evaluation by FT-IR spectrum..... | 99 |
| 5.2.3 Degradability evaluation by UV spectrum..... | 100 |
| 5.2.4 Degradability evaluation by TGA analysis..... | 102 |
| 5.2.5 The relationship between different evaluation methods..... | 103 |
| 5.2.6 The discussion on degradation mechanism..... | 108 |
| 5.3 Conclusion..... | 111 |
| | |
| CHAPTER 6 INVESTIGATION ON KERATIN AND POLY(L-LACTIC ACID) ELECTROSPUN NANOFIBROUS ANTI-TUMOR DRUG DELIVERY SYSTEM..... | 112 |
| 6.1 Materials and methods..... | 112 |

| | |
|---|------------|
| 6.1.1 Materials..... | 112 |
| 6.1.2 Preparation of the drug-loaded nanofibrous system..... | 113 |
| 6.1.3 Morphology of the drug-loaded nanofibrous system..... | 113 |
| 6.1.4 Chemical structure analysis of the drug-loaded nanofibrous system..... | 114 |
| 6.1.5 Thermal properties of the drug-loaded nanofibrous system..... | 114 |
| 6.1.6 Zeta potential analysis..... | 114 |
| 6.1.7 In vitro release experiments of the drug-loaded nanofibrous system..... | 115 |
| 6.2 Results and discussion..... | 116 |
| 6.2.1 Morphology of the composite nanofibers..... | 116 |
| 6.2.2 TEM morphology of the drug-loaded composite nanofibers..... | 118 |
| 6.2.3 Chemical structural evaluation by FT-IR Spectroscopy..... | 120 |
| 6.2.4 Thermal behavior evaluation by TGA-DTA diagrams..... | 122 |
| 6.2.5 Crystallinity analysis of the composite nanofibers by XRD patterns..... | 124 |
| 6.2.6 Drug release profile of anti-tumor drug-loaded nanofibers..... | 125 |
| 6.2.7 Mechanism study on controlled release effect of the anti-tumor drug-loaded nanofibers..... | 128 |
| 6.3 Conclusion..... | 133 |
| | |
| CHAPTER 7 PH-RESPONSIVE CONTROLLED RELEASE PERFORMANCE AND ANTI-TUMOR EFFECTS OF THE COMPOSITE ELECTROSPUN MEMBRANE..... | 135 |
| 7.1 Experiments and full factorial design..... | 136 |

| | |
|---|-----|
| 7.1.1 Sustained-release test in vitro..... | 136 |
| 7.1.2 Full-factorial design of experiments method..... | 136 |
| 7.1.3 Anti-tumor activity by MTS assay..... | 139 |
| 7.1.4 Observation of anti-tumor activity by SEM..... | 139 |
| 7.1.5 Anti-tumor activity by fluorescence images observation..... | 140 |
| 7.1.6 Anti-tumor activity by cell live/dead observation..... | 140 |
| 7.2 Results and discussion..... | 141 |
| 7.2.1 Morphology of the drug-loaded membranes after DOE..... | 141 |
| 7.2.2 Full-factorial design results..... | 142 |
| 7.2.3 Responsible surface design for drug controlled-release..... | 148 |
| 7.2.4 The antitumor activity results by cell live/dead assay..... | 150 |
| 7.2.5 Anti-tumor activity results by DAPI staining for cellular adhesion and proliferation studies..... | 156 |
| 7.2.6 Anti-tumor activity results by MTS assay..... | 161 |
| 7.3 Conclusion..... | 164 |

CHAPTER 8 INVESTIGATION OF ANTI-TUMOR NANOFIBROUS ELECTROSPUN MEMBRANE WITH ANTIMICROBIAL PEPTIDES..... 165

| | |
|----------------------------------|-----|
| 8.1. Materials and methods..... | 166 |
| 8.1.1 Sample preparation..... | 166 |
| 8.1.2 Cell culture..... | 167 |
| 8.1.3 Fluorescence staining..... | 167 |

| | |
|--|------------|
| 8.1.4 Cell Live/Dead assay..... | 167 |
| 8.1.5 Cell proliferation (viability) MTS assay..... | 168 |
| 8.2 Results and discussion..... | 169 |
| 8.2.1 Chemical structure analysis by FT-IR..... | 169 |
| 8.2.2 Morphology of anti-tumor activity of AMPs loaded nanofibers..... | 170 |
| 8.2.3 Cell live/die assay results..... | 175 |
| 8.2.4 DAPI staining for cellular adhesion and proliferation studies..... | 182 |
| 8.2.5 MTS assay for cells cytotoxicity studies..... | 190 |
| 8.3 Discussion and conclusion..... | 192 |
| CHAPTER 9 CONCLUSIONS AND FUTURE WORKS..... | 193 |
| 9.1 Conclusions..... | 193 |
| 9.2 Limitations and future works..... | 197 |
| REFERENCES..... | 198 |

LIST OF FIGURES

| | |
|---|----|
| Figure 2.1 Schematic demonstration of literature review structure..... | 13 |
| Figure 2.2 Basic scheme of tissue engineering process: cells are harvested from in vivo stem cells..... | 14 |
| Figure 2.3 Examples of artificial biomedical composite scaffold devices..... | 16 |
| Figure 2.4 SEM photographs of freeze-dried keratin sponge..... | 22 |
| Figure 2.5 Molecular structure of Cysteine..... | 25 |
| Figure 2.6 Molecular structure of Glycine..... | 26 |
| Figure 2.7 SEM photomicrographs of cross sections of PLLA sponge..... | 29 |
| Figure 2.8 Schematics of the molecular structure of a self-assembling nanofiber network..... | 33 |
| Figure 2.9 Schematic diagram of nanofibers formation by phase separation..... | 34 |
| Figure 2.10 Diagram to illustrate the working process of electrospinning device..... | 36 |
| Figure 2.11 Three modes of drug-loading on electrospun nanofibers..... | 39 |
| Figure 2.12 Diagram of the structure of cells membrane..... | 44 |
| Figure 3.1 XRD patterns of wool fibers, KP3 particles and KP5 particles by acidic hydrolysis..... | 58 |
| Figure 3.2 SEM images of different keratin polypeptides particles by acidic hydrolysis..... | 59 |
| Figure 3.3 TG-DSC curves of keratin polypeptides by acidic hydrolysis..... | 60 |
| Figure 3.4 FT-IR spectra of wool, KP3 particles and KP5 particles by acidic | |

| | |
|--|----|
| hydrolysis..... | 63 |
| Figure 3.5 XRD patterns of KP3 particles and KP5 particles by alkaline hydrolysis.. | 66 |
| Figure 3.6 SEM images of keratin polypeptides nanoparticles by alkaline hydrolysis..... | 67 |
| Figure 3.7 SDS-page image of keratin polypeptides by alkaline hydrolysis of KP3 articles and KP5 particles..... | 67 |
| Figure 3.8 TG-DSC curves of keratin polypeptides by alkaline hydrolysis..... | 69 |
| Figure 3.9 FT-IR spectra of pristine wool, KP3 articles and KP5 particles by alkaline hydrolysis..... | 72 |
| Figure 4.1 Schematic diagram of the formation process of keratin/PLLA nanofiber.. | 77 |
| Figure 4.2 SEM images of nanofibers..... | 81 |
| Figure 4.3 SEM images of keratin/PLLA nanofibers..... | 82 |
| Figure 4.4 Ranges of the diameter of keratin nanoparticles..... | 83 |
| Figure 4.5 The hypothesis mechanism diagram of re-dispersion of keratin in ethanol absolute..... | 84 |
| Figure 4.6 FT-IR spectra of keratin/PLLA membrane, pure PLLA membrane and pure keratin..... | 85 |
| Figure 4.7 TEM images of PLLA and keratin/PLLA nanofibers..... | 87 |
| Figure 4.8 XRD patterns of keratin/PLLA membrane, pure PLLA and pure keratin extracted from different solutions..... | 88 |
| Figure 4.9 Thermogravimetric curves of PLLA, pure keratin and keratin/PLLA membrane..... | 89 |

| | |
|---|-----|
| Figure 4.10 Cells proliferation performances on keratin/PLLA membrane..... | 92 |
| Figure 4.11 Cells morphology of fibroblast cells seeded on the keratin/PLLA nano-fibrous membrane and pure PLLA nanofibrous membrane..... | 92 |
| Figure 5.1 SEM of keratin/PLLA fibrous membrane..... | 98 |
| Figure 5.2 SEM of keratin/PLLA membrane after being immersed into PBS solution..... | 98 |
| Figure 5.3 FT-IR spectra of keratin/PLLA membrane, pure PLLA membrane and pure keratin..... | 99 |
| Figure 5.4 FT-IR spectrum of keratin/PLLA membrane as a function of degradation period..... | 100 |
| Figure 5.5 The calibration curve of keratin at a wavelength of 278nm in PBS solution..... | 101 |
| Figure 5.6 The degradation curve of the keratin/PLLA composite membrane by UV spectrum..... | 102 |
| Figure 5.7 TGA diagram of keratin/PLLA membranes as a function of degradation periods..... | 103 |
| Figure 5.8 Calculated diagram for TGA thermal stability..... | 104 |
| Figure 5.9 The schematic diagram of the degradation process of the composite nanofibers..... | 111 |
| Figure 6.1 Morphology observation of different fibers and their corresponding diameter range..... | 118 |
| Figure 6.2 TEM images of the electrospinning nanofibers..... | 119 |

| | |
|---|-----|
| Figure 6.3 FT-IR spectra of electrospinning PLLA fibers..... | 120 |
| Figure 6.4 The thermal behaviors of different composite nanofibers..... | 123 |
| Figure 6.5 The XRD patterns of nanofibers with different compositions..... | 124 |
| Figure 6.6 The controlled release profile..... | 126 |
| Figure 6.7 The fitted curves of drug release profile..... | 128 |
| Figure 6.8 The mechanism diagram of the release profile of 5-FU/PLLA nanofibers..... | 131 |
| Figure 6.9 The mechanism diagram of the controlled release profile of 5-FU/keratin/PLLA nanofibers..... | 132 |
| Figure 7.1 The morphology observation of the electrospinning nanofibers in different parameters..... | 141 |
| Figure 7.2 Normal probability plot of the standardized effects on drug controlled release..... | 144 |
| Figure 7.3 The residue plots diagrams..... | 145 |
| Figure 7.4 Main Effects plot (data means) for drug controlled release..... | 147 |
| Figure 7.5 Contour Plot of Drug release per vs. ratio of keratin/PLLA and pH value of the environments..... | 149 |
| Figure 7.6 Different membranes sustained-release performances based on various parameters..... | 150 |
| Figure 7.7 Fluorescence micrographs of the cells stained with FDA (living cells), PI (dead cells) and overlaid images after seeding HCT-116 on the surface of the different nanofibers for 4 hours..... | 152 |

| | |
|--|-----|
| Figure 7.8 Fluorescence micrographs of the cells stained with FDA (living cells), PI (dead cells) and overlaid images after seeding HCT-116 on the surface of the different nanofibers for 24 hours..... | 153 |
| Figure 7.9 Fluorescence micrographs of the cells stained with FDA (living cells), PI (dead cells) and overlaid images after seeding HCT-116 on the surface of the different nanofibers for 72 hours..... | 154 |
| Figure 7.10 Fluorescence micrographs of the cells stained with FDA (living cells), PI (dead cells) and overlaid images after seeding HCT-116 on the surface of the different nanofibers for 12 hours..... | 155 |
| Figure 7.11 Fluorescence micrographs of the cells stained with DAPI (cell nucleus), TRICE-phalloidin (cell skeleton) and overlaid images after seeding HCT-116 on the surfaces of the different nanofibrous for 4 hours..... | 157 |
| Figure 7.12 Fluorescence micrographs of the cells stained with DAPI (cell nucleus), TRICE-phalloidin (cell skeleton) and overlaid images after seeding HCT-116 on the surfaces of the different nanofibrous for 24 hours..... | 158 |
| Figure 7.13 Fluorescence micrographs of the cells stained with DAPI (cell nucleus), TRICE-phalloidin (cell skeleton) and overlaid images after seeding HCT-116 on the surfaces of the different nanofibrous for 72 hours..... | 159 |
| Figure 7.14 Fluorescence micrographs of the cells stained with DAPI (cell nucleus), TRICE-phalloidin (cell skeleton) and overlaid images after seeding HCT-116 on the surfaces of the different nanofibrous for 120 hours..... | 160 |
| Figure 7.15 MTS assay of the antitumor nanofibers..... | 161 |

| | |
|---|-----|
| Figure 7.16 The schematic diagram of illustrating the interaction between HCT-116 cells and 5-FU/keratin/PLLA nanofibers..... | 163 |
| Figure 7.17 The schematic diagram of illustrating the interaction between HCT-116 cells and 5-FU/PLLA nanofibers..... | 163 |
| Figure 8.1 The FT-IR spectra of different nanofibers..... | 169 |
| Figure 8.2 The photos of the dehydrated cell-seeded nanofibrous samples for further evaluations..... | 170 |
| Figure 8.3 The SEM images of HCT-116 cells cultured on the surface of the drug loaded membranes in 4 hour observation..... | 172 |
| Figure 8.4 The SEM images of HCT-116 cells cultured on the surface of the drug loaded membranes in 24 hour observation..... | 173 |
| Figure 8.5 The SEM images of HCT-116 cells cultured on the surface of the drug loaded membranes in 72 hour observation..... | 174 |
| Figure 8.6 The SEM images of HCT-116 cells cultured on the surface of the drug loaded membranes in 120 hour observation..... | 175 |
| Figure 8.7 Fluorescence micrographs of the cells stained with FDA (living cells), PI (dead cells) and overlaid images after seeding HCT-116 on the surface of the different Nanofibrous for 4 hours..... | 178 |
| Figure 8.8 Fluorescence micrographs of the cells stained with FDA (living cells), PI (dead cells) and overlaid images after seeding HCT-116 on the surface of the different Nanofibrous for 24 hours..... | 179 |
| Figure 8.9 Fluorescence micrographs of the cells stained with FDA (living cells), PI | |

| | |
|--|-----|
| (dead cells) and overlaid images after seeding HCT-116 on the surface of the different Nanofibrous for 72 hours..... | 180 |
| Figure 8.10 Fluorescence micrographs of the cells stained with FDA (living cells), PI (dead cells) and overlaid images after seeding HCT-116 on the surface of the different Nanofibrous for 120 hours..... | 181 |
| Figure 8.11 Fluorescence micrographs of the cells stained with DAPI (cell nucleus), TRICE-phalloidin (cell skeleton) and overlaid images after seeding HCT-116 on the surfaces of the different nanofibrous for 4 hours..... | 186 |
| Figure 8.12 Fluorescence micrographs of the cells stained with DAPI (cell nucleus), TRICE-phalloidin (cell skeleton) and overlaid images after seeding HCT-116 on the surfaces of the different nanofibrous for 24 hours..... | 187 |
| Figure 8.13 Fluorescence micrographs of the cells stained with DAPI (cell nucleus), TRICE-phalloidin (cell skeleton) and overlaid images after seeding HCT-116 on the surfaces of the different nanofibrous for 72 hours..... | 188 |
| Figure 8.14 Fluorescence micrographs of the cells stained with DAPI (cell nucleus), TRICE-phalloidin (cell skeleton) and overlaid images after seeding HCT-116 on the surfaces of the different nanofibrous for 120 hours..... | 189 |
| Figure 8.15 MTS assay of HCT-116 viability on different composite nanofibers in a function of time..... | 190 |
| Figure 8.16 MTS assay of HCT-116 viability on different composite nanofibers in a function of samples..... | 191 |

LIST OF TABLES

| | |
|---|-----|
| Table 2.1 List of natural biopolymers and their sources as well as main application fields..... | 19 |
| Table 2.2 Standard amino acid and their properties..... | 24 |
| Table 2.3 Comparison on Biodegradability and other Physical Properties of Selected Biopolymers..... | 30 |
| Table 2.4 Comparison among popular nanofibers fabrication technology methods... | 35 |
| Table 2.5 Different polymers used in electrospinning and their applications and assessment methods..... | 37 |
| Table 2.6 Comparison of Three modes of drug-loading on electrospun nanofibers... | 42 |
| Table 2.7 Comparison of pH-sensitive drug delivery system..... | 47 |
| Table 3.1 Major amino acids composition of keratin..... | 56 |
| Table 3.2 The summary of glass transition temperature, decomposition temperature and mass change of wool, KP3 and KP5..... | 61 |
| Table 3.3 The summary of glass transition temperature, decomposition temperature and mass change of KP3 and KP5 by alkaline hydrolysis..... | 70 |
| Table 4.1 TGA data under inert atmosphere..... | 90 |
| Table 5.1 TGA integral area data..... | 106 |
| Table 5.2 Relationship between TGA and UV analysis..... | 108 |
| Table 7.1 Design factors and their levels..... | 137 |

| | |
|--|-----|
| Table 7.2 Matrix design and experiments data..... | 138 |
| Table 7.3 Estimated effects and coefficients for controlled release in pH 6.0 PBS... | 142 |
| Table 7.4 Estimated effects and coefficients for controlled release in pH 7.4 PBS... | 143 |
| Table 7.5 Estimated effects and coefficients for controlled release difference between pH 7.4 PBS and pH 6.0 PBS..... | 143 |

LIST OF ABBREVIATIONS

| | |
|----------------|--|
| 5-FU | 5-Fluorouracil |
| DMF | N, N-dime-thylformamide |
| DSC | Differential scanning calorimetry |
| ECM | Extracellular matrix |
| FDA | Food and Drug Administration |
| FT-IR | Fourier Transform Infrared Spectroscopy |
| HCT-116 | Human colorectal carcinoma cell line |
| HFF-1 | Human foreskin fibroblasts |
| KP | Keratin |
| MTS | 3-(4,5-dimethylthiazol-2-yl)-5-(3-carboxymethoxyphenyl)-2-(4-sulfophenyl)-2H-tetrazolium, inner salt |
| PEG | Polyethylene glycol |
| PGA | Poly(glycolic acid) |
| pI | Isoelectric point |
| PLA | Poly(lactic acid) |
| PLGA | Poly(lactic-coglycolide) |
| PLLA | Poly--Lactide Acid |
| R ² | Coefficient of determination |
| SEM | Scanning electron microscopy |
| T _c | Crystallization temperature |

| | |
|----------------|----------------------------------|
| TEM | Transmission electron microscopy |
| TGA | Thermal gravimetric analysis |
| T _m | Melting temperature |
| UV | UV-Vis Spectroscopy |
| XRD | X-ray diffraction |
| Zeta | Zeta potential measurement |

CHAPTER 1 INTRODUCTION

1.1 Background

Tissue engineering is an emerging interdisciplinary field that applies the principles of biology and engineering to the development of viable substitutes that restore, maintain, or improve the function of human tissues and organs [1]. Tissue engineering, which applies methods from engineering and life sciences to investigate artificial constructs to direct tissue regeneration [2], has therefore attracted many scientists and surgeons with a hope to treat patients in a minimally invasive and less painful ways.

The crucial step in the whole tissue engineering process is the selection of proper scaffolds. The scaffolds, known as the artificial extracellular matrix (ECM), are defined as the carrier for cells, growth factors and other bio-molecular signals [3]. The major function of scaffolds is providing a framework and support for the cells to attach, proliferate and differentiate. Typically, artificial ECM constructs are developed using either naturally-occurring molecular polymers (e.g. collagen, fibrin) or synthetic polymers (PLGA, PEG, PVA). The adhesivity of the synthetic polymer scaffolds can be enhanced with ECM-derived peptides or protein fragments [4]. The RGD found in various ECM molecules (e.g. fibronectin, fibrin,) is the most commonly used adhesive ligand because most cells bind to ECM in an RGD-dependent manner [5]. These peptides can also further enhance the bio-interaction with cells by altering their chemical structure.

In the present study, in order to investigate a novel biomedical nanofibrous system with preferable bio-function and biocompatibility, Poly-*L*-lactic acid (PLLA) and wool keratin are selected as a result of their favorable physical and chemical properties, biocompatibility and biodegradability. Electrospinning is chosen as the fabrication technique since it's a well-developed methods and easily controllable on nanofibers fabrication process.

1.2 Objectives and significance

The present study is aimed at investigating a novel kind nanofibrous protein composite membrane and exploring its mechanism on degradation and drug sustained-release for the future applications in the field of clinic medicines, tissue engineering and implantable clinics devices. Keratin is utilized in the project for its high biocompatibility and beneficial impact on cells proliferation. Poly-(*L*-lactic acid) (PLLA) is selected as the host polymer of the membrane. The future application of the membrane could be in the realm of drug delivery and drug release. A detailed literature review has been carried out and reported in Chapter 2, through which several research gaps were identified. In order to fulfill the research gaps discussed in Chapter 2, the specific objectives are described as follows:

1. To explore the feasibility of transforming wool wastes into the functional protein biomaterials. Keratin polypeptides with different amino acids terminals can be applied based on specific biomedical purposes. Isoelectric precipitation process is introduced to produce the targeted bio-functional keratin polypeptides.

2. To investigate a method to apply keratin into PLLA organic electrospun solution and to produce the uniform electrospinning nanofibers with preferable chemical and physical properties. Especially, the novel synthesized nanofibers could be demonstrated for the high biocompatibility.
3. To explore the mechanism of the Keratin/PLLA nanofibers degradation process. Systematic evaluation methods should be introduced from different aspects.
4. To develop the antitumor drug loaded nanofibers drug delivery system. Mechanism study concerning interaction between keratin, drug and PLLA should be depicted. Systematic characterizations of the composite nanofibers should be examined.
5. To demonstrate the antitumor effect of the drug loaded system. A series of biological evaluation should be applied and explored the sustained-release effect of adding keratin into the PLLA nanofibers.
6. To explored the anti-tumor effect of the antimicrobial-peptides-loaded nanofibrous system. The antimicrobial peptides will be introduced into the system to work as an antitumor factor together with antitumor drug.

1.3 Research methodology

1.3.1 Nanofibers formation technology

To achieve the objectives a range of research methodologies were developed and employed as follows:

The keratin precipitation was extracted from raw wool by isoelectric precipitation

process. After that, the keratin precipitation was dehydrated by an ethanol-replacement process. Then the keratin-based blend suspension was loaded into a syringe with a metal capillary which was connected to high-voltage electricity. The feeding rate of the suspension from the syringe was set to form linear jet from the syringe. The nanofibers were collected on a grounded aluminum foil. 5-Fluorouracil was added into the keratin-based suspension as the drug model applied in the later dissolution test and anti-tumor test. A kind of anti-microbial peptides was added into the drug-loaded suspension to investigate the synergistic effect with chemical anti-tumor drug.

1.3.2 Characterization of nanofibers

The morphologies, crystal structures, physical properties and chemical properties of the keratin-based nanofibers, including keratin nanofibers, keratin/PLLA nanofibers, 5-FU/keratin/PLLA nanofibers and antimicrobial loaded 5-FU/keratin/PLLA nanofibers were characterized and analyzed with the use of advanced techniques such as scanning electron microscopy (SEM), transmission electron microscopy (TEM), Differential Scanning Calorimetry (DSC), thermal gravimetric analysis (TGA), Fourier Transform Infrared Spectroscopy (FT-IR), X-ray diffraction (XRD), Zeta potential measurement (Zeta) and UV-Vis Spectroscopy (UV).

1.3.3 Drug loading and in vitro release properties

The content of drug was analyzed by the ultraviolet (UV) spectrophotometer. Drug

load is the ratio of drug to the gross weight of the drug loaded polymer nanofibers. Encapsulation efficiency is the ratio of weight percentage of drug entrapped in nanofibers to the gross weight drug used in the experiment. The *in vitro* drug release property can be interpreted by the drug release curve based on the drug cumulative release percentage of drug (% , w/w) in PBS solution over predetermined periods of time. The different pH value PBS solutions were applied to mimic the normal tissue fluid and tumor issue fluid.

1.3.4 Biological evaluation of nanofibers

The morphology of cells proliferation was observed by SEM. The biocompatibility of keratin-based nanofibers can be evaluated by 3- (4,5- dimethylthiazol-2-yl)- 5- (3- carboxymethoxyphenyl)-2-(4-sulfophenyl)-2H-tetrazolium (MTS) assay , cell live/die assay and DAPI fluorescence staining assay. The *in vitro* cytotoxicity activity of anti-tumor drug loaded keratin-based nanofibers can be evaluated by MTS assay, Live/Dead assay. Cellular proliferation studies of nanofibers were observed by Fluorescent Microscopy (Nikon, Eclipse 80i). Fluorescent intensity was measured using Image J and was normalized to cell number per image. Besides, SEM images also provided a direct observation of cells proliferation morphology and confirmed the anti-tumor effect by utilizing the synergistic effect between anti-microbial peptide and anti-tumor drug to tumor cells by performing culture experiments with human colorectal carcinoma cell line (HCT-116).

1.4 Outline of the thesis

The thesis presents the studies on the exploration of keratin-based composite biofunctional materials. Various types of polymer systems, including keratin particles extracted from wool, keratin/PLLA composite nanofibers, 5-FU loaded keratin/PLLA composite nanofibers and Attacin-2 loaded 5-FU/keratin/PLLA composite nanofibers were exploited. Additionally, great effort has been made to disclose the sustained-release profile of keratin/PLLA nanofibers when loaded with hydrophilic anti-tumor drugs, the mechanism of the anti-tumor effect of drug-loaded electrospinning nanofibers and the generalized principle for developing this type of biofunctional polymers. The overall contents of the thesis are categorized as nine chapters, which are briefly described as follows:

Chapter 1 introduced the research background, the objectives and significance, and arrangement of the thesis respectively.

Chapter 2 gave a systematic literature review mainly on the three following topics: 1) materials candidates for scaffolds; 2) fabrication techniques of scaffolds; 3) evaluation methods on scaffolds' biofunctional properties. Research gaps of each part were summarized respectively. Finally, a brief summary was given at the end of the chapter.

Chapter 3 discussed the feasibility of transforming wool into the functional protein biomaterials. In order to achieve this objective, isoelectric precipitation process was introduced to produce the targeted bio-functional keratin polypeptides. Wool fibers were hydrolyzed and adjusted to predetermined pH values. The results suggested that

keratin polypeptides with different amino acids compositions could be tailored from wool hydrolyzed solution. Keratin particles at nanometer-scale were collected successfully. The chemical structure of keratin polypeptides endured the same as the pristine wool and the crystal structure of keratin polypeptides became more amorphous.

Chapter 4 presented applying keratin polypeptides into biofunctional tissue engineering scaffolds system. In order to achieve the keratin composite nanofibers, keratin polypeptides were blended with Poly (*L*-lactic acid) (PLLA) organic solution with an “ethanol replacement” process and electrospun into nanofibers. The results indicated that the nanofibrous composite membrane possessed ultrafine and homogenous structure without keratin aggregation. The Fourier transform infrared spectrometry (FT-IR) revealed the existence of keratin in the composite fibers. The thermal property of the composite membrane was more stable than pure keratin. XRD spectra revealed a crystal transformation of keratin after the process of electrospinning. The biocompatibility was examined by seeding cells on the surface of the composite nanofibers. Compared to pure PLLA nanofibers, keratin/PLLA fibrous membrane showed an enhanced impact on cells viability and affinity.

Chapter 5 explored the degradability of keratin/PLLA composite nanofibers. This chapter is foundation for chapter 6. In this chapter, the degradability of the nanofibrous biopolymer membrane is evaluated through several aspects. The morphology of the membranes is observed by SEM images which indicate that the thin keratin/PLLA nanofibers are unfolded after degradation in PBS solution. The UV

spectra further indicate the degradation rate of keratin. The FT-IR spectra demonstrate the same degradation trend by comparing the intensities of keratin characteristic peaks. The thermal properties of the degraded membranes are tested by TGA thermal analysis.

Chapter 6 developed a localized drug delivery system. The composite polymer-protein nanofibers containing hydrophilic drug 5-Fluorouracil were synthesized by electrospinning and characterized to determine the chemical properties, physical properties and drug release properties. The combination forces status of drug and protein was explored by Zeta potential analysis. The dispersion status of drug in the composite membrane was investigated by different characterization methods. Scanning electron microscopy and differential scanning calorimetry revealed that individual filament morphology and thermal properties are maintained in the bi-component filaments. The in vitro drug release profiles were examined. Drug release from a bi-component filament is an additive composite of the drug release profiles obtained from single component filaments, and multi-component filaments can control the release of drug over much longer times than a mono-component filament. Drug release from a tetra-component filament is calculated based on the individual component drug release profiles and shown to be a good predictor of experimentally determined drug release.

Chapter 7 investigated the optimized factors effect on the controlled release performance of the electrospun composite membrane in different pH environments, this study employs the full-factorial design with two factors at two-levels. The

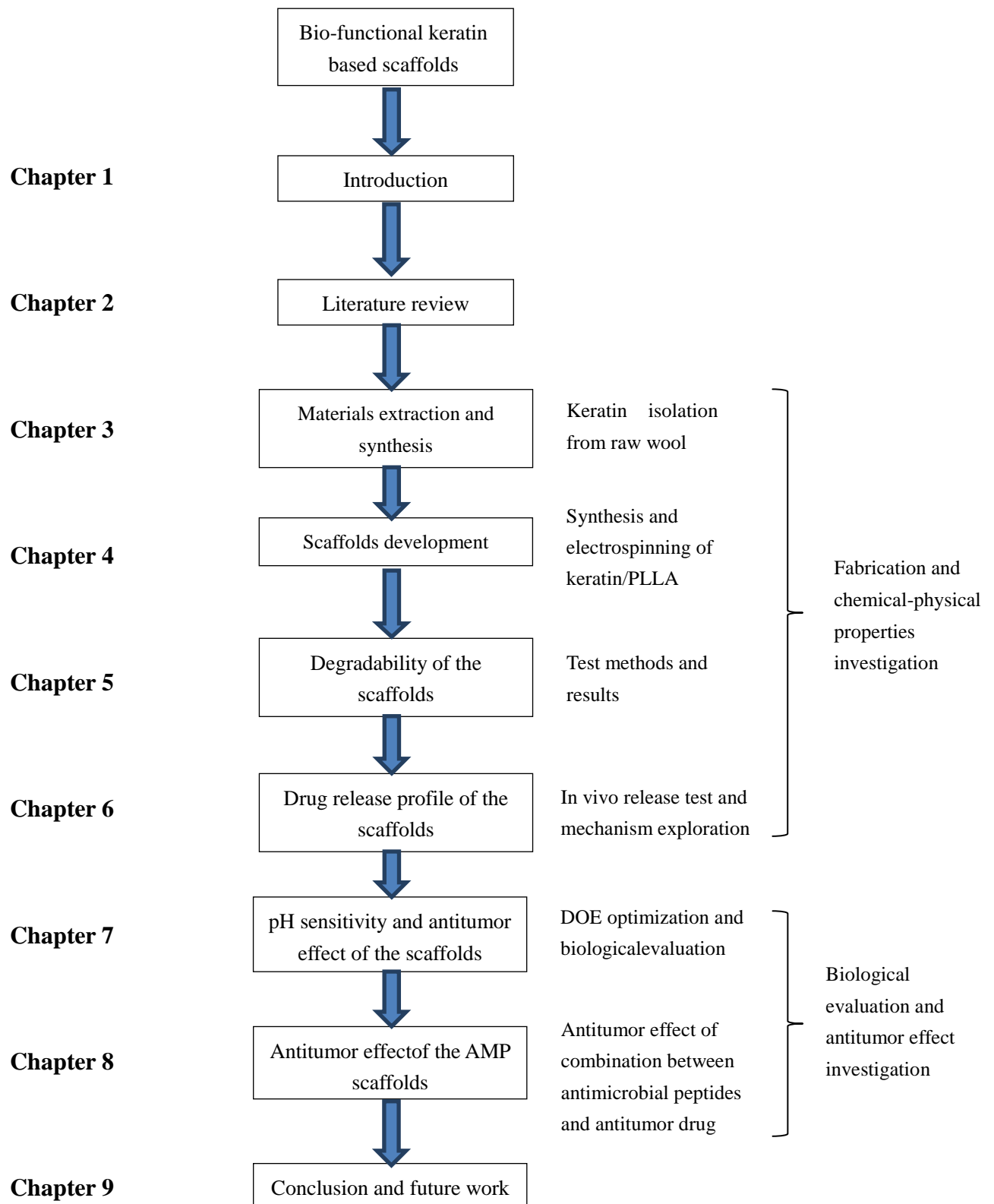
nanofibrous membranes with different processing parameters were tested in two different pH conditions: pH 7.4 PBS solution and pH 6.0 PBS solution. 5-fluorouracil was introduced in this experiment as the targeted drug. This full-factorial design of the experimental method indicates that it is possible to not only identify the main effects of this complex bio-mimetic system, but also investigate the effects of two-factor interactions. The antitumor effect was examined by a series of biological evaluations: cell live/dead assay, Fluorescence staining and MTS assay. The biological results indicated 5-FU/Keratin/PLLA nanofibers has a long-term inhibition effect on tumor cells (HCT-116) compared to 5-FU/PLLA nanofibers. The sustained effect can last from 4hours observation until 120 hours observation. The 5-FU/keratin/PLLA kept releasing the antitumor drug in the total 120 hours experiment and proliferation rate of tumor cells was inhibited steadily and sustainably. Adding keratin into the composite membranes can increase the antitumor effect dramatically.

Chapter 8 discussed the further investigation on bio-functions of PLLA and keratin nanofibrous membranes. Both the anti-tumor drug and anti-microbial peptides were loaded on the nanofibers. The antitumor effect between chemical drug and antimicrobial peptides was investigated. The experimental results indicated that after adding the antimicrobial peptides into the scaffolds, the antitumor effect could be observed, especially after 72 hours cultivation ($P<0.01$). Unlike the chemical antitumor drug with a short and strong inhibition effect on tumor cells, the biological antimicrobial peptides has a long and sustained inhibition on tumor cells which

compensates the short effect of chemical antitumor drugs. After the 72 hours observations, the antitumor effect of antimicrobial scaffolds dramatically inhibited the proliferation of tumor cells. The results indicated the feasibility of combining both chemical antitumor drugs and biological antimicrobial peptides together, which suggested the further direction of applying nanofibers in the realm of antitumor therapy.

Chapter 9 summarized all the conclusions and gave the suggested future work. The conclusions covered all the main findings obtained in this study. The suggested future work focused on three issues related to the optimization of dual drug formulation antitumor experiments and animal model experiments. References were attached in the end of the thesis. The frame work of this thesis could be well illustrated by the following.

Scopes and Outline of Thesis



CHAPTER 2 LITERATURE REVIEW

A primary driving force for the work in this thesis comes from a shifting biomaterials landscape of tissue engineering. In this chapter, an overview on tissue engineering and biomaterials applied in tissue engineering is presented. First of all, tissue engineering and the scaffolds are extensively introduced. Secondly, biomaterials as an important role in the tissue engineering process are introduced as two categories according to the diversified sources, compositions and functionalities. Thirdly, the applications of wool keratin, a kind of natural polymer, are summarized, such as the characterizations of the keratin and exploration of the keratin-based composite polymers. Fourthly, electrospinning technology and its corresponding applications in tissue engineering are summarized. Finally, the anti-tumor drug release system by electrospinning technology is introduced, which is followed by a brief summary.

2.1 Tissue engineering and scaffolds

2.1.1 Tissue engineering

Tissue engineering is an emerging interdisciplinary field that applies the principles of biology and engineering to the development of viable substitutes that restore, maintain or improve the function of human tissues and organs [1]. Tissue engineering, which applies methods from engineering and life sciences to investigate artificial constructs to direct tissue regeneration [2], has therefore attracted the attention of many scientists and surgeons with a hope to treat patients in a minimally invasive and less painful way.

A schematic diagram is given to display the whole structure of the literature review

section in Figure 2.1.

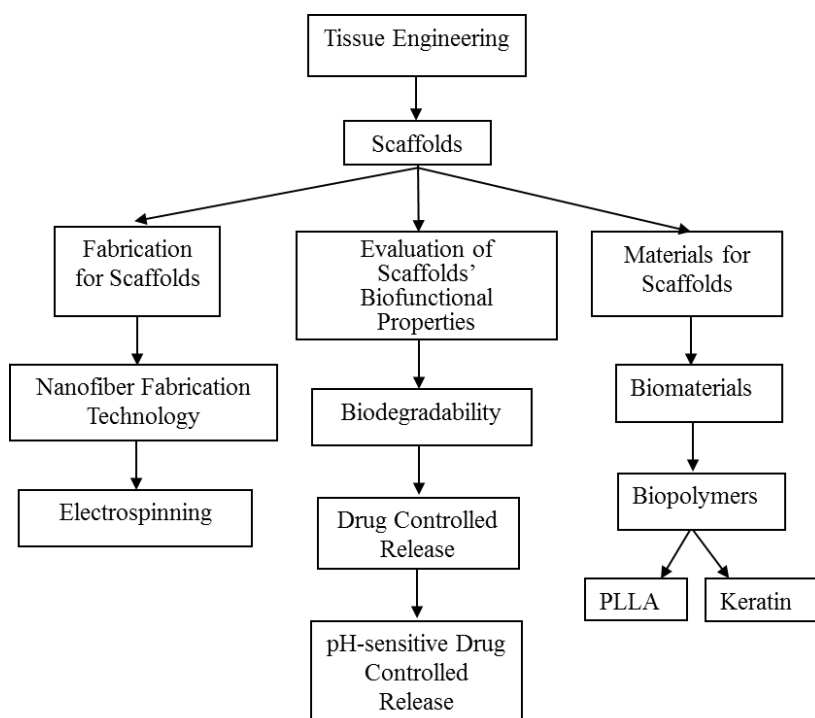


Figure 2.1 Schematic demonstration of literature review structure.

Tissue engineering also provides unique opportunities to investigate structural function relationship associated with new tissue formation in the laboratory and to predict the clinical outcome of the specific medical treatment. And some future applications for tissue engineering, for instance, drug carrier and drug targeted release have also been explored deeply recently. A general process of tissue engineering is explicated in Figure 2.2.

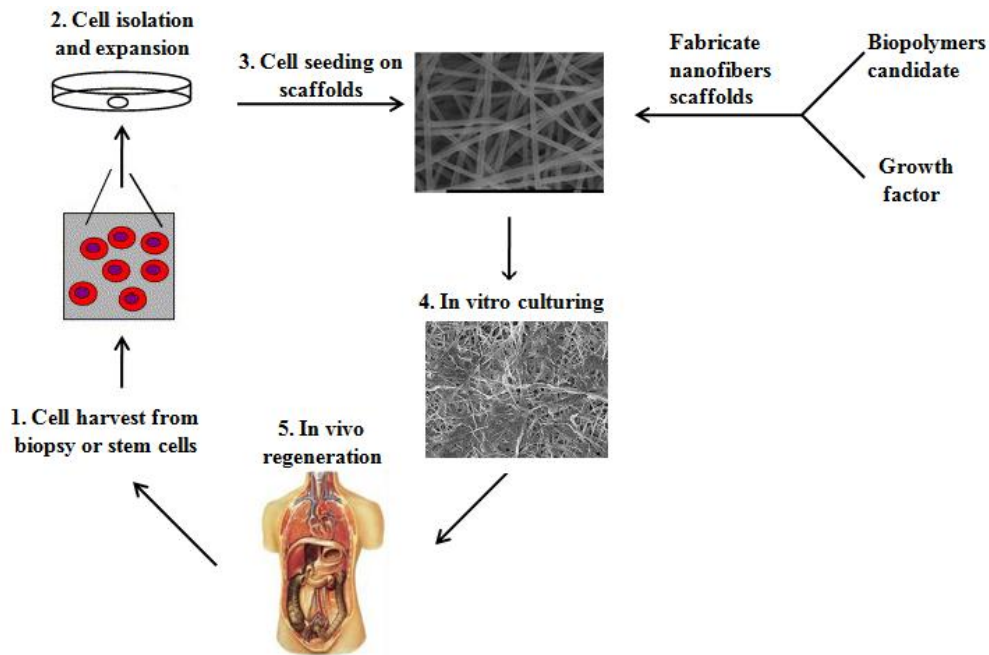


Figure 2.2 Basic scheme of tissue engineering process: cells are harvested from in vivo stem cells.

In order to achieve successful regeneration of wound organs or tissues based on the concept of tissue engineering, several critical elements should be considered. The first thing is the biomaterial scaffolds which serve as a mechanical support for cell growth. The second thing is the progenitor cells which can be differentiated into specific cell types. The final element is the inductive growth factors that can modulate cellular activities [6, 7]. The process of tissue engineering mainly involves the seeding of cells onto a scaffold, which as a whole part is cultured in vitro, and implanted into the body [8]. In general, tissue engineering requires three elements: 1) cells for seeding, 2) different kinds of scaffolds depending on the explored cells types; 3) bio-molecular signals between cells and scaffolds. It is obvious that the core issue of tissue engineering is to design suitable scaffolds and improve the properties of scaffolds. A

proper scaffold is the key step in achieving success in tissue engineering [9].

2.1.2 Scaffolds

The scaffolds, known as the artificial extracellular matrix (ECM), are defined as the carrier for cells, growth factors and other bio-molecular signals [3]. The major function of scaffolds is providing a framework and support for cells to attach to, proliferate and differentiate. Typically, artificial ECM constructs are developed by either natural-resourced molecular polymers (e.g. collagen, fibrin, keratin, etc.) or synthetic polymers (PLGA, PEG, etc.). The adhesivity of synthetic polymer scaffolds can be enhanced by ECM-derived peptides or protein fragments [4]. Found in various ECM molecules, RGD is considered as the most popular adhesive ligand for most cells bind to ECM through the RGD-dependent manner [5]. These peptides can also have better bio-interaction with cells by transforming their chemical structures. For instance, RGD can support better cell adhesion and proliferation when its physical structure is changed from linear to cyclic [10]. To mimic native tissue structures, ECM scaffolds have been developed in various physical forms such as hydrogels, nanofibers, woven and non-woven fabrics. Different crosslinking schemes are utilized to achieve stability prior to or during cell seeding [10-12]. Cells within these mechanically-conditioned and functionally-conditioned artificial tissues often display increased viability and ECM synthesis both in vitro and in vivo [13-15].

An ideal scaffold should have the following characteristics: 1) an extensive network of interconnecting pores so that cells can migrate, multiply and attach deep within the

scaffolds; 2) channels through which oxygen and nutrients are provided to cells deep inside the scaffold, and the waste products can be easily carried away; 3) biocompatibility of the substrate materials which do not elicit an unresolved inflammatory response nor demonstrate immunogenicity or cytotoxicity; 4) the right shape, however complex as desired by the surgeon; and 5) the mechanical properties of the scaffold must be sufficient and not collapse during handling and during the patient's normal activities [16-18]. Most materials widely used in the area of tissue engineering are adapted from other surgical uses, such as haemostatic agents and wound dressings. These materials include synthetic biodegradable materials, such as aliphatic polyesters (poly-glycolic acid, poly-lactic acid and their co-polymers) [19-21], hydroxyl-apatite (HA) [19, 22], and naturally derived materials, for example, collagen and chitin [23, 24]. The techniques of fabricating tissue engineering scaffolds include electrospinning [25-28], solvent casting particulate leaching, phase separation [18] and gas forming, emulsion freeze drying [29, 30]. The details regarding the biomaterial polymers and fabrication techniques will be illustrated more in subsequent chapters.

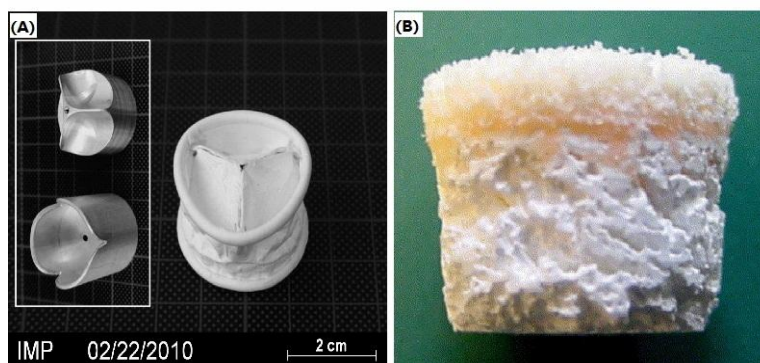


Figure 2.3 Examples of artificial biomedical composite scaffold devices: (A) Electrospun heart valve scaffold for tissue engineering; (B) Heterogeneous composite

scaffold for osteochondral repair [27, 28]

2.2 Biomaterials

2.2.1 Introduction about biomaterials

In the first Consensus Conference of the European Society for Biomaterials (ESB) in 1976, a biomaterial was defined as “a nonviable material used in a medical device, intended to interact with biological systems”. However, now the ESB's defined biomaterials as “material intended to interface with biological systems to evaluate, treat, augment or replace any tissue, organ or function of the body”. This subtle change in definition indicates how the field of biomaterials has evolved. Biomaterials have moved from merely interacting with the body to influence biological processes toward the goal of tissue regeneration [31-34]. The indispensable property of biomaterials is biocompatibility, which is defined as the ability of a material to perform with an appropriate host response in a specific application. The selection of biomaterials for a given application is determined by degraded surface, and bulk properties of the material. Generally there are three major categories in biomaterials:

1. Metals: Metals are inorganic materials with metallic bonds and highly mobile electrons which are strong and easily to form complex shapes.
2. Ceramics are inorganic materials with ionic bonds which are very hard and more resistant to degradation than metal. The disadvantage of ceramics is very brittle.
3. Biopolymers

Biopolymers have been widely investigated in the recent decades. Two major groups compose the biopolymers, the natural polymers and synthetic polymers. The natural

polymers are derived from sources within the body (e.g. collagen, fibrin, keratin.) or outside the body (chitosan, alginate). The synthetic polymers are man-made by certain chemical reactions in a certain purpose. The synthetic polymers can be easily mass-produced and sterilized and their physical, chemical, mechanical and other properties can be tailored for specific application. A detailed discussion concerning biopolymers will be conducted in the following section.

2.2.2 Natural biopolymers

A wide range of natural biopolymers have been found and studied such as collagen [35], gelatin [36], silk fibroin [37], fibrin (fibrinogen) and other poly-saccharide polymers (e.g. chitosan or alginate) [38, 39]. Natural polymers are mainly derived from sources within the biological body (e.g. collagen, fibrin) or outside the body (e.g. chitosan). The materials from bio-sources, especially the protein-based polymers are good at mimicking many features of ECM and therefore have the ability to improve the migration, growth and organization of cells during the period of tissue regeneration and wound healing, and for the stabilization of encapsulated and transplanted cells. They provide a natural substrate for cellular attachment, proliferation and differentiation in the native state. For the reasons mentioned above, naturally occurring polymers could be the preferred substrate for tissue engineering. Table 2.1 presents the major natural biopolymers and their sources as well as their applications. Among them, collagen, fibrin, gelatin and alginate have been extensively investigated for myocardial tissue engineering [40].

In summary, two major advantages of natural polymers are: 1) natural biopolymers possess similar chemical compositions as the tissues they are replacing; 2) natural biopolymers can be more easily integrated into the surrounding tissues over time. However, their drawbacks are obvious: 1) small existing amount in nature; 2) low mechanical properties; 3) are easily rejected by the host; 4) have possible batch variation.

Table 2.1 List of natural biopolymers and their sources as well as main application fields

| Polymer | Source | Applications |
|----------|---|---|
| Collagen | Tendons and ligament | Multi-applications, including cardiac tissue engineering, collagen gels [41]. |
| Elastin | Tissues and extracellular matrix | Multi-applications, including nano-composite scaffolds [42]. |
| Gelatin | Extracted from the collagen inside animals' connective tissue | Multi-applications, including nano-composite scaffolds [42]. |
| Chitosan | Shells of shrimp and crabs | Multi-applications, including nano-composite scaffolds [43]. |
| Keratin | Wools, nails and hairs | Multi-applications, including bio-functional membranes, sponge [44]. |
| Alginate | Cell walls of brown algae | Multi-applications, including composite alginate gels [45]. |

Collagen: An important natural biopolymer, which can be found in most body organs like skin, bone, tendon, cartilage and blood vessels. In humans, collagen represents

one-third of total proteins, accounting for three-quarters of the dry weight of skin, and is the most prevalent component of the extracellular matrix (ECM)

Chitosan: A copolymer of glucosamine and N-acetylglucosamine units obtained by deacetylation of chitin with a percentage of N-acetylglucosamine lower than 50%. It is often applied in the fields of wound healing, drug delivery systems, and tissue engineering because of its unique nontoxic and antimicrobial properties. However, it is only soluble in acetic solutions which limit its fabrication methods since many biopolymer fabrication methods (electrospinning, phase separation) are involved in organic or neutral environments.

Elastin: The protein component found during the process of the growth of tissues. Elastin is composed of cross-linked insoluble tropoelastin. Elastin is made by linking many soluble tropoelastin protein molecules, in a reaction catalyzed by lysyloxidase, to make a massive insoluble, durable cross-linked array. It is often utilized in biomaterials as a result of both mechanical strength and flexibility. However, elastin easily triggers the biological immune system and its low solubility limits its potential biomedical application.

Alginate: A biopolymer and polyelectrolyte that is considered to be biocompatible, non-toxic, non-immunogenic and biodegradable. It can be characterized as an anionic copolymer consisting of mannuronic acid (M block) and guluronic acid (G block)

units. Alginate has gained popularity in biomedical applications because of its gelling ability in the presence of divalent cations, and stability and viscosity in aqueous solutions. However, due to its weak mechanical properties and slow degradability, it is fraught with difficulties when applied in biomedical nanofibrous devices.

Keratin: The major structural fibrous protein providing an outer covering such as wool, hair, feathers and nails. From amino acid analysis, keratin is characteristically abundant in cysteine residues (7–20% of the total amino acid residues). Keratin is beneficial in wound healing and tissue regeneration as an artificial ECM. Due to its favorable mechanical strength, biodegradability and biocompatibility, keratin is considered a competitive biopolymer candidate to be applied as a biomedical scaffold. A detailed review of the literature on keratin is offered in the following.

2.2.3 Wool keratin

As a big family of cysteine-rich structural proteins formed in the epithelial cells of higher vertebrates, keratin belongs to the group of natural biopolymers. The natural sources of keratin are the stiff or filamentous organs such as hairs, nails, horns and feathers, all of which are present mostly as protein-rich waste [46, 47]. Unlike the kinds of protein materials (e.g. collagen) having been the target of extensive investigation, in the past keratin only attracted minor interest because of its water-insolubility and the limited number of methods available for its extraction and processing. However, in the last decade, and particularly over the last five years, new

methods have been described for the use of keratin or modified keratin, mainly obtained from wool, as a substrate or scaffold for cell cultivation and tissue engineering. Some reports have revealed the use of keratin, mainly derived from wool, as a substrate or scaffold for cell culture and tissue engineering. In one patent application, the suitability of keratin as a substrate and growth supplement was suggested [48]. Yamauchi *et al.* and Tachibana *et al.* reported an improved proliferation rate for fibroblasts (mouse cell line L929) on keratin-coated culture wells and spongy keratin scaffolds [49, 50]. Figure 2.4 displays the morphology of a keratin-based sponge.

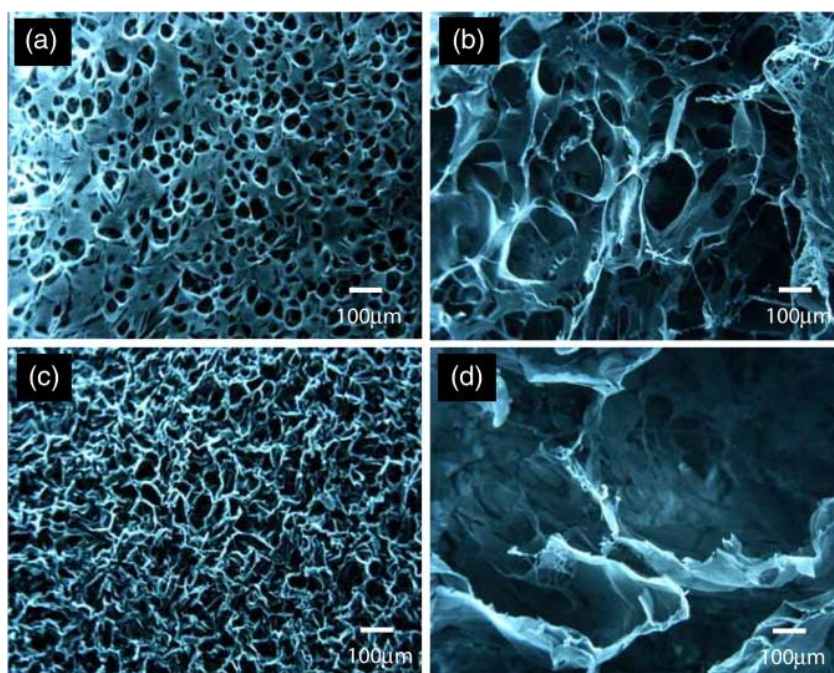


Figure 2.4 SEM photographs of freeze-dried keratin sponge (a) and (c) and keratin/calcium/alginate sponge (b) and (d). (a) and (b): surfaces, (c) and (d): cross-sections [45]

Moreover, chemically cross-linked keratin films and keratin-chitosan composite films have been investigated [51]. The essential element of the structure of the keratin

macromolecule is the alignment of amino acids residue along its chain. The sequence of amino acids defines the possibility of intermolecular links, the molecular cohesion of the keratin and the access of amino acids to the chemical reaction. The residue of cysteine in the keratin chain plays a fundamental role in chemical reactions of wool fibers. Keratin macromolecules in wool fiber takes on the following conformations [52-56]:

- Helical (α -keratin)
- Rectal (β -keratin)
- Undefined

Previous literature reports the study on extraction of protein material from wools by chemical cleavage of the disulphide bonds of the amino acid cysteine, responsible for the high stability of keratin, followed by successive purification and regeneration [54-56]. Keratin regenerated from wool fibers needs to be dissolved in proper solvents before processing for further applications. Generally speaking, aqueous solutions are employed to produce films, porous membranes, hydrogels. The cross-linking agents (such as formaldehyde or epoxy resins) are often applied to the regenerated keratin due to their mechanical strength. There is a consensus that protein is composed of amino acids. Different amino acids should have different chemical and medical properties. Table 2.2 gives a summary of amino acids characterization.

Table 2.2 Standard amino acid and their properties [57]

| Amino Acid | 3-Letter | 1-Letter | Side chain polarity | Side chain acidity or basicity | Hydropathy index |
|--------------------|----------|----------|---------------------|--------------------------------|------------------|
| Alanine | Ala | A | nonpolar | neutral | 1.8 |
| Arginine | Arg | R | polar | basic(strongly) | -4.5 |
| Asparagine | Asn | N | polar | neutral | -3.5 |
| Aspartic acid | Asp | D | polar | polar acidic | -3.5 |
| Cysteine | Cys | C | polar | neutral | 2.5 |
| Glutamic acid | Glu | E | polar | polar acidic | -3.5 |
| Glutamine | Gln | Q | polar | neutral | -3.5 |
| Glycine | Gly | G | nonpolar | neutral | -0.4 |
| Histidine | His | H | polar | basic(weakly) | -3.2 |
| Isoleucine | Ile | I | nonpolar | neutral | 4.5 |
| Leucine | Leu | L | nonpolar | neutral | 3.8 |
| Lysine | Lys | K | polar | basic | -3.9 |
| Methionin | Met | M | nonpolar | neutral | 1.9 |
| e Phenylalanine | Phe | F | nonpolar | neutral | 2.8 |
| Proline | Pro | P | nonpolar | neutral | -1.6 |
| Serine | Ser | S | polar | neutral | -0.8 |
| Threonine | Thr | T | polar | neutral | -0.7 |
| Tryptophan | Trp | W | nonpolar | neutral | -0.9 |
| Tyrosine | Tyr | Y | polar | neutral | -1.3 |
| Valine | Val | V | nonpolar | neutral | 4.2 |

The Hydropathy index indicates the hydrophobicity of amino acids. Normally, a larger number represents more hydrophobicity. Side chain acidity or basicity may be another factor related to the biomedical properties of amino acids. Based on the theory of isoelectric points, biological amphoteric molecules will precipitate at their pI point.

The iso-electric point (pI) can be calculated as indicated in Equation 2.1:

$$pI = \frac{pK_1 + pK_2}{2} \quad (\text{Equation 2.1})$$

In this equation, the pH of the amine terminal of an amino acid is denoted as pK_1 ; the pH of the carboxyl terminal of amino acid is denoted as pK_2 . Additionally, it is important to summarize the bio-functions of the major amino acids.

Cystine: A dimeric amino acid formed by the oxidation of two cysteine residues that covalently link to make a disulphide bond. Its chemical structure is $\text{HO}_2\text{CCH}(\text{NH}_2)\text{CH}_2\text{SH}$. The disulphide link is readily reduced to give the corresponding thiol cysteine. This reaction is typically effected with thiols [58]:



Disulphide bonds cleave more rapidly at higher temperatures.

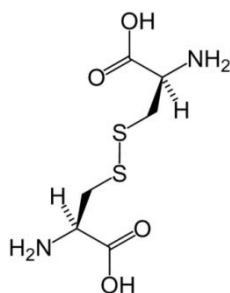


Figure 2.5 Molecular structure of Cysteine: $-\text{NH}_2$ group is hydrophobic and therefore the bi-sulfide binding is strengthened.

Glycine: with the molecular formula $\text{C}_2\text{H}_5\text{NO}_2$ it is the smallest amino acid molecule. It can fit into both hydrophilic and hydrophobic environments due to its two side chains. Glycine is degradable via three pathways. The predominant pathway in

animals involves the catalysis of the glycine cleavage enzyme, the same enzyme which is also involved in the biosynthesis of glycine. The degradation pathway is the reverse of its synthetic pathway [57]:

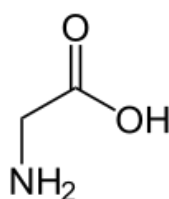
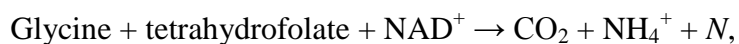


Figure 2.6 Molecular structure of Glycine.

Research Gap with regard to Wool Keratin

Wool keratin as a kind of cysteine-rich structural protein has been applied in some biomedical devices. However, previous studies mainly focused on the protein area. Little research has explored the mechanism of keratin applied as a biopolymer material. Based on the different bio-functions and solubility of the amino acid, hydrolyzed keratin could be separated into different polypeptides for specific biomedical purposes at different isoelectric points. Moreover because of the water solubility of wool keratin, many researchers have extracted keratin by dissolving in organic chemicals and spray drying wool keratin powder [59, 60] or lyophilizing the keratin powder [51, 61, 62].

Keratin powder can encounter several problems in electrospinning: firstly, the keratin powder is water soluble, so although the keratin particles have been embedded into the structure of membranes, films and scaffolds, it can be released into hydrophilic solutions rapidly. As a major functional part of a biomedical device, the loss of keratin could jeopardize the fibrous membranes, films and scaffolds. Also, keratin powder can become aggregated easily in a nanoscale structure which causes the average size of keratin particles to be larger than the diameter of nanofibers so the fibers cannot encapsulate the particles.

2.2.4 Synthetic biopolymers

As a matter of fact, instead of natural biopolymers, recently tailored synthetic polymers have been applied extensively in the realm of tissue engineering, drug delivery and medicine clinics, etc. Some polymer sub-classes are particularly suited to certain tissue types. Let's take elastomers as an example. Elastomers can sustain substantial deformation at low stresses and return rapidly to their initial dimensions upon release of the stress, which is suitable for cardiovascular applications, where tissue elasticity is an important property. Also, hydrogels are another instance. Their super-hydrophilic ability makes hydrogels swell in water and retain a significant amount of water within their structure. Due to their super water content, hydrogels can be explored for a variety of soft tissue applications (e.g. PEO/PEG). The advantages of synthetic polymers are: 1) they are easily sterilized; 2) their physical, chemical, mechanical and other properties can be tailored for specific applications;

and 3) they rarely trigger an immune system response. However, their major disadvantage is that most synthetic polymers do not interact with tissue in an active way and cannot improve wound healing and tissue regeneration.

2.2.5 Poly(L-lactic acid) (PLLA)

Poly(L-lactic acid) (PLLA) is one of the few synthetic degradable polymers approved by the Food and Drug Administration (FDA, USA) for human clinical applications [63]. The mechanism of the degradation of PLLA is hydrolytic attack of ester bonds. Through this hydrolytic attack, chemical chains are broken, causing it to degrade into lactic acid [64]. PLLA belongs to the saturated poly- α -hydroxy esters group, which contains most often utilized biodegradable synthetic polymer candidates like: poly(lactic acid) (PLA), poly(glycolic acid) (PGA) and poly(lactic acid-co-glycolide) (PLGA) copolymers [13, 65]. The chemical properties of these polymers allow hydrolytic degradation through de-esterification. In the process of degradation, the monomeric components of each polymer are removed by natural pathways. The human body already contains highly regulated mechanisms for completely removing monomeric components of lactic and glycolic acids. Studies confirmed that PLLA, as a stable synthetic polymer candidate, has been employed in tissue engineering. A Poly (D-lactic acid) (PDLA) oligomer was used to blend with PLLA to form a stereo complex possessing good thermal resistance [66]. An in vitro interaction of MG-63osteosarcomacells with PLLA membranes was investigated which showed that a particulate membrane can improve cell adhesion growth [67]. PLLA has also been

fabricated with collagen as cartilage scaffolds. The big pore size, however, can only maintain its original mechanical strength and structure for a matter of weeks. SEM morphology is shown in Figure 2.7 [15].

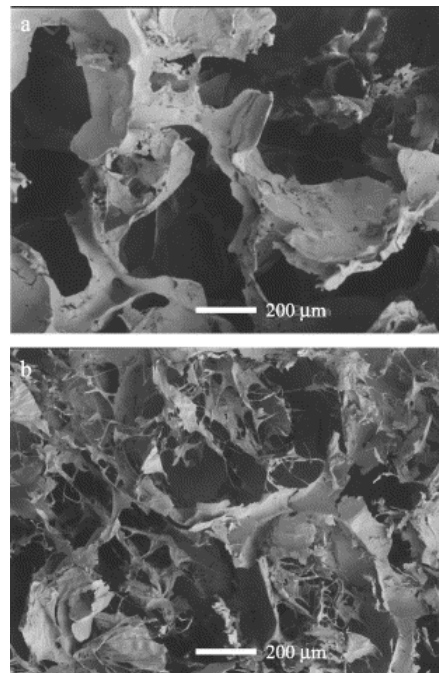


Figure 2.7 SEM photomicrographs of cross sections of PLLA sponge (a) and PLLA–collagen sponge (b) at original magnification $\times 80$

Research Gap for the application of PLLA

PLLA as a kind of safety materials as demonstrated by the FDA (Food and Drug Admission, USA) has been investigated widely. With high biocompatibility and biodegradability, a major problem encountered in PLLA application is the lack of ECM and cell growth signals. Due to this, merely based on PLLA nanofibrous membrane, no significant impact has been observed concerning improvement of wound healing and tissue regeneration.

2.2.6 Degradability of biopolymers

Degradability is the key issue in the selection of biomaterials in tissue engineering. A degradable product has the ability to break down in a safe, reliable, and relatively fast way, by biological processes, into the raw materials of nature and thus disappear into nature. A comparison [15, 68, 69] of the degradability and other properties of different kinds of polymers is as shown in Table 2.3.

Table 2.3 Comparison on Biodegradability and other Physical Properties of Selected

| Biopolymers | | | | |
|--------------------------------|--|-----------------------------|---------------------------|------------|
| Polymer | Melting Temperature (T _m /°C) | Biodegradation Time(Months) | Modulus (Gpa) | Mechanism |
| Poly-L-lactide (PLLA) [68, 70] | 173-178 | 12--24 | Film or disk: 1.2--3.0 | Hydrolytic |
| Poly-DL-lactide (PDLLA) [71] | Amorphous | 12--16 | Film or disk: 1.9--2.4 | Hydrolytic |
| Polyglutamic acid(PGA) [72] | 225—230 | 4--6 | Fiber: 7--14 | Hydrolytic |
| Poly-caprolactone (PCL) [71] | 58 | >24 | ---- | Hydrolytic |
| Collagen [73] | ---- | 2--24weeks | ---- | Enzymetic |
| Chitosan [74] | ---- | 100days | ---- | Enzymetic |

From Table 2.3, the first four kinds of materials are synthetic and have a relatively longer degradation time. The last two polymers are protein-based natural polymers

which have a shorter degradation period due to the enzymatic mechanism rather than hydrolytic degradation. In general, the degradation time should not last too long or too short. Since the substantial structure serves as a cell host, a short degradation time makes these polymers unable to fulfill this basic aim. However, on the other hand, if the polymers' degradation lasts for too long, when the tissue completes the regeneration process, the residue of polymers in vivo can be restrictive for new tissue growth. A proper degradation time is what researchers are looking for. The chemical properties of these polymers allow hydrolytic degradation in the process of de-esterification. After degradation, the monomeric components of each polymer are removed by natural pathways. The human body already contains highly regulated mechanisms for completely removing monomeric components of lactic and glycolic acids. PLA and PGA can be processed easily and their degradation rates and physical and mechanical properties are adjustable over a wide range by using various molecular weights and copolymers. However, these polymers undergo a bulk erosion process such that they can cause scaffolds to fail prematurely. In addition, abrupt release of these acidic degradation products can cause a strong inflammatory response [75, 76]. In general, PGA degrades faster than PLA, as found in Table 2.2. Their degradation rates decrease in the following order:



Biodegradable polyester degradation begins by being attacked by water molecules followed by the hydrolysis of ester bonds. Various factors affect the de-esterification kinetics. For example, chemical composition and configurational structure, processing

history, molar mass (Mw), environmental conditions, stress and strain, crystallinity, device size, morphology (e.g. porosity) and chain orientation, distribution of chemically reactive compounds within the matrix, additives, presence of original monomers, and overall hydrophilicity [77, 78].

2.3 Fabrication technology applied in tissue engineering

2.3.1 Fabrication technology for nanofibers

Polymer nanofibers have been fabricated using a number of different techniques. The methods of nanofibers fabrication are varied and utilize physical, chemical, thermal, and electrostatic fabrication techniques. The methods of polymer nanofibers fabrication most commonly associated with tissue engineering scaffolds in the literature are electrospinning, self-assembling peptide reactions and phase separation. The following part will discuss the nanofibers fabrication technology in detail.

Electrospinning: This method is an electrostatically driven method for fabricating polymer nanofibers. Nanofibers are formed from the polymer solution that is fed through a capillary tube into a region of high electric field. The electric field is most commonly generated by connecting a high voltage power source in the kilovolt range to the capillary tip. As electrostatic forces overcome the surface tension of the liquid, a Taylor cone is formed and a thin jet is rapidly accelerated to a grounded or oppositely charged collecting target. The size and microstructure of the nanofibers can be controlled by varying parameters such as solution viscosity, voltage, feed rate,

solution conductivity, capillary-to-collector distance, and orifice size [79]. The electrospinning technique is a mature technology. It is very versatile and a wide range of polymer and copolymer materials with a wide range of fiber diameters (several nanometers to several microns) can be fabricated using this technique.

Self-assembly: This is a process whereby molecules organize and arrange themselves into patterns or structures through non-covalent forces such as hydrogen bonding, hydrophobic forces, and electrostatic reactions. Nanofibers with diameters around 5-25 nm can be formed by the self-assembly process, and systems have been developed wherein nanofibers assembly can be induced by appropriate pH values. While peptides are most commonly used in self-assembly of tissue engineering structures, synthetic polymer nanofibers have also been fabricated by self-assembly [80-83]. Figure 2.8 displays the peptide-amphiphile self-assembling structure [79].

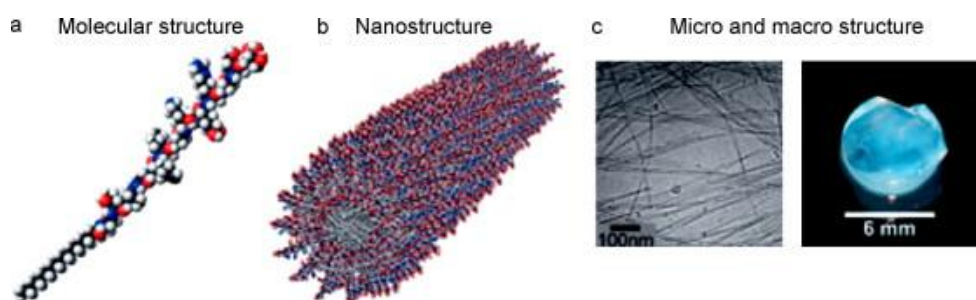


Figure 2.8 Schematics of the (a) molecular structure and (b) nanostructure, and images of the (c) micro and macro structure of a self-assembling nanofibers network.

Phase separation: Nanofibrous foam materials have been fabricated by a technique called thermally induced liquid-liquid phase separation. This fabrication procedure

involves four steps in general [84]. A schematic diagram is shown in Figure 2.9.

- (1) Dissolution of polymer in solvent
- (2) Phase separation and polymer gelatination at low temperature
- (3) Solvent exchange by immersion in water
- (4) Freezing and freeze-drying.

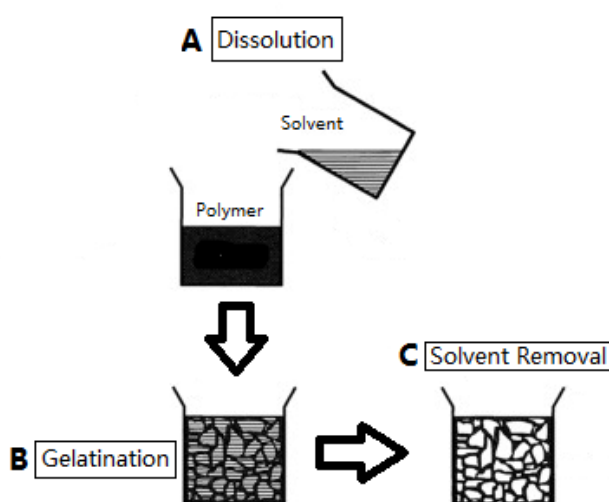


Figure 2.9 Schematic diagram of nanofibers formation by phase separation.

The morphology of these structures can be controlled by fabrication parameters such as gelatination temperature and polymer concentration. Interconnected porous nanofiber networks have been formed from polymers such as PLLA, PLGA and poly-DL-lactic acid(PDLLA) with fiber diameters from 50-500 nm, and porosities up to 98.5% [84-86]. Table 2.4 is a summary for a more detailed comparison.

Table 2.4 Comparison among popular nanofibers fabrication technology methods

| Technology Methods | Application Area | Ease of Processing | Advantages | Disadvantages |
|--------------------|--------------------|--------------------|--|--|
| Electrospinning | Lab and Industrial | Easy | <ol style="list-style-type: none"> 1. Cost Effective 2. Easy set-up 3. Tailorable mechanical properties, size, shape at satisfactory level 4. Wide range of polymers selection | <ol style="list-style-type: none"> 1. Use of Toxic organic solvent 2. limited application in 3-D pore structures |
| Self-assembly | Lab | Difficulty | <ol style="list-style-type: none"> 1. Achieves fiber diameters on lowest ECM scale (normally, 5–8 nm) 2. Injectable for in vivo assembly 3. Achieves 3Dimensional pore arrangement | <ol style="list-style-type: none"> 1. Low yield and commercial 2. Only short fibers can be created (< 1 μm) 3. Limited selection on polymer candidates |
| Phase Separation | Lab | Easy | <ol style="list-style-type: none"> 1. Batch-to-batch consistency 2. Achieves 3-Dimensional pore arrangement | <ol style="list-style-type: none"> 1. Low yield 2. Complex operations |

2.3.2 Electrospinning technology applied in tissue engineering

Among the popular nanofibers fabrication methods so far, electrospinning is attracting people's attention due to its easy operation, high yield and wide selection range of polymer candidates. Electrospinning is an electrostatic fiber fabrication technique which has evinced more interest and attention in recent years due to its versatility and potential for applications in diverse fields. The notable applications include tissue engineering, biosensors, filtration, wound dressings, drug delivery and enzyme immobilization. The working process of electrospinning is shown in Figure 2.10.

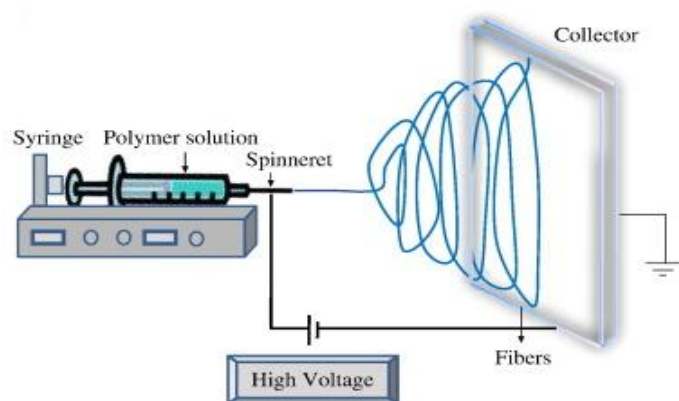


Figure 2.10 Diagram to illustrate the working process of electrospinning device [87].

With smaller pores and higher surface area than regular fibers, electrospun fibers have been successfully applied in various fields, such as nano-catalysis, tissue engineering scaffolds, protective clothing, filtration, biomedical, pharmaceutical, optical electronics, health care, biotechnology, defense and security, and environmental engineering. Overall, this is a relatively robust and simple technique to produce nanofibers from a wide variety of polymers. In Table 2.5 previous studies and medical applications utilizing the electrospinning technique are summarized in detail [88-94].

Spun nanofibers also offer several advantages such as an extremely high surface-to-volume ratio, tunable porosity, malleability to conform to a wide variety of sizes and shapes, and the ability to control the nanofiber composition to achieve the desired results from its properties and functionality.

Table 2.5 Different polymers used in electrospinning and their applications and assessment methods

| Polymers | Application and Devices | Assessment Methods |
|---------------------------------------|---|---|
| Poly(glycolide) (PGA) | Nonwoven TE scaffolds | SEM,TEM, in vitro rat cardiac fibroblast culture, in vivo rat model |
| Poly(lactide-co-glycolide)(PLGA) | Biomedical applications, wound healing | SEM, WAXD, SAXS, degradation analysis |
| Poly(ϵ -caprolactone) (PCL) | Bone tissue engineering | SEM, in vitro rat mesenchymal stem cell culture |
| Poly(l-lactide) (PLLA) | 3D cell substrate | SEM, in vitro human chondrocyte culture |
| Poly(l-lactide) (PLLA) | Nanofibrous Membrane | SEM,FTIR,XRD and vitro fibroblast cells culture |
| Silk fibroin | Nanofibrous scaffolds for wound healing | SEM, ATR-IR, ¹³ C CP/MAS NMR, WAXD, NMR, in vitro human keratinocyte culture |

Because of these advantages, electrospun nanofibers have been widely investigated in the past several years regarding their use in various applications, such as filtration, optical and chemical sensors, electrode materials, and biological scaffolds [95].

Research gap of electrospinning technology applied in the biomaterials area

Apart from the huge success, the advantages of the electrospinning method and electrospun nanofibers, there are still some challenges that need to be overcome. A major challenge which arises when using electrospun membranes for tissue engineering is the non-uniform cellular distribution and lack of cellular migration in the scaffold with increasing depth under normal passive seeding conditions. It has also been reported that with a decrease of the electrospun fiber diameter there is an increase in the number of fiber-to-fiber contacts per unit length and a decrease in the mean pore radius in the mesh. Nam *et al.* have used an interesting technique which involves simultaneous mechanical dispersion of NaCl particles and electrospinning of fibers followed by salt leaching [96]. However, this method creates very large pores though very dense fiber sheaths are observed in between the created macropores which help only in surface migration and not into the interior of the fibers. Ekaputra *et al.* studied the method of co-electrospinning, where they used medical-grade poly (ϵ -caprolactone)/collagen as the main fiber with water-soluble polymers PEO and gelatin to increase the void volume in the structure with selective removal of solid material from the mesh [97]. The method of blending with water soluble polymers offers very limited improvements compared to conventionally electrospun fibers in terms of cell infiltration. Therefore, it would be beneficial to fabricate a kind of electrospun membrane with a homogenous structure and improve the non-uniform cellular distribution.

2.4 Bio-functionalized electrospun nanofibers for tissue engineering

2.4.1 Target drug loading and controlled-release from nanofibers

Drug loading on the surface can be completed by utilizing surface-modified nanofibrous membranes which have an extremely high surface area to volume ratio, leading to higher drug loading dosage per unit mass than any other devices. The immediate release of drugs from the nanofiber surface can enable facile dosage control of certain therapeutic agents. It was especially suitable for some specific applications, e.g., prevention of bacterial infection occurring within a few hours of surgery [98].

A schematic diagram is given in Figure 2.11 to illustrate three modes of drug-loading on the electrospinning nanofibers.

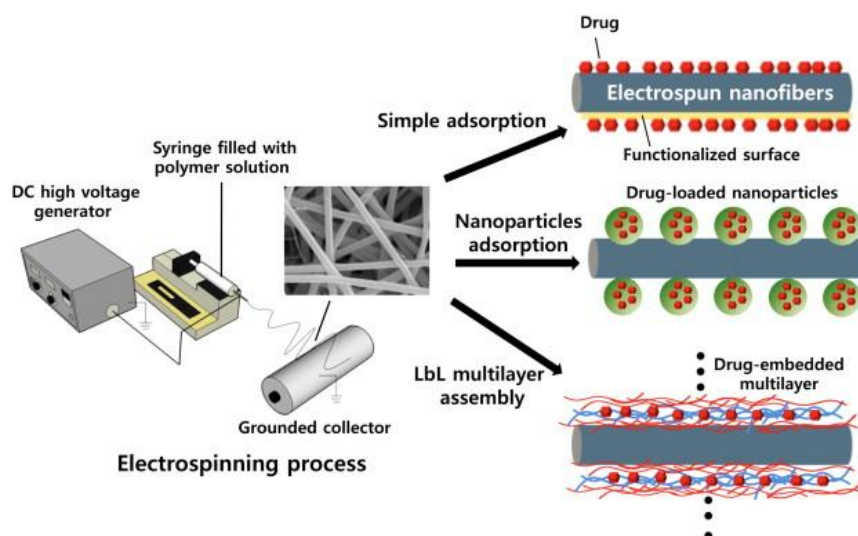


Figure 2.11 Three modes of drug-loading on electrospun nanofibers [98]

Simple Adsorption: Physical surface adsorption is the most achievable approach for loading drugs on nanofibrous membranes. Electrostatic interaction, hydrogen bonding, hydrophobic interaction and Van Der Waals interaction can be utilized as the driving force for surface adsorption [99]. A typical example is the use of the specific

interaction between heparin and growth factors. Heparin has strong binding affinity with various growth factors such as fibroblast growth factor (FGF), vascular endothelial growth factor (VEGF), heparin-binding epidermal growth factor (HBEGF) and transforming growth factor- β (TGF- β). This approach can last for a long period of biological activity by preventing early degradation of growth factors. Heparin immobilization of biomaterial surface and subsequent attachment of growth factor can be the most efficient approach to local delivery of growth factors and consequent variations [100].

Drug-loaded nanoparticle adsorption: The assemble nanoparticle on the surface of nanofibers has been developed for various applications such as electronic, catalysis and sensor devices [101, 102]. The large interfacial area of the nanofibers leads to high-performance devices. Such hierarchical nano-structure can also be constructed using therapeutically or biologically functional nanoparticles such as silver or hydroxyapatite nanoparticles.

Layer-by-layer multilayer adsorption: This method allowed surface coating with a thickness from different scales, e.g., nanometers or micrometers to achieve controlled-release by layer-by-layer (LbL) polyelectrolyte multilayer assembly. Driven by an electrostatic force on charged substrates, layer-by-layer multilayer adsorption comprises layer-by-layer deposition of poly-anions and poly-cations principally, as a result of self-assembled multilayer coating or free standing membranes. This technique attracted extensive attentions for the ease of its synthesis, universality for any complex structure of substrate and the feasibility of using any composition for the coating layer. While charged therapeutic component scan be

easily incorporated into the multilayer assembly, the incorporation of insoluble and uncharged drugs appears to be difficult. Recent approaches have included the encapsulation of drugs into charged particles [103, 104].

Table 2.6 Comparison of Three modes of drug-loading on electrospun nanofibers

| | Ease of Processing | Advantages | Disadvantages |
|--------------------------------------|--------------------|--|--|
| Simple Adsorption | Easy | <ol style="list-style-type: none"> 1. The most achievable methods to control drug slow-release. 2. High yield of drug loading. 3. wide range of selection on drug and biopolymers | <ol style="list-style-type: none"> 1. Limited on application in specific biological environment (e.g. capillary blood vessel) |
| Drug-loaded nanoparticles adsorption | Difficulty | <ol style="list-style-type: none"> 1. Nanoparticles can be applied in capillary blood vessel. 2. More precisely targeted drug release | <ol style="list-style-type: none"> 1. Difficulty to fabricate specific nanoparticles 2. Low yield of drug loading. 3. narrow range of selection on drug and biopolymers |
| Layer-by-layer multilayer adsorption | Difficulty | <ol style="list-style-type: none"> 1. Precisely targeted drug release. | <ol style="list-style-type: none"> 1. Difficulty to fabricate LPL multilayer. 2. Low yield of drug loading. 3. narrow range of selection on drug and biopolymers |

2.4.2 pH-sensitive drug delivery system

The pH-sensitive system was first introduced for the clinical treatment of tumors. In the 1930s, Warburg noted ‘the remarkable extent to which living tumor cells are able to convert carbohydrate into lactic acid [105, 106]. Within the past decades of research, there is consensus that pH 6.4 is regarded as the ideal condition for the growth and invasiveness of solid tumors. In cancer therapy, the tumor microenvironment has become one of many areas which are studied in order to design new therapies. Especially, knowledge and understanding of the tumor microenvironment allow researchers to elaborate different therapeutic strategies, based on numerous differences compared with normal tissue, including vascular abnormalities, oxygenation, perfusion, pH and metabolic states. The differences in terms of the morphology of tumor vasculature and pH are two basic properties which will be particularly described since they are the more relevant characteristics in regard to the design of tumor-targeted drug delivery systems [38].

The measured acidic pH of the extracellular fluid of tumor cells has been extensively reported [106]. The lower extracellular pH is an intrinsic feature of tumor cells. Two causes are: acid export from the tumor cells and clearance of extracellular acid. In fact, lower pH benefits tumor cells because it promotes invasiveness and gives them a competitive advantage over normal cells for growth. Figure 2.12 illustrates the structure of cell membrane. Tumor cells have neutral or slightly alkaline intracellular pH values whereas its extracellular fluid is relatively acidic [107]. The extracellular pH (pH_e) of normal tissues and blood pH are kept constant at pH 7.4 and their intracellular pH (pH_i) at pH 7.2 [108]. However, in tumor cells, this gradient is

Reversed as: $pH_i > pH_e$.

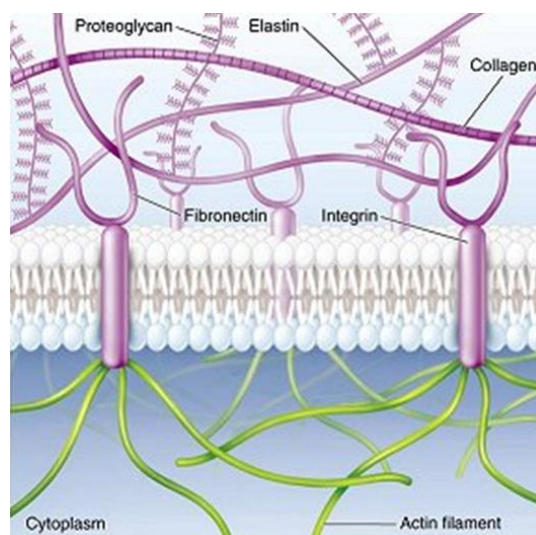


Figure 2.12 Diagram of the structure of cells membrane [108].

Materials with pH sensitivity can work efficiently in the therapy of tumors because of the significant acidic extracellular fluid of tumor cells. These materials have a wide range of potential applications in photography, drug delivery, cosmetics, sensors, cell encapsulation, food processing and the textile industry. As a result, numerous efforts have been made to develop various biodegradable pH-sensitive materials. Based on the previous research, three major groups of pH-sensitive drug delivery systems are identified.

pH-sensitive polymer micelles: A polymeric micelle is defined as a super-molecular assembly of block copolymers, having a characteristic core-shell structure; the drug-loaded core is surrounded by biocompatible poly (ethylene glycol) (PEG) outer shells (or other polymers) [109, 110]. And polymeric micelles can be utilized in drug delivery systems and are currently recognized as promising formulations for enhancing the efficacy of anticancer drugs [111, 112]. The polymeric micelles function by responding to intracellular signals from cells. Among all these

intracellular signals, low pH in endosomes and lysosomes are used as a chemical stimulus for designing pH-sensitive drug carriers since the macromolecular carriers are taken up by the cells and finally localized in the endosomes and/or lysosomes [113]. Kataoka *et al.* at the University of Tokyo (Tokyo, Japan) have recently fabricated a micelle-forming PEG-block-P(Asp-Hyd-DXR) copolymer, which is prepared by chemically conjugating doxorubicin (DXR) to the side chain of PEG-b-poly (aspartic acid) copolymers via an acid-labile hydrazone bond [114, 115].

pH-sensitive hydrogels: Hydrogel is considered a polymeric material which is able to absorb more than 20% of its weight of water and still retain a distinct 3D structure. The water-insoluble property of hydrogels is attributed to the presence of chemical or physical cross-links, which provide a network structure and physical integrity to the system. The pH-responsive hydrogel systems are of great importance due to their unique pH dependent swelling-deswelling behavior [116]. Hydrogels made of cross-linked polyelectrolytes display big differences in swelling properties depending on the pH of the environment. The pendant acidic or basic groups on polyelectrolytes undergo ionization just like acidic or basic groups of monoacids or monobases. Ionization on polyelectrolytes, however, is more difficult due to the electrostatic effects exerted by other adjacent ionized groups [117]. The swelling and pH-responsiveness of polyelectrolyte hydrogels can be adjusted by using neutral co-monomers [117, 118].

pH-sensitive polymer fibers: The pH-sensitive polymers show a big change in properties in response to small variations in physical or chemical stimuli. The property transition happens through changes in phase, shape, conformation

characteristics, swelling behavior, solubility and optical properties, as well as permeability via various molecular mechanisms [119]. In general, conventional pH-sensitive polymers are mostly based on those containing ionized groups of a weak acid (carboxylic acid) or a weak base (e.g. amino group). The pKa of carboxylic acid or pKb of the amino group in polymers changes depending on the surrounding molecular environment in order to lead to the phase or swelling transition in the similar pH range [120]. Such behavior has been used to induce the controlled release of model drugs like indomethacin or cationic proteins like lysozyme. The poly-amidoamine designed by Duncan *et al.* has a different structure since it combines positive and negative charges within the polymer backbone [121].

Table 2.7 Comparison of pH-sensitive drug delivery system

| | | Ease of Processing | Advantages | Disadvantages |
|------------------------|----------|--------------------|---|---|
| pH-sensitive micelles | polymer | Difficulty | <ol style="list-style-type: none"> 1. Precise targeted drug release. 2. Apply in specific biological environment(e.g. vessels) | <ol style="list-style-type: none"> 1. Challenge to control its pH sensitivity 2. Low yield of drug loading. |
| pH-sensitive hydrogels | | Easy | <ol style="list-style-type: none"> 1. Easy to fabricate 2. Controllable pH-sensitivity | <ol style="list-style-type: none"> 1. Low mechanical strength 2. Low yield of drug loading 3. Can't be applied in specific biological environment(e.g. vessels) |
| pH-sensitive fibers | polymers | Easy | <ol style="list-style-type: none"> 1. Easy to fabricate 2. Controllable pH-sensitivity. 3. Strong mechanical strength. 4. High yield of drug loading. | <ol style="list-style-type: none"> 1. Can't be applied in specific biological environment(e.g. vessels) |

2.4.3 Synergistic effect between anti-tumor drugs and antimicrobial peptides

Antimicrobial peptides, also known as AMPs, were initially discovered in the late nineteenth century. They are considered to be promising alternatives to antibiotics because of their properties of rapid reaction to invading pathogens and the ability to overcome the problem of antimicrobial resistance. AMPs are widely found in a variety of animal and plant species. Besides the broad antimicrobial spectrum, the extensive existence of this kind of peptide indicates that microbes have not effectively developed a means to resist their action yet [122]. Although bacterial resistance to AMPs has already been observed, there are numerous bacterial species that remain sensitive to AMPs' actions. The modifications required for resistance to AMPs may be metabolically expensive for the maintenance and host colonization of microbes [123]. As early as the 1980s, AMPs had been introduced into the anti-tumor therapy reported by Kingsbury et al. with an AMP-5-fluorouracil peptide conjugate [124]. Obeid et al. reported that in order to improve the anticancer activity of the proapoptotic peptides, several targeted chimeric inhibitor peptides, were synthesized by coupling antimicrobial peptides together. The results indicated that the targeted peptides combination approach could serve as a new powerful autonomous anticancer therapy [125]. The general membrane-targeted method of cell lysis shows potential in synergistic effects when applied together with conventional chemotherapeutics [126]. For example, Chen et al. reported that cecropin which displays anticancer activity against ovarian, carcinoma, breast carcinoma and leukaemia cells could synergize the anticancer drugs S-fluorouracil [127] and cytarabine against acute lymphoblastic leukaemia cells [128]. AMPs with cytotoxic activity against tumor cells have potential application for conquering problems with multiple-drug resistant (MDR) proteins because AMPs are not selected for resistant cancer cells. MDR proteins arouse

problems for current treatments as a result of they give a cancerous cell the ability to resist treatment by simply ejecting anti-tumor drugs out of the cell where they can do no harm. AMPs, however, kill the cell simply by membrane disruption and avoid this resistance mechanism. Other beneficial merits of AMPs as antitumor agents include their wide range of activity, their ability to kill cancer cells effectively, their ability to destroy primary tumors as well as prevent metastasis, and the fact that they do not harm on vital organs [129].

Research Gap of nanofibrous system for drug controlled-release

Since drug delivery, especially in regard to controlled drug-release is attracting great attention and intensive interest. Some studies have explored different modes of applying nanofibers in drug delivery. However, as a developing area, the research on controlled release is still theoretical and limited. The mechanism for drug adsorption and drug slow-release remains an unresolved question and needs to be further explored. Additionally, the field of pH-sensitive drug delivery systems is very new. Few studies have investigated the mechanism concerning nanopolymeric scaffolds in pH-sensitive systems. Besides the unknown mechanism, the optimization of this area is still in its infancy.

2.5 Summary of the knowledge gaps

In summary, six research gaps have been identified by the literature review, including:

1. Keratin is a kind of protein composed of different amino acids. Different amino acids have different bio-functions as a result of the differences of their chemical

structures. However, little research has explored the impact on biofunctions by the different amino acids of keratin. Besides, the large bead-shaped keratin particles and aggregations are still an unresolved problem. These large particles can damage the uniformity and homogenous structure of nanofibrous membranes. It is important to develop a novel fabrication method.

2. The PLLA organic electrospinning solution requires insoluble keratin samples because PLLA cannot dissolve in aqueous environments. However, the relevant studies about keratin samples so far mainly suggest collecting keratin from a hydrolyzed keratin solution. It is necessary to explore how to prepare keratin in a water-free environment while retaining its original structure and properties as well.
3. In the fabrication process, current research has barely explored how to optimize the parameters of electrospinning technology to fabricate keratin/PLLA nanofibrous membrane with satisfactory porosity and uniformity and how to evaluate its biodegradability.
4. The potential applications of keratin/PLLA composite devices, such as controlled drug-release systems and drug delivery systems need to be explored but to date there have been limited studies on this area.
5. The optimized experimental design hasn't been introduced in the composite membrane fabrication procedures. The biofunctional and anti-tumor evaluation of the keratin composite membrane hasn't been explored before.
6. The anti-tumor effect of AMP scaffolds (e.g. Attacin2) hasn't been discovered

and studied before. It needs to confirm that the AMP possesses its original anti-tumor activity and antimicrobial activity after being processed by electrospinning techniques.

On the basis of the knowledge gaps identified, five objectives were derived, as reported in Section 1.2 in Chapter 1.

CHAPTER 3 ISOLATION AND CHARACTERIZATION OF BIOFUNCTIONAL KERATIN ISOELECTRIC PRECIPITATES

This chapter focuses on completing objective 1 by developing natural functional biomaterials. Based on the extensive literature review in Chapter 2, the feasibility of extracting the functional biomaterials from wool keratin was studied. During the extraction process, wool fibers were hydrolyzed and the hydrolysate was adjusted to predetermined pH values to collect keratin polypeptides. The morphology of keratin polypeptides was analyzed and determined by SEM investigation. Afterwards, the chemical and crystal structure and thermal properties were analyzed by FT-IR spectra, XRD and TGA, respectively. These results suggested that keratin polypeptides with different amino acid compositions can be tailored from wool hydrolyzed solution based on isoelectric-point precipitation and have potential application in the future as biomaterials for wound healing, drug delivery, and so on.

3.1. Materials and Methods

3.1.1 Materials

Wool was purchased from Australia. Hydrochloric acid 37% GR for analysis ACS (IL, USA, analytical purity) and sodium hydroxide powder (IL, USA, analytical purity) were employed to hydrolyze wool fibers.

3.1.2 Hydrolysis of raw wool fibers

Both acidic and alkaline hydrolysis methods were introduced in this chapter. The first method was acidic hydrolysis of wool fibers. Wool fibers were hydrolyzed and

adjusted to predetermined pH value by chloride acid (HCl). After that, keratin polypeptides precipitates were collected and characterized. The results indicated that it was viable to extract keratins with different compositions of polypeptides for future application. The keratin polypeptides could be developed as the tailored biofunctional raw materials for specific purposes in tissue engineering. Wool fibers were hydrolyzed in the acidic environment. 60g of wool was immersed into 4 mol/L hydrochloric acid (400ml) solution, and then incubated in 95 °C water bath to hydrolyze the wool fibers until the wool fibers were dissolved thoroughly. Then the prepared hydrolysis solution was filtered twice for further process. The pH value of wool hydrolyzed solution was adjusted based on the principle of isoelectric precipitation. Two kinds of keratin polypeptide precipitates were collected at pH 3.22 and pH 5.55, respectively.

The second method in this chapter was alkaline hydrolysis of wool fibers. The basic procedures were almost the same as the acidic hydrolysis. Raw wool was immersed into 2 wt. % sodium hydroxide solution which was kept thermostatic in water bath (95 °C). After the wool fibers were dissolved completely, the hydrolyzed solution was kept at room temperature for 48 h. Then the solution was adjusted to pH 5.55 by 0.1 M HCl. Keratin precipitate was observed at its isoelectric value (pI). Then the precipitate was collected by centrifuge. The precipitate was re-dispersed in distilled water and collected by centrifugation again. Subsequently the precipitate was dispersed in absolute ethanol and centrifuged again. This procedure was repeated 4 times.

3.1.3 Isoelectric-point precipitation process of keratin polypeptides

Isoelectric point (pI) is defined as the pH value at which a particular molecule or surface carries zero net electrical charge. Isoelectric precipitation is a process in which proteins or amino acids are precipitated at pH value close to their isoelectric points [130, 131]. In this study, the pH value of the prepared wool hydrolysis solution was adjusted to pH 3.22 with 1 M NaOH, a thick layer of precipitate was observed at the bottom of the solution after 24 h. After the precipitate was collected and denoted as keratin polypeptides (KP3), the rest wool hydrolysis solution was adjusted to pH 5.55. The present precipitate was also collected and denoted as keratin polypeptides (KP5). In order to wash away salt and any other impurities, KP3 and KP5 were dispersed in DI water and centrifuged 3 times, respectively. Finally, KP3 and KP5 suspensions were spray-dried to obtain keratin polypeptide powders, respectively.

3.1.4 The crystal structure analysis by XRD measurement

The differences on the crystal structures of wool fibers, KP5 and KP3 were compared by X-ray diffractometer (XRD, D8 Advance, Bruker AXS, Germany). The patterns were obtained by a diffractometer with a Cu K α radiation source. The 2α Bragg angles were scanned over a range of 10-80° using a 0.05° step size and 10°/min scan speed.

3.1.5 Surface morphology observation

The surface morphology of KP5 and KP3 was observed by scanning electron microscope (SEM, JEOL, JSM-6490, Japan). In the preparation step, the samples were adhered directly onto an aluminum stub with a thin self-adherent carbon film and then coated with a thin layer of gold.

3.1.6 The thermal stability evaluation by TG-DSC measurement

The phase change temperature and decomposition temperature were measured by thermogravimetry and differential scanning calorimetry (TG-DSC, Netzsch STA 449C, Burlington, Germany) at a heating rate of 10 °C/min over a temperature range of 30 °C to 400 °C.

3.1.7 Chemical bonding evaluation by FT-IR measurement

The chemical structures of KP5 and KP3 were examined by Fourier transform infrared spectroscopy (FTIR, Perkin Elmer 1720, Perkin Elmer, USA) in the transmission mode with the wave number ranging from 4,000 to 400 cm⁻¹. KBr pellets were prepared by gently mixing the sample powders with KBr.

3.2 Results and discussion

3.2.1 The characterizations of acidic hydrolysis peptides

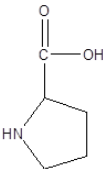
In the process of acidic hydrolysis of wool fibers, disulfide bond (S-S) and partial peptide bonds of keratin in wool were split apart. The acidic hydrolysis reaction of wool fiber could be described as following:



Ninhydrin reaction and biuret reaction were used to measure the amino acid content and the protein content, respectively. Based on these two reactions, the known hydrolysis degree of wool keratin was about 33% under the following operating conditions: 4.0 mol/L HCl, 95 °C and 24 h. When the time was prolonged to 48 h and 72 h, there was no significant increase on the hydrolysis degree of wool keratin, which was kept at 33%. It was indicated that the prolonged hydrolysis time couldn't

increase the degree of hydrolysis at the fixed temperature and certain acidic concentration. Table 3.1 summarized the major amino acids existing in keratin and their chemistry formula as well as their isoelectric points [132, 133].

Table 3.1 Major amino acids composition of keratin

| Amino acid | Formula | Isoelectric point |
|------------|---|-------------------|
| Cys | $\begin{array}{c} \text{O} \\ \parallel \\ \text{H}_2\text{N}-\text{CH}-\text{C}-\text{OH} \\ \\ \text{CH}_2 \\ \\ \text{SH} \end{array}$ | 5.07 |
| Glu | $\begin{array}{c} \text{O} \\ \parallel \\ \text{H}_2\text{N}-\text{CH}-\text{C}-\text{OH} \\ \\ \text{CH}_2 \\ \\ \text{CH}_2 \\ \\ \text{C}=\text{O} \\ \\ \text{OH} \end{array}$ | 3.22 |
| Gly | $\begin{array}{c} \text{O} \\ \parallel \\ \text{H}_2\text{N}-\text{CH}-\text{C}-\text{OH} \\ \\ \text{H} \end{array}$ | 5.97 |
| Leu | $\begin{array}{c} \text{O} \\ \parallel \\ \text{H}_2\text{N}-\text{CH}-\text{C}-\text{OH} \\ \\ \text{CH}_2 \\ \\ \text{CH}_2 \\ \\ \text{C}=\text{O} \\ \\ \text{OH} \end{array}$ | 5.98 |
| Proline |  | 6.48 |
| Tyrosine | $\begin{array}{c} \text{O} \\ \parallel \\ \text{H}_2\text{N}-\text{CH}-\text{C}-\text{OH} \\ \\ \text{CH}_2 \\ \\ \text{C}_6\text{H}_4 \\ \\ \text{OH} \end{array}$ | 5.67 |

From Table 3.1, the isoelectric points of the amino acids in keratin was mainly in two ranges: more acidic range (e.g. pH 3.22) and less acidic range (e.g. pH 5-6). The purpose of the present study was to verify the feasibility of tailoring bio-functional polypeptides from pristine wool keratin through isoelectric precipitation process. The different pH ranges of precipitation environments led to different isoelectric precipitates. It has been proved that two kinds of polypeptides with different compositions were collected successfully. Additionally, both chemical and physical properties of polypeptides will be examined through a series characterizations and biological evaluations.

XRD analysis

XRD is an important technique to determine the crystal phase of the samples. Figure 3.1 showed the XRD patterns of wool, KP3 and KP5. The result of XRD indicated that the two kinds of keratin polypeptides mainly existed in an amorphous form instead of crystal form. Compared with wool fiber before hydrolysis, a broad peak at 20.2° disappeared after hydrolysis. The arrows pointed at the crystalline peaks were shown in Figure 3.1. Under high temperature and acidic environment, most of the hydrogen bonds existing in wool fibers were broken down, therefore some crystals were destroyed thoroughly as a result of the amorphous structure of wool keratin polypeptides [134, 135]. Since the total crystallinity of wool equals the sum of α and β -crystallinity, the hydrolysis process of wool decreased the presence of both α -helix and β -sheet structures. Compared to the alkaline hydrolysis procedures [136], the acidic hydrolysis were intend to produce more amorphous keratin polypeptides. This might due to a higher and more thoroughly degree of hydrolysis by acid.

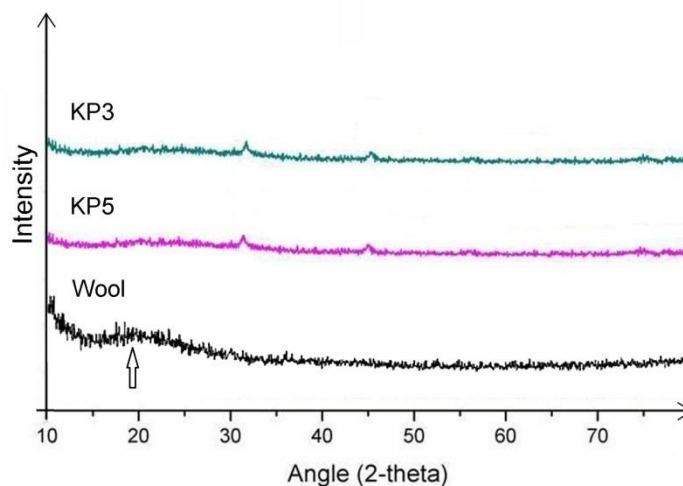


Figure 3.1 XRD patterns of wool fibers, KP3 particles and KP5 particles by acidic hydrolysis.

Surface morphology

SEM images could identify the morphology of the surface layer directly. Figure 3.2 displayed the SEM images of KP3 and KP5 powders respectively. The smooth micro-spheres could be observed for both KP3 and KP5 particles. The spherical shape might be a result of the process of spray drying. There were insignificant differences concerning surface morphology and shapes between KP3 and KP5 particles. Both of KP3 and KP5 possessed the smooth, round and uniform surfaces. However, the diameter ranges of the micro-sphere were obviously different. For the diameter of KP3 particles, the range was from 8 μm to 12 μm and some micro-spheres were in hollow structure. The KP5 particles possessed a smaller diameter lying in the range of 1-5 μm . The difference of diameter range could be a result of the different concentrations of KP5 and KP3 suspensions. The hollow structure of KP3 particle might due to the evaporation of water. In the process of spray-drying, after the KP3 suspension pumped into the chamber, the high-speed air flow dispersed the liquid into

small droplets. The droplets were dried rapidly and water on the surface of droplets kept releasing into the environment. The droplets shrank to smaller droplets consequently. If the concentration of the droplets reached a certain level, the inside water could hardly penetrate the shell of droplets. Finally, the evaporated molecules had to break through the shell and left the hollow spheres as shown in Figure 3.2.

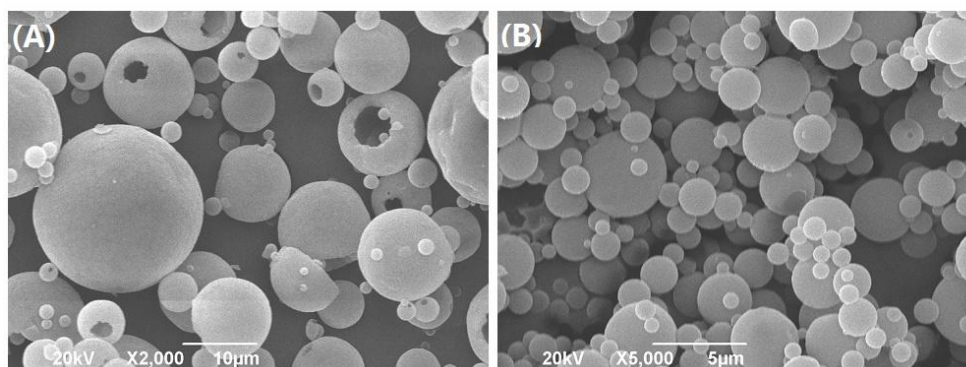


Figure 3.2 SEM images of different keratin polypeptides particles by acidic hydrolysis: (A) KP3 powders; (B) KP5 powders.

TG-DSC measurement

TG-DSC analysis was an important technique to measure the content of the components with different phase change temperature and fusion temperature. In this study, the TG-DSC curves revealed the thermal properties of the two kinds of keratin polypeptides as well as the wool fibers. Figure 3.3(A), (B) and (C) displayed the TG-DSC curves of wool, KP3 and KP5 powders, respectively.

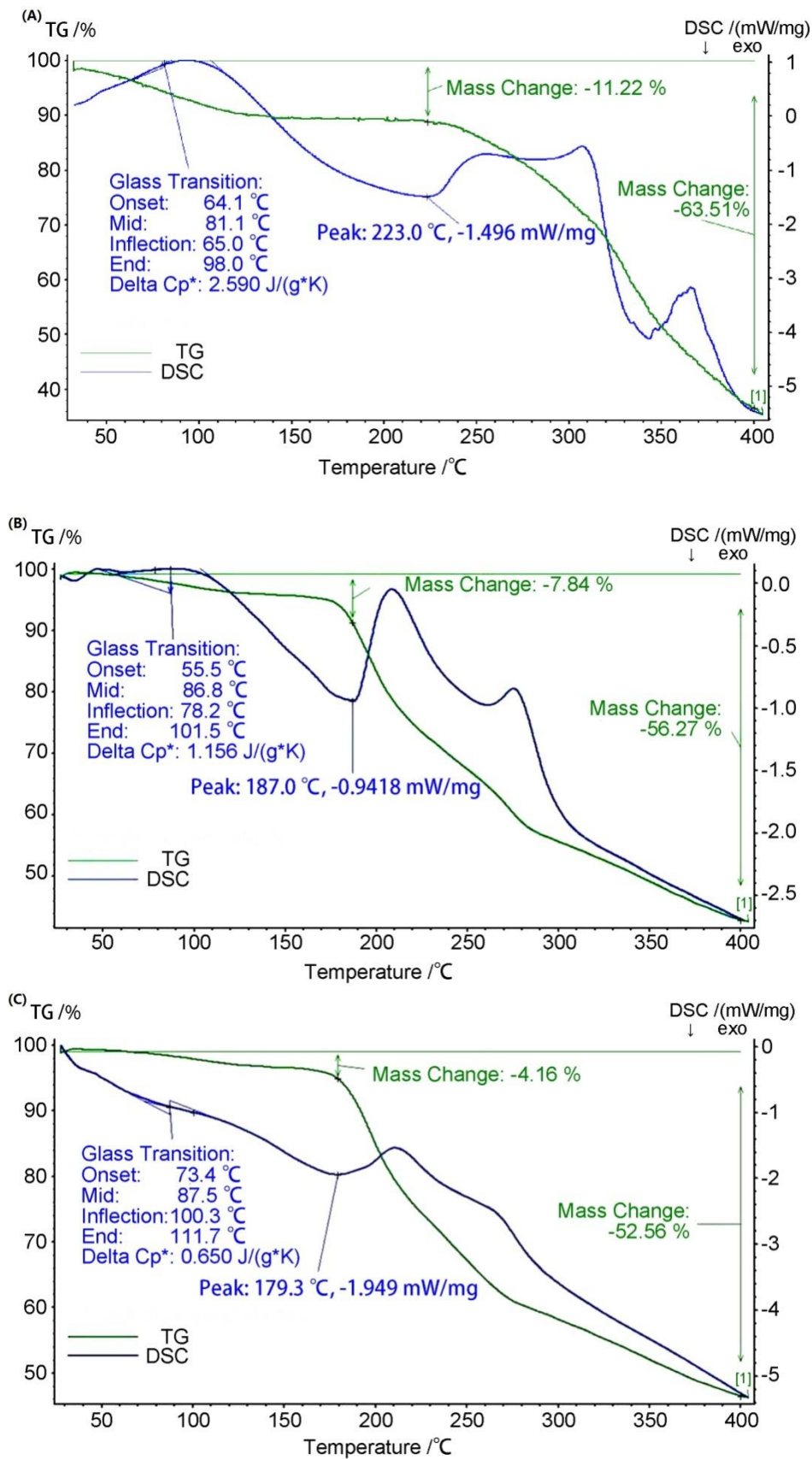


Figure 3.3 TG-DSC curves of keratin polypeptides by acidic hydrolysis: (A) wool; (B) KP3 particles; (C) KP5 particles.

Table 3.2 summarized the glass transition temperature, decomposition temperature and mass change (400 °C) consequently. The glass transition temperature of KP3 and KP5 were 100.3 °C, 78.2 °C respectively. Comparing with 100.3 °C, 78.2 °C, the wool sample had a lower glass transition temperature at 65.0 °C. The lower glass transition temperature was a result of the higher water-content in the original wool [137]. However, a reverse trend occurred concerning the decomposition temperature. The decomposition temperature of the acidic and neutral polypeptide was 179.3 °C and 187.0 °C, respectively, which were lower than that of wool at 223.0 °C.

Table 3.2 The summary of glass transition temperature, decomposition temperature and mass change of wool, KP3 and KP5

| Sample | Glass transition temperature (°C) | Decomposition temperature (°C) | Mass change (400 °C) |
|---------------|-----------------------------------|--------------------------------|----------------------|
| Pristine wool | 65.0 | 223.0 | 63.51% |
| KP3 | 100.3 | 179.3 | 52.56% |
| KP5 | 78.2 | 187.0 | 56.27% |

In Figure 3.3 (A) and (C), a decrease-trend sloping portion was observed at 110.0 °C. This was a result of the evaporation of the bound water in the keratin structure. This was also referred to as the “denaturation” temperature [138]. With temperature increasing, an endotherm peak at 223.0 °C was observed on the DSC curve in Figure 3.3 (A), which was corresponding to the melting of the α -form crystallites. The slope in Figure 3.3 (B) was slow due to a low hydroscopicity of PK3 particles. In Figure 3.3 (A), a sharp exothermic peak was observed at 347.0 °C indicted decomposition of keratin fractions with intermediate and high thermal stability [138]. For KP3 particles,

this temperature shifted to a lower temperature of 270.0 °C. According to the equation: $T_M = \Delta H / (\Delta S + R \ln C_T)$ [139], in which R as the gas constant equals to 1.987 cal $K^{-1} mol^{-1}$, it could be explicated that when increasing the melting entropy, the melting point decreased correspondingly. Comparing with wool sample, KP3 and KP5 possessed lower mass change. The better thermal-stability of wool was a result of the cross-linking between the macromolecules by hydrogen bonds. After acidic hydrolysis, the decrease of hydrogen-bonds weakens the cross-linking. The same results were also found in the XRD patterns. In fact, there were two main thermal events existing in the DSC curves. One was the melting of α -helix and β -sheet structures and the crystallites were changed correspondingly in Figure 3.3(A); the other one was the thermal degradation of components in Figure 3.3(A), (B) and (C). The variations of the temperature concerning the thermal degradation indicated that the different crystal structures transformed after acidic hydrolysis and isoelectric precipitations of wool.

FT-IR analysis

FT-IR spectrum can explicate the chemical structure changes by detecting the vibration of chemical bonds in molecules. Figure 3.4 showed the FTIR spectra of pristine wool, KP3 and KP5. Their corresponding characteristic peaks were marked correspondingly. The disulphide bond (S-S) of the wool keratin was broken down in the process of acidic hydrolysis, and its characteristic peak disappeared in both the KP3 and KP5. According to the curve of wool, the peak at 617 cm^{-1} and 473 cm^{-1} should be assigned to C-S bond stretching and S-S bond stretching as well as the C-C bond deformation [140]. After the acidic hydrolysis, due to the cleavage of S-S bond in cysteine, there was no peak at this region from the two polypeptides curves. Apart from the deformation of cysteine, the hydrolysis also generated many small peaks

around the region from 1121-1022 cm^{-1} which were related the sulphate oxides.

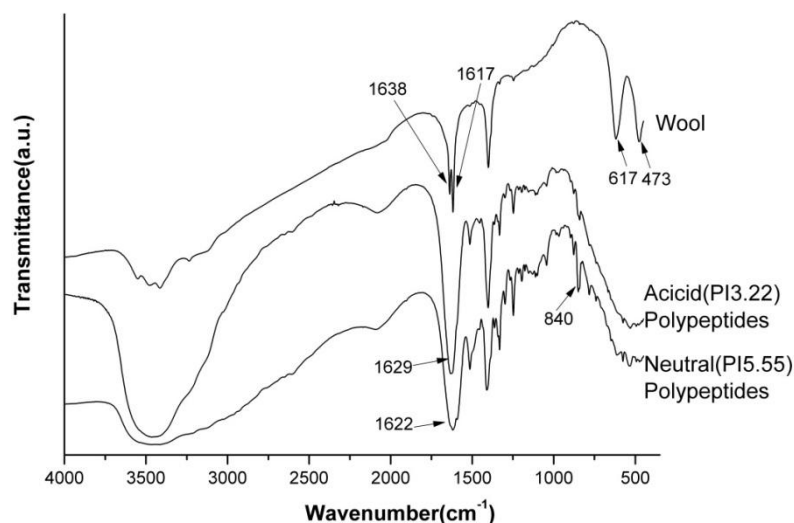


Figure 3.4 FT-IR spectra of wool, KP3 particles and KP5 particles by acidic hydrolysis.

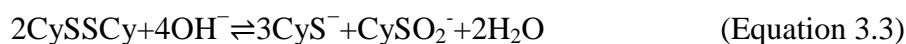
In Figure 3.4, there were mainly three major band regions, which were assigned as amide I, II, III. The amide I band was related to C=O stretching, which occurred within the range of 1600-1700 cm^{-1} . The amide II within the region of 1400-1500 cm^{-1} came from N-H bending and C-H stretching. The amide III band laid in the range of 1220–1300 cm^{-1} and it was the result from the combination of C-N stretching and N-H in plane bending as well as some distribution from C-C stretching and C=O bending [141]. From the wool curve, there were two split peaks at 1617 cm^{-1} and 1638 cm^{-1} . These two peaks were yielded because of the α -helix structure and β -sheet structure. After the acidic hydrolysis, due to a change on the structures of keratin, two split peaks combined as amide I band. The differences between the KP3 and KP5 could be observed although not strikingly significant. As shown in Table 3.1, polypeptides with different amino acids composition could be generated as a result of collection on different isoelectric points. For example, from the spectra of KP5, the

presence of benzene could be demonstrated by three bands at 1600, 1500 and 1400 cm^{-1} [142]. The additional peak at 840 cm^{-1} appeared at fingerprint region because of the substituent positioning effects of benzene which probably establishes presence of tyrosine. For both KP3 and KP5, a group of small peaks around the region from 1121-1022 cm^{-1} with different intensities, were related to the content of different sulphate oxides [141]. Since different amino acids have their specific bio-functions, there would be remarkable application potential of tailoring specific polypeptides with different amino acid compositions [143]. Furthermore, the tailored polypeptides can be applied with both the synthetic and natural polymers to be considered as proper candidates in tissue engineering.

3.2.2 The characterizations of alkaline hydrolysis peptides

Wool and isoelectric precipitation of keratin polypeptide

In the process of alkaline hydrolysis of wool fibers, disulfide bond (S-S) and partial peptide bonds of keratin in wool were split apart. Treatment of wool at temperatures above 70 °C and within a pH range of pH 9–11, with exposure time within 4-12 h, in the presence of excess alkali, can lead to the conversion of disulfide groups to cystyl residues (CyS-) [144, 145]. The alkaline hydrolysis reaction of wool fiber could be described as following [144]:



Keratins extracted from wool can be fractionated into two groups. One fraction with less sulfur than the parent wool and is believed to originate in the microfibrils. The other group contains more sulfur than wool and can be applied in the matrix. Low-

and high-sulfur fractions are the major components of the fiber and represent 50–60% and 20–30% by weight of wool, respectively. Alkali-assistance gives negative charges on the ionizable acid groups of wool to form electrostatic repulsion between them. Often a hydrogen-bond breaking agent, such as urea, is included in the formulation to unfold or denature the protein.

XRD analysis

XRD is an important technique to determine the crystal phase of the samples. Figure 3.5 showed the XRD patterns of KP3 and KP5 by alkaline hydrolysis. The result of XRD indicated that the two kinds of keratin polypeptides existed in a certain crystal form. A broad peak at 20.2° can be observed after alkaline hydrolysis. Under high temperature and acidic environment, most of the hydrogen bonds existing in wool fibers were broken down, therefore some crystals transformed between pristine wool to keratin polypeptides. Since the total crystallinity of wool equals the sum of α and β -crystallinity, the hydrolysis process of wool decreased the presence of both α -helix and β -sheet structures. Compared to the acidic hydrolysis procedures [136], the alkaline hydrolysis were intended to keep the crystal structure of keratin polypeptides. This might be due to a different hydrolysis mechanism and different degree of hydrolysis in alkaline environments.

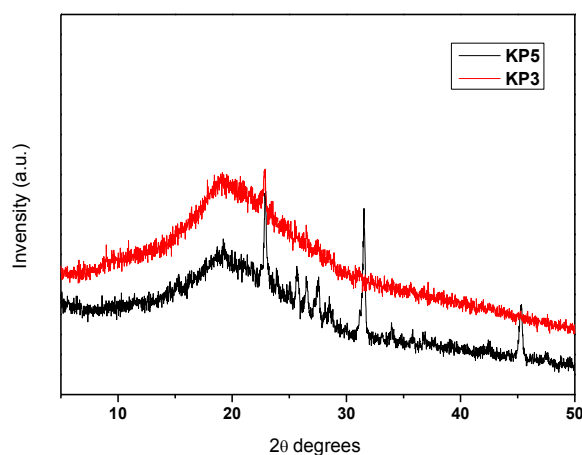


Figure 3.5 XRD patterns of KP3 particles and KP5 particles by alkaline hydrolysis.

Surface morphology

SEM images could identify the morphology of the surface layer directly. Figure 3.6 displayed the SEM images of KP3 and KP5 powders respectively. The smooth micro-spheres could be observed for both KP3 and KP5 particles by alkaline hydrolysis. The spherical shape might be a result of the process of spray drying. There were insignificant differences concerning surface morphology and shapes between KP3 and KP5 particles. Both of KP3 and KP5 possessed the smooth, round and uniform surfaces. However, the diameter ranges of the micro-sphere were obviously different. For the diameter of KP5 particles, the range was from 4 μm to 5 μm which is smaller than the acidic hydrolysis particle sizes. The KP3 particles however, possessed a bigger diameter than 5 μm . The difference of diameter range could be a result of the different concentrations of KP5 and KP3 suspensions. Compared with acid hydrolysis particle, the alkaline particles possessed a smaller diameter range. The rough surfaces are a result of different concentration of keratin polypeptides hydrolyzed solutions.

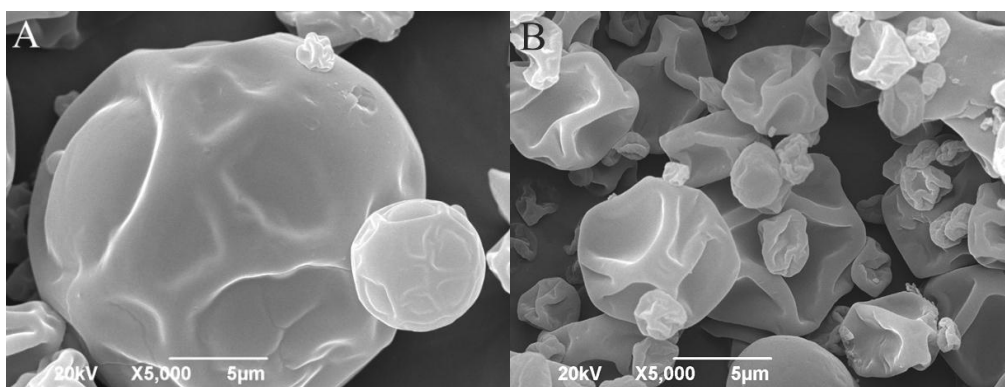


Figure 3.6 SEM images of keratin polypeptides nanoparticles by alkaline hydrolysis:
(A) KP3 powders; (B) KP5 powders.

SDS-Page analysis

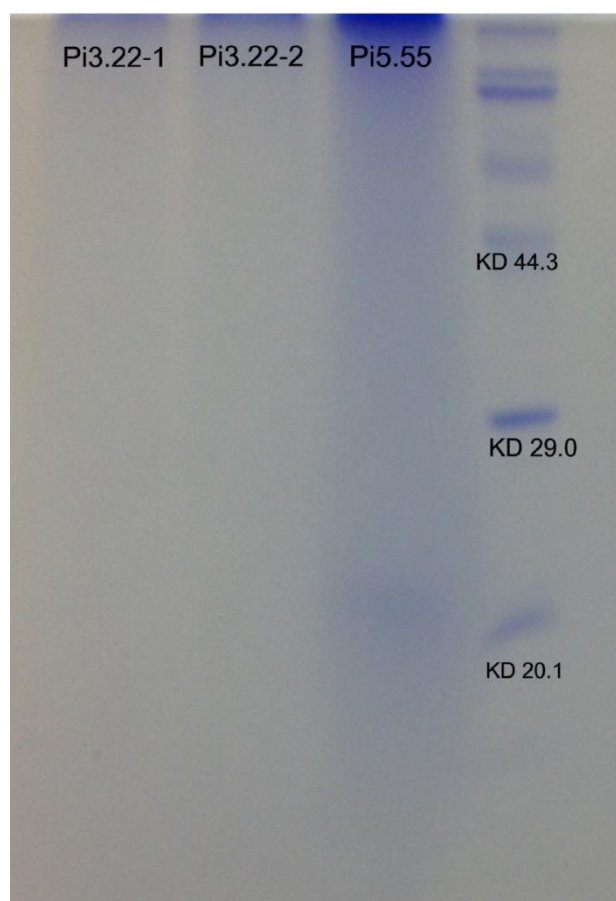


Figure 3.7 SDS-page images of keratin polypeptides by alkaline hydrolysis of KP3articles and KP5particles.

The SDS-page experiments have been done according to the protocol as below:

High-Range Rainbow Molecular Weight Markers (GE Healthcare, MW 1200–225,000 D) were applied as control. SDS-PAGE analysis was performed according to following steps: Electrophoresis was conducted in a GeneMate electrophoresis system (IscBioexpress, Kaysville, UT) equipped with a 12% Gel, $0.1 \times 10 \times 8 \text{ cm}^3$ (NuSep, Lawrenceville, GA) and running buffer of 10× diluted to 1× Samples, 0.5 mg/mL sample concentrations, were prepared in pH 9 loading buffer containing 10 mM TRIS–HCl: 1 mM EDTA medium with sodium dodecyl sulfate (SDS electrophoresis purity reagent, Bio-Rad Laboratories, Hercules, CA), 2-mercaptoethanol (Bio-Rad Electrophoresis Grade #161-0710), and 1% w/v Coomassie Brilliant Blue (Amresco, Solon, OH). The gels were processed at 90v in running buffer. Coomassie R 350 stain (Pharmacia Biotech) was used to stain the gels. A dilute solution of methanol and glacial acetic acid in deionized water was used for destaining. In Figure 3.7, it can be observed that most of KP3 and KP5 possessed a molecular weight below 24K. Moreover, no clear bands could be detected. It meant that both KP3 and KP5 have wide molecular weight distribution. In the harshly alkaline hydrolysis environment, not only the S-S bonds between protein chains were broken, but the amide bonds of protein were also snipped un-specifically. As a result, KP3 and KP5 with different molecular weights were collected from the hydrolysis of the peptide bonds. Unlike the reduction hydrolysis, the severe hydrolysis produced fragmented keratin peptides with low molecular weight.

TG-DSC measurement

TG-DSC analysis was an important technique to measure the content of the components with different phase change temperature and fusion temperature. In this study, the TG-DSC curves revealed the thermal properties of the two kinds of keratin

polypeptides as well as the wool fibers. Figure 3.8 (A) and (B) the TG-DSC curves of KP3 and KP5 powders by alkaline hydrolysis respectively.

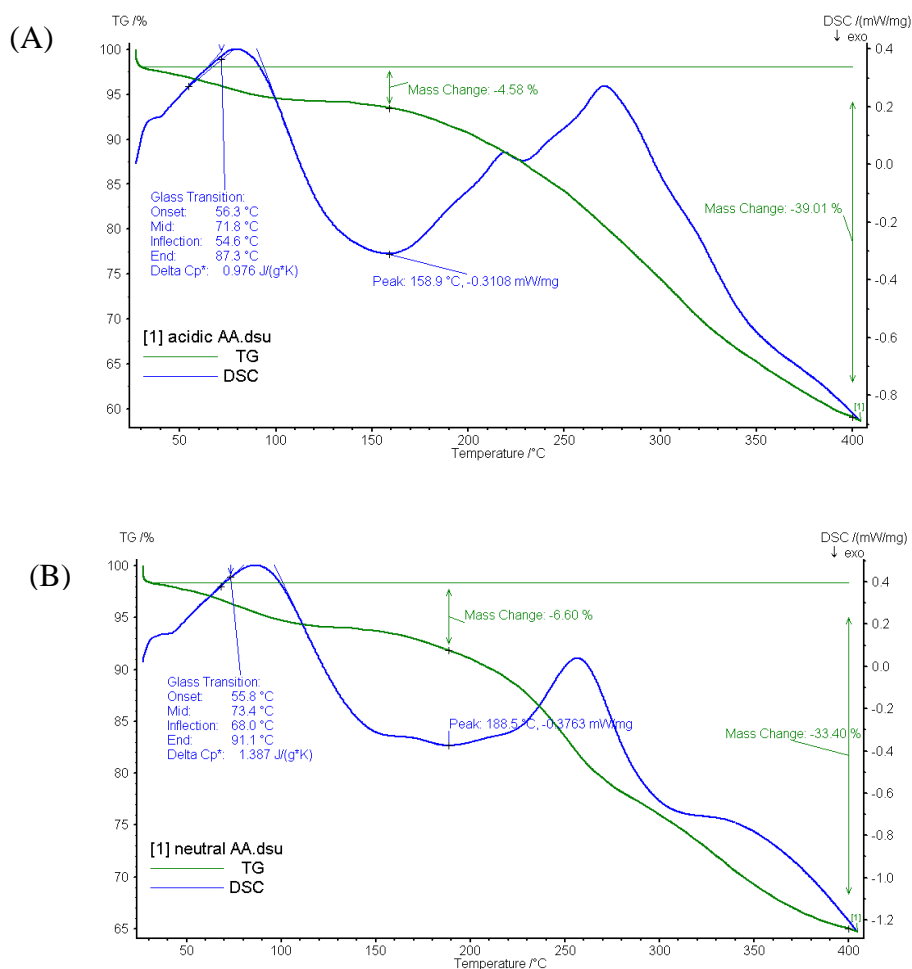


Figure 3.8 TG-DSC curves of keratin polypeptides by alkaline hydrolysis: (A) KP3 particles; (B) KP5 particles.

The glass transition temperature of KP3 and KP5 were 100.3 °C, 78.2 °C respectively. Comparing with 100.3 °C, 78.2 °C, wool sample had a lower glass transition temperature at 65.0 °C. The lower glass transition temperature was a result of the higher water-content in the original wool [137]. However, a reverse trend occurred concerning the decomposition temperature. The decomposition temperature of the acidic and neutral polypeptide was 179.3 °C and 187.0 °C, respectively, which were

lower than that of wool at 223.0 °C.

Table 3.3 The summary of glass transition temperature, decomposition temperature and mass change of KP3 and KP5 by alkaline hydrolysis

| Sample | Glass transition temperature (°C) | Decomposition temperature (°C) | Mass change (400 °C) |
|--------|------------------------------------|---------------------------------|----------------------|
| KP3 | 71.8 | 158.9 | 39.01% |
| KP5 | 73.4 | 188.5 | 33.40% |

In Figure 3.8 (A) and (B), a decrease-trend sloping portion was observed at 110.0 °C. This was a result of the evaporation of the bound water in the keratin structure. This was also referred to as the “denaturation” temperature [138]. With temperature increasing, an endotherm peak at 223.0 °C was observed on the DSC curve in Figure 3.8 (A), which was corresponding to the melting of the α -form crystallites. The slope in Figure 3.8 (B) was slow due to a low hydroscopicity of PK3 particles. In Figure 3.8 (A), a sharp exothermic peak was observed at 347.0 °C indicted decomposition of keratin fractions with intermediate and high thermal stability [138]. For KP3 particles, this temperature shifted to a lower temperature of 270.0 °C. According to the equation: $T_M = \Delta H / (\Delta S + R \ln C_T)$ [139], in which R as the gas constant equals to 1.987 cal $K^{-1} mol^{-1}$, it could be explicated that when increasing the melting entropy, the melting point decreased correspondingly. Comparing with wool sample, KP3 and KP5 possessed lower mass change. The better thermal-stability of wool was a result of the cross-linking between the macromolecules by hydrogen bonds. After acidic hydrolysis, the decrease of hydrogen-bonds weakens the cross-linking. The same results were also found in the XRD patterns. In fact, there were two main thermal events existing in the DSC curves. One was the melting of α -helix and β -sheet structures and the crystallites were changed correspondingly in Figure 3.8 (A); the other one was the

thermal degradation of components in Figure 3.8 (A), (B). The variations of the temperature concerning the thermal degradation indicated that the different crystal structures transformed after acidic hydrolysis and isoelectric precipitations of wool.

FT-IR analysis

FT-IR spectrum can explicate the chemical structure changes by detecting the vibration of chemical bonds in molecules. Figure 3.9 showed the FT-IR spectra of pristine wool, KP3 and KP5. Their corresponding characteristic peaks were marked correspondingly. The disulphide bond (S-S) of the wool keratin was broken down in the process of acidic hydrolysis, and its characteristic peak disappeared in both the KP3 and KP5. According to the curve of wool, the peak at 617 cm^{-1} and 473 cm^{-1} should be assigned to C-S bond stretching and S-S bond stretching as well as the C-C bond deformation [140].

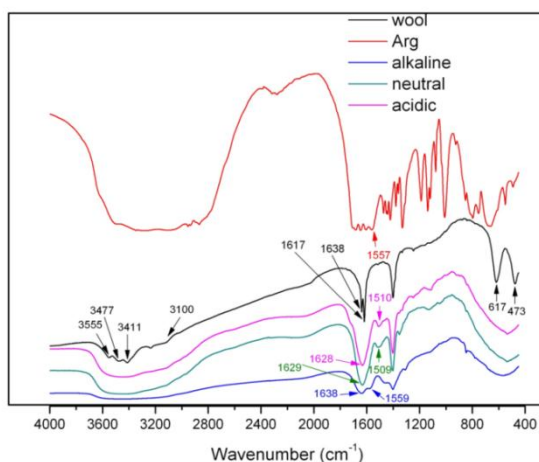


Figure 3.9 FT-IR spectra of pristine wool, KP3 articles and KP5 particles by alkaline hydrolysis.

After the alkaline hydrolysis, due to the cleavage of S-S bond in cysteine, there was no peak at this region from the two polypeptides curves. Apart from the deformation

of cysteine, the hydrolysis also generated many small peaks around the region from 1121-1022 cm^{-1} which were related to the sulphate oxides. The peaks appeared at 1510 cm^{-1} and 1628 cm^{-1} represented the Amide I and Amide II of keratin polypeptides.

In Figure 3.9 there were mainly three major band regions, which were assigned as amide I, II, III. The amide I band was related to C=O stretching, which occurred within the range of 1600-1700 cm^{-1} . The amide II within the region of 1400-1500 cm^{-1} came from N-H bending and C-H stretching. The amide III band laid in the range of 1220–1300 cm^{-1} and it was the result from the combination of C-N stretching and N-H in plane bending as well as some distribution from C-C stretching and C=O bending [141]. From the wool curve, there were two split peaks at 1617 cm^{-1} and 1638 cm^{-1} . These two peaks were yielded because of the α -helix structure and β -sheet structure. After the acidic hydrolysis, due to a change on the structures of keratin, two split peaks combined as amide I band.

3.2.3 The comparison between the acidic hydrolysis and alkaline hydrolysis

In this chapter, both the acidic hydrolysis and alkaline hydrolysis were introduced and investigated by extensive studies. The main difference between these two hydrolysis methods is the hydrolysis efficiency and hydrolysis strength. As discussed before, when keratin, such as wool or feathers, is treated with thioglycolic acid at a pH of 10 or higher the reaction appears to be identical with that on simpler disulfides. The reaction is a simple reduction; no loss of sulfur occurs. The sulfhydryl protein can be re-oxidized to the disulfide state, and this disulfide protein is still soluble in acid or alkali and digestible by trypsin or pepsin. The action of cyanide on wool is not quite so simple. A higher alkalinity is required (pH 12 to 13) and the proteins lose sulfur;

however, the substances obtained behave as true proteins, not as products of hydrolysis. From mild reduction hydrolysis of wool, high- and low-sulfur and high-glycine–tyrosine groups have been identified. Hypothetically, mild 2-mercaptoethanol reduction can cleave disulfide bonds to solubilize wool while leaving the microstructure of keratin intact. In the presence of excess reducing agent extensive reduction can occur to reduce 96% of the cysteine residues of wool at pH 5.0–7.5 according to two reversible nucleophilic displacement reactions by mercaptide ion (RS^-) on the symmetrical wool (W) keratin disulfide (WSSW). The XRD curves revealed that the alkaline treatment intended to produce polypeptides with crystal forms and the acidic hydrolysis intended to produce amorphous form polypeptides. The chemical structure from both acidic and alkaline hydrolysis indicated few differences chemical bonding interactions. The SDS-page analysis indicated that alkaline hydrolysis could produce polypeptides with smaller molecular weight. The future application of keratin extracted from wools is to be component part in functional nanofibers, the smaller molecular weight could benefit the potential application in nanofibers due to a lower Gibbs free energy. A lower Gibbs free energy could enhance the interactions between nanofibers and biological tissues.

3.3 Conclusion

In this chapter, the first objective has been achieved by developing techniques to extract functional peptides from wool keratin. The targeted bio-functional keratin polypeptides through the isoelectric precipitation process were fabricated successfully by both the acidic hydrolysis and alkaline hydrolysis. In each hydrolysis methods, based on the major amino acid compositions of keratin and their specific isoelectric precipitation points, two kinds of keratin polypeptide precipitations, denoted as KP3

and KP5, were collected at predetermined pH value (pH 3.22 and pH 5.55), respectively. The physical chemical properties of the KP3 and KP5 powders were investigated through a series of experimental analyses. SEM images displayed the sphere-like structures of KP3 and KP5 particles. The alkaline hydrolysis KP3 and KP5 possessed a smaller diameter ranges than that of acidic hydrolysis. Due to different concentrations of spray-dried suspensions, the surfaces of KP3 and KP5 by alkaline hydrolysis had more wrinkles. FT-IR spectra revealed that the bi-sulphate bonds of wool were cleaved and different amino acid compositions were found accordingly by both acidic hydrolysis and alkaline hydrolysis. TG-DSC curves indicated that both KP3 and KP5 by acidic hydrolysis retained a little lower stability compared to wool due to the loss of α -helix and β -sheet structures. The thermal stability of KP3 and KP5 by alkaline hydrolysis were more stable which also confirmed by XRD patterns. The SDS-page confirmed that the molecular weight of KP5 can be detected at around 20 KD. The experimental results indicated that these bio-functional keratin polypeptides have been extracted from wool successfully. By compared both physical and chemical properties of keratin polypeptides, KP5 by alkaline hydrolysis was selected for future exploration discussed in later chapters.

CHAPTER 4 INVESTIGATION ON KERATIN AND POLY(L-LACTIC ACID) BIOFUNCTIONAL ELECTROSPUN MEMBRANE

Previous chapter explored on utilizing keratin polypeptides extracted from wool fibers. This chapter focuses on completing Objective 2 by fabricating biofunctional tissue engineering scaffolds system with introduction of keratin polypeptides. Biocompatible membrane composed of Poly (*L*-lactic acid) (PLLA) and keratin is firstly electrospun. To begin with, water-insoluble keratin was extracted from the wool hydrolyzed solution based on a principle of isoelectric precipitation. These keratin precipitates were dispersed uniformly within ethanol absolute to form non-aqueous homogenous suspension. Ultrafine nanofibrous membranes were successfully prepared by electrospinning the blend of PLLA and keratin suspension. Uniform structure of the composite nanofibers was observed by scanning electron microscopy (SEM). Transmission electron microscopy (TEM) pictures indicated keratin was evenly distributed within the composite fibers. The result of FTIR spectra revealed the composition of keratin/PLLA membrane. X-ray differential spectroscopy (XRD) suggested that higher crystallinity of keratin can be observed from keratin/PLLA composite nano-fibers than the original keratin precipitates. The thermogravimetric analyzer (TGA) spectra indicated that keratin/PLLA composite fibers possessed constant better thermal stability than pure keratin precipitates. The biocompatibility of keratin/PLLA composite membrane was examined by MTS assay.

The cells proliferation profile was observed by fluorescent micrographs. The results indicated that with promoting effect on cell adherence and proliferation, this composite material was suitable as a potential candidate for tissue engineering.

4.1 Materials and Methods

4.1.1 Materials

Poly(*L*-lactic acid) (PLLA) with an inherent viscosity of 6.5dl/g was supplied by PURAC (Netherlands). Chloroform and *N,N*-dimethylformamide (DMF) were purchased from Acors (Belgium). The wool fiber was purchased commercially.

4.1.2 Preparation of wool keratin precipitate

The alkaline hydrolysis keratin peptides were utilized in this chapter. The procedures followed the same experimental conditions as described in Chapter 3. Raw wool was immersed into 2 wt. % sodium hydroxide solution which was kept thermostatic in 95 °C water bath. After the wool fibers were dissolved completely, the hydrolyzed solution was kept stable 48 h at room temperature. Then the solution was adjusted to pH 5.55 by HCl (0.1M). Precipitate was observed at the bottom of the hydrolyzed solution. Then the precipitate was collected by centrifuge (5000 r/min). The precipitate was re-dispersed in DI water and collected by centrifuge again. Subsequently the precipitate was dispersed in absolute ethanol and centrifuged again. This procedure was repeated 4 times.

4.1.3 Electrospinning the keratin/PLLA fibrous membrane

PLLA was dissolved completely at a concentration of 1.0 % in a mixed organic solution of chloroform (wt 90%) together with DMF (wt 10%). Then the wool keratin precipitate was added to form the keratin/PLLA (wt 1:9) suspension. The suspension was loaded into a syringe with a metal capillary which was connected to high-voltage electricity at 22 KV. The feeding rate of the suspension from the syringe was set at 0.4ml/min. The distance between the capillary and the receptor, a grounded aluminum foil, was 10cm. Pure PLLA membrane was also electrospun as the control based on the same parameters. The detailed process of keratin/PLLA composite nanofiber formation was described in Figure 4.1.

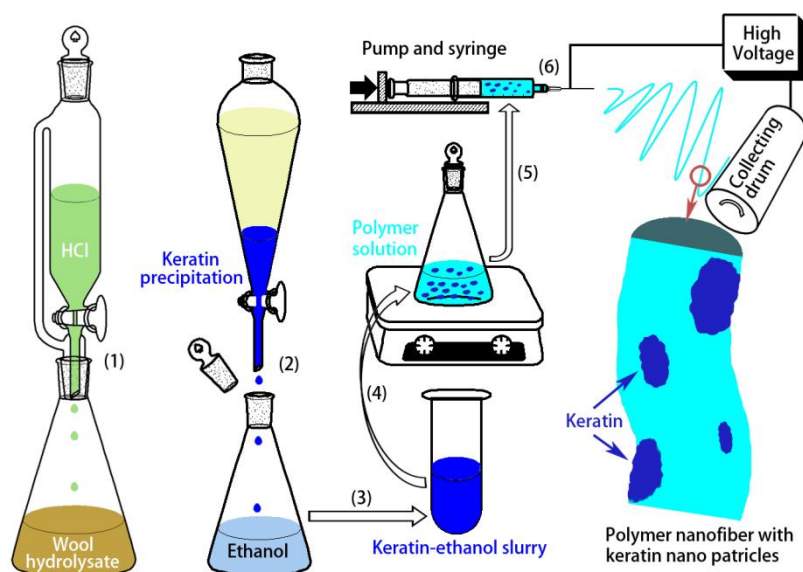


Figure 4.1 Schematic diagram of the formation process of keratin/PLLA nanofiber.

4.1.4 Extraction of keratin from membrane

The fabricated keratin/PLLA membrane was immersed into pure chloroform solution until thoroughly dissolved. Then the solution was centrifuged (5000 r/min) to remove

PLLA which dissolved in chloroform solution from keratin. The same procedure was repeated 4 times until all PLLA was removed from keratin. The keratin precipitates were collected and dispersed in absolute ethanol. After centrifuged, the keratin precipitates was collected for further characterizations.

4.1.5 Characterizations of the keratin composite nanofibrous membranes

The morphology of the keratin/PLLA composite membrane was observed by the scanning electron microscopy (SEM, JEOL Model JSM-6490). The average diameters of both original keratin precipitate before electrospinning and keratin extracted from keratin/PLLA electrospinning membrane were analyzed by a dynamic light scattering (DLS) instrument (Zetaplus particle size analyzer, Brookhaven Ins., U.S.A.). The experiment was processed on a 90° angle detector, with 35 mW solid state laser detector at a wavelength of 658 nm. For each sample, ten consecutive measurements were examined with an integration time of 2s. Transmission electron micrographs were acquired by JEOL 2011 transmission electron microscope (TEM). The keratin/PLLA membrane fibers were deposited on 3mm/400mesh carbon-coated copper grids. Pure PLLA fibers were observed as a control in both SEM and TEM observation. The microstructure of the electrospun membranes were measured by Fourier transform infrared spectrometry (FTIR, Nicolet 5700, Thermo Co. USA). Four groups of samples were prepared: original keratin precipitate from water, keratin precipitate treated by ethanol absolute, keratin/PLLA fibers, pure PLLA fibers. X-ray diffraction experiments were performed on x-ray diffractometer Bruker D8 Advance with a Cu

source at room temperature. The voltage and current was 40 kV and 30 mA respectively and X-ray beam was falling on a sample area of about $7 \times 12 \text{ mm}^2$ with the angle (2θ) shifting from 5° to 50° at a rate of $3^\circ/\text{min}$. Four groups of samples were prepared: original keratin precipitate from water, keratin precipitate treated by ethanol absolute, keratin/PLLA fibers, pure PLLA fibers. The thermogravimetric analyzer (Netzsch STA 449C Jupiter) was utilized to examine the thermal properties. The pure PLLA and keratin powders, which were made from the dried precipitations being collected at pH 5.55, were tested as a control.

4.1.6 Cells culture on the keratin composite membranes

The keratin/PLLA fibrous membrane samples were prepared in the same size and shape. Then they were exposed to 365 nm wavelength UV for sterilization. After that, they were placed into 24 well-cell culture plates rinsed with culture medium for 2 hour prior to cell seeding. Human foreskin fibroblasts cell line, HFF-1, was obtained from ATCC and cultured in T25 culture flasks (SPL, Korea) in an incubator at 37°C and 5% CO_2 . Dulbecco's modified medium, DMEM (Invitrogen, USA), was supplemented with 10% foetal bovine serum, FBS (Invitrogen, USA), 1% penicillin (Invitrogen, USA), 1% streptomycin (Invitrogen, USA). All cells used in this study were at passage 10 or less. Cells were harvested by adding 0.25% trypsin with EDTA (Invitrogen, USA). The trypsin was neutralized by adding DMEM media with 10% FBS. Then the cell suspension was centrifuged and seeded on the treated substances. Seeding 5×10^4 cells per well ($n=3$) for prepared sample. Cells were incubated at 37°C with 5% CO_2 until

the evaluation. CellTiter 96® Aqueous One Solution Reagent (Promega, USA) was added to the culture medium in each well as a ratio of 1:5. The plates were kept in the incubator (protect from light) for 4 hours. The absorbency of the solution from each well via 492 nm wavelength was read by Micro-plate reader infinite F200 (TECAN, Switzerland). This assay was conducted at 24 hours of incubation. The MTT (Sigma) assay was employed to identify the cellular energy metabolism and cell proliferation. After HFF-1 was cultured in 24-well plates for 3 days, the cell proliferation was examined by MTT assay. 50 µl of MTT (5 mg/ml) were added to each well and incubated at 37 °C for 4 h in humidified atmosphere of 5% CO₂ in air. At the end of the assay, blue formazan reaction product was dissolved by adding 200 µl dimethyl sulfoxide and 100 µl solution was transferred to a 96-well plate. The solution of each sample was placed in a microtiter plate and the absorbance at 490 nm was measured on a SS-3000 Immunoanalyser (MB-Ir, Beijing, China).

4.2 Results and Discussion

4.2.1 Morphology of keratin/PLLA membrane by SEM

The SEM photos about the membrane structure were shown in Figure 4.2 and Figure 4.3. These images indicated that the fibrous membrane with homogenous structure was fabricated. In these pictures, no agglomeration was found and keratin blended with PLLA was formed a fine fibrous membrane. The average diameter of the keratin/PLLA fiber was $1.1 \pm 0.4 \mu\text{m}$. It was noticeable that the diameter of keratin/PLLA fiber was smaller than the diameter of pure PLLA ($1.5 \pm 0.3 \mu\text{m}$). This

could be contributed by decrease in viscosity and increase in conductivity when adding keratin in the electrospun solution [146]. It has been confirmed that lower viscosity enhanced the formation of finer fibers and higher charge density by jet formed smoother and finer fibers for the stronger whipping instability of the jet that enhanced the fibers stretching [147].

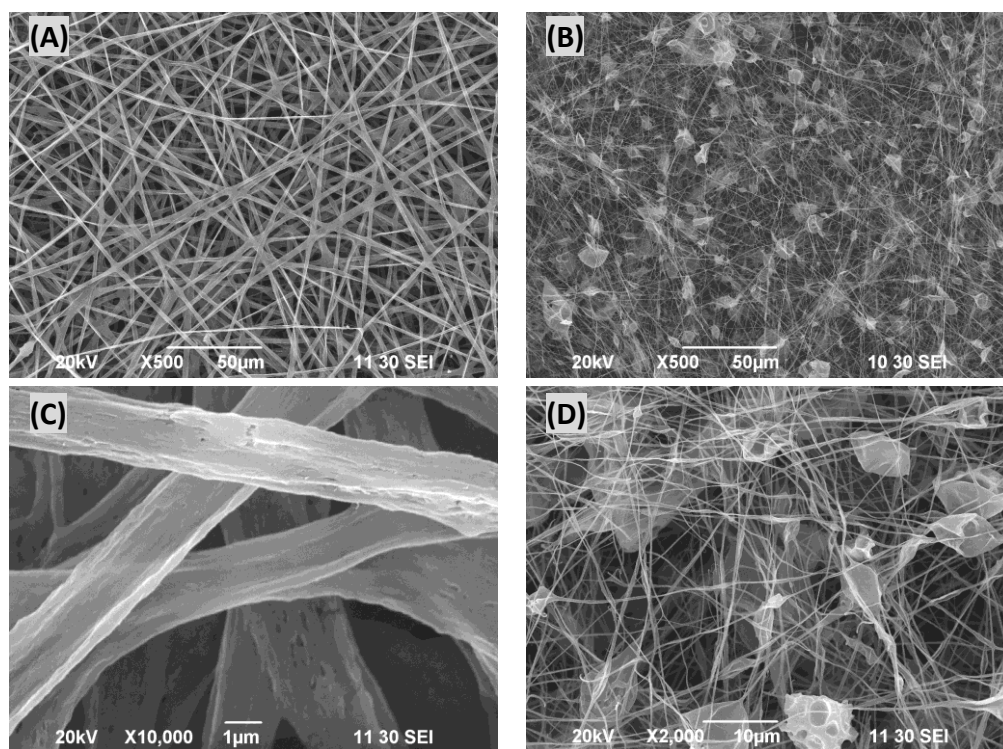


Figure 4.2 SEM images of nanofibers: (A) and (C) were obtained from keratin/PLLA (wt 1:9) membrane; (B) and (D) were obtained from keratin/PLLA (wt 1:1) membrane. The homogenous structures without any agglomeration can be observed from keratin/PLLA (wt 1:9) membrane.

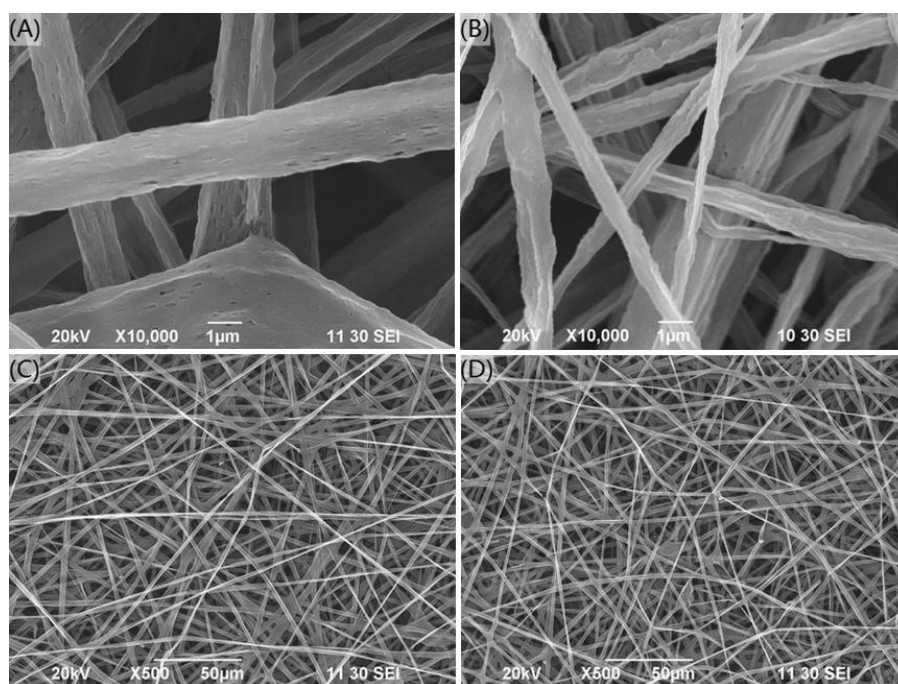


Figure 4.3 SEM images of keratin/PLLA nanofibers: (A) and (C) were obtained from pure PLLA membranes; (B) and (D) were obtained from keratin/PLLA nanofibrous membranes (wt 1:9). The homogenous structures without any agglomeration can be observed from both of the two membranes.

Figure 4.4 displayed the comparison of the diameter between the keratin extracted from the membrane and the original keratin precipitates. The impact of the electrospinning force could be observed on the physical change of keratin particle. Unlike the larger diameter distribution of 1000-1400 nm, the keratin particle was observed to become much smaller after processed through electrospinning. It was believed that in the process of electrospinning, a stretching force was applied on the suspension of PLLA and keratin. Hence keratin was affinitive with PLLA fibers more closely and its physical morphology was changed correspondingly.

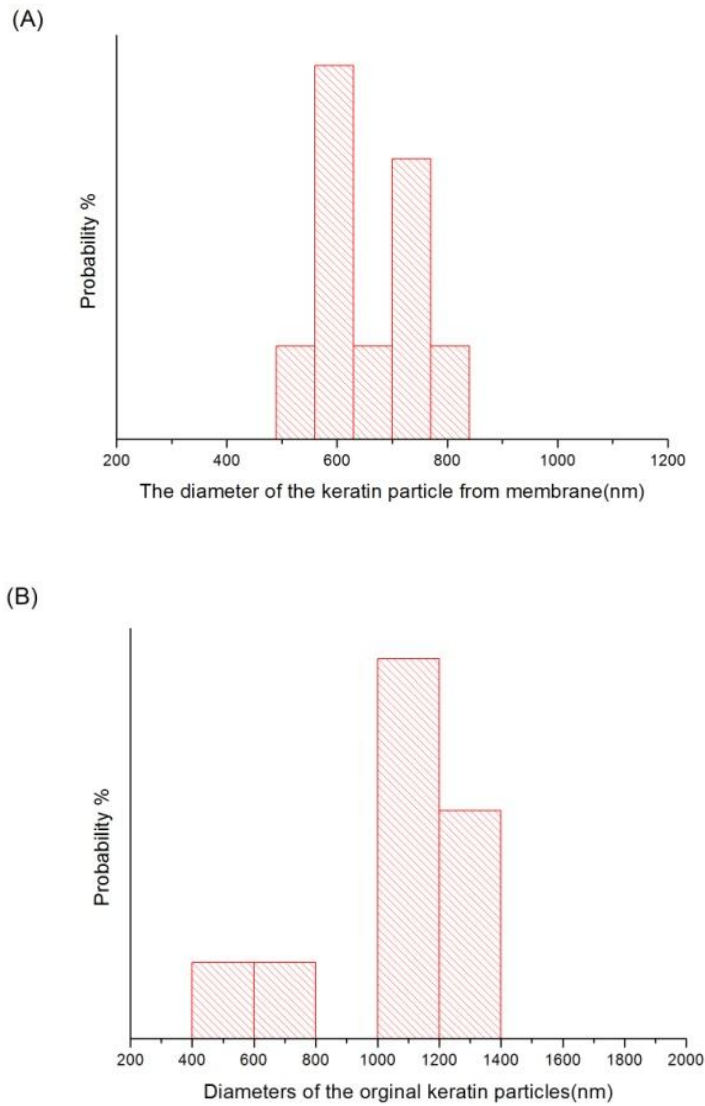


Figure 4.4 Ranges of the diameter of keratin nanoparticles: (A) shows the diameter of the keratin particle extracted from the keratin/PLLA electrospinning membrane; (B) shows the diameter of the original keratin particle.

It was a tangled problem that spray-dried keratin particles aggregated in the composite fibers [148]. The big particles aggregation can easily destroy the initial structure of composite fibers. The present study was employed a method of isoelectric precipitation instead of spray-drying the keratin hydrolyzed solution. The possible

mechanism was described in Figure 4.5. Firstly, in the process of alkaline hydrolysis of wool fibers, disulfide bond (S-S) and partial peptide bonds of keratin in wool were split apart. The negative Cys^- group was unveiled at keratin surface. The same negative charge repelled the keratin particles from each other to prevent their aggregation. Based on the principle of isoelectric precipitation, the acid was then added into the environment. When it came close to the pI value, the positive charges came to the surface of Cys^- group and keratin had no net charge. This directly reduced solubility of keratin because it was unable to interact with the medium and will fall out of solution. The keratin precipitates were then re-dispersed in a alcohol system to form uniform suspension. There're two purposes of utilizing alcohol: firstly, organic PLLA solution was resistance to aqueous system. The previous study was spray-drying the keratin hydrolyzed solution. But the keratin particles aggregation was aroused correspondingly. The alcohol re-dispersion treatment can prevent this problem; Moreover, a replacement of water by ethanol can achieve the uniform blend of keratin and PLLA.

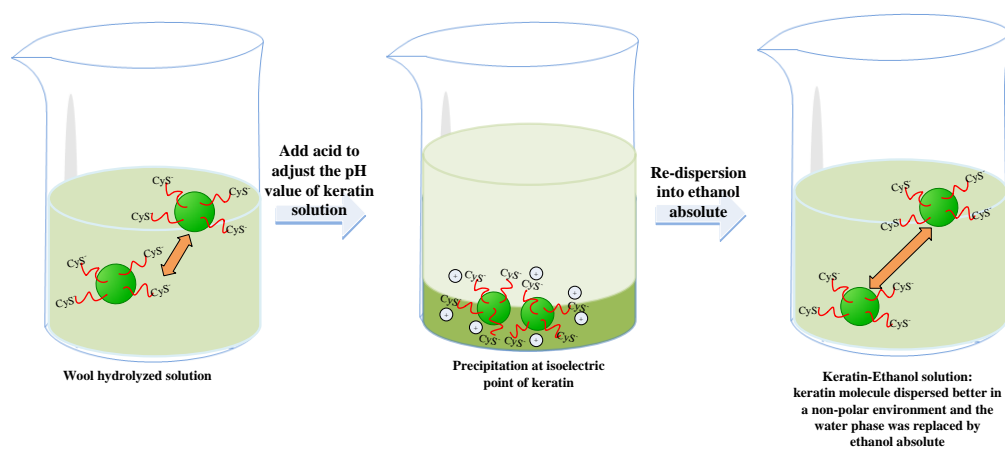


Figure 4.5 The hypothesis mechanism diagram of re-dispersion of keratin in ethanol absolute.

4.2.2 FT-IR spectrum of keratin/PLLA membrane

Although the morphology of keratin/PLLA membrane had few differences with the pure PLLA membrane from SEM observation, the FTIR spectrum revealed the microstructure of the keratin/PLLA membrane. In Figure 4.6, two absorption peaks were observed respectively at 1630 and 1550 cm^{-1} , which were the characteristic peaks of keratin. They were believed to identify amide I and II bands of keratin. As a matter of fact, amide I absorption peak, ranging between 1700 to 1600 cm^{-1} , was considered being especially sensitive to the secondary structure of the proteins. The absorption peak at 1650 cm^{-1} indicated the presence of the α -helix structure; the bands related to the β -sheet structure fell in the range of 1631 to 1515 cm^{-1} . The peaks at low intensity of α -helix structure implied the disordered keratin conformations [149].

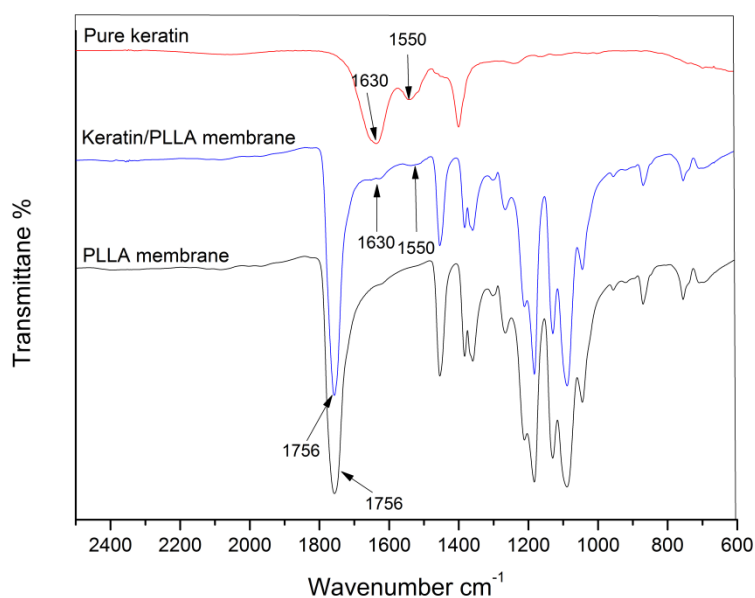


Figure 4.6 FT-IR spectra of keratin/PLLA membrane, pure PLLA membrane and pure keratin. Two characteristic peaks of keratin were observed respectively at 1630 and

1550 cm^{-1} from both pure keratin sample and keratin/PLLA fibrous membrane sample. The FT-IR spectrum revealed the composition of keratin/PLLA membrane.

4.2.3 TEM morphology of keratin/PLLA membrane

Since FT-IR spectra have demonstrated that keratin existed in the membrane, a detailed morphology of keratin/PLLA fibers was further investigated by TEM. Figure 4.7(A) indicated the morphology of pure PLLA fibers, while Figure 4.7(B) displayed the keratin/PLLA fibers. The notable dark shadow indicated the existence of keratin pH 5.55.

Both the TEM graphs and the FTIR spectrum demonstrated the existence of keratin in the membrane. From the SEM pictures, it was difficult to observe the morphology differences between the pure PLLA membrane and the keratin/PLLA membrane. This phenomenon implied that the keratin pH 5.55 has been dispersed uniformly within the net-structure of the fibers. It demonstrated that the new preparation and fabrication method of adding keratin/ethanol into PLLA organic suspension has conquered the poor structure uniformity of the keratin/PLLA membrane which was made from wool keratin particles [148]. The diameter of spray-dried keratin particles was much greater than the average diameter of PLLA fibers. Although keratin particles maintained the PLLA fibers as a membrane with high porosity, the porous structure collapsed sharply after the keratin particle dissolved or removed during degradation which was a negative impact on cell seeding and culturing. Now with the new fabrication method, PLLA and

keratin mixed uniformly.

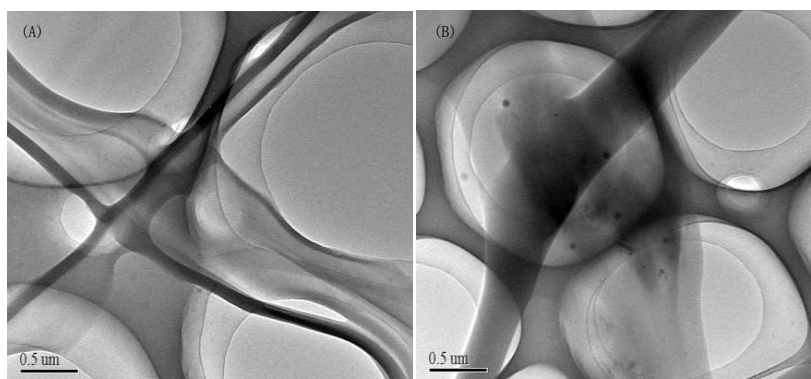


Figure 4.7 TEM images of PLLA and keratin/PLLA nanofibers: (A) pure PLLA fibers and (B) keratin/PLLA fibers. The dark shadow area in image (B) was keratin precipitates blended into nanofibers.

4.2.4 XRD spectra of keratin/PLLA membrane

The XRD spectra in Figure 4.8 illustrated the crystal structure of pure PLLA, keratin precipitates from water, keratin precipitates from ethanol, keratin/PLLA membrane and keratin extracted from membrane. From XRD spectrum of pure keratin from water and ethanol, a broad peak can be observed at $19.6\ 2\theta^\circ$, which represented α -helix structure and the sharp peak at $23.3\ 2\theta^\circ$ represented the β -sheet structure. These corresponded to the β -sheet crystalline spacing of 4.7 and 3.8 Å. There was no difference between keratin obtained from water environment and keratin obtained from ethanol environment. This indicated that the ethanol-treatment of keratin didn't affect its initial crystallinity. The initial α -helix and β -sheet were kept after the keratin re-dispersed in the ethanol solution. In XRD spectrum for keratin/PLLA membrane, a sharp peak appeared at around 16.5° . This was attributed to the keratin crystal structure

transformation. There were two major secondary structures in keratin: α helix and β -sheet [150]. The crystallinity could be higher with more α -helix structures. It was observed from Figure 4.6 that in the curve of keratin/PLLA membrane the peak of α helix reduced dramatically, which suggested that keratin lost the ordered structures in the process of being formed as the electrospun nanofibrous membrane. In order to explore the impact of electrospinning process on crystallinity of keratin, keratin was extracted from electrospun composite membrane. Compared with pure PLLA fiber, the keratin extracted from membrane barely had any significant differences compared with pure PLLA which has less crystallinity.

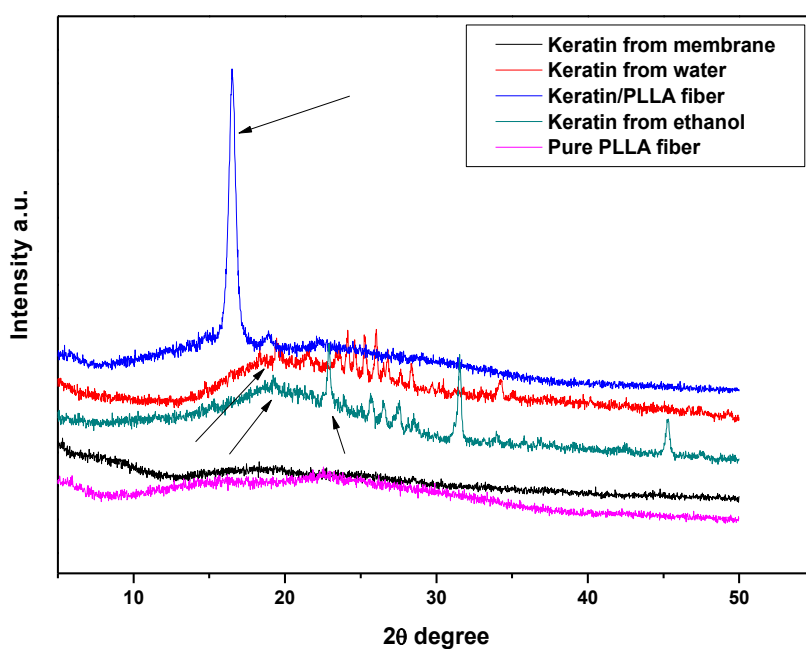


Figure 4.8 XRD patterns of keratin/PLLA membrane, pure PLLA and pure keratin extracted from different solutions. In the curves of keratin from water and ethanol, the broad peak at 19.6° represented α helix structure and the acute peak at 23.3° represented the β -sheet structure. In the curve of keratin/PLLA, a new peak appeared at 16.5° which was caused by the keratin crystal structure transformation.

4.2.5 Thermal property of keratin/PLLA membrane

The thermal-stability of the keratin/PLLA membrane has been examined through thermo-gravimetric analysis by determining the changes concerning samples weight in relation to the changes in temperature. From Figure 4.9, it was noticeable that keratin had the lowest decomposition temperature at 210 °C while the PLLA had the decomposition temperature up to more than 350 °C due to its polymeric structure and van der waals force between the bonds.

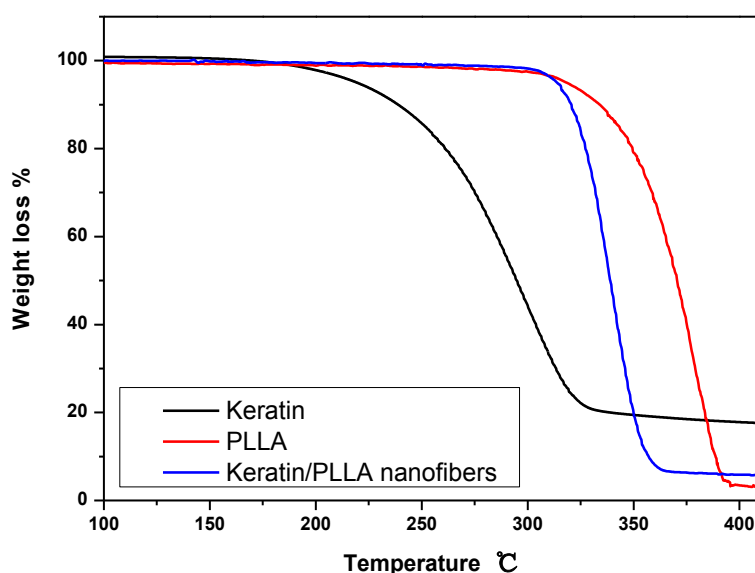


Figure 4.9 Thermogravimetric curves of PLLA, pure keratin and keratin/PLLA membrane. The decomposition temperature of keratin/PLLA nanofibrous membrane was at 307.5 °C which lay in the range between pure PLLA and keratin.

The decomposition temperature of keratin/PLLA membrane lay in the range between pure PLLA and keratin. At 307.5 °C, a sharp decomposition trend occurred since there was an acute decrease in weight loss of keratin/PLLA membrane. Comparing with

PLLA, keratin has almost completed its decomposition led by its weight loss down to more 80% in total at 307.5 °C. When the keratin in the membrane has decomposed at a large scale, the membrane appeared to be thermal-unstable and was quickly burned out subsequently. After being heated up to 350.0 °C, the keratin/PLLA membrane almost thoroughly decomposed. The weight loss of keratin/PLLA membrane was close to 95% which was slightly lower than the weight loss of pure PLLA, however much higher than the weight loss of pure keratin. This phenomenon might be changed according to the content percentage of keratin in the membrane.

Table 4.1 TGA data under inert atmosphere

| Sample | T _i (°C) | T _{mr} (°C) | R (wt.%) |
|--------------|---------------------|----------------------|----------|
| PLLA | 315.0 | 394.0 | 4.3 |
| Keratin | 198.0 | 323.0 | 21.4 |
| Keratin/PLLA | 312 | 361 | 7.1 |

4.2.6 Cells culture on keratin/PLLA nanofibrous membrane

The biocompatibility of keratin/PLLA membrane was tested by MTT assay. This assay worked on the principle that the mitochondrial dehydrogenase enzyme reduced the salt to a colored formazan product [147]. The result was shown in Figure 4.10. This bar chart showed that keratin/PLLA membrane had a beneficial impact on cells viability compared with pure PLLA membrane. The cell viability test demonstrated the biocompatibility of keratin/PLLA membrane and made its further application in

medicine clinics possible. Figure 4.11 showed the fluorescent micrographs of adherence performance of fibroblast HFF-1 on the electrospun membranes of keratin/PLLA and pure PLLA after 24h and 48h cultivation. It was observed that more cells adhered and proliferated better on the keratin/PLLA (Figure 4.11 A and C) membrane surfaces compared to the pure PLLA membrane (Shown in Figure 4.11 B and D). The cell growth performance on the membrane surfaces after 48h showed similar trend to the cell adhesion performance after 48 h cultivation: the cells had grown on all surfaces of the keratin/PLLA composite membranes, but had grown less on the surface of the pure PLLA membranes. This is attributed by the hydrophilicity of keratin/PLLA membrane, on the surface of which the cells adhered, spread and grew more on hydrophilic surface rather than a hydrophobic one. The reduced cell adhesion and growth on the PLLA membrane surface may be explained by the high surface hydrophobicity and the high mobility of the hydrated PLLA chains exposed on the surfaces. Therefore, the affinity from surface to cells could be interrupted. Compared with pure PLLA scaffolds, a greater density of viable cells was seen on the composite fibrous membranes. Cell culture results indicated that these composite fibers have promoting effect on cell growth and attachment. In future they could be utilized as scaffold materials for tissue engineering and wound healing dressing.

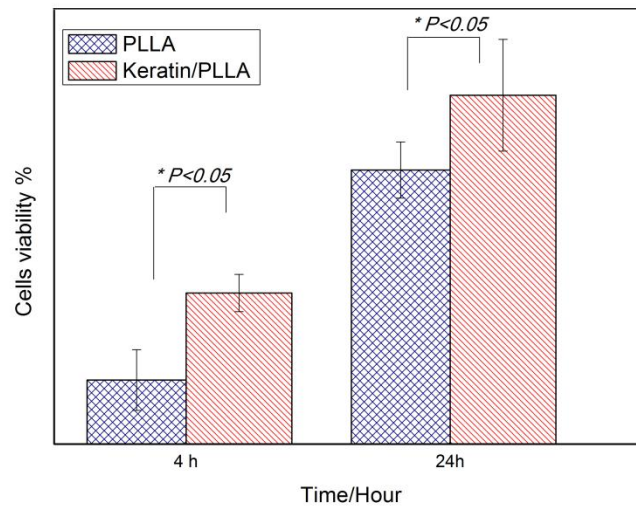


Figure 4.10 Cells proliferation performances on keratin/PLLA membrane (pure PLLA membrane worked as control) for 4 hour and 24 hour. The left bar which represented keratin/PLLA membrane was higher than the right bar which stood for pure PLLA. This trend demonstrated the positive impact of keratin/PLLA membrane on cells viability.

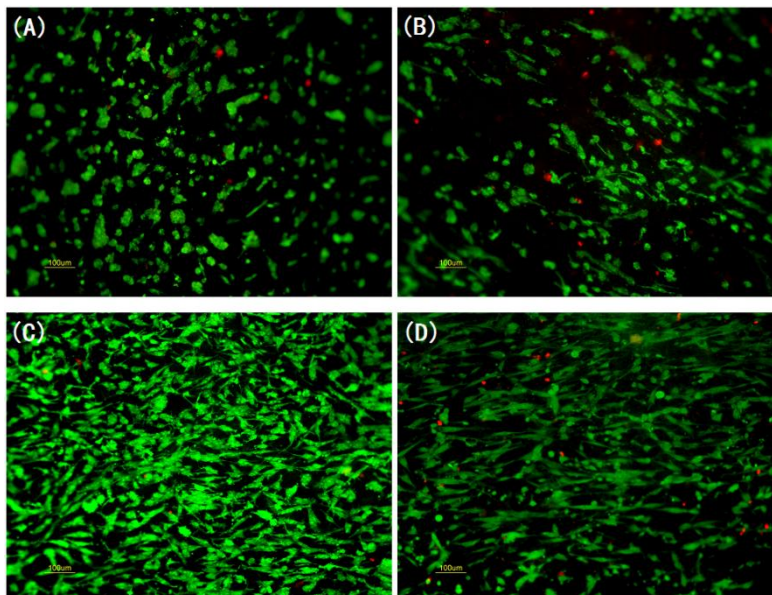


Figure 4.11 Cells morphology of fibroblast cells seeded on the keratin/PLLA nanofibrous membrane and pure PLLA nanofibrous membrane separately: (A) and (B)

display the cells proliferation profiles after cultivation on keratin/PLLA and PLLA for 24 h; (C) and (D) display the cultivation after 48 h.

4.3 Conclusion

Objective 2 has been achieved in this chapter. Isoelectric keratin precipitates have been introduced into the composite nanofibrous scaffolds successfully. The detailed problems of procedures have been conquered as well. In order to resolve the aggregation of protein embedded within nanofibers, the keratin precipitates were re-dispersed in alcohol system instead of being fabricated as spray-dried particles. The composite nanofibrous membrane was successfully electrospun from the blend of isoelectric keratin precipitates and PLLA organic solution subsequently. The morphological images indicated the composite nanofibrous membrane possessed ultrafine and homogenous structure without keratin aggregation embedded. The FT-IR spectrum observed the existence of keratin in the composite fibers. The thermal property of the composite membrane was more stable than pure keratin tested by TGA. XRD spectra revealed a crystal transformation of keratin after the process of electrospinning. An MTS assay was employed to identify the biocompatibility of keratin/PLLA composite nanofibrous membrane. Compared with pure PLLA membrane, keratin/PLLA fibrous membrane showed a dramatically beneficial impact on cells viability. The combined results of characterizations and cell culture experiments indicated that keratin/PLLA nanofibrous membrane was preferable for tissue engineering with its stable chemical property and good biocompatibility.

CHAPTER 5 DEGRADATION EVALUATION OF KERATIN AND POLY(L-LACTICACID)ELECTROSPUN NANOFIBROUS MEMBRANE

Chapter 5 aims to achieve Objective 3 by studying the degradability of nanofibrous biopolymer membrane. The morphology of the membrane was observed by SEM images which indicated that the thin keratin/PLLA nanofibers unfold after degradation in PBS solution. The UV spectra further indicated the degradation rate of keratin. The FTIR spectra demonstrated the same degradation trend by comparing the intensities of keratin characteristic peaks. The thermal properties of the degraded membranes were tested by TGA thermal analysis. The mechanism of the degradation process was also explored and the results indicated that adding keratin into PLLA nanofibers increases their degradation rate compared to pure PLLA nanofibers.

5.1 Materials and methods

5.1.1 Materials

Poly(*L*-lactic acid) (PLLA) with an inherent viscosity of 6.5dl/g was supplied by PURAC (Netherlands). Chloroform and *N,N*-dimethylformamide (DMF) were purchased from Acors (Belgium). The wool fiber was purchased commercially.

5.1.2 Preparation of keratin/PLLA electrospun nanofibers

As described in Chapter 4, the keratin/PLLA nanofibrous membrane was fabricated following the conditions as: keratin/PLLA electrospun suspension was loaded into a syringe with metal capillary which was connected with high-voltage electricity at

22KV. The feeding rate of the suspension from the syringe was set at 0.4ml/min. The distance between the capillary and the receptor, a grounded aluminum foil, was 10cm. Pure PLLA membrane was electrospun as the control.

5.1.3 Methodology of degradability evaluation of keratin/PLLA nanofibrous membrane

The morphology of the fibrous membrane was observed using the Scanning Electron Microscopy (SEM) (Netzsch STA 449C Jupiter). The samples being tested were pure PLLA membrane, the original keratin/PLLA membrane and keratin/PLLA membrane after biodegradation respectively. Also, TEM test further investigated the structure of keratin/PLLA membrane and pure PLLA membrane.

Before the UV test on PBS solution, a keratin calibration curve was got based on a series of experiments concerning the relationship between the concentration of keratin and OD value. Then, the sample membrane was immersed into PBS solution (PH7.4, 1 L), which is mimicking the inner environment of human body, and settled in a shaking table at 60rpm at 37 °C constantly. After 1 hour, 10 ml solution was collected from the PBS bottle and another amount of 10 ml pure PBS solution was added to make sure the keratin/PLLA membrane was kept in the volume-constant solution. A series of 10 ml solution samples were ready to be tested after a certain time interval subsequently. Then all the collected solutions were tested with UV spectrum under the wavelength of 278 nm. Through the keratin calibration curve, the OD value data were transferred into concentration data.

Another group of keratin/PLLA membrane degradation was done in the following

way: 6 groups of samples were cut from a same keratin/PLLA electrospinning membrane. Each group was immersed in 1 L of PBS solution at pH 7.4 in a shaking table at 60 rpm and was kept thermostat at 37 °C. The PBS solutions were collected respectively in the intervals of 3 hours, 24 hours, 3 days, 7 days, 14 days and 28 days. The membrane samples were taken based on the same time interval. The samples were then thoroughly rinsed using DI water and then dried in room temperature. keratin/PLLA membrane was examined using Fourier transform infrared spectrometry (FTIR, Nicolet 5700, Thermo Co. USA). The characteristic absorption peaks of keratin were observed. A series of biodegraded membranes taken in different intervals as mentioned before were also examined in order to recognize the ratio changes of keratin in membranes.

The Thermogravimetric analysis/Differential scanning calorimeter (Netzsch STA 449C Jupiter) was used in examination on thermal properties of keratin/PLLA fibrous membrane. The degraded membranes with different degradation time were examined. The pure keratin and pure PLLA were tested as a control.

5.2 Results and discussion

5.2.1 Morphology of keratin/PLLA electrospinning membrane

The SEM photos of the structure of membranes are shown in Figure 5.1. These images indicated that the nanofibrous membranes with homogenous structure were fabricated. From the fiber structures, no big agglomeration was found and the keratin polypeptides were surrounded by PLLA to form a fine fibrous membrane. The average diameter of the keratin/PLLA fiber is $1.1\pm 0.4\ \mu\text{m}$. It is noticeable that the diameter of keratin/PLLA fiber is smaller than that of pure PLLA, which is 1.5 ± 0.3

μm . This could be contributed by the decrease in electrospinning solution viscosity and the increase in conductivity when adding keratin in the solution [20]. Indeed, it has been confirmed that lower viscosity may enhance the formation of finer nanofibers and higher charge density by jet forms smoother and finer nanofibers for the stronger whipping instability of the jet that enhances the fibers stretching [21].

The morphology of the degraded nanofibers was observed from SEM and these photos are shown in Figure 5.2. It is obviously that the fiber structures changed dramatically in the process of degradation. Firstly, the width of the fibers extended to $4.1\pm 0.8 \mu\text{m}$ and within certain volume the thickness of each bundle became much smaller. Secondly, the clear and homogenous structure of original membrane changed to a sticky and dense structure after being immersed in PBS solution. Thirdly, after being immersed in PBS, there's no dramatic difference in the fiber structure no matter how long the fiber was immersed as shown in Figure 5.2. The membranes degraded after 3 hours and 7 days were displayed as similar structures. The expansion behavior of membrane fibers might be attributed to the hydrophobicity of PLLA. After being immersed in PBS solution, water molecules penetrated the free space of fibers which were hollow inside and the fibers were forced to be unfolded. Since the whole membrane was in a crisscross and loose structure the penetration of water molecules would be very quick. So there's no significant difference in structure between the membranes degraded respectively for 3 h and 7 day. In addition this demonstrated the improvement of our new fabrication method. The membrane made in previous method [4] has a lot of keratin beads in the fibrous structure and when the fiber was unfolded, the keratin beads were released firstly which is not our expectation during the long-term keratin degradation processes. A fine and homogenous structure could

be helpful to slow the keratin degradation.

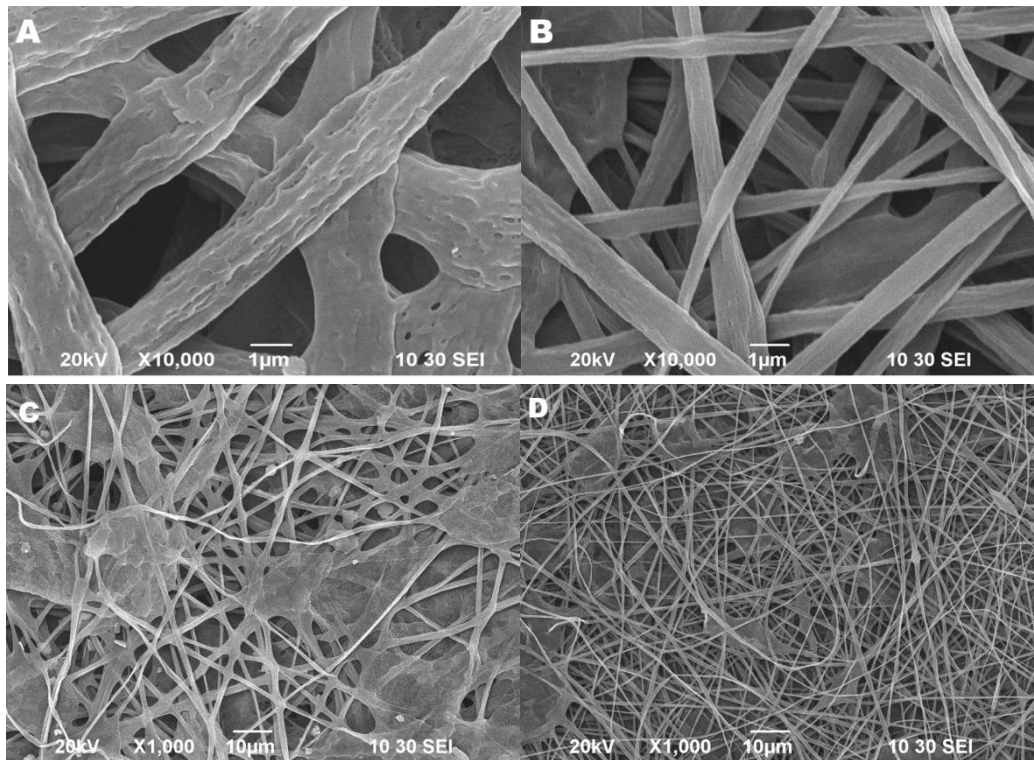


Figure 5.1 SEM of keratin/PLLA fibrous membrane, (A) and (C) were from pure PLLA membrane; (B) and (D) were from keratin/PLLA membrane.

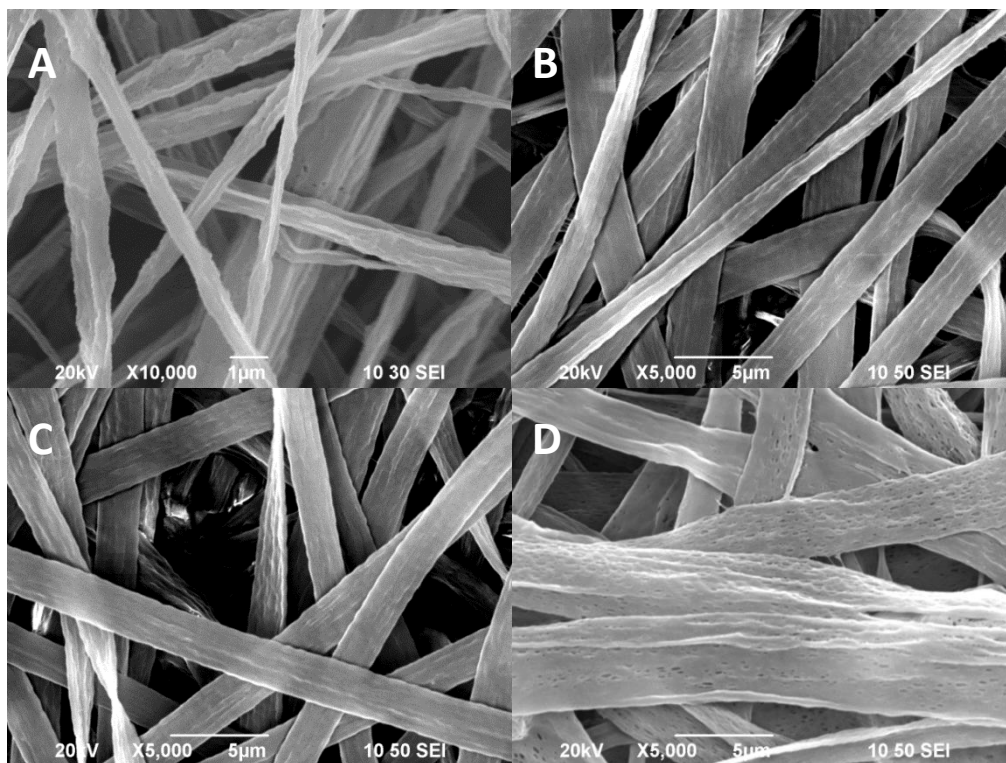


Figure 5.2 SEM of keratin/PLLA membrane after being immersed into PBS solution

for (A): 0 hour (original membrane); (B) 3 hours (C) 3 days and (D) 7 days.

5.2.2 Degradability evaluation by FT-IR spectrum

The FT-IR test mainly focused on the composition of keratin/PLLA membrane and that of the degraded. From the FT-IR graph shown in Figure 5.3, the characteristic peaks of keratin could be observed from the composite membranes as indicated with arrows.

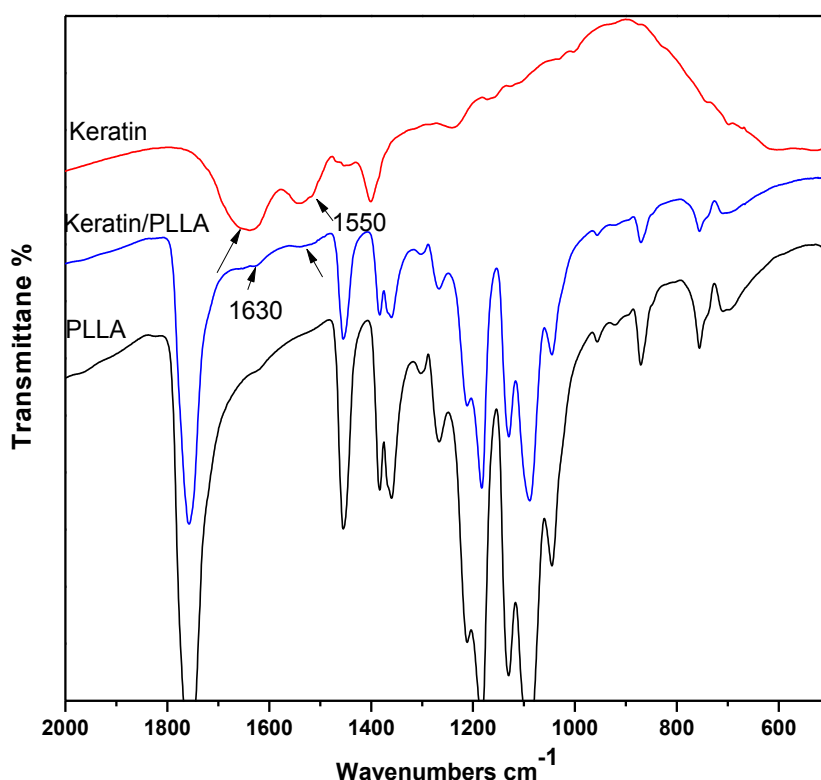


Figure 5.3 FT-IR spectra of keratin/PLLA membrane, pure PLLA membrane and pure keratin.

There were two absorption peaks respectively at 1630 and 1550 cm^{-1} , which are the characteristic peaks of keratin. They are assigned to the amide I and II bands of protein. As a matter of fact, the amide I absorption, respectively at 1700 to 1600 cm^{-1} , is known to be especially sensitive to the secondary structure of proteins. On the basis

of literature data the absorption at 1650 cm^{-1} suggests the presence of the α -helix structure, whereas the bands related to the β -sheet structure fall in the $1631\text{--}1515\text{ cm}^{-1}$ range. The peaks at low intensity in the $1697\text{--}1670\text{ cm}^{-1}$ range indicate disordered keratin conformations [22]. In Figure 5.4, it can be found that along with the degradation the content of keratin left in the membrane was getting smaller for the peaks were getting weaker.

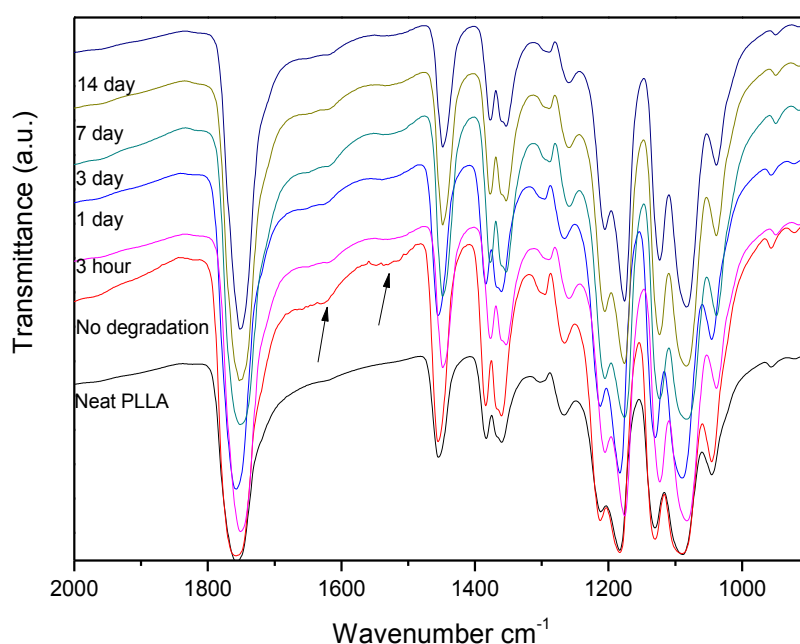


Figure 5.4 FT-IR spectrum of keratin/PLLA membrane as a function of degradation period and along with the degradation the two characteristic peaks at 1630 cm^{-1} and 1550 cm^{-1} gradually became weaker.

5.2.3 Degradability evaluation by UV spectrum

Keratin calibration curve was drawn at wavelength 278 nm , which interpreted a relationship between the concentration of keratin released into PBS solution and OD value as shown in Figure 5.5. The reason to choose 278 nm as the absorbance

wavelength is that the absorbance peak of keratin 278 nm is an effect of absorption of aromatic amino acids in keratin chains [24]. In Figure 5.6, the degradation profile of the membrane can be observed. A steady increase can be observed concerning the amount of keratin polypeptides released into PBS solution as a function of time. Within 180 hours, $18.34 \pm 0.49\%$ keratin has been released into the solution. Comparing with the previous methods [4] which stated that more than half keratin polypeptides were released in the first 3hour, our new methods improved the stability of the fibrous membrane and made it a lasting degradation period. The purpose of the keratin/PLLA electrospinning membrane is working as a candidate material in the area of orthopedics clinic and bone regeneration. Normally, the bone regeneration lasts a long period of time, correspondingly in need of a material of long period of degradation. This is the purpose of this new fabrication method.

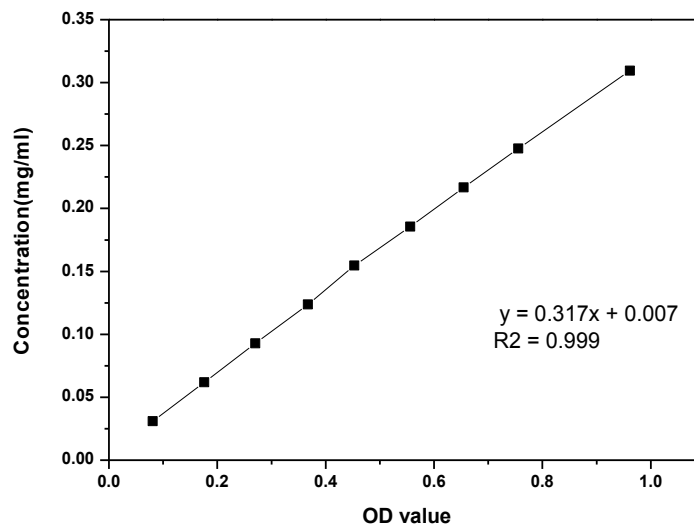


Figure 5.5 The calibration curve of keratin at a wavelength of 278nm in PBS solution.

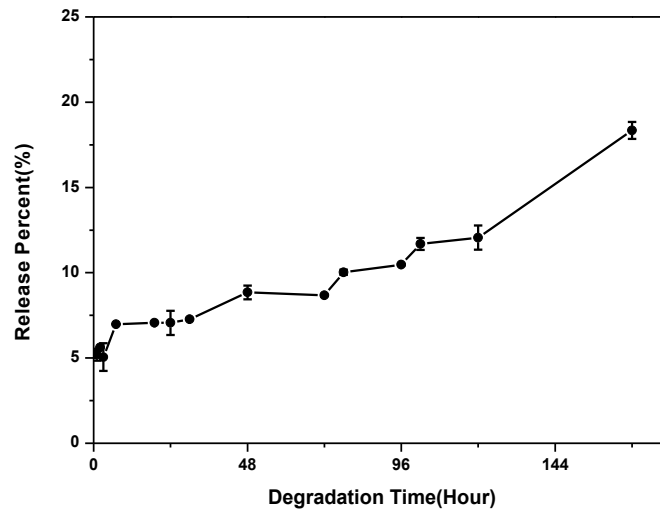


Figure 5.6 The degradation curve of the keratin/PLLA composite membrane by UV spectra.

5.2.4 Degradability evaluation by TGA analysis

TGA spectra of keratin/PLLA membranes as a function of degradation periods are shown in Figure 5.7. It displayed the thermal-stability of a series of membranes. The curves in the left graph are respectively for pure keratin, 3 hours degraded membrane, 24 hours degraded membrane, 3 days degraded membrane, 7 days degraded membrane and 14 days degraded membrane. It is obvious that pure keratin decomposed at a lower temperature at 210 °C and for other membranes the lower content of keratin left, the higher decomposed temperature it had.

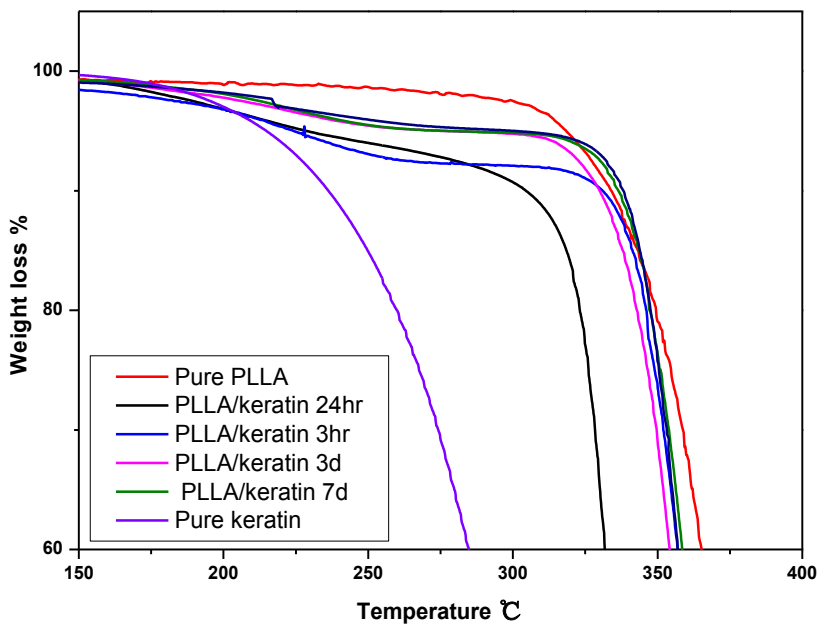
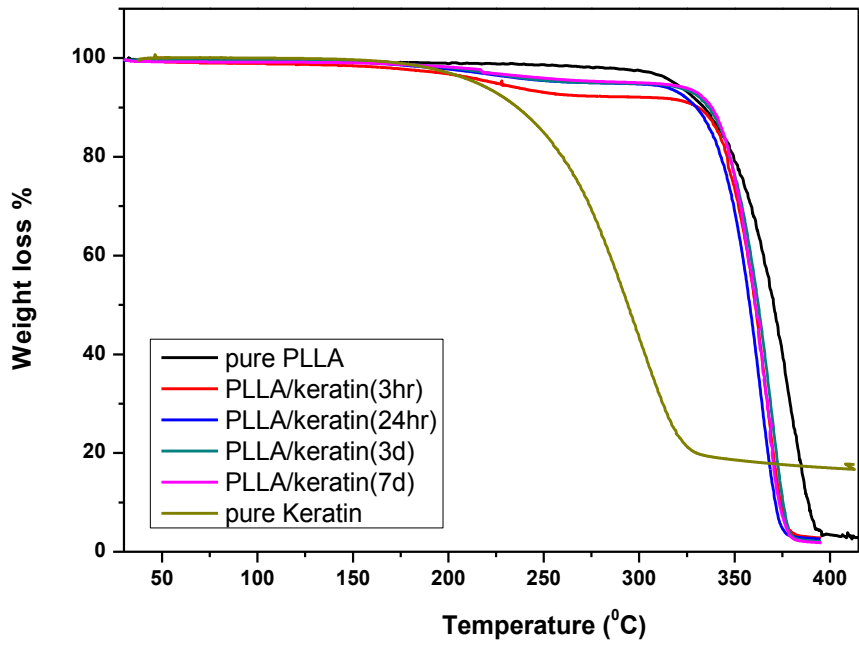


Figure 5.7 TGA diagrams of keratin/PLLA membranes as a function of degradation periods. The bottom graph has amplified the curve zones from the top diagram.

5.2.5 The relationship between different evaluation methods

Different characterization methods represented the keratin release status and the

keratin degradability in the nanofibrous membrane. TGA curves revealed the keratin status remained in the composite nanofibers. With the degradation time passing, the keratin/PLLA nanofiber curve was approaching to the pure PLLA fibers closely. The UV spectra, on the contrary, reflected the situation of released keratin in the PBS solution which equaled to the losing amount of keratin of the composite fibers. In order to evaluate the correlations between different evaluation methods, several indexes were extracted from different characterization methods.

The thermogravimetric analyzer was used to examine the thermal properties of keratin/PLLA nanofibrous membrane. The pure PLLA and keratin powders, which were collected and dried from wool hydrolyzed at pH 5.55, were tested as a control. In this paper, TGA curves were defined to explicate a quantitative change on biodegradation. In Figure 5.8, the area below TGA curve was regarded as the thermal stability of compound. Then formula 1, 2 and 3 could be derived as follows:

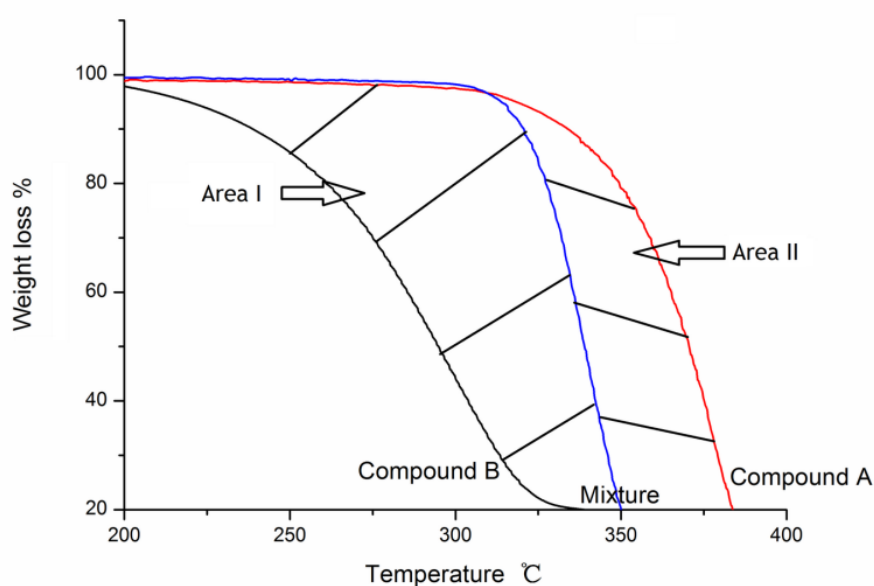


Figure 5.8 Calculated diagram for TGA thermal stability.

Area I was the difference on thermal stability between compound A and mixture; Area II was the difference on thermal stability between compound B and mixture. The content percentage of compound A in mixture was denoted as $K_A = \text{Area I} / (\text{Area I} + \text{Area II})$

$$\text{Area}_I = \int_{T_1}^{T_2} f(x_A) dt \quad \text{Equation 5.1}$$

$$\text{Area}_{\text{mixture}} = \int_{T_1}^{T_2} f(x_m) dt \quad \text{Equation 5.2}$$

$$\text{Area}_{II} = \int_{T_1}^{T_2} f(x_B) dt \quad \text{Equation 5.3}$$

In these formulas, $f(x_A)$, $f(x_B)$ and $f(x_m)$ stood for the curves of compound A, compound B and mixture respectively. T_1 was the initial temperature and T_2 was the end temperature when the process of heating was finished. Area I denoted as the difference on thermal stability between compound A and mixture and Area II denoted as the difference on thermal stability between compound B and mixture.

The content percentage of compound A in mixture was expressed as $K_A = \text{Area I} / (\text{Area I} + \text{Area II})$. While, the content percentage of compound B in mixture was expressed as $K_B = \text{Area II} / (\text{Area I} + \text{Area II})$. The bigger was Area I, the higher percentage of compound A was there in mixture.

In the UV spectra, the index was set as the release amount of keratin after 24 hour degradation time. The index data was shown in Tables 5.1 and 5.2.

Table 5.1 TGA integral area data

Input

iy = [Book1]Sheet1!(C1,D1)
type = 0 (math:Mathematical Area)
plot = 0

Output

oy = [Book1]Sheet1!(,C"Integrated Y1")[936:1567]
x1 = 189.55299
x2 = 367.22601
i1 = 1
i2 = 632
area = 16663.539363124
y0 = 99.08521
x0 = 202.106
dx = 272.13380536697

integ1

Input

iy = [Book1]Sheet1!(E1,E2)
type = 0 (math:Mathematical Area)
plot = 0

Output

oy = [Book1]Sheet1!(,C"Integrated Y1")[949:2130]
x1 = 189.998
x2 = 367.148
i1 = 1
i2 = 1182
area = 15711.0141255
y0 = 97.26372
x0 = 189.998
dx = 266.2870525

[2013/7/25 20:40 "" (2456498)]

integ1

Input

iy = [Book1]Sheet1!(F1,F2)
type = 0 (math:Mathematical Area)
plot = 0

Output

oy = [Book1]Sheet1!(,C"Integrated Y1")[865:1559]
x1 = 189.776
x2 = 367.168

i1 = 1
i2 = 695
area = 15831.55078843
y0 = 98.13862
x0 = 189.776
dx = 263.38452965051

[2013/7/25 20:42 "" (2456498)]

integ1

Input

iy = [Book1]Sheet1!(G1,G2)
type = 0 (math:Mathematical Area)
plot = 0

Output

oy = [Book1]Sheet1!(,C"Integrated Y1")[1097:2278]
x1 = 189.855
x2 = 367.005
i1 = 1
i2 = 1182
area = 16151.3912115
y0 = 98.43286
x0 = 189.855
dx = 267.76552426898

[2013/7/25 20:44 "" (2456498)]

integ1

Input

iy = [Book1]Sheet1!(H1,H2)
type = 0 (math:Mathematical Area)
plot = 0

Output

oy = [Book1]Sheet1!(,E"Integrated Y3")[866:1549]
x1 = 189.88699
x2 = 367.03201
i1 = 1
i2 = 684
area = 16137.28779691
y0 = 98.42951
x0 = 189.88699
dx = 266.43836626764

[2013/7/25 20:45 "" (2456498)]

integ1

Input

iy = [Book1]Sheet1!(A,B)

```

type = 0 (math:Mathematical Area)
plot = 0
Output
oy = [Book1]Sheet1!(,F"Integrated Y4")[1018:2199]
x1 = 189.899
x2 = 367.049
i1 = 1
i2 = 1182
area = 10591.21477725
y0 = 98.30388
x0 = 189.899
dx = 200.24603754941

```

Table 5.2 Relationship between TGA and UV analysis

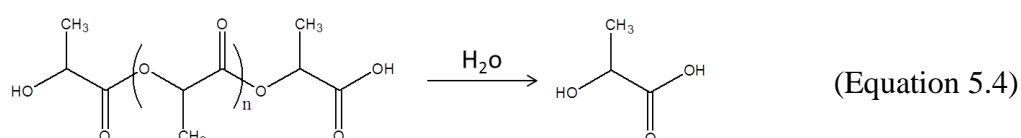
| | UV data (%) | TGA data | |
|---------|-------------|----------------|-----------|
| | | Area of curves | Ratio (%) |
| 3 hour | 5.05 | 15711.0 | 0.84 |
| 24 hour | 7.06 | 15831.5 | 0.86 |
| 3 days | 8.67 | 16137.4 | 0.91 |
| 7 days | 15.34 | 16151.3 | 0.93 |

5.2.6 The discussion on degradation mechanism

Based on the mechanism of polyesters degradation process, two types were categorized: bulk degradation and surface degradation. PLLA usually underwent bulk degradation. In the case of bulk degradation, water molecules penetrated into the matrix faster than polymer itself degraded. The bulk degradation process, it occurred at a uniform rate throughout the polymer matrix and therefore was considered as homogeneous. On the contrary, when polymers involved in surface or heterogeneous

degradation, the rate of water penetration into the matrix was slower than the rate of polymer degradation [9-11]. Because of the carboxylic end groups, bulk degradation rate could be enhanced by auto-catalysis. The biodegradation rate of polyesters depended on several factors, for example, the polymer crystallinity and purity, copolymer type (composition and initial molecular weight), sample size, pH and temperature of the degradation medium, processing and sterilization methods, as well as the presence of additives [11]. Previous explorations have been carried out for controlling the hydrolytic degradation of polyesters. It is important to understand the degradation characteristics of the polyesters to control their degradation rates according to certain purposes. Using additives for controlling polyesters, e.g., PLLA, degradation is performed in order to reduce microclimate pH, a result of carboxylic acid end groups during polyester hydrolysis.

In Figure 5.9, degradation schematic diagrams were shown to describe the whole degradation process for both pure PLLA nanofibers and keratin/PLLA nanofibers. For pure PLLA nanofibers, the degradation mainly came from the broken of terminal and backbone ester bonds. The chemical reaction was described as below:



Normally, the degradation of PLLA was slow and it took several months and years based on different molecular weight. After adding keratin, the degradation rate

increased due to the release of keratin from the composite nanofibers. After keratin precipitates left, the surface of keratin/PLLA became rough and porous. Water molecule could attack the PLLA polymer chain because of the more interface were unfolded between PLLA and water. The degradation rate could be controlled by adjusting the amount of keratin in the composite nanofibers and therefore the future drug controlled-release could be achieved by adjusting the weight ratio between keratin, PLLA and targeted drug model.

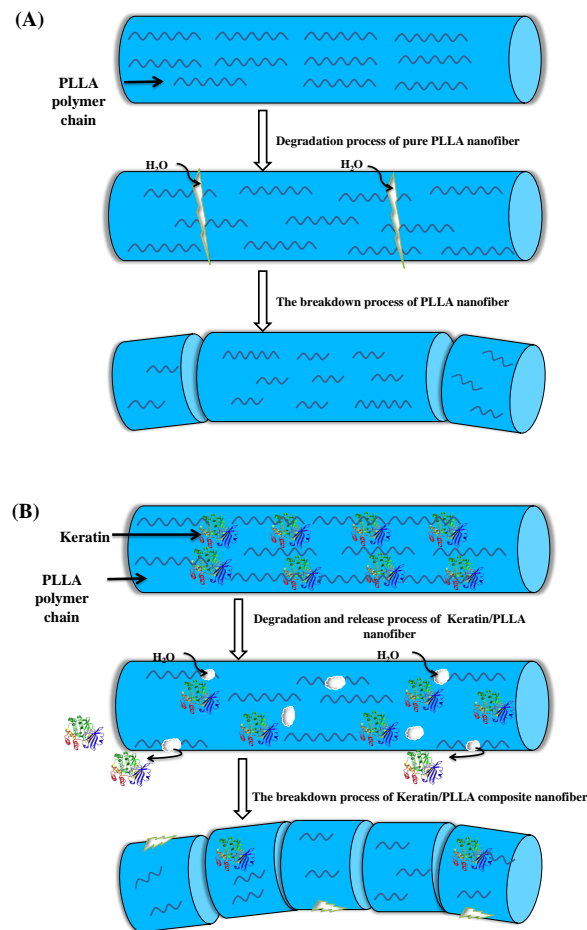


Figure 5.9 The schematic diagram of the degradation process of the composite nanofibers: (A) the pure PLLA nanofibers; (B) keratin/PLLA nanofibers.

5.3 Conclusion

In this part, the degradability of keratin composite nanofibers was examined using three different methods. Objective 3 was achieved by using different degradation evaluation methods. The degradation morphology of PLLA/keratin composite membrane was observed from SEM images. The thin fiber unfolded in the PBS solution. The UV spectra further indicated the degradation of keratin. In the first week, 15.34% of the keratin composition was released into the PBS solution. The FT-IR spectra demonstrated the same degradation by comparing the characteristic peaks of keratin. The thermal property of the membrane was tested by TGA. The results indicated that in comparison to previous keratin composite membranes, the present study successfully explored keratin/PLLA membrane with longer degradation periods. The new fabrication method improved the stability of the fibrous membrane. Since keratin offers affinity between tissues and scaffolds, sustained release of keratin could be beneficial for its future application, e.g. controlled drug release and cellular responses.

CHAPTER 6 INVESTIGATION ON KERATIN AND POLY(L-LACTIC ACID) ELECTROSPUN NANOFIBROUS ANTI-TUMOR DRUG DELIVERY SYSTEM

In Chapter 6, Objective 4 aims to be achieved through the study of a localized drug delivery system. Compared to the nanofibers discussed in previous chapters, a tetra-component nanofibrous system was built by introducing a drug model, e.g., 5-Fluorouracil. The composite polymer-protein nanofibers containing a hydrophilic drug, e.g., 5-Fluorouracil were electrospun and characterized to explore the chemical properties, physical properties and drug release properties. The morphology of composite nanofibers was observed by SEM and TEM. The combination forces status of the drug and keratin was explored by Zeta potential analysis. The crystallinity status of the drug in the composite nanofibers was investigated by XRD analysis. TGA curves revealed the thermal properties of the tetra-component nanofibers. The biofunction of keratin composite nanofibers in controlled drug release was studied. The in vitro drug release performances were examined within a period of 120 hours. Finally, the drug release mechanism was revealed by fitting the drug release curves.

6.1 Materials and methods

6.1.1 Materials

N, N-dimethylformamide (DMF) was purchased from Acors (Belgium). The targeted drug model 5-Fluorouracil was purchased from Sigma USA. PLLA polymer with the inherent viscosity of 7.0 dl/g was supplied by PURAC (Netherlands). The phosphate

buffer powder (pH 7.4) was purchased from Sigma USA. All samples were vacuum dried at 60 °C for 12 hours to remove solvents before characterization.

6.1.2 Preparation of the drug-loaded nanofibrous system

The keratin precipitates were prepared following the routines discussed in Chapter 3. PLLA was dissolved completely at the concentration of 1.0 wt. % in a mixed organic solution of 90 wt. % chloroform together with 10 wt. % DMF. 5-FU was added into keratin alcohol precipitates. The 5-FU/keratin suspension was blended with PLLA organic solution to form an electrospinning suspension. The electrospinning suspension was loaded into a syringe with a metal capillary which was connected to high-voltage electricity at 22 KV. The feeding rate of the suspension from the syringe was set at 0.4 ml/min. The distance between the capillary and the receptor, grounded aluminum foil, was 10 cm. Pure PLLA membrane was electrospun as the control under the same experimental conditions.

6.1.3 Morphology of the drug-loaded nanofibrous system

The morphology of the nanofibers was observed by Scanning Electron Microscopy (SEM) (Netzch STA 449C Jupiter). The samples being tested were pure PLLA membrane, keratin/PLLA membrane and 5-FU/keratin/PLLA membrane. The structural morphology of nanofibers was observed by Transmission Electron Microscopy (TEM) (JEOL Model JEM-2011).

6.1.4 Chemical structure analysis of the drug-loaded nanofibrous system

The chemical structure and molecular interactions of the anticancer drug with PLLA of the membranes were examined by FT-IR spectra in transmittance mode. The wavenumber (cm^{-1}) of absorption bands or peaks in specific regions corresponding to characteristic stretching vibrations of specific group wave-numbers can be examined in detail. The FT-IR wave number was set from 4000 to 500 cm^{-1} during eight scans, with 2 cm^{-1} resolution (Paragon 1000, Perkin-Elmer, USA). The FT-IR spectra were normalized and the major vibration bands were attributed to the specific chemical groups. The samples being tested were pure PLLA membrane, keratin/PLLA membrane, 5-FU/keratin/PLLA membrane and pure 5-FU.

6.1.5 Thermal properties of the drug-loaded nanofibrous system

Thermo-gravimetric analysis differential scanning calorimeter (Netzch STA 449C Jupiter) was used to examine the thermal properties of keratin/PLLA fibrous membrane. The samples being tested were pure PLLA membrane, keratin/PLLA membrane, 5-FU/keratin/PLLA membrane and pure 5-FU. The pure 5-FU and pure PLLA were tested as a positive and negative control respectively.

6.1.6 Zeta potential analysis

The zeta potential and translational diffusion coefficient measurements of dispersions containing keratin and 5-FU/keratin samples were carried out using a dynamic light scattering instrument (Malvern Zetasizer Nano ZS, Worcestershire, UK) at room

temperature, i.e., 25 °C. Ethanol was applied as a dispersant for all samples during both measurements to mimic the synthesis process of keratin alcohol precipitates and 5-FU/keratin suspension. Keratin and 5-FU/keratin samples were dispersed at a weight ratio of 0.1% in ethanol. The concentrations of electrospun keratin samples in ethanol were calculated automatically and presented in. Equation 6.1 describes the factors which may affect the zeta potential.

$$\zeta = \frac{dU}{dp} \times \frac{\eta}{\varepsilon \times \varepsilon_0} \times K \quad (\text{Equation 6.1})$$

where ζ is the zeta potential, dp is the pressure, and η represents electrolyte viscosity, ε_0 the vide permittivity and ε the electrolyte electric constant [151].

6.1.7 In vitro release experiments of the drug-loaded nanofibrous system

Nanofibrous samples that were prepared were incubated in 500 ml phosphate buffer solution (PBS, pH7.4) at a constant temperature of 37.0 °C. At predetermined intervals, a preset amount of PBS solution was collected and the same amount of fresh PBS solution was added into the sample bottles for further release. In the whole experimental process, the volume of PBS solution in the sample bottles was kept at a constant level. By using the incubated solution of blank fiber as control, the 5-FU concentration in the release solution was monitored by a UV-VIS spectrophotometer at 265 nm according to the calibration curve of 5-FU in the same buffer. The accumulative release of 5-FU from the nanofibers was calculated as the function of incubation time.

6.2 Results and discussion

6.2.1 Morphology of the composite nanofibers

Nano-scaled electrospun fibers were produced from a solution of polymers. Polymer concentration, electrospinning voltage and solution conductivity mainly influenced the spinability of electrospinning solutions. A high voltage was applied to a droplet of polymer solution at the end of a metallic needle, or spinneret. Then the droplet stretched until a critical point was reached. A stream of liquid then burst from the droplet surface, forming a Taylor cone. Under favorable conditions, the stream of polymer solution was continuous, and the solvent evaporated while the nanofibers were in flight. In the typical case the fibers were then deposited on an electrically grounded collector, which was usually cylindrical. In the present study, the process usually produced smooth fibers with a diameter range of 0.7-1.8 μm . Nanofibrous membranes can be fabricated by collecting the nanofibers on a grounded surface. The nanofibrous membrane had a large surface area and porosity in comparison to bulk matter. Synthetic polymers were usually simpler to be processed than natural polymers and were more likely to yield controlled nanofiber morphology.

As shown in Figure 6.1, superfine composite nanofibers were observed. Due to the ethanol treatment of keratin, the prepared electrospinning solution contained a certain amount of ethanol. Since the force that caused the stretching of the solution can be attributed to the repulsive forces between the charges on the electrospinning jet, and the stretching process was enhanced due to the increase of solution conductivity.

electrospinning technology was applied to prepare nanofibrous scaffolds. The microstructure and morphology of nanofibers and scaffolds should not or only slightly change during the modification. As shown in Figure 6.1, after each step of treatment, the surface morphology of modified PLLA scaffolds was analyzed by SEM and it can be observed that the nanofiber diameters maintained very well and surface smoothness changed. The surface of the pure PLLA nanofibers was comparatively smooth. After adding keratin, the surface of the nanofibers remained the same. Then adding 5-FU still kept the original smooth surface. These images indicated that no aggregation or particles were induced during the synthesis process and electrospinning process.

The diameters of the nanofibers, however, appeared to be significantly different. The average fiber diameter of pure PLLA nanofibers was $1.89 \pm 0.06 \mu\text{m}$. The diameter of keratin/PLLA nanofibers decreased to $1.51 \pm 0.05 \mu\text{m}$. After adding 5-FU the average diameter of 5-FU/keratin/PLLA decreased to $0.82 \pm 0.04 \mu\text{m}$. The decreased diameter range of nanofibers was related to the viscosity of the electrospinning solution. The polymer weight ratio decreased most in a tetra-component electrospinning solution which led to thinner and finer nanofibers.

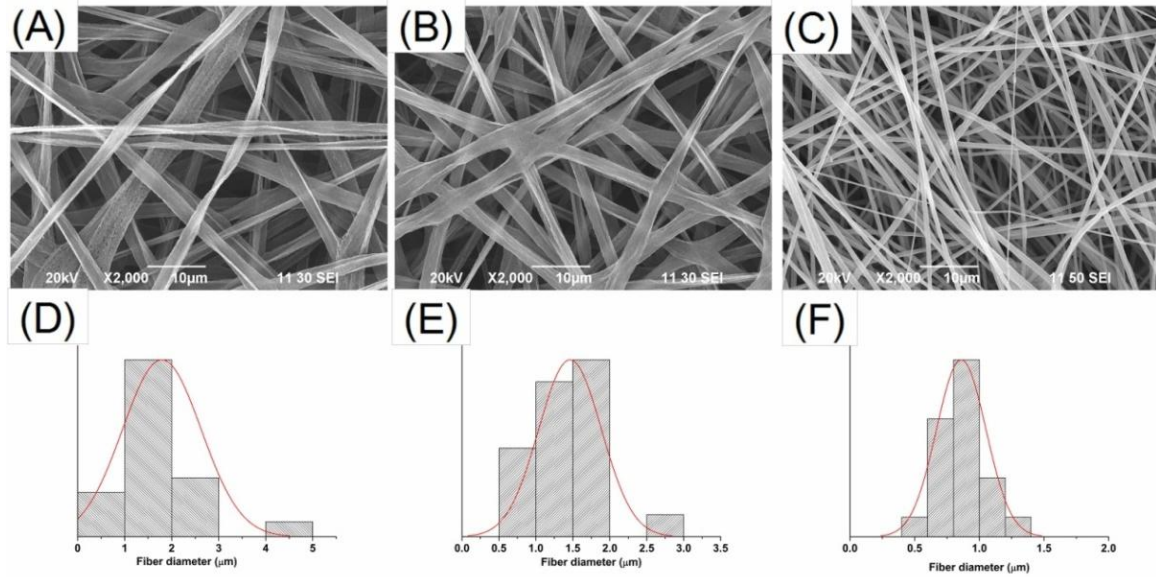


Figure 6.1 Morphology observation of different fibers and their corresponding diameter range: (A) SEM image of pure PLLA fiber; (B) SEM image of keratin/PLLA fiber; (C) SEM image of 5-FU/keratin/PLLA fiber; (D) Normalized histogram of pure PLLA fiber diameter; (E) Normalized histogram of keratin/PLLA fiber; (F) Normalized histogram of 5-FU/keratin/PLLA fiber diameter.

6.2.2 TEM morphology of the drug-loaded composite nanofibers

It is well-known that TEM images can be utilized to explore the inner structure of nanofibers. In order to verify the effect of the electrospinning process on the dispersion of the 5-FU molecules and keratin in the polymer matrix, a TEM technique was utilized to explore the inner structure of the electrospun nanofibers containing the 5-FU and keratin.

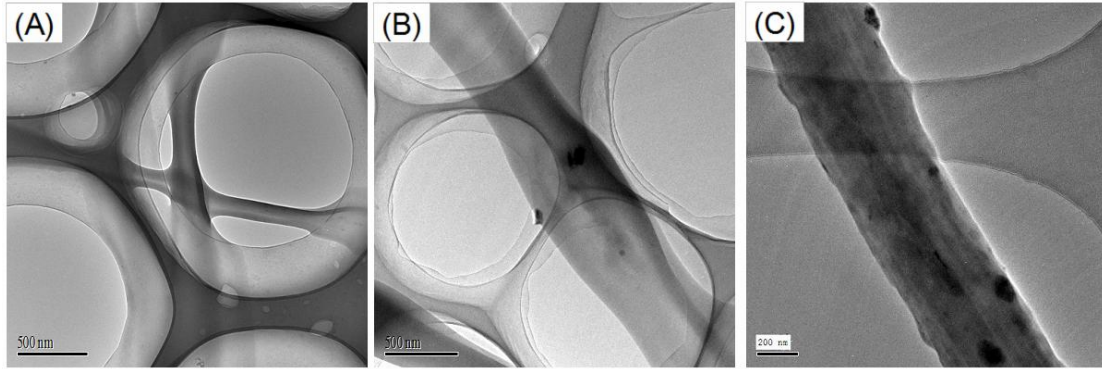


Figure 6.2 TEM images of the electrospinning nanofibers: (A) Pure PLLA composite nanofibers; (B) Keratin/PLLA composite nanofibers; (C) 5-FU/keratin/PLLA composite nanofibers.

In Figure 6.2, the TEM images of pure PLLA, keratin/PLLA nanofibers and 5-FU/keratin/PLLA nanofibers were observed respectively. Figure 6.2 (A) reveals the structure of pure PLLA electrospun nanofibers. Figure 6.2 (B) reveals the keratin/PLLA composite nanofibrous structure. There is a dark shadow dispersed with and within nanofibers. The phenomenon is evidence of keratin being dispersed amorphously together with PLLA fibers. Figure 6.2 (C) reveals the structure of 5-FU/keratin/PLLA drug-loaded nanofibers. The inside part of a single fiber is darker than the surface area. In the TEM image, the darker part reflects matter with higher density. Hence the TEM images indicate that the drug and keratin are more likely to disperse within the central part of the nanofibers. The reasons will be explained in later subsections.

6.2.3 Chemical structural evaluation by FT-IR Spectroscopy

The chemical structures of the drug-loaded composite electrospun membranes were revealed by FT-IR spectra as shown in Figure 6.3. Five groups of samples were tested, specifically described as: pure 5-FU, pure PLLA, 5-FU/PLLA nanofibers, keratin/PLLA nanofibers and 5-FU/keratin/PLLA nanofibers. The existence of 5-FU loaded into the composite nanofibers was detected by FT-IR spectra. The characteristic peaks of 5-FU include 3300 cm^{-1} (N-H stretch), 1730 cm^{-1} (C=O vibration), 1673 cm^{-1} (-C=O and -C=C overlapping peak of vibration), and 1247 cm^{-1} (-C-N vibration) [152].

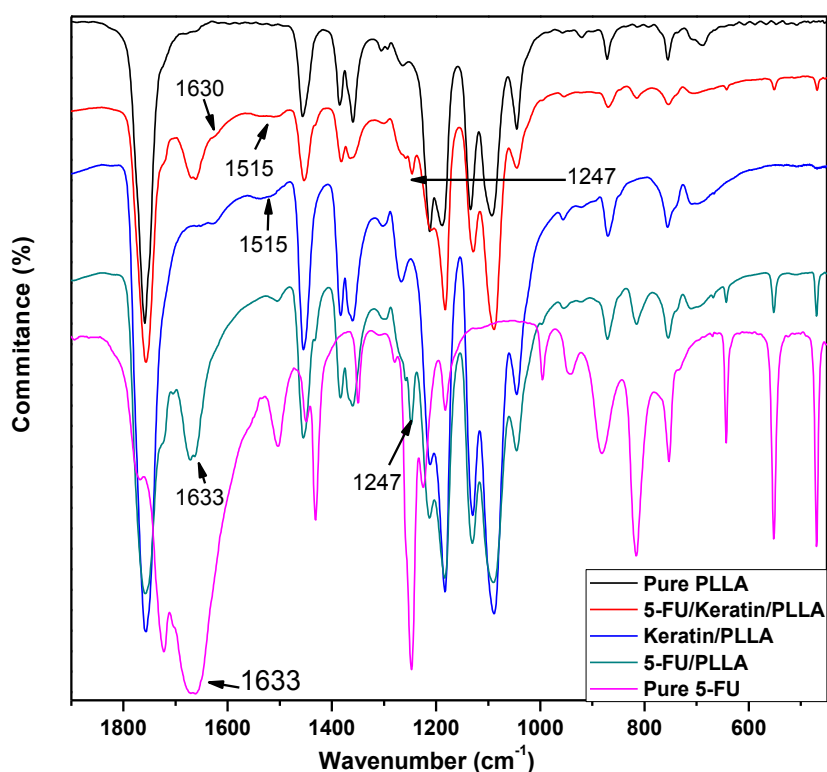


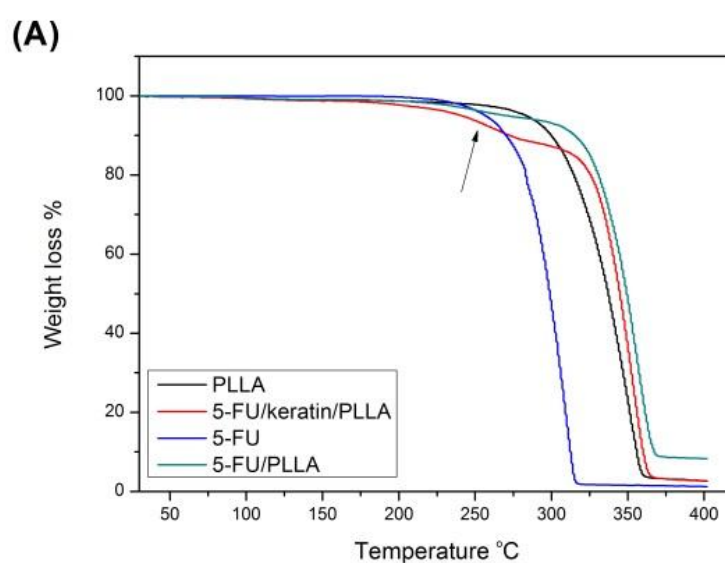
Figure 6.3 FT-IR spectra of electrospinning PLLA fibers, 5-FU/keratin/PLLA fibers, keratin/PLLA fibers, 5-FU/PLLA fibers and pure 5-FU powder. For PLLA/keratin composite membrane, two peaks appeared at 1630 cm^{-1} and 1515 cm^{-1} which belong to keratin.

In Figure 6.3, all three groups of samples: pure 5-FU, 5-FU/PLLA nanofibers and 5-FU/keratin/PLLA nanofibers displayed the certain peaks of 5-FU. The FT-IR spectra indicated that the anti-tumor drug, e.g., 5-FU, had been successfully introduced into the composite nanofibers through an electrospinning process. The basic chemical properties of 5-FU remained the same which indicated that 5-FU resisted the high voltage environment of the electrospinning process. The anti-tumor effect of 5-FU is another factor which will be examined and discussed in later chapters.

The existence of keratin was also detected from FT-IR spectra in three groups of samples: keratin/PLLA nanofibers, 5-FU/keratin/PLLA composite nanofibers. Since proteins are comprised of amino acids joined together by amide bonds, the polypeptide and protein units were repeating and produced different characteristic FT-IR absorption bands, e.g., amide A, B, and I-VII. Amide bands represent different vibrational modes of the peptide bond. In Figure 6.3, two absorption peaks can be observed at 1630 and 1550 cm^{-1} , which were the characteristic peaks of keratin respectively. They were believed to identify amide I and II bands of keratin. Amide I absorption peak, ranging from 1700 to 1600 cm^{-1} , was considered especially sensitive to the secondary structure of the proteins. The absorption peak at 1650 cm^{-1} indicated the presence of the α -helix structure; the bands related to the β -sheet structure fell in the range of 1631 to 1515 cm^{-1} . The peaks at low intensity of α -helix structure implied the disordered keratin conformation [153].

6.2.4 Thermal behavior evaluation by TGA-DTA diagrams

The thermal stability of electrospun PLLA, 5-FU/PLLA, 5-FU/keratin/PLLA and pure 5-FU blend nanofibers was measured using TGA in a nitrogen atmosphere. Figure 6.4 shows the TGA thermograms of different decomposition temperatures with different compositions. Three weight loss peaks were observed in the TGA curve. Because all the samples were dried before testing, the peak water vaporization which usually lies in the range of 25-95 °C was eliminated. For the pure 5-FU sample, a sharp peak could be observed at 305 °C which was the decomposition temperature of 5-FU. For the 5-FU/keratin/PLLA samples, a broad peak at 230-270 °C was due to the thermal degradation of both keratin and 5-FU, and the third peak at 300-400 °C was due to the byproduct formation of PLLA during the TGA thermal degradation process. For the 5-FU/keratin samples, a similar peak occurred at 230-270 °C. This peak appeared to be weaker than that of pure 5-FU due to the low weight ratio of the drug in nanofibers.



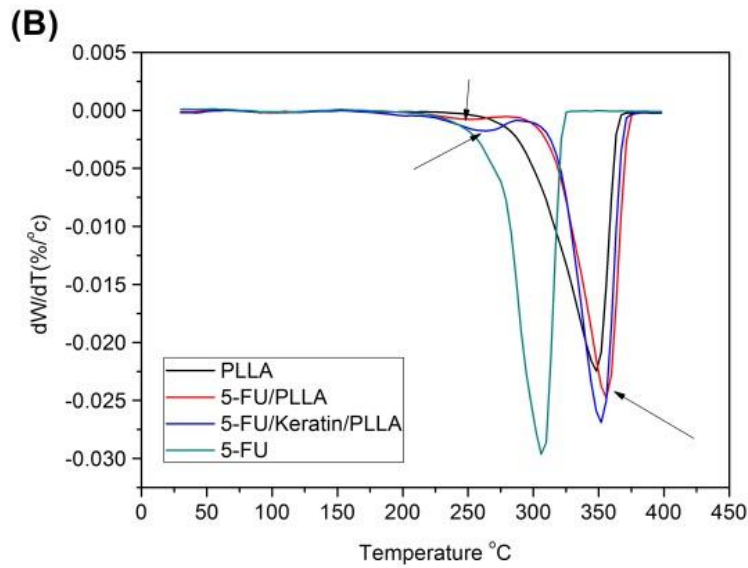


Figure 6.4 The thermal behaviors of different composite nanofibers: (A) TGA diagram of pure PLLA, 5-FU/PLLA, 5-FU/keratin/PLLA and pure 5-FU and (B) DTA diagram of PLLA, 5-FU/PLLA, 5-FU/keratin/PLLA.

Figure 6.4 (B) displays the similar thermograms trend of differential curves. It can safely reach to a conclusion that lower thermal stability at the mid-point temperature of the degradation of PLLA could be obtained with a higher mass ratio of keratin in the keratin/PLLA blend electrospun nanofibers. Moreover, with a higher percentage of keratin in the keratin/PLLA blend nanofibers, superior thermal stability could be obtained at higher temperatures (above 350 °C). In addition, the thermal stability of the composite nanofibers was measured using DTG in a nitrogen atmosphere. The lower most curve of the TGA data represents the PLLA/keratin blend without 5-FU and the upper most curve the composite nanofibers with 4 wt. % of 5-FU. Thermal stability is increased from the keratin/PLLA blend nanofibers in the polymer blends of the composite nanofibers. The higher thermal stability of 5-FU content material might

be attributed to the higher chain compactness in the polymer blend due to the protection of 5-FU which was encapsulated in the keratin/PLLA blend.

6.2.5 Crystallinity analysis of the composite nanofibers by XRD patterns

The XRD spectra in Figure 6.5 illustrates the crystal structure of pure PLLA, 5-FU/PLLA, 5-FU/keratin/PLLA and pure 5-FU. The physical combination of 5-FU, keratin and PLLA was examined as a control to explore the electrospinning process effect on the interaction between the anti-tumor drugs, keratin and PLLA.

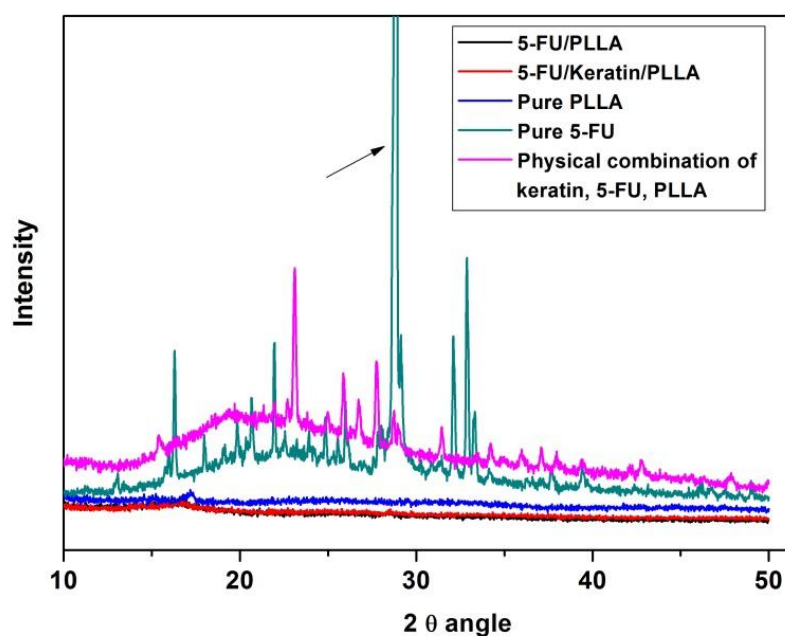


Figure 6.5 The XRD patterns of nanofibers with different compositions: pure PLLA, 5-FU/PLLA, 5-FU/keratin/PLLA and pure 5-FU. The physical combination of 5-FU, keratin and PLLA was examined as a control to explore the electrospinning process effect on the interaction between antitumor drug, keratin and PLLA.

As shown in Figure 6.5, 5-FU displayed the characteristic intense peaks at 2θ of 16.2° , 19.0° , 20.5° and 28.6° , indicating the typical crystalline structure [154]. For the pure PLLA samples, there existed no observable peak indicating an amorphous structure of PLLA. A physical blend of 5-FU powder, keratin and PLLA was introduced for comparison with the electrospun nanofibers to explore the crystalline transformation during the electrospinning process. The characteristic peaks of 5-FU still could be observed for the physically blended samples. However, after being processed by electrospinning technology, the peaks were eliminated for both 5-FU/PLLA nanofibers and 5-FU/keratin/PLLA nanofibers. The results revealed that there was a crystallinity transformation of 5-FU after being electrospun. A crystal structure shifted to a more amorphous structure. Even with the presence of 5-FU, both 5-FU/PLLA and 5-FU/keratin/PLLA nanofibers showed no peak for 5-FU, suggesting that 5-FU molecules are homogeneously dispersed within the PLLA layer at a molecular level without forming an evident crystalline structure [155].

6.2.6 Drug release profile of anti-tumor drug-loaded nanofibers

The cumulative release profiles of 5-FU from drug-loaded composite nanofibers and the pure 5-FU in a phosphate buffered solution (PBS, pH7.4) are shown in Figure 6.6.

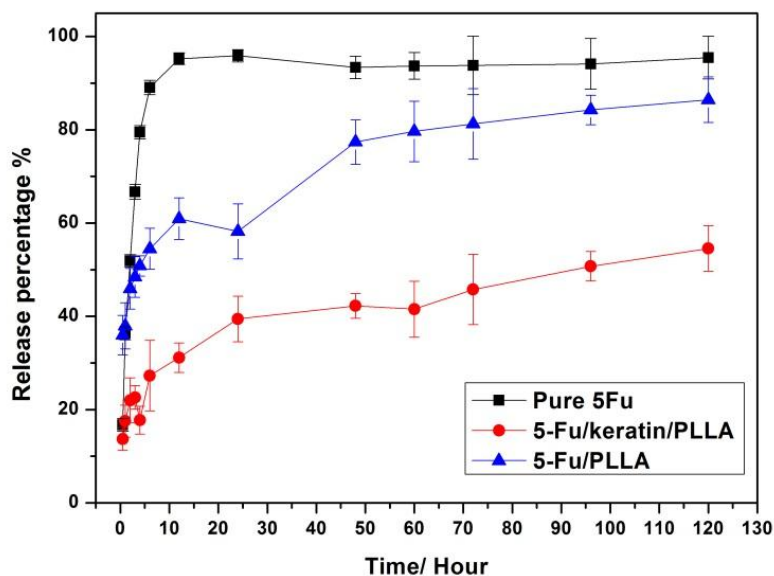


Figure 6.6 The controlled release profile of pure 5-FU, 5-FU/PLLA and 5-FU/keratin/PLLA nanofibers in PBS solution (pH 7.4) in a periods of 120 hours.

The amount of 5-FU was the same for all samples during the release experiments. As shown in Figure 6.6, the pure 5-FU was rapidly dissolved and released and the release amount reached 90% within 10 hours due to its strong hydrophilicity. However, a significant sustained release curve could be observed from the nanofibers sample. For the release of 5-FU loaded PLLA composite nanofibers, approximately 55% of 5-FU was released within the first 10 hours. Only 29% of 5-FU was released for 5-FU/keratin/PLLA composite nanofibers. It is clear that the release of 5-FU loaded composites was much slower than that of pure 5-FU. 5-FU/keratin/PLLA had the slowest release ratio of all which indicated that the tetra-component nanofibers prevented and hindered the burst release of 5-FU compared with bi-component nanofibers. After the burst release phase, the cumulative release curve of 5-FU

reached a flat release phase. The release profile for the drug-loaded composites can be described as follows. At the first stage, a burst release occurred. This burst release of 5-FU was associated with 5-FU molecules adsorbed or trapped near the surface of or close to the product's surface, which diffused out easily during the initial incubation time. The release of these molecules creates a concentration gradient, which favors the transportation of drug molecules toward this release boundary. The drug molecules from the inner part have to travel a greater distance, and therefore the release rate slows down with time. At the second stage, the inner drugs gradually diffuse to the buffer solutions through the carrier and reach release equilibrium by the end. Additionally, 5-FU/PLLA nanofibers released the drug relatively faster than 5-FU/keratin/PLLA nanofibers. As there is a certain charge interaction between 5-FU and keratin, the keratin molecules assemble and trap more 5-FU molecules towards the inner part of nanofibers during the electrospinning process due to a phase separation effect and static electric absorption effect. As a result, the 5-FU mainly laid within the centre of 5-FU/keratin/PLLA nanofibers and this led to the longer release time of 5-FU. Therefore, it was clear that the release of 5-FU/keratin/PLLA nanofibers was much slower than that of 5-FU/PLLA nanofibers. After 120 hours, the cumulative releases of 5-FU/keratin/PLLA nanofibers reached 50%. The result demonstrated that these composite nanofibers could be a suitable polymeric carrier for drug release in vitro.

6.2.7 Mechanism study on controlled release effect of the anti-tumor drug-loaded nanofibers

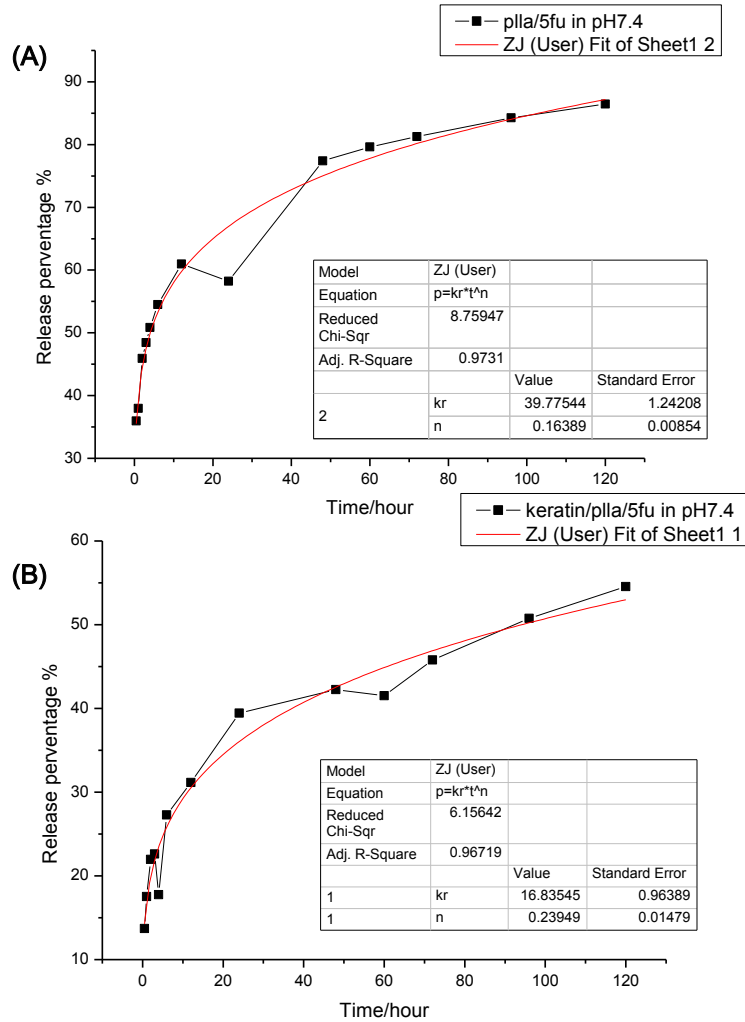


Figure 6.7 The fitted curves of drug release profile of (A) 5-FU/PLLA nanofibers, (B) 5-FU/keratin/PLLA nanofibers.

To determine the mechanism of the targeted drug release from nanofibers, the above in vitro release data were fitted to the Korsmeyer–Peppas kinetic model which were describer in equation (2) [156, 157].

$$\frac{M_t}{M_\infty} = \partial t^n \quad (\text{Equation 6.2})$$

Where θ is a constant incorporating structural and geometric characteristic of the drug dosage form, n is the release exponent, indicative of the drug release mechanism, and the function of it is Mt/M_{∞} .

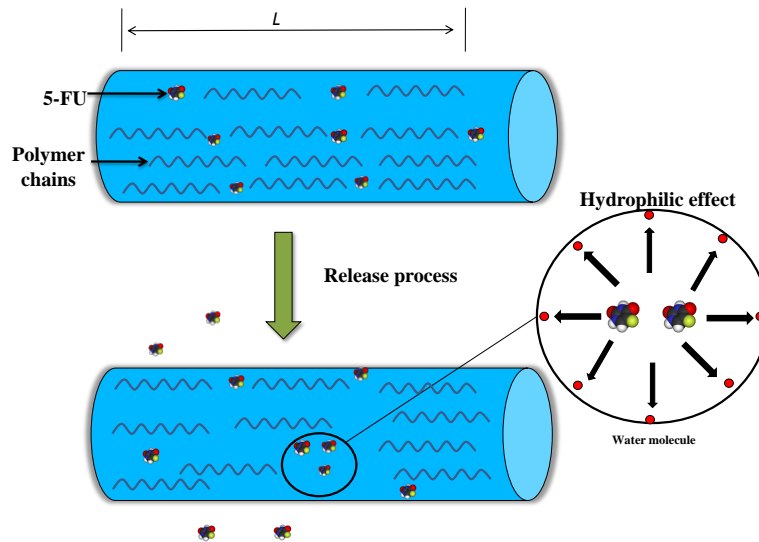


Figure 6.8 The mechanism diagram of the release profile of 5-FU/PLLA nanofibers.

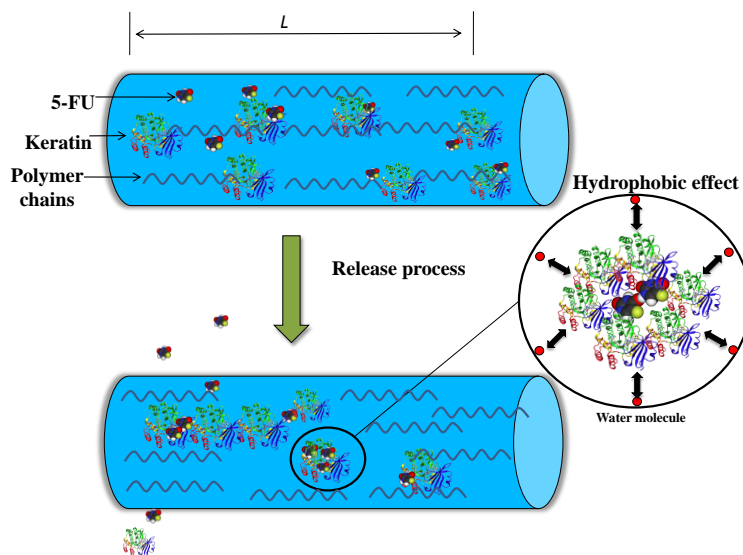


Figure 6.9 The mechanism diagram of the controlled release profile of 5-FU/keratin/PLLA nanofibers.

In Figure 6.8, the water molecule directly attacked the 5-FU molecules at the surface of the nanofibers. This caused the burst release of 5-FU. The 5-FU embedded within the nanofibers, however, had to wait for a long degradation periods to release due to the slow degradation rate of PLLA. The situation improved after adding keratin into the system. In Figure 6.9, 5-FU achieved a controlled and steady release from the 5-FU/keratin/PLLA nanofibers. In the fabrication process, because of the phase separation effect, 5-FU and keratin composites were likely to be repelled by the organic electrospun solution. The little amount of 5-FU left at the surface of nanofibers can avoid a burst release at some extent. After that, water molecules attacked the PLLA polymer chain and the inner 5-FU/keratin composites were contacted with the water molecules. As revealed by Zeta potential analysis, the static charge interaction occurred between 5-FU and keratin. Therefore, when contacting with water molecules, the hydrophobic keratin aggregated and 5-FU was surrounded by keratin and prevented from the hydra environment. Finally, after all the keratin released from the nanofiber, 5-FU begun to release from nanofibers. The controlled-release of 5-FU was achieved.

6.3 Conclusion

In this chapter, the objective 4 has been achieved. The drug loaded keratin composite nanofibrous membranes were fabricated successfully. The composite nanofibrous membrane, tetra-component nanofibrous membrane and pure PLLA membrane as the control group were fabricated by electrospinning technology. Detailed

characterizations examined both the physical and chemical properties of the composite nanofibers. The membrane morphology, chemical structure, degree of crystallinity, thermal stability zeta potential and drug release property *in vitro* were examined subsequently. The drug release mechanism of the 5-FU-loaded membrane and relationships among drug and keratin were identified. Morphology results indicated that the relationships between fiber diameters were inversely proportional to the composition of electrospinning solution. The FT-IR results suggested that 5-FU molecules were loaded successfully in the membrane and no chemical interaction occurred between 5-FU, keratin and PLLA. The XRD patterns revealed that that 5-FU was dispersed within both 5-FU/PLLA nanofibers and 5-FU/keratin/PLLA nanofibers. No characteristic peak of 5-FU could be observed after the electrospun process which indicated the dispersion of 5-FU reached to a molecular level. For the controlled release profile, 5-FU release more slowly in 5-FU/keratin/PLLA nanofibers than in 5-FU/PLLA nanofibers. The fitted release curves demonstrated the release profile followed the Korsmeyer–Peppas kinetic model.

CHAPTER 7 PH-RESPONSIVE CONTROLLED RELEASE PERFORMANCE AND ANTI-TUMOR EFFECTS OF THE COMPOSITE ELECTROSPUN MEMBRANE

In Chapter 7, Objective 5 aims to be achieved by optimizing the experimental factors which effecting the controlled release performance of the electrospun composite membrane in different pH environments. This chapter describes a full-factorial design with two factors at two-levels. The factors considered in the present study included: ratio of the two components in the membrane and fabrication electrospinning voltage. Keratin and PLLA are the two components of the membrane and the components ratio was set as 1:1 and 1:9. The fabrication electrospinning voltage was selected at two levels: 15 KV and 25 KV. Then the membranes with different processing parameters were tested under two different pH conditions: pH7.4 PBS solution and pH6.0 PBS solution. 5-fluorouracile was introduced in this experiment as the targeted drug model. This full-factorial design of the experimental method indicates that it is possible to not only identify the main effects of this complex bio-mimetic system, but also investigate the effects of two-factor interactions. The results illustrate that the ratio between two components is a main factor affecting controlled release performance. The result also indicates that this composite electrospun membrane can be used as a potential candidate for pH sensitive drug release materials.

7.1 Experiments and full factorial design

7.1.1 Sustained-release test in vitro

Different 5-FU-loaded fibers samples that were prepared were incubated in 500 ml phosphate buffer solution (PBS) (pH 7.4 and pH 6.0 respectively) at a temperature of 37.0 °C. At predetermined interval, a preset amount PBS solution was collected and the same amount of fresh PBS solution was added into the sample bottles for further release. In the whole experimental process, the volume of PBS solution in the sample bottles was kept at a constant level. By using the incubated solution of blank fiber as control, the 5-FU concentration in the release solution was monitored by UV–VIS spectrophotometer at 265 nm according to the calibration curve of 5-FU in the same buffer. The accumulative release of 5-FU from the fiber was calculated as the function of incubation time.

7.1.2 Full-factorial design of experiments method

The design of the experimental (DOE) method has been used frequently to examine the quality of products based on some essential design factors and levels during the manufacturing process. DOE has the structured and organized analysis capability. To explore the main and interaction effects of factors and obtain the maximum power density output, this study employs a full-factorial method with two factors and two-levels applied in two conditions. Table 7.1 displayed the matrix for design factors and their corresponding levels.

Table 7.1 Design factors and their levels

| Factors | Symbol | Units | Low | High |
|--------------------------------|--------|-------|----------|----------|
| | | | Level(-) | Level(+) |
| Ratio between Keratin and PLLA | B | N/A | 1:9 | 1:1 |
| Electrospun Voltage | C | KV | 15 | 25 |

The factors considered in this study include: 1) ratio of the two components in the membrane, and 2) fabrication electrospun voltage of the membrane. Two different pH value environments were introduced: pH 6.0 and pH 7.4. Keratin and PLLA were two components of the electrospun membrane and the components ratio was set as 1:1 and 1:9. The fabrication electrospun voltage was selected at two levels: 15 KV and 25 KV. 5-fluorouracile was introduced in this experiment as the targeted drug. Both the main effects of this complex bio-mimetic system and the effects of two-factor interactions were explored. Table 7.1 showed the experimental design and related response variables. Table 7.2 displayed the matrix design and experiments data.

Table 7.2 Matrix design and experiments data

| Run No. | Voltage | Ratio of keratin and PLLA(RKP) | Drug controlled release percentage at 24hours in pH6.0 PBS (%) (DR6.0) | | | Drug controlled release percentage at 24hours in pH6.0 PBS (%) (DR7.4) | | | Difference of DR6.0 and DR7.4 (%) (DDR) | | |
|------------|---------|--------------------------------------|---|-------|-------|---|-------|-------|--|-------|-------|
| | | | I | II | III | I | II | III | I | II | III |
| | | | 1 | -1 | -1 | 34.89 | 32.38 | 33.89 | 23.3 | 25.77 | 26.78 |
| 2 | +1 | -1 | 29.42 | 27.89 | 26.92 | 23.98 | 24.25 | 23.25 | 5.44 | 3.64 | 3.67 |
| 3 | +1 | +1 | 38.19 | 34.89 | 37.8 | 28.91 | 26.65 | 29.91 | 9.28 | 8.24 | 7.89 |
| 4 | -1 | +1 | 35.78 | 32.68 | 34.1 | 27.01 | 28.9 | 27.34 | 8.77 | 3.78 | 6.76 |

7.1.3 Anti-tumor activity by MTS assay

HCT-116 cells were seeded into 24-well plates (Nunclon™ Surface, Nunc, Denmark) at the density of $1 \times 10^4/\text{cm}^2$ and were cultured until become confluent. After the incubation with three parts of polypeptides for 24 hours, the cells were detached. Cells were then centrifuged, re-suspended into the medium contained 0.4% trypan blue (Invitrogen, U.S.A.) and the cells numbers were counted using haemocytometer (Precicolor HBG, Germany). The cell numbers were normalized by that of control group and expressed as the percentage of cell viability. HCT-116 are incubated at $37\text{ }^\circ\text{C}/5\% \text{CO}_2$ in DMEM or RPMI 1640 medium with 10% FBS and 100 IU/mL penicillin and 100 $\mu\text{g}/\text{mL}$ streptomycin. HCT-116 cells were plated on 96-well plates for 24 hours to reach 70% confluence (5000 cells, 10000 cells/well respectively). After washing with PBS, cells were incubated with either control culture medium or peptides contained medium for 24 hours. Medium was removed and the cells were washed with fresh PBS. 100 μl fresh medium was added to each well. MTS solution was added to each well in the ratio of 1:5. The plates were incubated at $37\text{ }^\circ\text{C}/5\% \text{CO}_2$ for 3-4 hours. Then, optical density (OD) values of the medium were evaluated at 492 nm using micro-plate reader.

7.1.4 Observation of anti-tumor activity by SEM

The HCT-116 cells were seeded in glass disks placed in 24-well plates at the concentration of 6×10^4 cells / cm^2 and allowed to grow for 4 hours, 24 hours, 72 hours and 120 hours, respectively. After incubation for 4 hours, 24 hours, 72 hours and 120 hours, cells on glass disks were fixed with 2.5% glutaraldehyde for 1 hour at room temperature followed by dehydration with a series of graded ethanol/water solutions (50%, 70%, 80%, 95% and 100% respectively). The samples were kept in fume hood

to dry at room temperature. The samples were coated with gold before observation under a scanning electron microscope (JEOL Model JSM-6490, Japan) to determine their morphology.

7.1.5 Anti-tumor activity by fluorescence images observation

For fluorescent observation, the cell contained glass disks were also gently washed with 37°C phosphate buffered saline, fixed with 4% paraformaldehyde in phosphate buffered saline at room temperature for 15 min, and permeabilized with 0.1% Triton X-100 in phosphate buffered saline for 5 min at room temperature. Then cells were incubated with 10 µg /mL TRICE-phalloidin in dark for 30 min, and the nucleuses of cells were additionally counterstained with 1 µg/mL DAPI in phosphate buffered saline. The glass disks were visualized using fluorescent microscope Eclipse 80i (Nikon, Japan).

7.1.6 Anti-tumor activity by cell live/dead observation

The cell permeable esterase-substrate fluorescein diacetate (FDA) and the cell nucleic acid stain propidium iodide (PI) were combined and used to assess the viability of HCT-116 grown on the coated disks. The HCT-116 cells were seeded in glass disks placed in 24-well plates at the concentration of 6×10^4 cells/cm². Cells were incubated at 37°C for 4 hours to allow cell attachment and then add 1 mL growth medium to each well to incubate for 4 hours, 24 hours, 72 hours and 120 hours respectively. Then the cells contained scaffolds were rinsed in phosphate buffered saline three times and the cells were stained by rinsing in the phosphate buffered saline that contained 1 µg/ml FAD and 1 µg/mL PI for 5 minutes at dark and room temperature. Images were taken by fluorescent microscope Eclipse 80i (Nikon, Japan).

7.2 Results and discussion

7.2.1 Morphology of the drug-loaded membranes after DOE

From Figure 7.1, differences of the nano-scaled structures could be observed due to the impacts of various factors. Figure 7.1 (A) revealed the structure of the membrane with a ratio between keratin and PLLA at 1:9. With the lower electrospinning voltage, the structure of the membrane tends to be formed more homogeneously. With a high voltage of 25 KV, as shown in Figure 7.1(C) and (D), both kinds of membranes with different compositions have more beads-shaped knots in the structures. These pictures indicated that a lower electrospun voltage and lower composition ratio between keratin and PLLA have more beneficial impacts on the uniformity of the membranes nano-scaled structures.

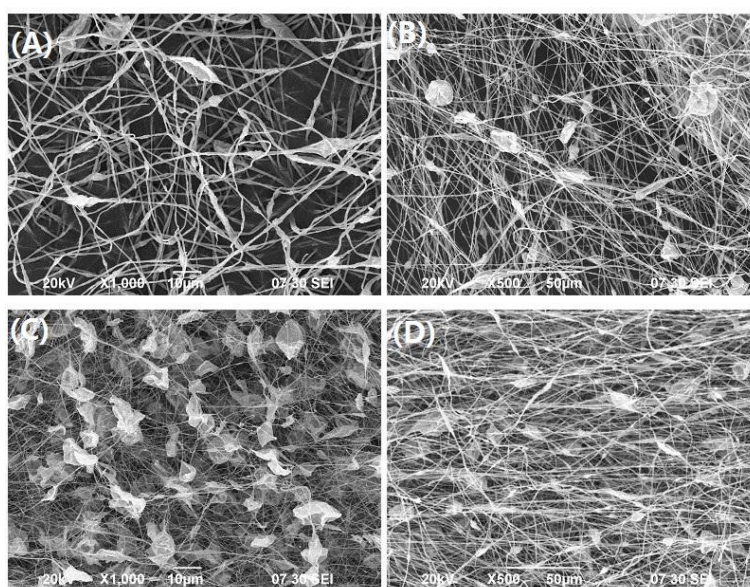


Figure 7.1 The morphology observation of the electrospun nanofibers in different parameters: (A) Ratio between keratin and PLLA is 1:9 at 15 KV; (B) Ratio between keratin and PLLA is 1:1 at 15 KV; (C) Ratio between keratin and PLLA is 1:9 at 25 KV; (D) Ratio between keratin and PLLA is 1:1 at 25 KV.

7.2.2 Full-factorial design results

A mathematical model describing the main effect and interactions of various factors on a given response variable could be defined by full factorial analysis. In the present study, two pH value environments have been introduced. Table 7.3 displayed the estimated effects and coefficients for controlled release in pH 6.0 PBS solution which was mimicking the acidic tumor environment. Table 7.4 displayed the estimated effects and coefficients for controlled release in pH 7.4 PBS solution which represented the healthy human organ environment. Table 7.5 illustrated the estimated effects and coefficients for controlled release differences between pH 7.4 PBS solution and pH6.0 PBS solution.

Table 7.3 Estimated effects and coefficients for controlled release in pH 6.0 PBS

| Term | Effect | Coefficient | SE Coefficient | T | P |
|--|--------|-------------|-------------------|--------|-------|
| Constant | --- | 33.23 | 0.4293 | 77.42 | 0.000 |
| Electrospinning voltage | -4.208 | -2.104 | 0.4293 | -4.900 | 0.001 |
| Ratio between keratin and PLLA(RKP) | 4.675 | 2.337 | 0.4293 | 5.450 | 0.001 |
| Voltage*RKP | 1.435 | 0.718 | 0.4293 | 1.670 | 0.133 |
| S = 1.48704 PRESS = 39.8032 R-Sq = 87.59% R-Sq(pred) = 72.08% | | | | | |
| R-Sq(adj) = 82.94% | | | | | |

Table 7.4 Estimated effects and coefficients for controlled release in pH 7.4 PBS

| Term | Effect | Coef | SE Coef | T | P |
|---|--------|---------|---------|--------|--------|
| Constant | --- | 26.33 | 0.3895 | 67.62 | 0.000 |
| Voltage | -1.098 | -0.5492 | 0.3895 | -1.410 | 0.1960 |
| RKP | 3.565 | 1.782 | 0.3895 | 4.580 | 0.0020 |
| Voltage*RKP | 0.3583 | 0.1792 | 0.3895 | 0.4600 | 0.6580 |
| S = 1.34918 PRESS = 32.7652 R-Sq = 74.31% R-Sq(pred) = 42.21% | | | | | |
| R-Sq(adj) = 64.68% | | | | | |

Table 7.5 Estimated effects and coefficients for controlled release difference between pH 7.4 PBS and pH 6.0 PBS

| Term | Effect | Coef | SE Coef | T | P |
|--|--------|--------|---------|--------|--------|
| Constant | --- | 6.898 | 0.5666 | 12.18 | 0.0000 |
| Voltage | -3.110 | -1.555 | 0.5666 | -2.740 | 0.0250 |
| RKP | 1.110 | 0.5550 | 0.5666 | 0.9800 | 0.3560 |
| Voltage*R KP | 1.077 | 0.5380 | 0.5666 | 0.9500 | 0.3700 |
| S = 1.96269 PRESS = 69.3385 R-Sq = 54.01% R-Sq(pred) = 0.00% | | | | | |
| R-Sq(adj) = 36.76% | | | | | |

Table 7.3 showed the sum of squares being used to estimate the factors' effect and the F-ratios, which were defined as the ratio of the respective mean-square-effect to the mean-square-error. The significance of these effects was evaluated using the t-test, and had a significance level of 5%. The P-value in Table 7.3 is 0.001 and 0.001 for the main effect and the interaction effects separately. $P < 0.05$ indicated that the main effects of each factor and the interaction effects were statistically significant.

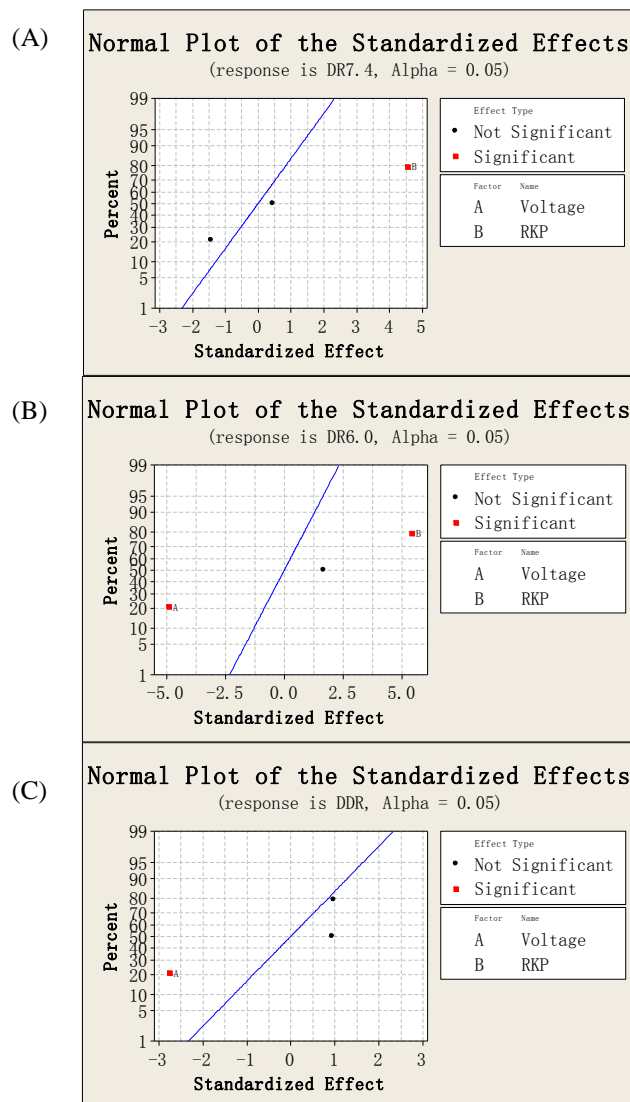


Figure 7.2 Normal probability plot of the standardized effects on drug controlled release: (A) Normal plot of the standardized effects of the membrane controlled release performances in pH 7.4 solution; (B) Normal plot of the standardized effects of the membrane controlled release performances in pH6.0 solution; (C) Normal plot of the standardized effects of the difference of the membrane controlled release performances in pH6.0 and pH 7.4 solution.

A normal probability plot of the standardized effects was used to determine the statistical significance of both main and interaction effect which is shown in Figure 7.2. As shown in Figure 7.2 (A), the ratio of keratin and PLLA had a significant

impact on the controlled release effect of composite membrane in the neutral environment. However, Figure 7.2 (B) illustrated that both the ratio of keratin and PLLA and electrospinning voltage played as significant impact factors on the controlled release performance of the composite membrane in the acidic environment. Figure 7.2 (C) displayed that the electrospinning voltage was a main factor in enlarge the difference of controlled release performances in different pH value environments.

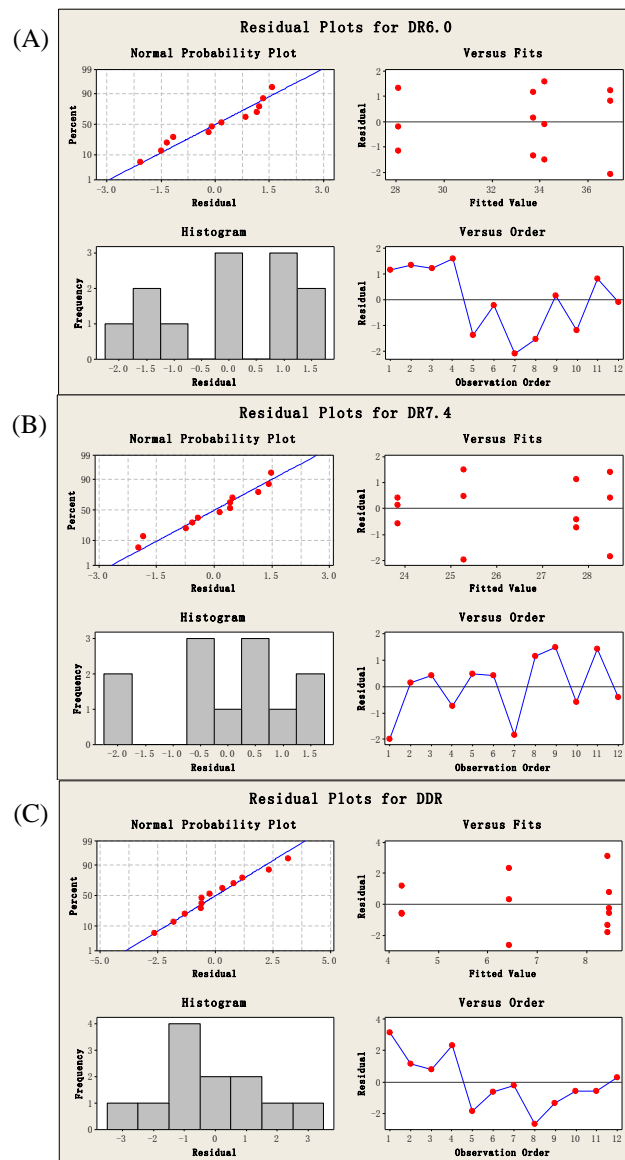


Figure 7.3 The residue plots diagrams for: (A) Controlled release performance in pH 7.4; (B) Controlled release performance in pH 6.0; (C) Differences of the controlled release performances in pH 6.0 and pH 7.4 solution.

After reviewing the regression output, it was necessary to review the fits and the residuals in the graphs. The residuals were the difference between the calculated release value and the observed value. It was necessary that the residuals are normally distributed in order for the regression analysis to be valid. The graphs in Figure 7.3 illustrated the shape of the residuals data – a histogram and a normal probability plot. These graphs could help to determine whether the residuals were normally distributed. It was necessary to perform a Normality test to determine it for sure. Since it was expected that a significant controlled release performance in different pH environment could be achieved, the ideal controlled release nanofibrous system was described as following: low drug release dosage in neutral environment (pH 7.4) and maximum drug release dosage in pH 6.0 which represented the existence of tumor cells.

In Figure 7.4 the main effects plot diagrams were displayed. In Figure 7.4 (A), in a more acidic environment, the electrospinning voltage had a negative impact whereas the ratio of keratin and PLLA had a positive impact to maximize the sustained drug delivery dosage. In a neutral environment as shown in Figure 7.4 (B), in order to minimize the release performance of the drug delivery system, increasing of the ratio of keratin and PLLA was considered as an important factor while the electrospinning voltage was insignificant factor to be considered in the membrane fabrication process. In Figure 7.4 (C), to enlarge the difference of the sustained release performances, voltage was considered a main element in the membrane fabrication process: increasing the electrospinning voltage could lead to a larger dosage difference in different pH-scaled environments. The main effects of each parameter on the controlled release performance are shown in Figure 7.4. The main effect plots were generated to represent the results of the regression analysis. It showed only the factors

that were significant at the 95% confidence interval. The main effects represent deviations of the average between the high and low levels for each factor. When the effect of a factor was positive, the rate increased as the factor changed from low to high levels. In contrast, if the effects were negative, a reduction in controlled release percentage occurred for high level of the same factor.

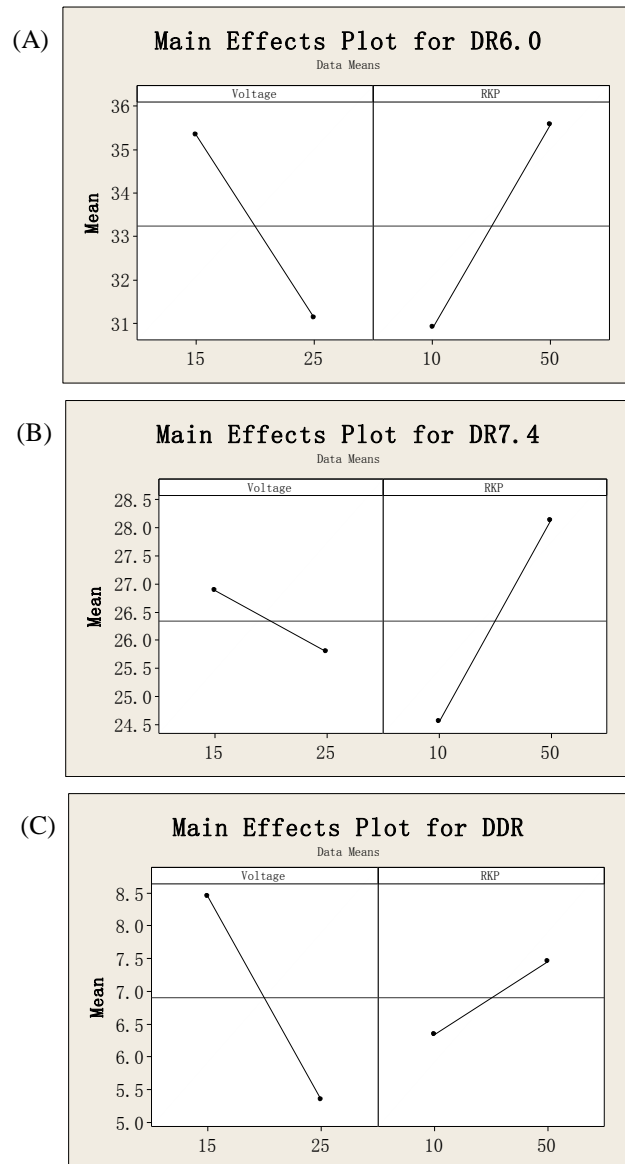


Figure 7.4 Main Effects plot (data means) for drug controlled release

7.2.3 Responsible surface design for drug controlled-release

After determining the model to be valid, the surface plots of the evenness versus two of the variables were generated. There were three variables and three surface plots that allowed us to qualitatively find a minimum or maximum for evenness. For each of the plots, the hold value on the parameters was set as: pH 7.4 (pH value), 0.1 (ratio between keratin and PLLA) and 15KV (electrospinning voltage) for a better controlled-release effect. Figure 7.5 illustrated the main factor effects of in different pH value environment concerning the drug controlled-release performance. In Figure 7.5 (A), the neutral environment required minimum release drug dosage. The trend of the color indicated that with higher electrospun voltage and lower ratio of keratin in the membrane, fewer drugs would be release into the environment PBS solution. On the contrary, in the acidic pH solution, a lower electrospun voltage and higher keratin composition ration in the membrane can lead to a large drug releasing dosage. To enlarge the drug dosage difference in different pH-scaled environment, Figure 7.5(C) compared the release result in both pH7.4 and pH6.0 and explored that lower electrospun voltage can contribute a more significant dosage difference in variable pH value environments.

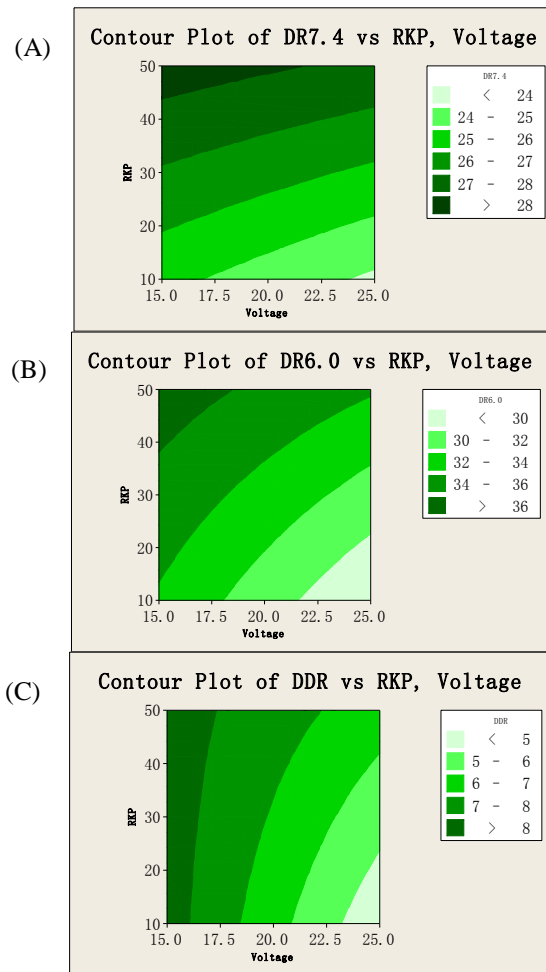


Figure 7.5 Contour Plot of Drug release per vs. ratio of keratin/PLLA and pH value of the environments.

Actually, the different drug sustained-release effect performance in different pH value environment indicated an important property of this composite membrane. The membrane endows the property of pH sensitivity. This can be utilized widely in the area of anti-tumor treatment. In terms of controlled drug release, ideally, anticancer drug should not be released during circulation in the bloodstream. However, a sufficient amount of anticancer drug should be released relative quickly to kill the cancer cells effectively while the drug arrived at the targeted site of cancer cells. The tumoral pH variation has been considered as an ideal trigger for the selective release of anticancer drugs in tumor tissues as well as tumor-targeted drug delivery. The pH

value of the normal tissue is approximately 7.4, while the existing tumoral pH generally decreased to pH 4.0-pH 6.0 [159, 160]. In Figure 7.6, a series of controlled release experiments demonstrated the pH sensitivity of the composite nano-fibrous membrane. Within the first 20 hours, a burst release could be observed from the membrane with higher keratin composition. After 20 hours release, a dramatic release performances difference could be observed from the membrane with lower keratin composition.

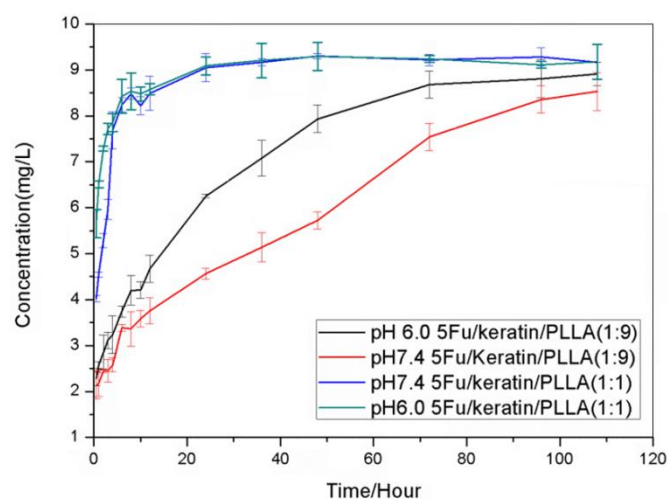


Figure 7.6 Different membranes sustained-release performances based on various parameters.

7.2.4 The antitumor activity results by cell live/dead assay

The fluoresces images displayed the cells proliferation performances on different nanofibers surfaces. The second columns represented the cells which are proliferated healthily and the third columns represented the cells which were dead. The last columns represented the overlaid images of both live cells and dead cells. Blank PLLA samples in this experiment worked as a control. Five groups of samples were tested and the whole experimental period was 120 hours. The predetermined time intervals were settled as: 4 hours, 24 hours, 72 hours and 120 hours. At those time

intervals, the cells proliferation morphologies were observed and analyzed. From Figure 7.7, the blank PLLA nanofibers provided preferable environments for tumor cells compared to PLLA/5-FU nanofibers, PLLA/keratin nanofibers and PLLA/keratin/5-FU nanofibers. These results indicated that both PLLA/5-FU nanofibers and PLLA/keratin/5-FU nanofibers had significant inhibition effect on tumor cells proliferations. Between these two groups, the PLLA/keratin/5-FU nanofibers possessed an enhanced and prolonged inhabitation on HCT-116 cells. This trend was increased after 120 hours cultivation.

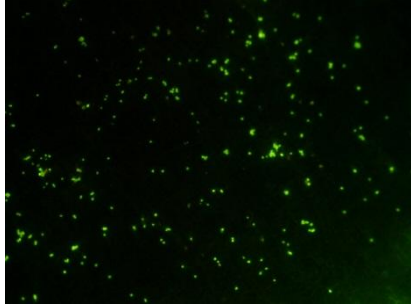
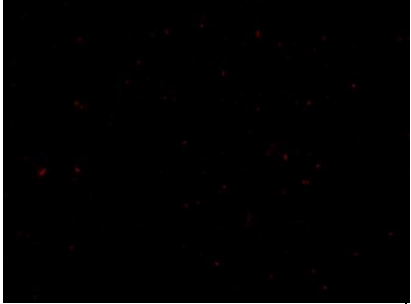
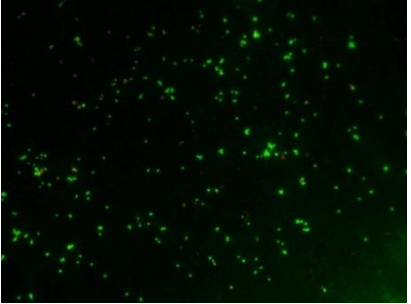
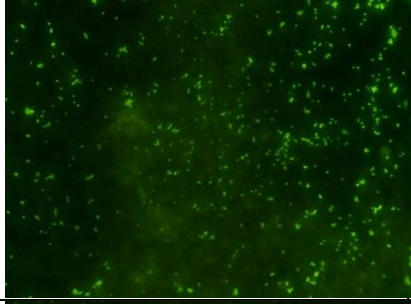
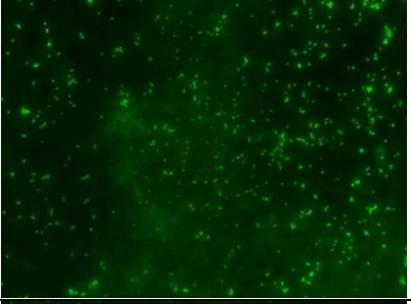
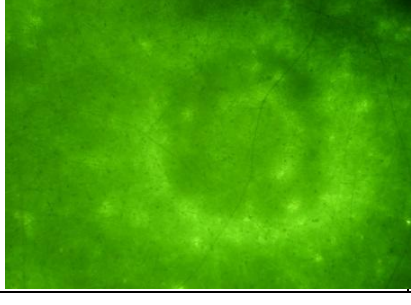
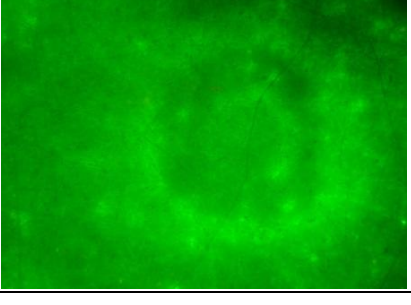
| Sample | Live | Dead | Overlay |
|-----------------------|---|--|---|
| PLLA |  |  |  |
| PLLA/5-FU |  |  |  |
| PLLA/Keratin |  |  |  |
| PLLA/keratin/ 5-FU |  |  |  |

Figure 7.7 Fluorescence micrographs of the cells stained with FDA (living cells), PI (dead cells) and overlaid images after seeding HCT-116 on the surface of the different nanofibers for 4 hours.

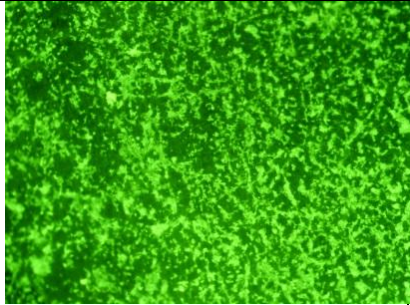
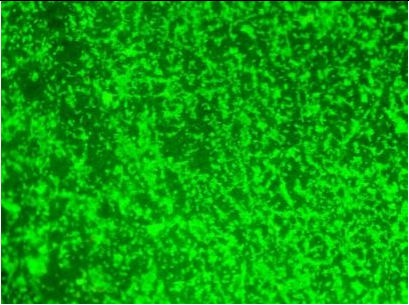
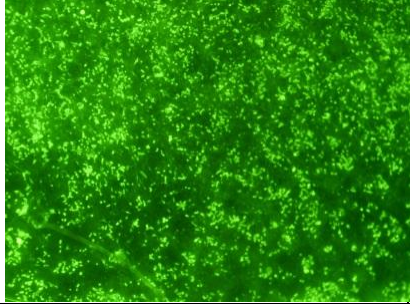
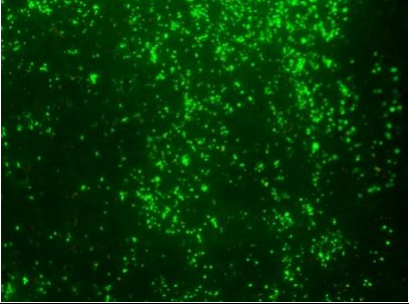
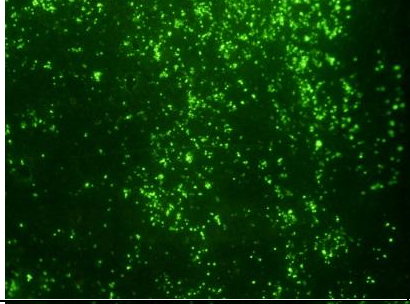
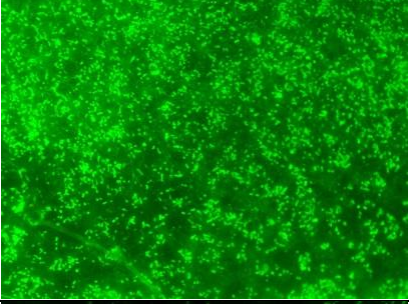
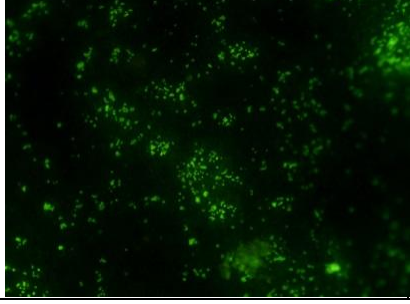
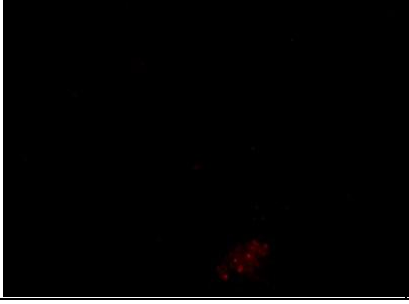
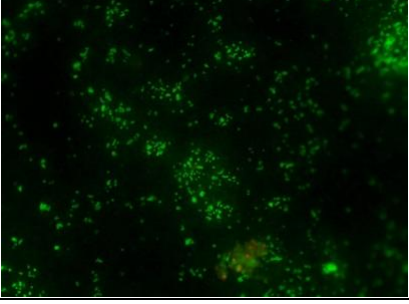
| Sample | Live | Dead | Overlay |
|-----------------------|---|--|---|
| PLLA |  |  |  |
| PLLA/5-FU |  |  |  |
| PLLA/Keratin |  |  |  |
| PLLA/keratin/ 5-FU |  |  |  |

Figure 7.8 Fluorescence micrographs of the cells stained with FDA (living cells), PI (dead cells) and overlaid images after seeding HCT-116 on the surface of the different nanofibers for 24 hours.

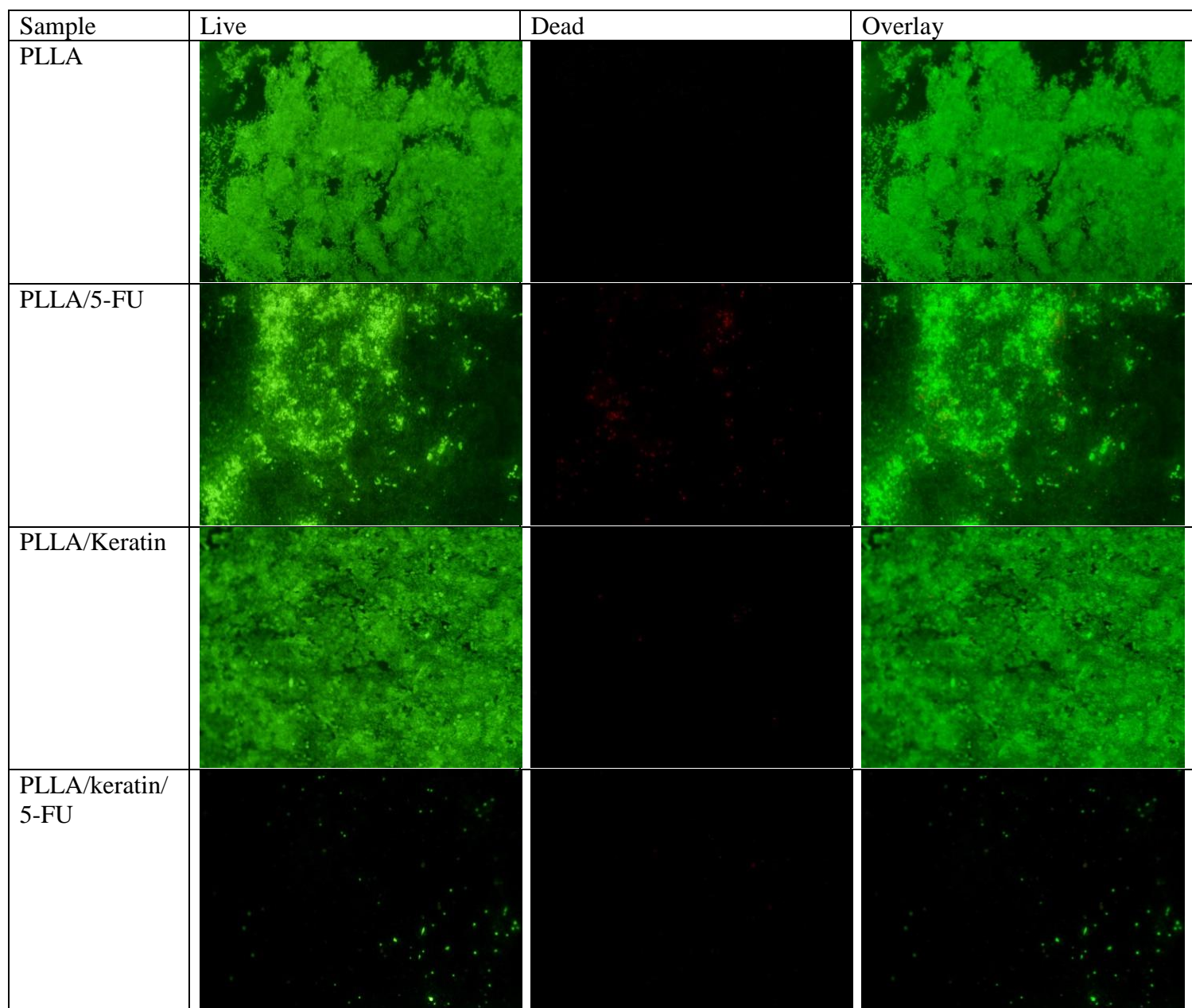


Figure 7.9 Fluorescence micrographs of the cells stained with FDA (living cells), PI (dead cells) and overlaid images after seeding HCT-116 on the surface of the different nanofibers for 72 hours.

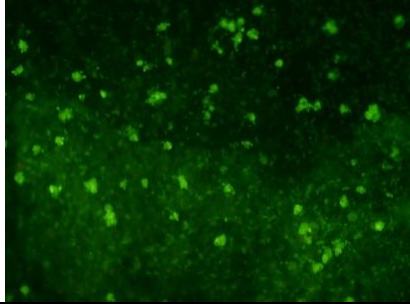
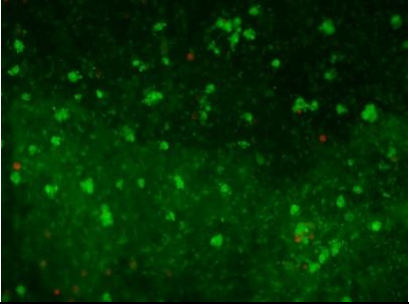
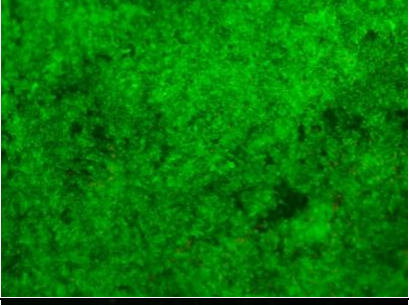
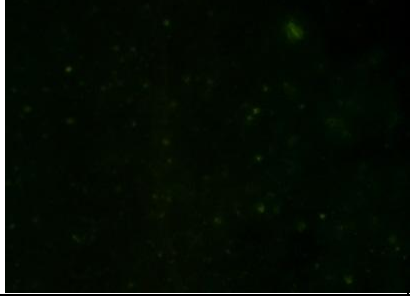
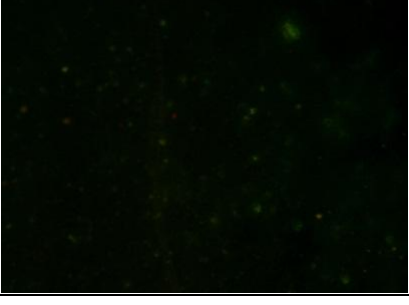
| Sample | Live | Dead | Overlay |
|-----------------------|---|--|---|
| PLLA |  |  |  |
| PLLA/5-FU |  |  |  |
| PLLA/Keratin |  |  |  |
| PLLA/keratin/ 5-FU |  |  |  |

Figure 7.10 Fluorescence micrographs of the cells stained with FDA (living cells), PI (dead cells) and overlaid images after seeding HCT-116 on the surface of the different nanofibers for 120 hours.

7.2.5 Anti-tumor activity results by DAPI staining for cellular adhesion and proliferation studies

In order to test the responses of HCT-116 tumor cells to different composite nanofibers samples, cells were cultured on the new scaffold containing: pure PLLA, PLLA/5-FU, PLLA/keratin and PLLA/keratin/5-FU. Double staining with FITC-phalloidin and DAPI was used to elucidate the cytoskeletal arrangement of HCT-116 cells. As shown in Figure 7.11, the cells responded differently to different compositions of the scaffolds. HCT-116 on the 5-FU loaded nanofibrous surface remained aggregated, presumably due to their poor adhesive interaction with the substrate. By contrast, HCT-116 cells cultured on blank PLLA showed well-dispersed cell bodies and extensive arborization. These results suggest an ability of 5-FU loaded nanofibers of inhibiting the tumor cells proliferation. Especially, cells on the PLLA/keratin/5-FU composite nanofibers showed a vague cytoskeleton shape which indicated the PLLA/keratin/5-FU composite nanofibers has a strong inhibition effect on the tumor cells. In Figure 7.11, the second columns represented the cells skeletons which were stained by TRICE-phalloidin and the third columns represented the cell nucleus which were stained by DAPI. The last columns represented the overlaid images of both cells skeletons and cells nucleuses. Blank PLLA samples in this experiment worked as a control. Four groups of samples were tested and the whole experimental period was 120 hours. The predetermined time intervals were settled as: 4 hours, 24 hours, 72 hours and 120 hours. At those time intervals, the cells proliferation morphologies were observed and analyzed. The staining images indicated that both PLLA/keratin/5-FU and PLLA/5-FU had anti-tumor activity on tumor cells proliferations. The PLLA/keratin/5-FU nanofibers had a stronger and more prolonged inhibition effect on the tumor cells proliferations.

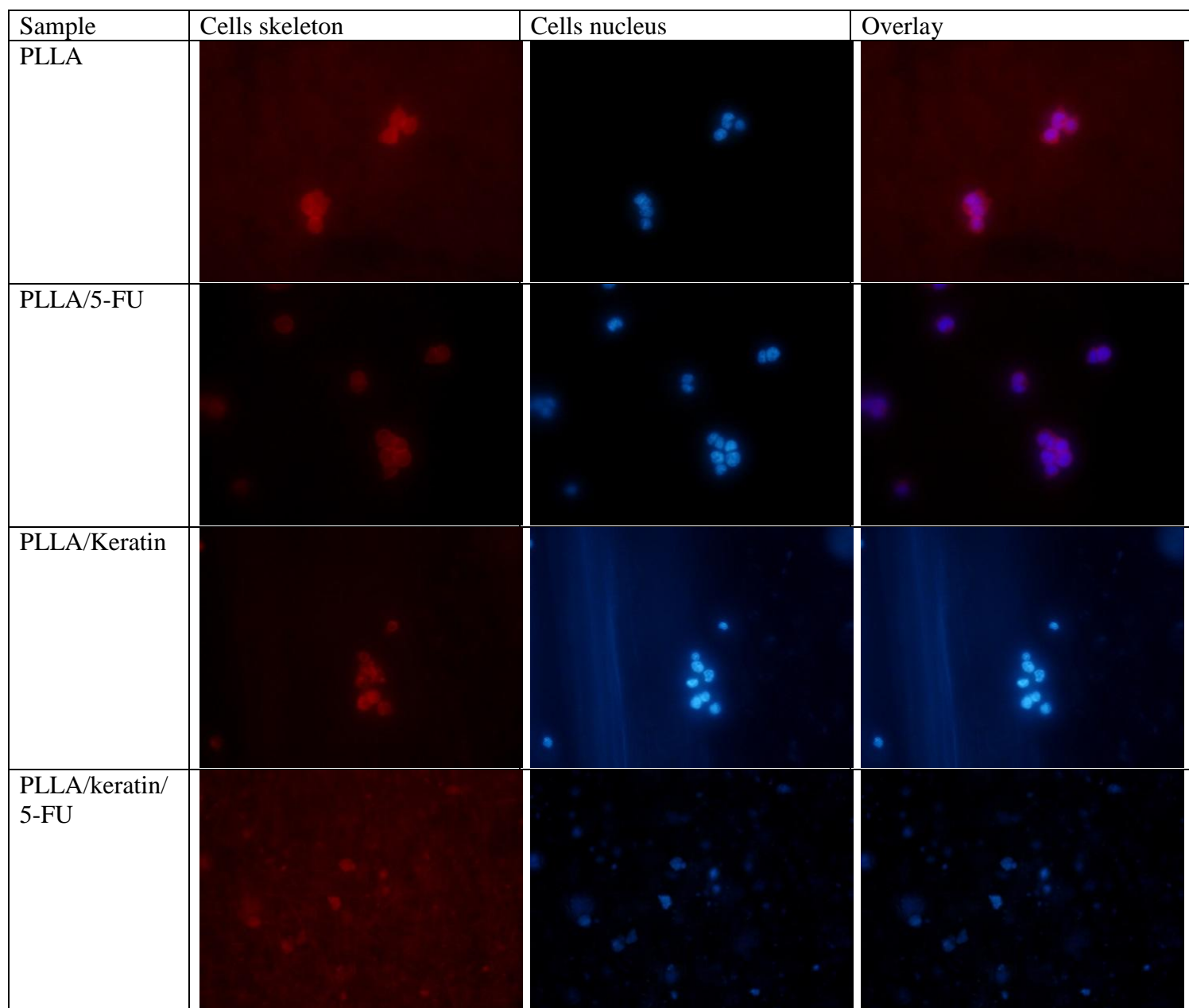


Figure 7.11 Fluorescence micrographs of the cells stained with DAPI (cell nucleus), TRICE-phalloidin (cell skeleton) and overlaid images after seeding HCT-116 on the surfaces of the different nanofibrous for 4 hours.

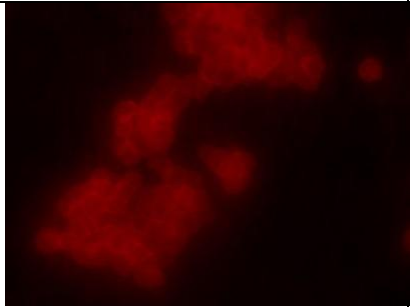
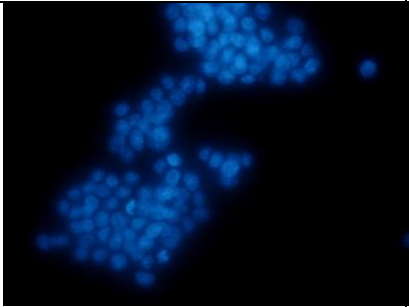
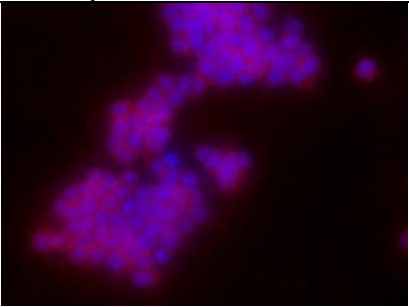
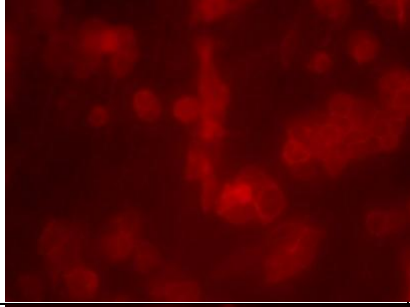
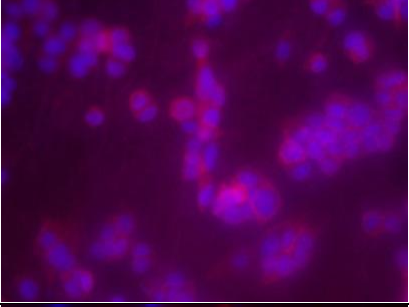
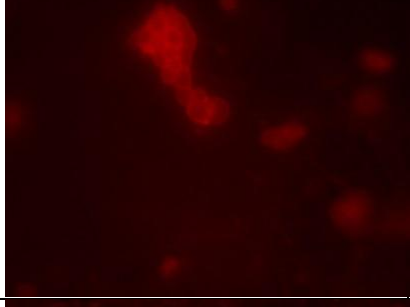
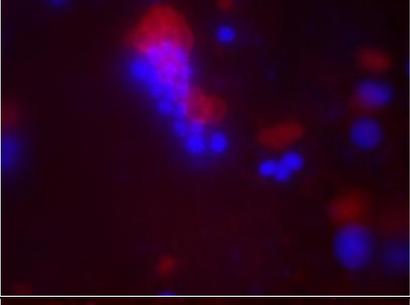
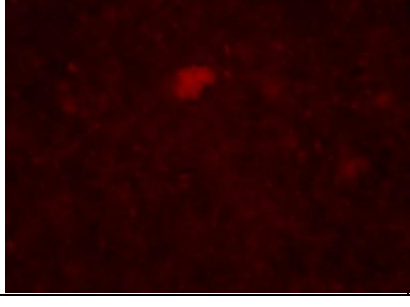
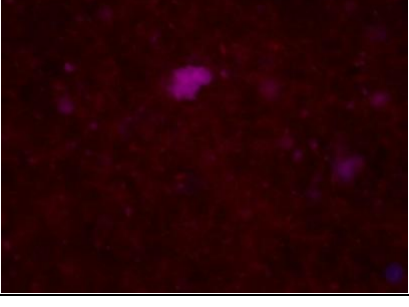
| Sample | Cells skeleton | Cells nucleus | Overlay |
|-----------------------|---|--|---|
| PLLA |  |  |  |
| PLLA/5-FU |  |  |  |
| PLLA/Keratin |  |  |  |
| PLLA/keratin/ 5-FU |  |  |  |

Figure 7.12 Fluorescence micrographs of the cells stained with DAPI (cell nucleus), TRICE-phalloidin (cell skeleton) and overlaid images after seeding HCT-116 on the surfaces of the different nanofibrous for 24 hours.

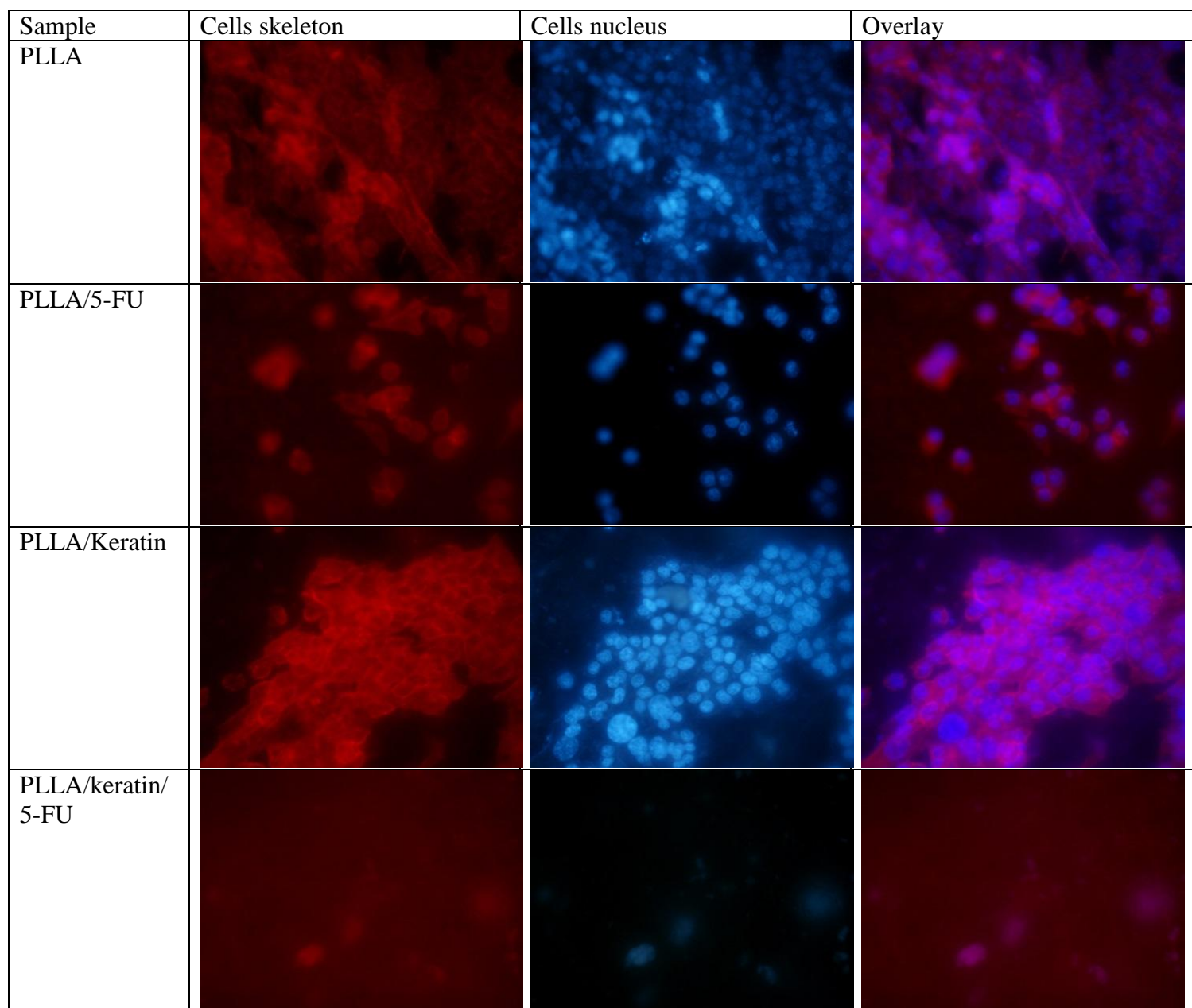


Figure 7.13 Fluorescence micrographs of the cells stained with DAPI (cell nucleus), TRICE-phalloidin (cell skeleton) and overlaid images after seeding HCT-116 on the surfaces of the different nanofibrous for 72 hours.

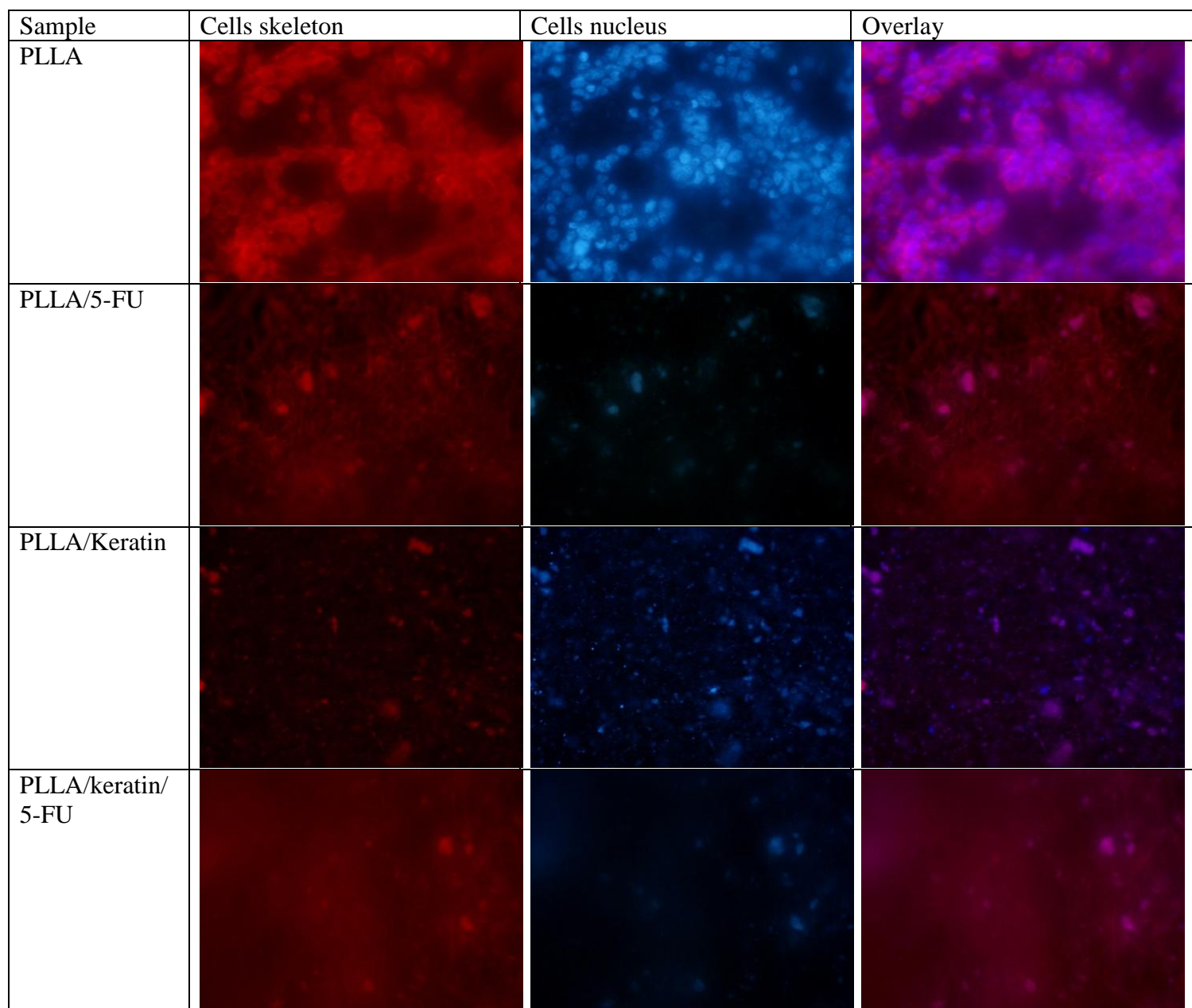


Figure 7.14 Fluorescence micrographs of the cells stained with DAPI (cell nucleus), TRICE-phalloidin (cell skeleton) and overlaid images after seeding HCT-116 on the surfaces of the different nanofibrous for 120 hours.

7.2.6 Anti-tumor activity results by MTS assay

The Anti-tumor activity was analyzed quantitatively by MTS assay. In Figure 7.15, a comparison between different composite nanofibers has been displayed. The total experimental period lasted to 120 hours. Pure PLLA nanofibers which fabricated at the same experimental conditions were employed as a control. Compared with pure PLLA nanofibers, both 5-FU/PLLA nanofibers and 5-FU/keratin/PLLA nanofibers possessed a more significant anti-tumor inhibition effects on HCT-116 cells. Keratin/PLLA nanofibers didn't show any anti-tumor inhabitation effect in the present study. Instead of inhibit the tumor cells, the function of keratin was to achieve the controlled-release of 5-FU. Without keratin, 5-FU could be released into the system fast and decayed soon since its half-life only last decade minutes in plasma [161]. After adding keratin, there was a significantly controlled release effect on 5-FU release profile. Hence, a prolonged and sustaining anti-tumor effect was observed in 5-FU/keratin/PLLA nanofibers.

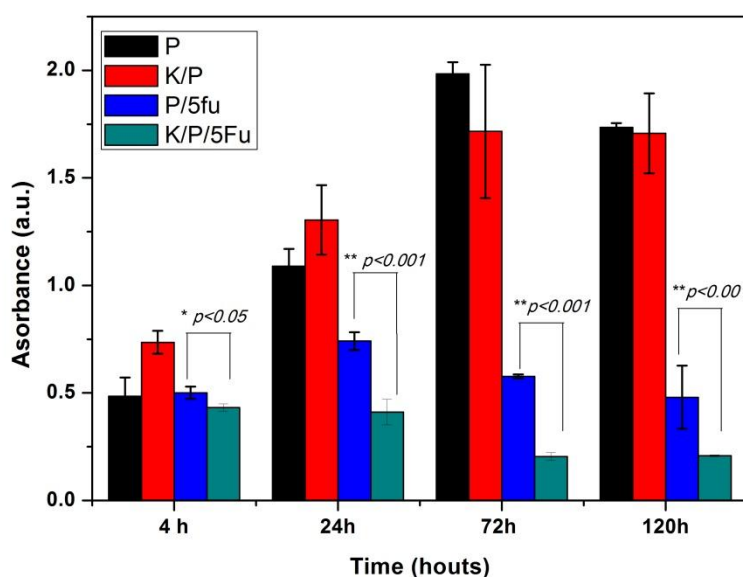


Figure 7.15 MTS assay of HCT-116 viability on different nanofibers surfaces. Statistical analysis revealed a difference between 5-FU/PLLA nanofibers and the

5-FU/keratin/PLLA nanofibers on the viability of MSCs (* $p < 0.05$; $n = 3$).

The potential anti-tumor mechanisms of both 5-FU/PLLA and 5-FU/keratin/PLLA nanofibers were described in Figure 7.16 and Figure 7.17. Instead of inhibit the tumor cells, the function of keratin was to achieve the controlled-release of 5-FU in the nanofibers. Without keratin, 5-FU could be released into the system fast and decayed soon since its half-life only last decade minutes in plasmas as described in Figure 7.17. After tumor cells attached on the surface of nanofibers, a burst-release occurred in the group of 5-FU/PLLA due to its lack the controlled-release component. After the burst-release, 5-FU decayed soon in the solution and its anti-tumor function was impaired after adding keratin, there was a significantly controlled release effect on 5-FU release profile. Hence, a prolonged and sustaining anti-tumor effect was observed in 5-FU/keratin/PLLA nanofibers. As discussed previously, both fluoresces images and the MTS assay results demonstrated the same trend, which was that the composite 5-FU/keratin/PLLA nanofibers can enhance the anti-tumor effect compared to 5-FU/PLLA nanofibers.

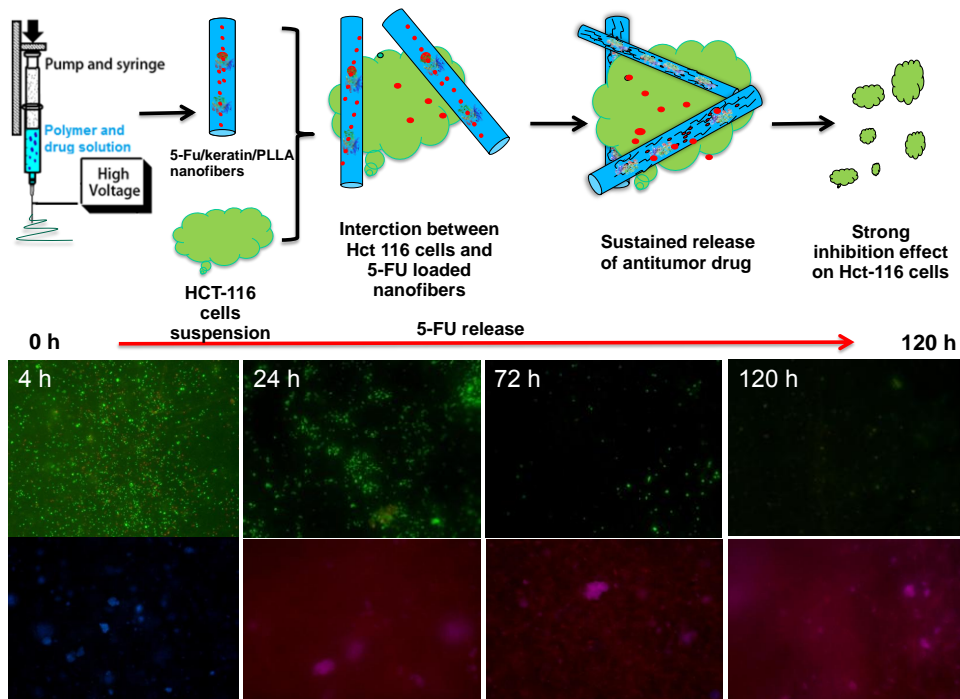


Figure 7.16 The schematic diagram of illustrating the interaction between HCT-116 cells and 5-FU/keratin/PLLA nanofibers.

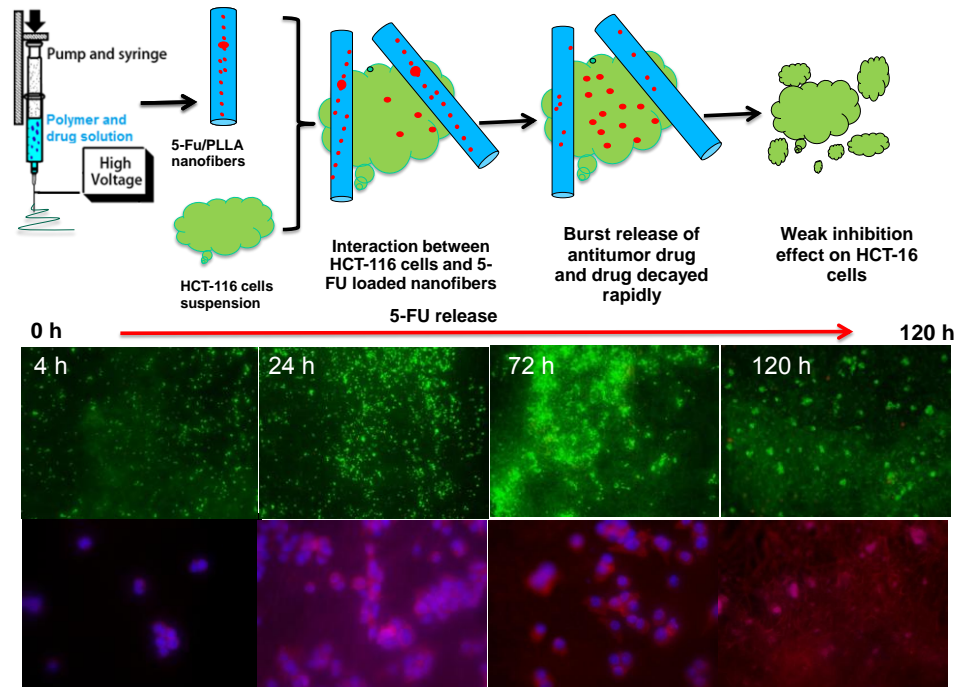


Figure 7.17 The schematic diagram of illustrating the interaction between HCT-116 cells and 5-FU/PLLA nanofibers.

7.3 Conclusion

In this chapter, Objective 5 has been completed. DOE design was applied to analyze and optimize the drug sustained release performance. Two factors were considered in the present study: ratio of the two components in the membrane and fabrication electrospinning voltage of the membrane. Two different pH value environments were introduced: pH 6.0 and pH 7.4. Keratin and PLLA were the two components of the membrane and the components ratio was set as 1:1 and 1:9. The fabrication electrospinning voltage was selected at two levels: 15 KV and 25 KV. 5-fluorouracil was introduced in this experiment as the targeted drug. This full-factorial design of the experimental method indicated that it was possible to not only identify the main effects of this complex bio-mimetic system, but also investigate the effects of two-factor interactions. The results indicate that the composite membrane has pH sensitivity and lowering the electrospinning voltage can lead to significant pH sensitive controlled release performance. The ratio between two components can affect the release performance in a neutral environment. The result suggests that nanofibrous composite electrospun membrane can be considered a preferable potential candidate for pH sensitive controlled drug release systems. The biological evaluation confirmed the anti-tumor activity of different composite nanofibers. After comparing fluorescent images and MTS assay, adding keratin helped to achieve the controlled drug-release model (e.g. 5-FU). The anti-tumor activity in a controlled release nanofibrous system was confirmed by cell live/dead assay, cellular adhesion, proliferation studies and MTS assay.

CHAPTER 8 INVESTIGATION OF ANTI-TUMOR NANOFIBROUS ELECTROSPUN MEMBRANE WITH ANTIMICROBIAL PEPTIDES

In this chapter, Objective 6 aims to be achieved by introducing antimicrobial peptides Attacin2 into the 5-FU/keratin/PLLA system. In traditional surgical operation treatments, infection would be hardly avoided. As a group of antimicrobial peptides (AMPs), Attacin possessed both anti-bacterial and anti-tumor function as been discovered. In this chapter, both the anti-tumor drug and AMP was introduced into the anti-tumor nanofibrous drug delivery system. The synergistic effect between anti-tumor drug and AMPs were investigated. The experimental results indicated that after adding the antimicrobial peptides into the membrane, the synergistic effect could be observed, especially after 72 hours observation. Unlike the chemical antitumor drug has a short and strong inhibition effect on tumor cells, the biological antimicrobial peptides has a long and sustained inhibition on tumor cells which compensates the short effect of chemical antitumor drugs. The experiments demonstrated that the synergistic effect between chemical antitumor drug and antimicrobial peptides could inhibit the proliferation of tumor cells. The results indicated the feasibility of combining both chemical antitumor drugs and biological antimicrobial peptides together, which suggested the further direction of applying nanofibers in the realm of antitumor therapy.

8.1. Materials and methods

8.1.1 Sample preparation

Attacin2, known as gloverin, is a group of AMPs containing high components of glycine but less of cysteine. The activity presented by this group is mainly to fight against gram-negative bacteria. Compared with another kind of AMPs, the molecular mass of Attacin2 is generally higher, which is around 20 kD. Two Attacin2 genes, *BmAttacin1* and *BmAttacin2*, have been found in silkworm which are synthesized primarily in fat body [162]. Traditionally, it is very difficult to isolate Attacin2 from the fat body of silkworm since it is a minor content group of inducible AMPs, even though their cDNA sequences already have been revealed [163, 164]. Heterologous expression is quite necessary for the further study to obtain this kind of protein. *E.coli* is a universal prokaryotic expression system for heterologous expression. In this study, we succeeded to clone the cDNA fragment encoding mature peptide of *BmAttacin2*(*MBmAttacin2*) into the prokaryotic vector pET28a(+) and obtain the *MBmAttacin2* after induced expression in *E.coli* [165]. The prepared Attacin2 samples were collected from other lab-mates.

The electrospun solutions with different components were fabricated on the square glass disks size in 0.64 cm^2 which were stick on the aluminum foil as nanofibers. The membranes were: pure PLLA membrane, PLLA/Attacin2 membrane, PLLA/keratin/Attacin2 membrane and PLLA/keratin/5-FU/Attacin2 membrane respectively. The electrospun parameters were followed strictly as same as the previous study in the present thesis. The coated glass disks and the films were placed in 24-well tissue culture plates (Nunc, Demark) and were sterilized by 70% ethanol for 24 hours in $4\text{ }^{\circ}\text{C}$. After that, they were rinsed in PBS three times and then

pre-warmed at 37 °C for 2 hours prior to cell seeding.

8.1.2 Cell culture

Colon cancer cells HCT-116, (Sigma, U.S.A.) were cultured in 25cm² culture flasks (SPL, Korea) with Dulbecco's modified medium (DMEM, Sigma, U.S.A.) in 37 °C, 5% CO₂. DMEM was supplemented with 10% fetal bovine serum (FBS, Caisson, U.S.A.), 1% penicillin-streptomycin solution (Caisson, U.S.A.) as growth medium. Cells were harvested by adding 0.25% trypsin with EDTA Tetrasodium (Caisson, U.S.A.). After cells were detached, trypsin was neutralized by adding growth medium. Cell suspension was then centrifuged, re-suspended with fresh medium and was counted using haemocytometer (Precicolor HBG, Germany) and were subcultured for particular experiments.

8.1.3 Fluorescence staining

For fluorescent observation, the cell contained glass disks were also gently washed with 37°C phosphate buffered saline, fixed with 4% paraformaldehyde in phosphate buffered saline at room temperature for 15 min, and permeabilized with 0.1% Triton X-100 in phosphate buffered saline for 5 min at room temperature. Then cells were incubated with 10 µg /mL TRICE-phalloidin in dark for 30 min, and the nucleuses of cells were additionally counterstained with 1 µg/mL DAPI in phosphate buffered saline. The glass disks were visualized using fluorescent microscope Eclipse 80i (Nikon, Japan).

8.1.4 Cell Live/Dead assay

The cell permeable esterase-substrate fluorescein diacetate (FDA) and the cell nucleic

acid stain propidium iodide (PI) were combined and used to assess the viability of HCT-116 grown on the coated disks. The cells were seeded in glass disks placed in 24-well plates at a concentration of 6×10^4 cells / cm^2 . Cells were incubated at 37°C for 4 hours to allow cells attachment and then 1 mL growth medium was added to each well to incubate for 24 hours and 72 hours. Then the cells contained scaffolds were rinsed in phosphate buffered saline three times and the cells were stained by rinsing in the phosphate buffered saline that contained $1\mu\text{g/mL}$ FAD and $1\mu\text{g/mL}$ PI for 5 minutes in dark at room temperature. Images were taken by fluorescent microscope Eclipse 80i (Nikon, Japan).

8.1.5 Cell proliferation (viability) MTS assay

HCT-116 cells were seeded into 24-well plates (Nunclon™ Surface, Nunc, Denmark) at a density of $1 \times 10^4/\text{cm}^2$ and were cultured until become confluent. After the incubation with three parts of polypeptides for 24 hours, the cells were detached. Cells were then centrifuged, re-suspended into the medium which contained 0.4% trypan blue (Invitrogen, U.S.A.) and the cells numbers were counted by haemocytometer (Precicolor HBG, Germany). The cell numbers were normalized by that of control group and expressed as the percentage of cell viability. HCT-116 are incubated at $37^\circ\text{C}/5\% \text{CO}_2$ in DMEM or RPMI 1640 medium with 10% FBS and 100 IU/mL penicillin and $100 \mu\text{g/mL}$ streptomycin. HCT 116 cells were plated on 96-well plates for 24h to reach 70% confluence (5000cells, 10000cells/well respectively). After washing with PBS, cells were incubated with either control culture medium or peptides contained medium for 24 h. Medium was removed and the cells were washed with fresh PBS. $100 \mu\text{l}$ fresh medium was added to each well. MTS solution was added to each well in the weight ratio of 1:5. The plates were incubated at $37^\circ\text{C}/5\%$

CO₂ for 3-4 h. Then, OD values of the medium were evaluated at 492 nm using micro-plate reader.

8.2 Results and discussion

8.2.1 Chemical structure analysis by FT-IR

In order to detect the existence of Attacin2 in the nanofibers, the FT-IR spectra were applied to examine the microstructure of different composite nanofibers. Four groups of samples were examined: pure PLLA nanofibers, Attacin2/PLLA nanofibers, 5-FU/Attacin2/PLLA nanofibers and 5-FU/Attacin2/keratin/PLLA nanofibers. Because Attacin2 was a kind of antimicrobial, the characteristic peaks of Attacin2 came from Amide I and Amide II in protein.

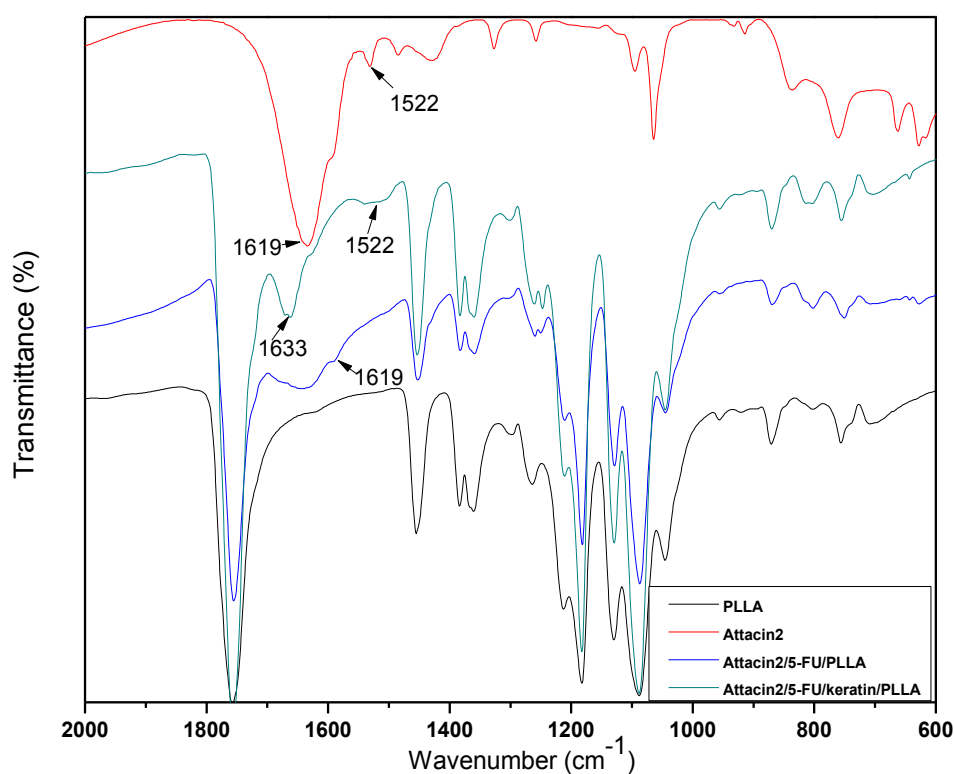


Figure 8.1 The FT-IR spectra of different nanofibers: PLLA, Attacin2/PLLA, 5-FU/Attacin2/PLLA, Attacin2/5-FU/keratin/PLLA nanofibers.

In Figure 8.1, the curve of Attacin2/PLLA displayed two peaks pointed 1619 cm^{-1} and 1522 cm^{-1} which demonstrated the existence of Amide I and Amide II. This demonstrated that Attacin2 has been fabricated into the membrane successfully. In the 5-FU/Attacin2/keratin/PLLA nanofibers, keratin belong to protein therefore, the characteristic peaks of keratin might overlap with the two peaks from Attacin2. Hence the existence of Attacin2 has been confirmed, the next work was moved to examine the anti-tumor activity of Attacin2 worked with anti-tumor drug model (e.g. 5-FU).

8.2.2 Morphology of anti-tumor activity of AMPs loaded nanofibers

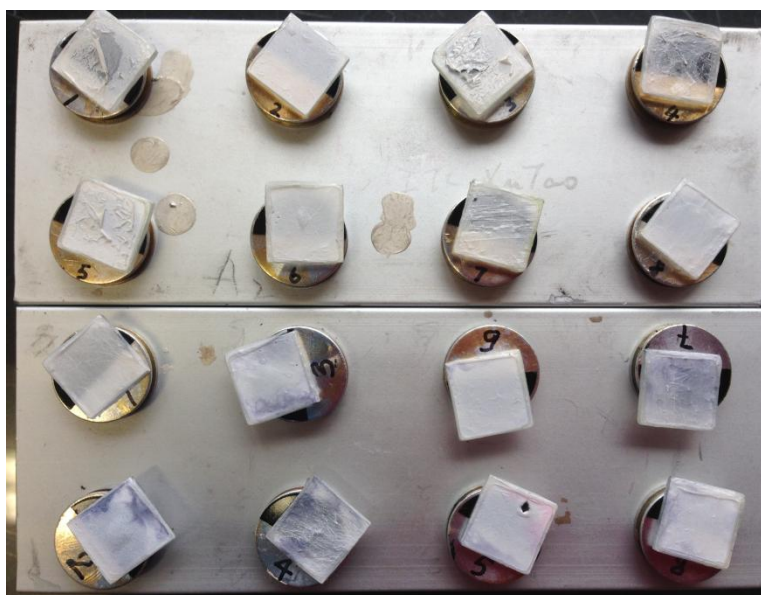


Figure 8.2 The photos of the dehydrated cell-seeded nanofibrous samples for further evaluations (e.g. SEM)

In the present study, all the samples cultured in the cells medium were collected after predetermined time intervals. Then the samples were prepared and treated based on different evaluation purposes. As shown in Figure 8.2, the samples were dehydrated and affixed on the metal holder for SEM observation. The unsmooth surface might be due to the aggregation of cells after the dehydration of nanofibers, especially to

samples with large cells concentration, e.g., pure PLLA and PLLA/keratin nanofibers. At each time interval, three pieces of glass samples were collected for each kind of nanofibers. Besides SEM observation, the other pieces of glass samples were prepared fluoresces observation and DAPI staining observation. The left sample mediums were examined by MTS assay. All the samples were tested three times ($p<0.05$).

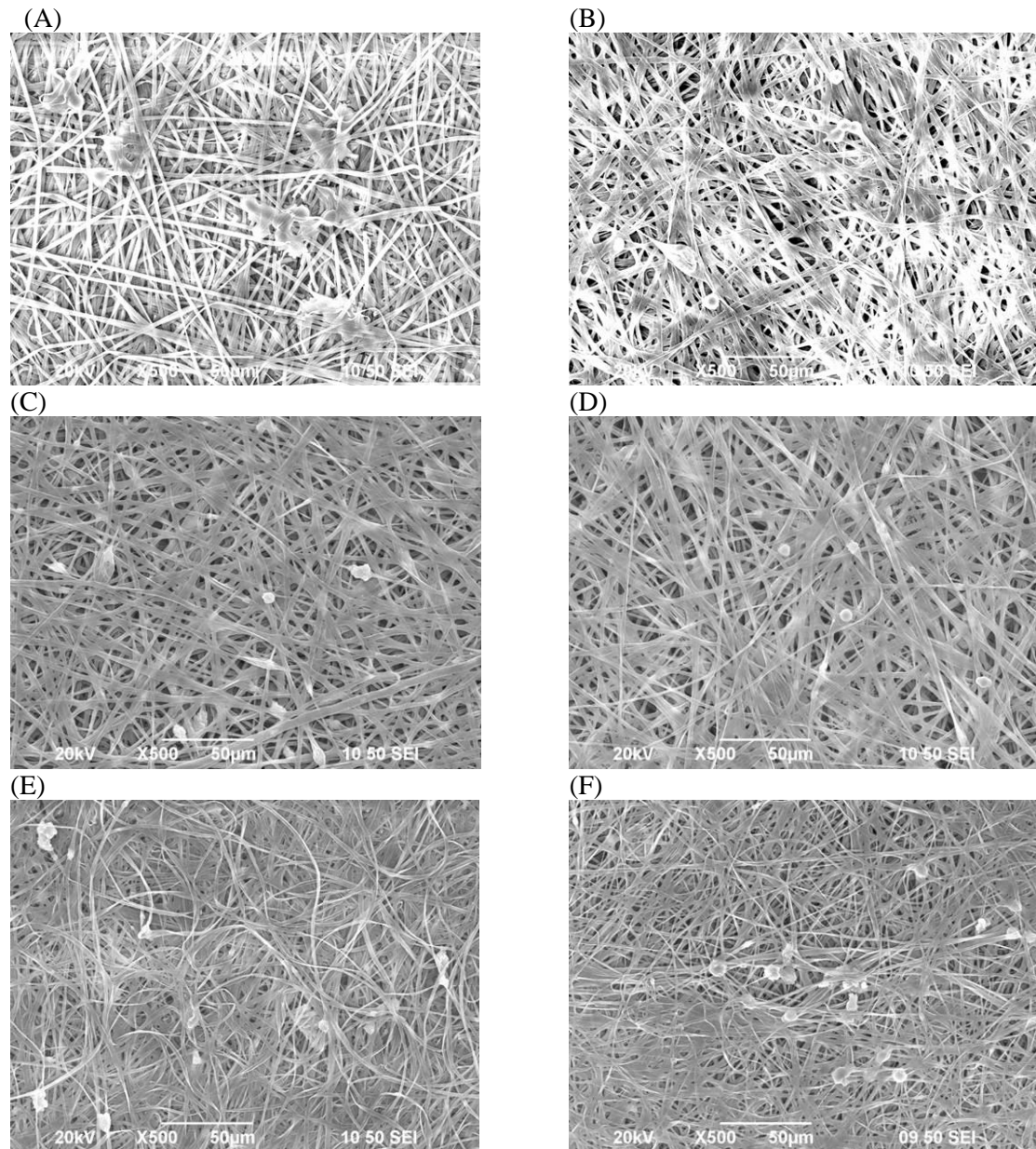


Figure 8.3 The SEM images of HCT-116 cells cultured on the surface of the drug loaded membranes in 4 hour observation: (A) pure PLLA; (B) 5-FU/PLLA; (C) Keratin/PLLA; (D) 5-FU/keratin/PLLA; (E) Attacin2/keratin/PLLA; (F) Attacin2/5-FU/keratin/PLLA nanofibers.

In Figure 8.3, the interaction between nanofibers and HCT-116 was observed directly. More cells adhered on the surface of PLLA and PLLA/keratin nanofibers. Few cells could be detected on the surface of 5-FU/keratin/PLLA, Attacin2/keratin/PLLA and Attacin2/5-FU/keratin/PLLA nanofiberous surfaces. Due to short time of cultivation (e.g. 4 h), there was no significant cells proliferation behavior difference observed.

Figure 8.4 displayed the interaction between cells and nanofibers after 24 h cultivation. More cells attached on the surfaces of nanofibers compared with 4 h observation. Cells proliferated significantly on the surface of PLLA nanofibers and Keratin/PLLA nanofibers. On the surface of Attacin2/keratin/PLLA nanofibers and Attacin2/5-FU/keratin/PLLA nanofibers, although there're certain amount of cells adhered, the proliferated cells could be hardly observed. This might be due to low biocompatible of these nanofibers. Normally cells didn't proliferate well in the un-friendly environment.

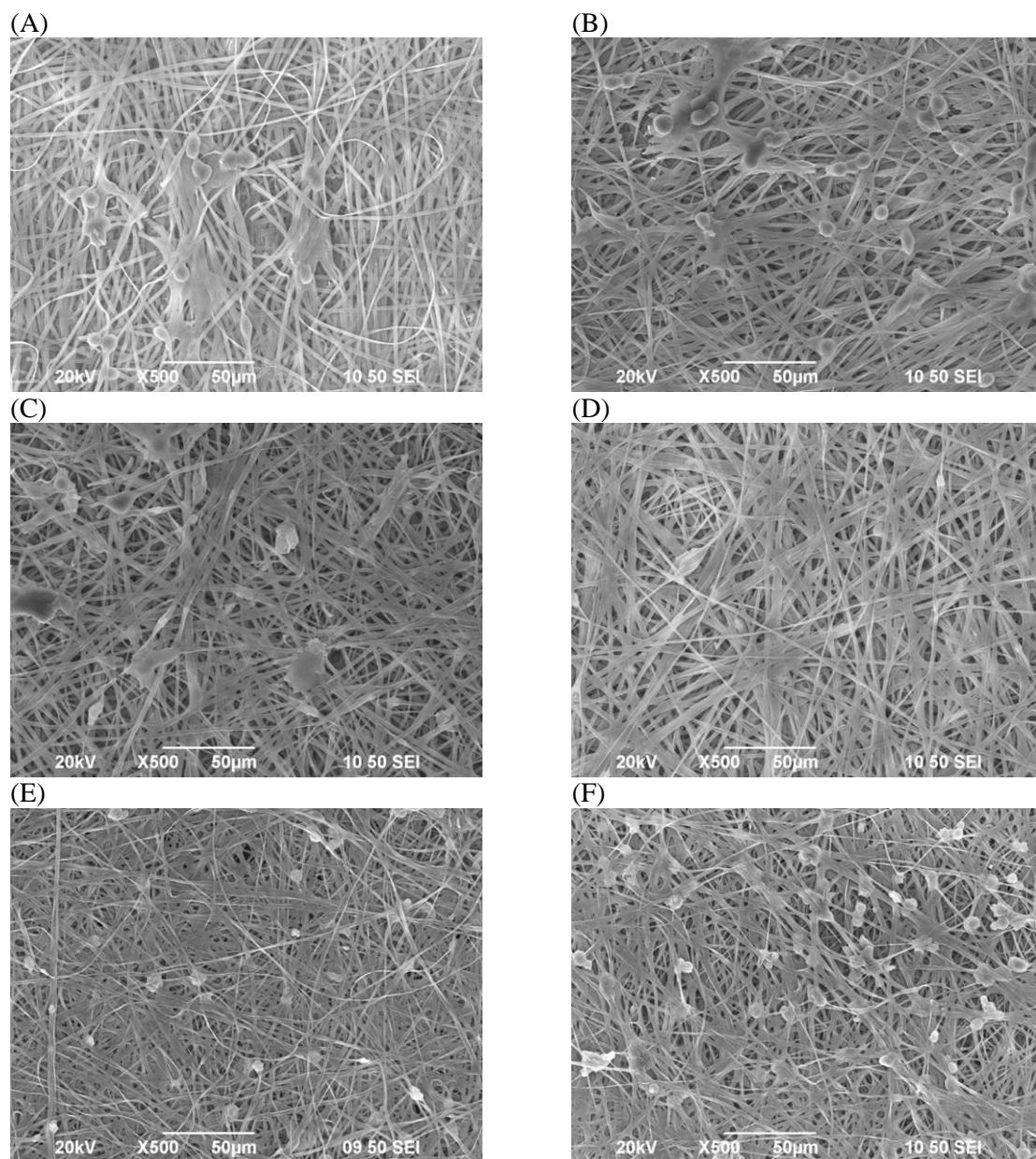


Figure 8.4 The SEM images of HCT-116 cells cultured on the surface of the drug loaded membranes in 24 hour observation: (A) pure PLLA; (B) 5-FU/PLLA; (C) Keratin/PLLA; (D) 5-FU/keratin/PLLA; (E) Attacin2/keratin/PLLA; (F) Attacin2/5-FU/keratin/PLLA nanofibers.

After longer observation of 72 hours and 120 hours as shown in Figure 8.5 and Figure 8.6, respectively, significant difference between different samples could be observed. Cells proliferated healthily on the surface of PLLA nanofibers, Keratin/PLLA nanofibers and Attacin2/keratin/PLLA nanofibers. The results illustrated that the

anti-microbial peptide could have the antitumor effect when worked with drug, e.g., 5-FU together to achieve the synergistic effect. Few cells adhered and none proliferated on the surface of 5-FU/keratin/PLLA and Attacin2/5-FU/keratin/PLLA nanofibers.

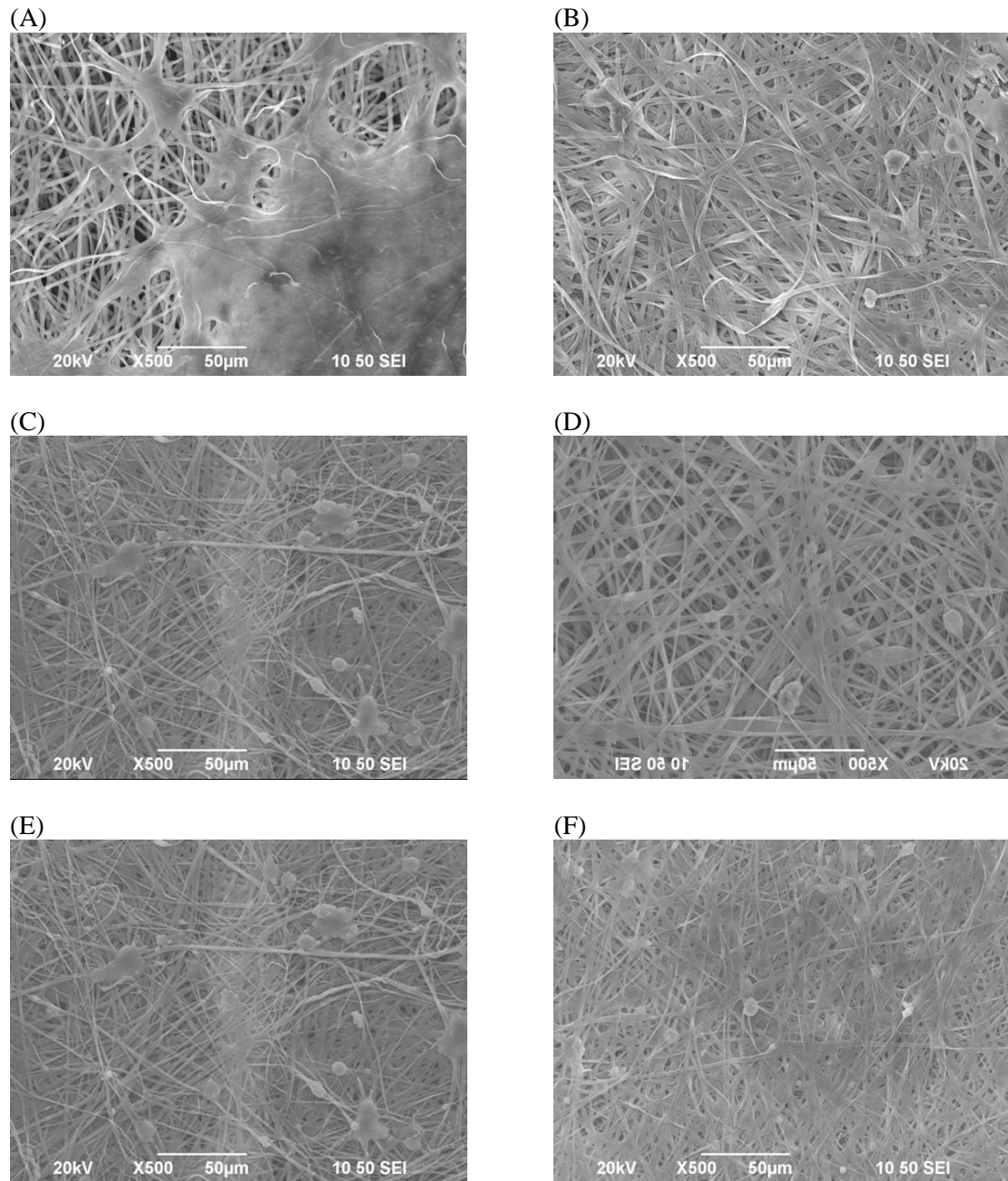


Figure 8.5 The SEM images of HCT-116 cells cultured on the surface of the drug loaded membranes in 72 hour observation: (A) pure PLLA; (B) 5-FU/PLLA; (C) Keratin/PLLA; (D) 5-FU/keratin/PLLA; (E) Attacin2/keratin/PLLA; (F) Attacin2/5-FU/keratin/PLLA nanofibers.

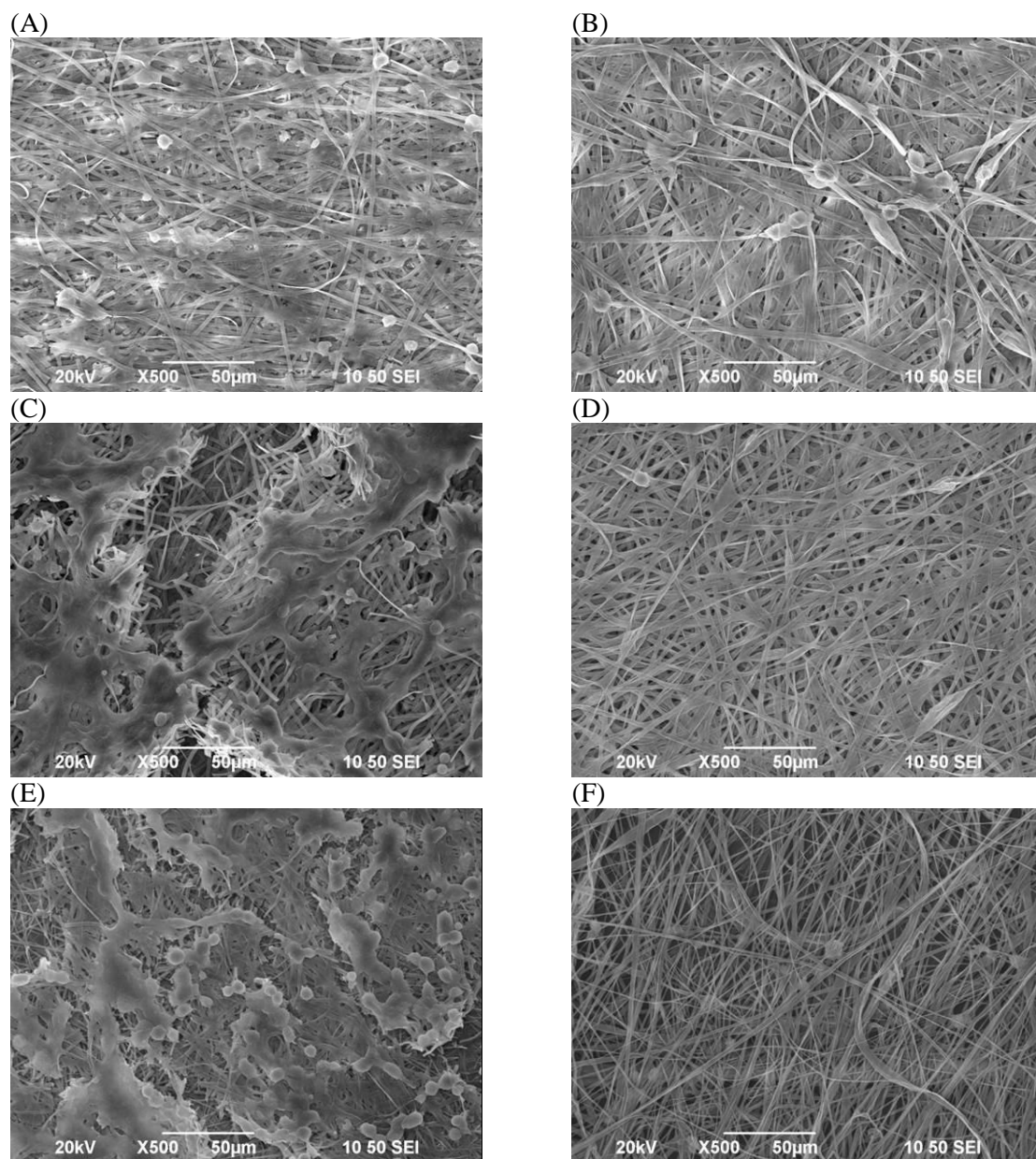


Figure 8.6 The SEM images of HCT-116 cells cultured on the surface of the drug loaded membranes in 120 hour observation: (A) pure PLLA; (B) 5-FU/PLLA; (C) Keratin/PLLA; (D) 5-FU/keratin/PLLA; (E) Attacin2/keratin/PLLA; (F) Attacin2/5-FU/keratin/PLLA nanofibers.

8.2.3 Cell live/die assay results

In Figure 8.7, the images displayed the cells proliferation performances on different nanofibers surfaces. The second columns represented the cells which are proliferated

healthily and the third columns represented the cells which were dead. The last columns represented the overlaid images of both live cells and dead cells. Blank PLLA samples in this experiment worked as a control. Five groups of samples were tested and the whole experimental period was 120 hour. The predetermined time intervals were settled as: 4 hour, 24 hour, 72 hour and 120 hour. At those time intervals, the cells proliferation morphologies were observed and analyzed. In Figure 8.7, the blank PLLA nanofibers provided preferable environments for tumor cells compared to PLLA/Attacin2 nanofibers, PLLA/keratin/Attacin2 nanofibers, PLLA/keratin/5-FU nanofibers and PLLA/keratin/Attacin2/5-FU nanofibers. These results indicated that both 5-FU and Attacin2 had a significant inhibition effect on tumor cells proliferations. In Figure 8.8, the images displayed the cells proliferation performances on different nanofibers surfaces after 24 hours cultivation. The blank PLLA nanofibers provided preferable environments for HCT-116 compared to PLLA/Attacin2 nanofibers, PLLA/keratin/Attacin2 nanofibers, PLLA/keratin/5-FU nanofibers and PLLA/keratin/Attacin2/5-FU nanofibers. Both PLLA/keratin/Attacin2 and PLLA/keratin/5-FU displayed the most inhibition effect on the tumor cells proliferation. The cells growth rate on PLLA/keratin/Attacin2/5-FU nanofibers obviously decreased compared to the 4 hour cultivation group. In Figure 8.9 and Figure 8.10, cells growths performances displayed significant differences after long period's cultivation. The synergistic effect between antimicrobial and anti-tumor drug could be observed. The images displayed the cells proliferation performances on different nanofibers surfaces. For the control group, cells almost spread on the whole surface of PLLA membrane. For the group of PLLA/Attacin2 and PLLA/keratin/Attacin2, cells growths were dampened compared with PLLA group. The two most significant group samples which inhibited the tumor cells were

PLLA/keratin/5-FU and PLLA/keratin/Attacin2/5-FU membranes. Especially after 120 hour cultivation, large amount of dead cells could be observed in the group of PLLA/keratin/Attacin2/5-FU membranes then that of PLLA/keratin /5-FU membranes. The results indicated that the synergistic effect between anti-microbial and anti-tumor drug occurred at the late stage of cells cultivations, e.g., 72 hour and 120 hour. As a kind of natural protein, Attacin2 performed a “soft” but sustained effect on inhibiting the tumor cells.

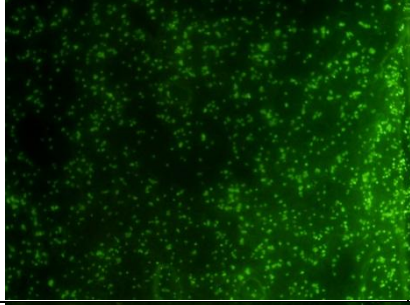
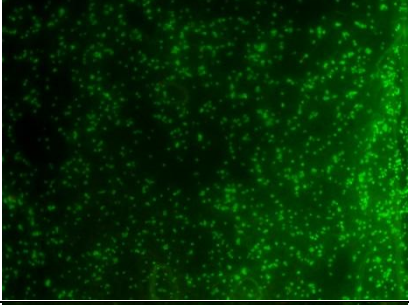
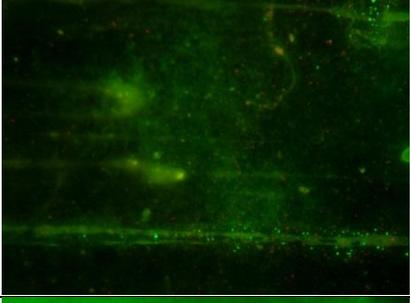
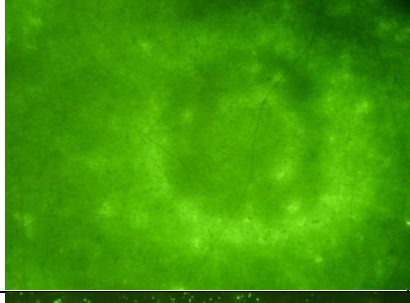
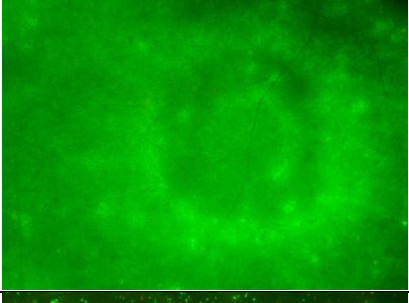
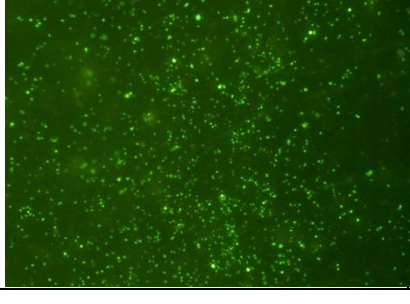
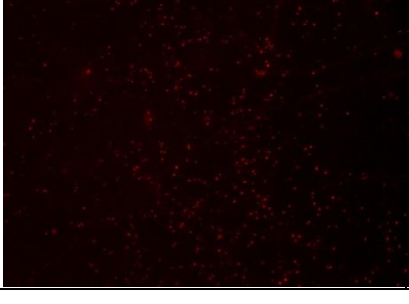
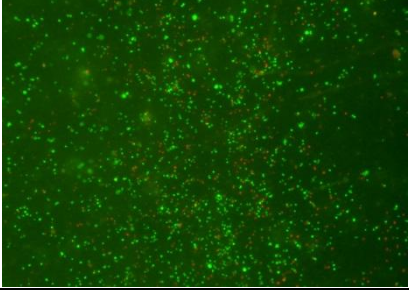
| Sample | Live | Dead | Overlay |
|----------------------------|---|--|---|
| PLLA |  |  |  |
| PLLA/Attacin 2 |  |  |  |
| PLLA/keratin/Attacin2 |  |  |  |
| PLLA/keratin/5-FU |  |  |  |
| PLLA/keratin/Attacin2/5-FU |  |  |  |

Figure 8.7 Fluorescence micrographs of the cells stained with FDA (living cells), PI (dead cells) and overlaid images after seeding HCT-116 on the surface of the different nanofibers for 4 hours.

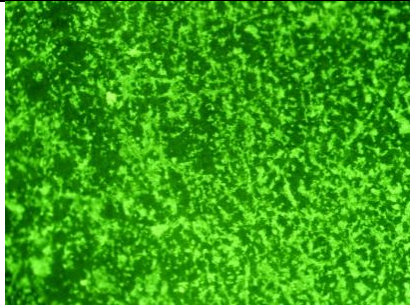
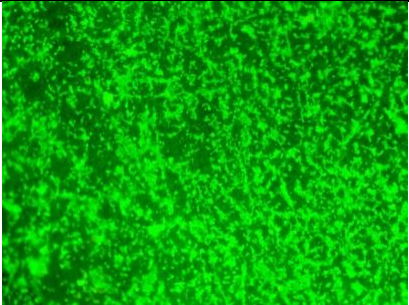
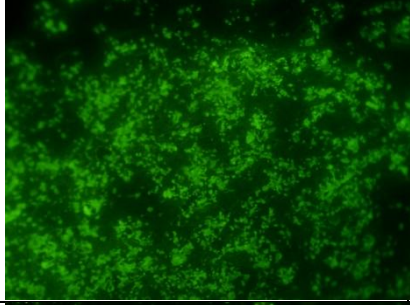
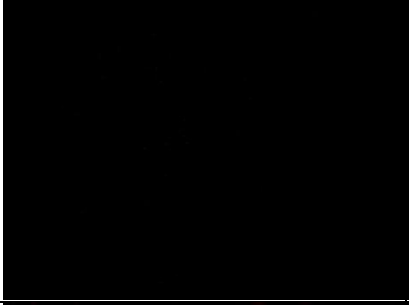
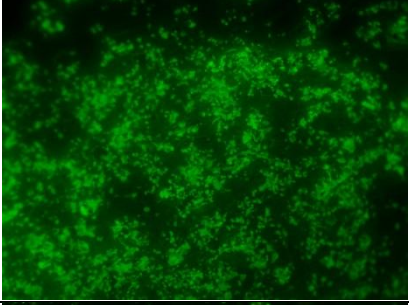
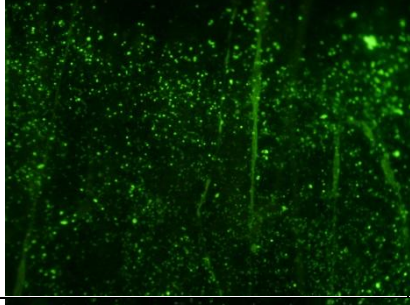
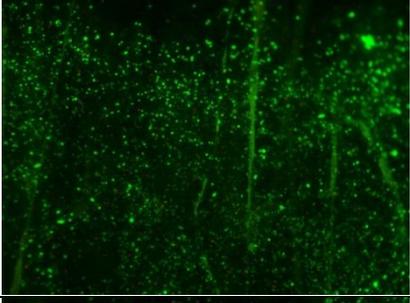
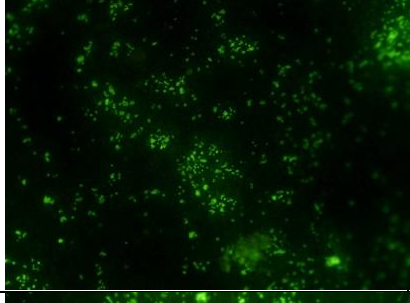
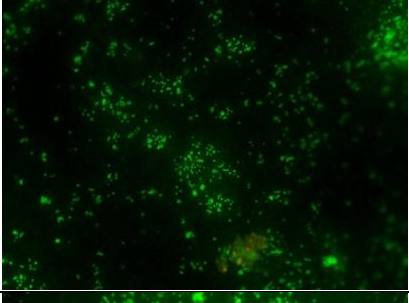
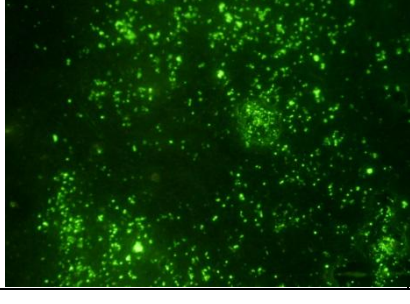
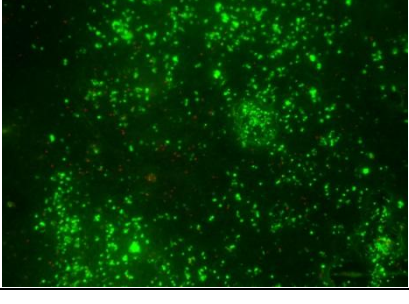
| Sample | Live | Dead | Overlay |
|----------------------------|---|--|---|
| PLLA |  |  |  |
| PLLA/Attacin 2 |  |  |  |
| PLLA/keratin/Attacin2 |  |  |  |
| PLLA/keratin/5-FU |  |  |  |
| PLLA/keratin/Attacin2/5-FU |  |  |  |

Figure 8.8 Fluorescence micrographs of the cells stained with FDA (living cells), PI (dead cells) and overlaid images after seeding HCT-116 on the surface of the different nanofibers for 24 hours.

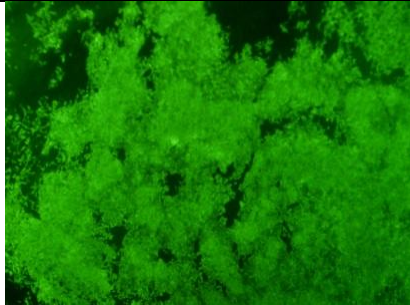
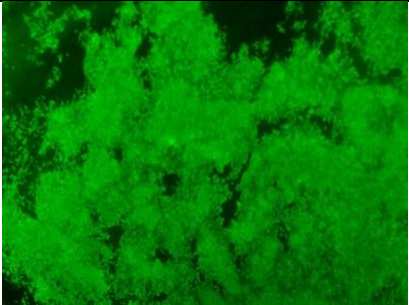
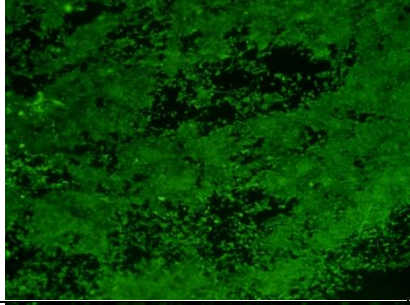
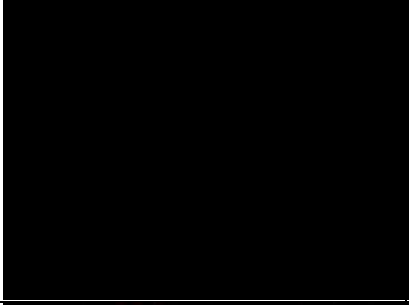
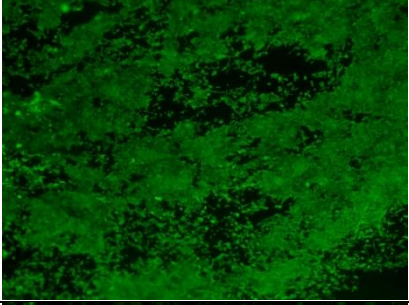
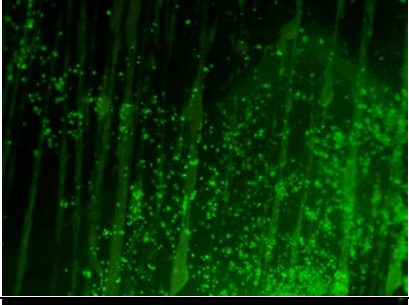
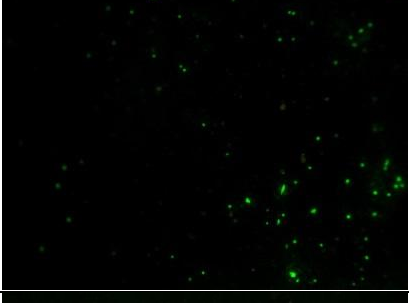
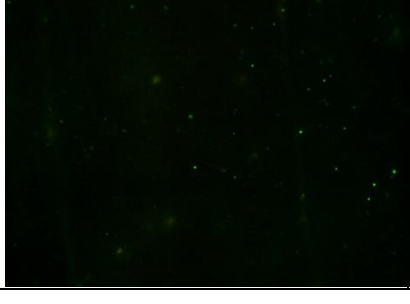
| Sample | Live | Dead | Overlay |
|----------------------------|---|--|---|
| PLLA |  |  |  |
| PLLA/Attacin 2 |  |  |  |
| PLLA/keratin/Attacin2 |  |  |  |
| PLLA/keratin/5-FU |  |  |  |
| PLLA/keratin/Attacin2/5-FU |  |  |  |

Figure 8.9 Fluorescence micrographs of the cells stained with FDA (living cells), PI (dead cells) and overlaid images after seeding HCT-116 on the surface of the different nanofibers for 72 hours.

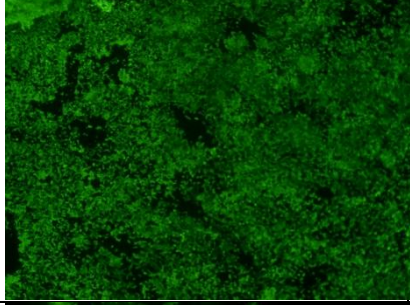
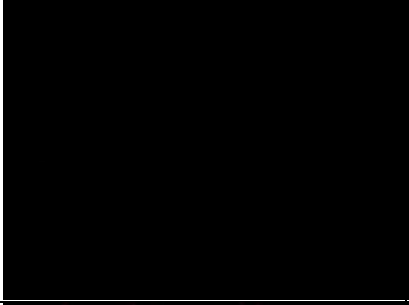
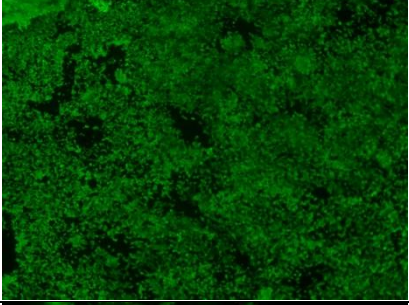
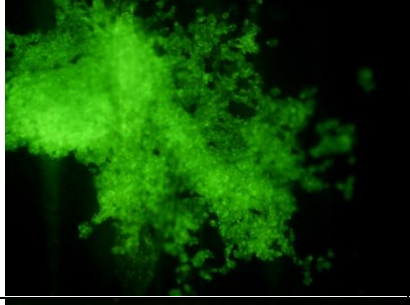
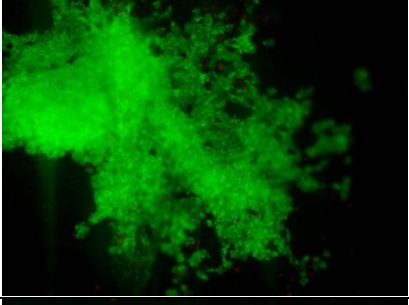
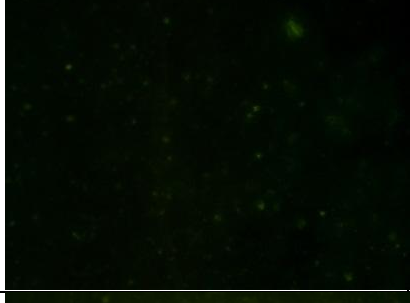
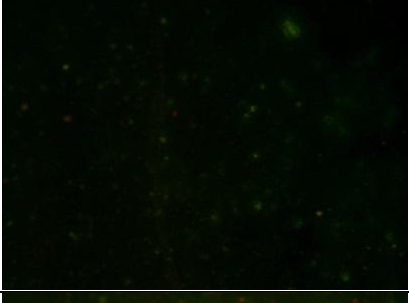
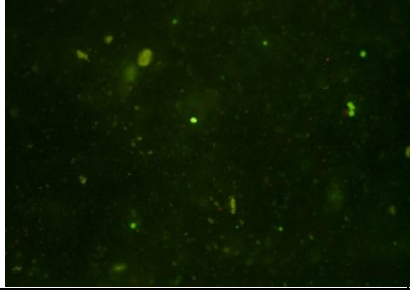
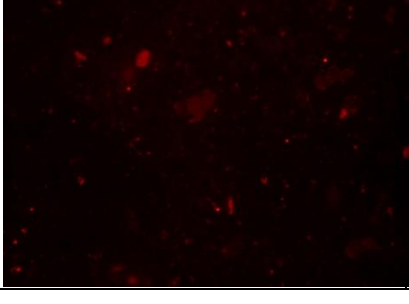
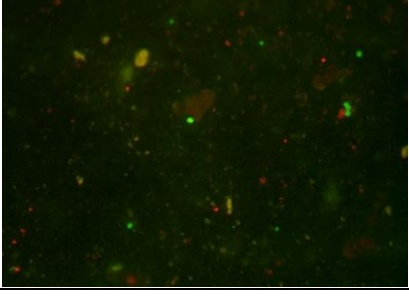
| Sample | Live | Dead | Overlay |
|----------------------------|---|--|---|
| PLLA |  |  |  |
| PLLA/Attacin 2 |  |  |  |
| PLLA/keratin/Attacin2 |  |  |  |
| PLLA/keratin/5-FU |  |  |  |
| PLLA/keratin/Attacin2/5-FU |  |  |  |

Figure 8.10 Fluorescence micrographs of the cells stained with FDA (living cells), PI (dead cells) and overlaid images after seeding HCT-116 on the surface of the different nanofibers for 120 hours.

8.2.4 DAPI staining for cellular adhesion and proliferation studies

In order to test the responses of HCT-116 tumor cells to different composite nanofibers samples, cells were cultured on the new scaffold containing: pure PLLA, PLLA/Attacin2, PLLA/keratin/Attacin2, PLLA/keratin/5-FU and PLLA/keratin/Attacin2/5-FU. Double staining with FITC-phalloidin and DAPI was used to elucidate the cytoskeletal arrangement of HCT-116 cells. As shown in Figure 8.11, the cells responded differently to different compositions of the scaffolds. HCT-116 on the both 5-Fu loaded nanofibrous surface and Attacin2 loaded nanofibrous surfaces remained aggregated, presumably due to their poor adhesive interaction with the substrate. By contrast, HCT-116 cells cultured on blank PLLA showed well-dispersed cell bodies and extensive arborization. These results suggest an ability of both 5-FU loaded nanofibers and Attacin2 loaded nanofibers to inhibit the tumor cells proliferation. Especially, cells on the Attacin2 composite nanofibers showed a vague cytoskeleton shape which indicated the antimicrobial peptides has an inhibition effect on the tumor cells. In Figure 8.11, the second columns represented the cells skeletons which were stained by TRICE-phalloidin and the third columns represented the cell nucleus which were stained by DAPI. The last columns represented the overlaid images of both cells skeletons and cells nucleuses. Blank PLLA samples in this experiment worked as a control. Five groups of samples were tested and the whole experimental period was 120 hours. The predetermined time intervals were settled as: 4 hours, 24 hours, 72 hours and 120 hours. At those time intervals, the cells proliferation morphologies were observed and analyzed. The blank PLLA nanofibers provided preferable environments for tumor cells compared to PLLA/Attacin2 nanofibers, PLLA/keratin/Attacin2 nanofibers, PLLA/keratin/5-FU nanofibers and PLLA/keratin/Attacin2/5-FU nanofibers. These results indicated that

both 5-FU and Attacin2 has a significant inhibition effect on tumor cells proliferations. The same trend could be observed in Figure 8.12. The cells responded differently to different compositions of the scaffolds. HCT-116 on the both 5-FU loaded nanofibrous surface and Attacin2 loaded nanofibrous surfaces remained aggregated, presumably due to their poor adhesive interaction with the substrate. By contrast, HCT-116 cells cultured on blank PLLA showed well-dispersed cell bodies and extensive arborization. These results suggest an ability of both 5-FU loaded nanofibers and Attacin-2 loaded nanofibers to inhibit the tumor cells proliferation. Especially, cells on the Attacin2 composite nanofibers showed a vague cytoskeleton shape which indicated the antimicrobial peptides has an inhibition effect on the tumor cells. In Figure 8.12, the second columns represented the cells skeletons which were stained by TRICE-phalloidin and the third columns represented the cell nucleus which were stained by DAPI. The last columns represented the overlaid images of both cells skeletons and cells nucleuses. Blank PLLA samples in this experiment worked as a control. Five groups of samples were tested and the whole experimental period was 120 hours. The predetermined time intervals were settled as: 4 hours, 24 hours, 72 hours and 120 hours. At those time intervals, the cells proliferation morphologies were observed and analyzed. The blank PLLA nanofibers provided preferable environments for tumor cells compared to PLLA/Attacin2 nanofibers, PLLA/keratin/Attacin2 nanofibers, PLLA/keratin/5-FU nanofibers and PLLA/keratin/Attacin2/5-FU nanofibers. These results indicated that both 5-FU and Attacin2 has a significant inhibition effect on tumor cells proliferations. In order to test the responses of HCT-116 tumor cells to different composite nanofibers samples, cells were cultured on the new scaffold containing: pure PLLA, PLLA/Attacin2, PLLA/keratin/Attacin2, PLLA/keratin/5-FU and

PLLA/keratin/Attacin2/5-FU. Double staining with FITC-phalloidin and DAPI was used to elucidate the cytoskeletal arrangement of HCT-116 cells. As shown in Figure 8.5, the cells responded differently to different compositions of the scaffolds. HCT-116 on the both 5-FU loaded nanofibrous surface and Attacin2 loaded nanofibrous surfaces remained aggregated, presumably due to their poor adhesive interaction with the substrate. By contrast, HCT-116 cells cultured on blank PLLA showed well-dispersed cell bodies and extensive arborization. These results suggest an ability of both 5-FU loaded nanofibers and Attacin2 loaded nanofibers to inhibit the tumor cells proliferation. Especially, cells on the Attacin2 composite nanofibers showed a vague cytoskeleton shape which indicated the antimicrobial peptides has an inhibition effect on the tumor cells. In Figure 8.7, the second columns represented the cells skeletons which were stained by TRICE-phalloidin and the third columns represented the cell nucleus which were stained by DAPI. The last columns represented the overlaid images of both cells skeletons and cells nucleuses. Blank PLLA samples in this experiment worked as a control. Five groups of samples were tested and the whole experimental period was 120 hours. The predetermined time intervals were settled as: 4 hours, 24 hours, 72 hours and 120 hours. At those time intervals, the cells proliferation morphologies were observed and analyzed. In Figure 8.7, the blank PLLA nanofibers provided preferable environments for tumor cells compared to PLLA/Attacin2 nanofibers, PLLA/keratin/Attacin2 nanofibers, PLLA/keratin/5-FU nanofibers and PLLA/keratin/Attacin2/5-FU nanofibers. These results indicated that both 5-FU and Attacin2 has a significant inhibition effect on tumor cells proliferations. In order to test the responses of HCT-116 tumor cells to different composite nanofibers samples, cells were cultured on the new scaffold containing: pure PLLA, PLLA/Attacin2, PLLA/keratin/Attacin2, PLLA/keratin/5-FU

and PLLA/keratin/Attacin2/5-FU. Double staining with FITC-phalloidin and DAPI was used to elucidate the cytoskeletal arrangement of HCT-116 cells. As shown in Figure 8.14, the cells responded differently to different compositions of the scaffolds. HCT-116 on the both 5-FU loaded nanofibrous surface and Attacin2 loaded nanofibrous surfaces remained aggregated, presumably due to their poor adhesive interaction with the substrate. By contrast, HCT-116 cells cultured on blank PLLA showed well-dispersed cell bodies and extensive arborization. These results suggest an ability of both 5-FU loaded nanofibers and Attacin2 loaded nanofibers to inhibit the tumor cells proliferation. Especially, cells on the Attacin2 composite nanofibers showed a vague cytoskeleton shape which indicated the antimicrobial peptides has an inhibition effect on the tumor cells. In Figure 8.13, the second columns represented the cells skeletons which were stained by TRICE-phalloidin and the third columns represented the cell nucleus which were stained by DAPI. The last columns represented the overlaid images of both cells skeletons and cells nucleuses. Blank PLLA samples in this experiment worked as a control. Five groups of samples were tested and the whole experimental period was 120 hours. The predetermined time intervals were settled as: 4 hours, 24 hours, 72 hours and 120 hours. At those time intervals, the cells proliferation morphologies were observed and analyzed. In Figure 8.1, the blank PLLA nanofibers provided preferable environments for tumor cells compared to PLLA/Attacin2 nanofibers, PLLA/keratin/Attacin2 nanofibers, PLLA/keratin/5-FU nanofibers and PLLA/keratin/Attacin2/5-FU nanofibers. These results indicated that both 5-FU and Attacin2 has a significant inhibition effect on tumor cells proliferations.

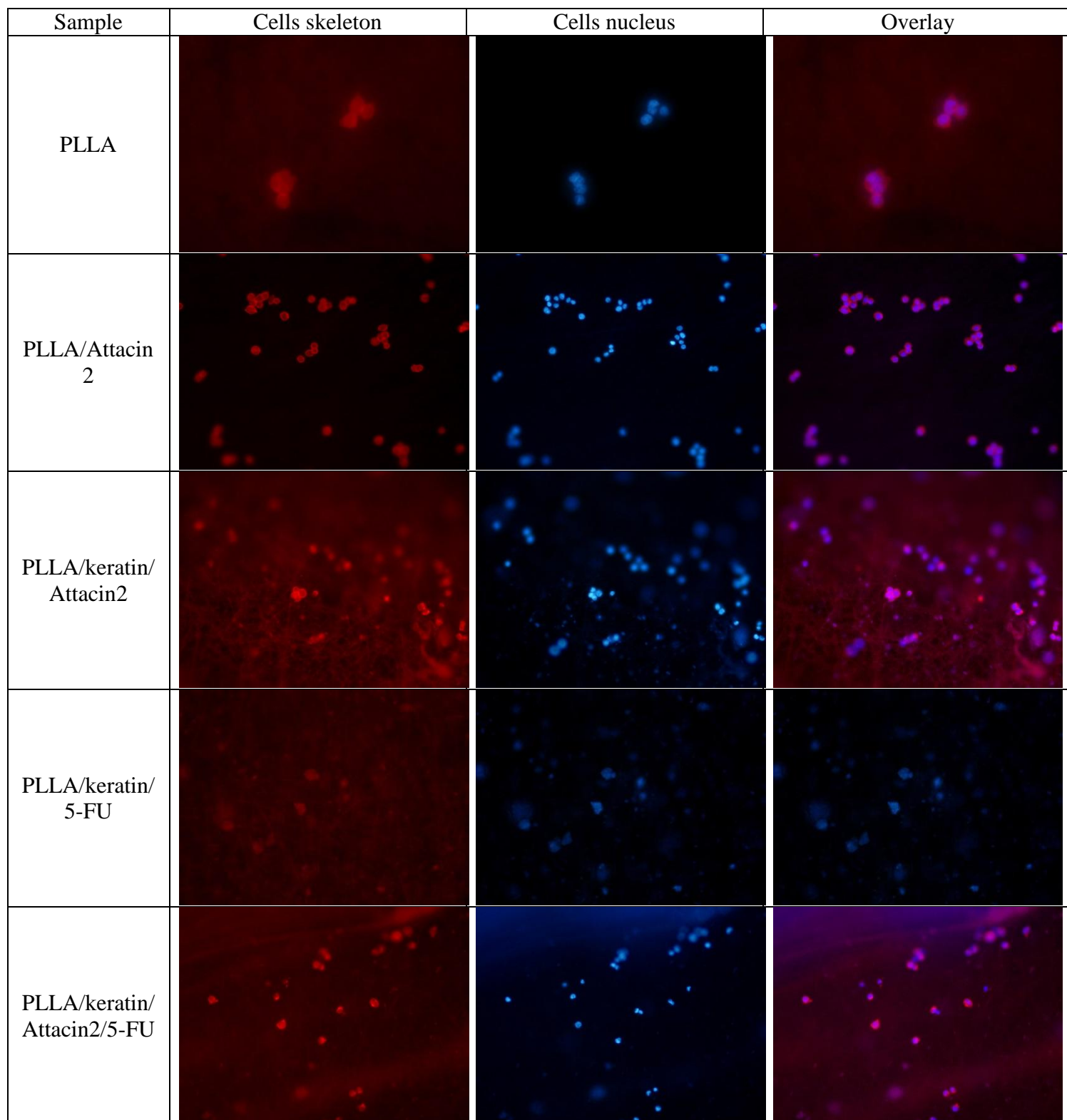


Figure 8.11 Fluorescence micrographs of the cells stained with DAPI (cell nucleus), TRICE-phalloidin (cell skeleton) and overlaid images after seeding HCT-116 on the surfaces of the different nanofibrous for 4 hours.

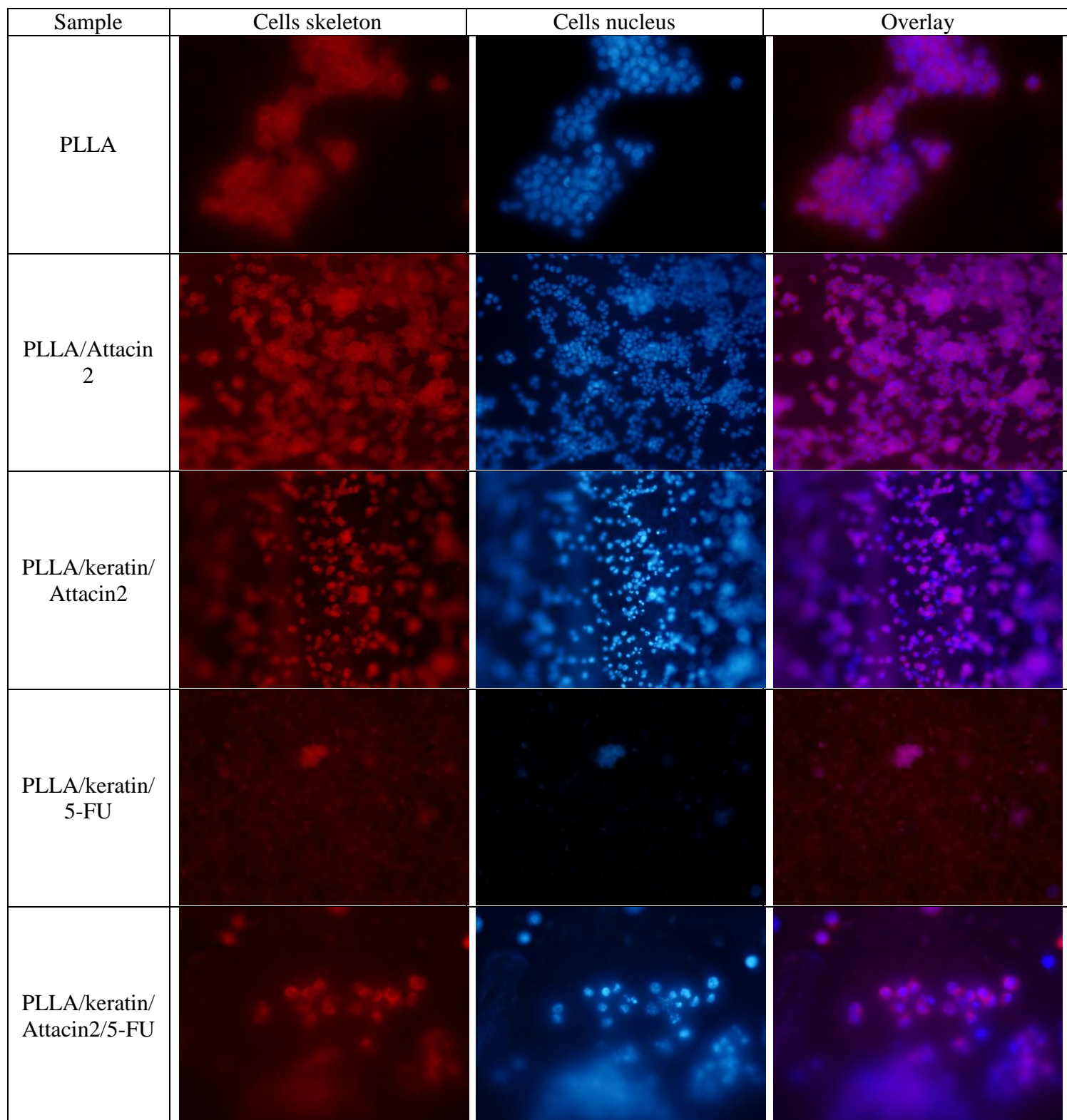


Figure 8.12 Fluorescence micrographs of the cells stained with DAPI (cell nucleus), TRICE-phalloidin (cell skeleton) and overlaid images after seeding HCT-116 on the surfaces of the different nanofibrous for 24 hours.

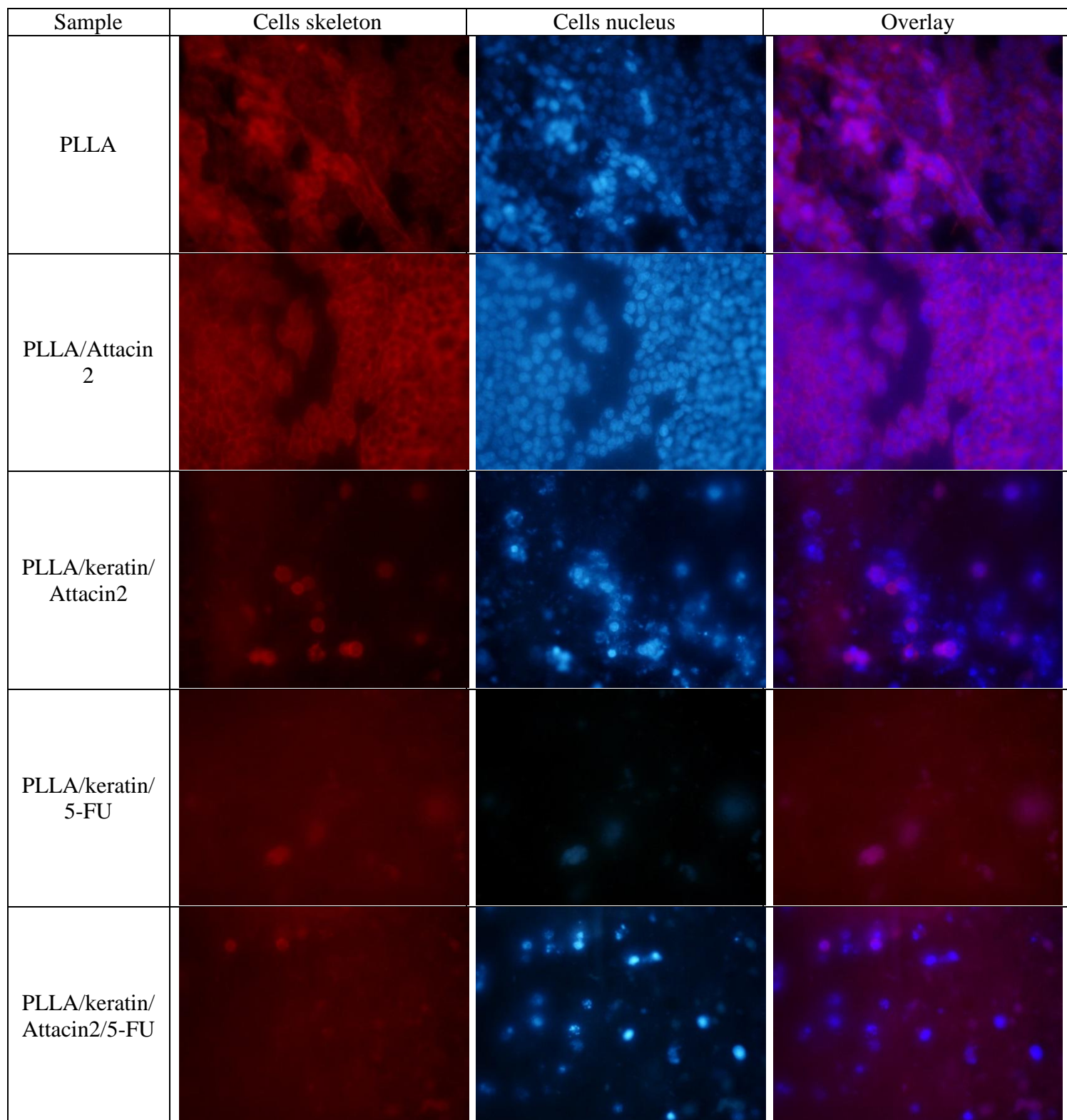


Figure 8.13 Fluorescence micrographs of the cells stained with DAPI (cell nucleus), TRICE-phalloidin (cell skeleton) and overlaid images after seeding HCT-116 on the surfaces of the different nanofibrous for 72 hours.

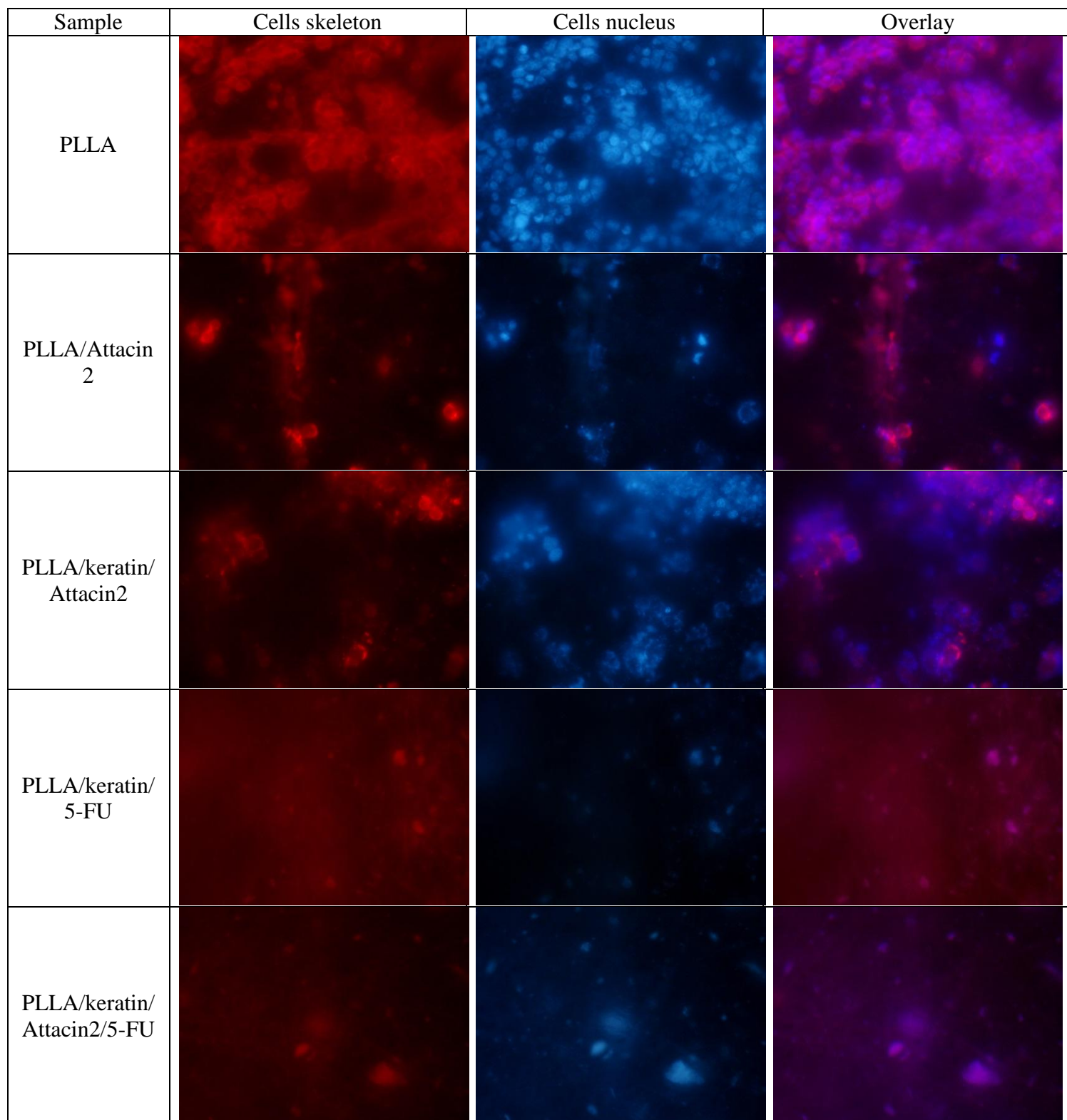


Figure 8.14 Fluorescence micrographs of the cells stained with DAPI (cell nucleus), TRICE-phalloidin (cell skeleton) and overlaid images after seeding HCT-116 on the surfaces of the different nanofibrous for 120 hours.

8.2.5 MTS assay for cells cytotoxicity studies

Figure 8.14 and Figure 8.15 displayed the MTS results for the inhibition efficiency of the Attacin2 and 5-FU loaded membranes to the human colorectal cancer HCT-116 cells. After 72 hour of cultivation, all Attacin2 and 5-FU loaded membrane groups displayed significantly different anti-tumor performance compared to the pure 5-FU loaded group. The cell inhibition efficacy of the keratin/5-FU membrane group was much higher than the PLLA group at 24, 48 and 72 hours due to the sustainable release of 5-FU in the drug membranes.

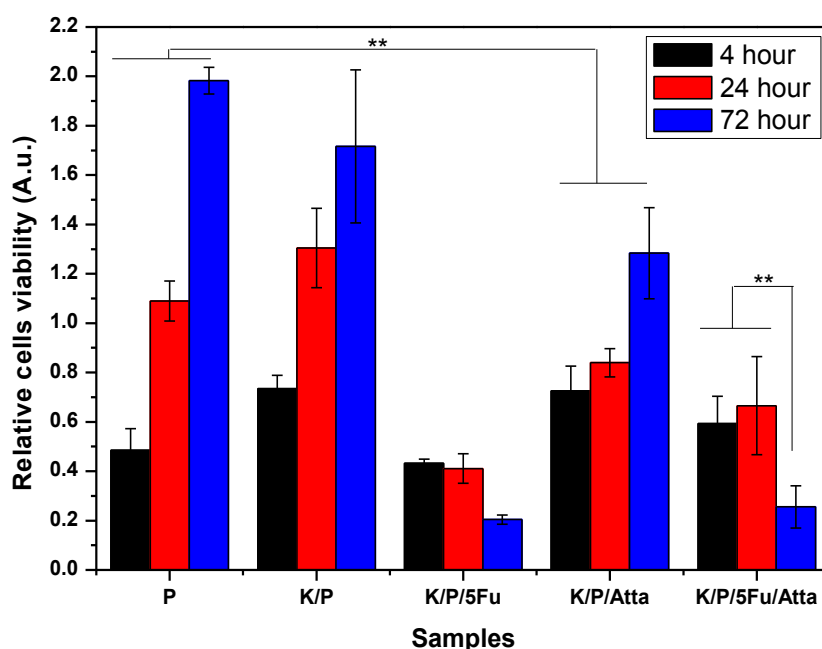


Figure 8.15 MTS assay of HCT-116 viability on different composite nanofibers. Statistical analysis revealed a difference between the 500–1,000-nm nanofibers and the polystyrene control on the viability of MSCs (** $p < 0.01$; $n = 3$).

In Figure 8.15, the PLLA/keratin/5-FU samples, the cells viability ceased decreasing after 72 hour cultivation. However, a significant decrease in cell viability could be observed for the group of PLLA/keratin/Attacin2/5-FU even after 72 hour

cultivation ($P < 0.05$). This difference indicated that at late stage of cultivation, Attacin increased the anti-tumor effect together with the anti-tumor drug. This process needs a long and sustained period to achieve.

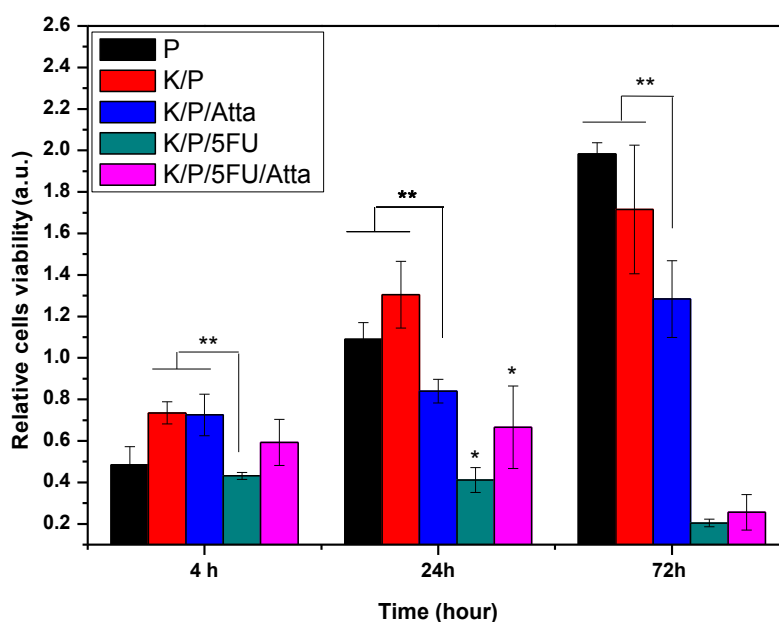


Figure 8.16 MTS assay of HCT-116 viability on different composite nanofibers. Statistical analysis revealed a difference between the 500–1,000-nm nanofibers and the polystyrene control on the viability of MSCs (* $p < 0.05$; ** $p < 0.01$; $n = 3$).

In Figure 8.16, the cells viability was displayed as a function of time in order to observe the effect between cultivation times to the cells viability. At early stage, the PLLA/keratin/5-FU membrane performed a more significant effect on anti-tumor activity than PLLA/keratin/Attacin2/5-FU. However, this trend changed after 48 hour cultivation. After a 72 hour cultivation, there's no significant difference between PLLA/keratin/Attacin2/5-FU membranes and PLLA/keratin/5-FU membranes ($p < 0.05$). Moreover, the group of PLLA/keratin/Attacin2/5-FU possessed significantly difference with the groups of PLLA/Attacin2, PLLA/keratin/Attacin2 membranes

($p < 0.01$). A conclusion might be safely conducted that the synergistic effect between antimicrobial (e.g. Attacin2) and anti-tumor drug (e.g. 5-FU) occurred at the late stage of drug release profile. Normally, the chemical drug decayed and therefore decreased its anti-tumor performance at the late stage of drug release. Adding antimicrobial compensated this weakness. The “soft” and sustained synergistic effect could last till several weeks and this could suggest new components of anti-tumor agents.

8.3 Discussion and conclusion

Combination therapy for the treatment of cancer is becoming more popular because it generates synergistic anticancer effects, reduces individual drug-related toxicity and suppresses multi-drug resistance through different mechanisms of action [166]. In recent years, nanotechnology-based combination drug delivery to tumor tissues has emerged as an effective strategy by overcoming many biological, biophysical and biomedical barriers that the body stages against successful delivery of anticancer drugs [167]. The sustained, controlled and targeted delivery of chemotherapeutic drugs in a combination approach enhanced therapeutic anticancer effects with reduced drug-associated side effects.

In this chapter, the main explorations focused on the interaction between anti-tumor chemical drug and antimicrobial peptides and their corresponding synergistic effect on the antitumor therapy. The results indicated that adding Attacin2 into the drug loaded membrane can increase the anti-tumor effect in the whole therapy. After 48 hours observation, the synergistic effect gradually became significant comparing with single drug formulation. The tumor cells proliferation rate was inhibited by the dual drug formulation in the late phase of the total 72 hours observations. The future work and challenges of the dual drug formulation would be discussed in chapter 9.

CHAPTER 9 CONCLUSIONS AND FUTURE WORKS

In this thesis, a systematic exploration has been carried out to establish understanding on the scientific problems and engineering issues of developing anti-tumor drug delivery nanofibrous system. After the literature review, the knowledge gaps have been filled by completing the objectives which were summarized in this chapter. The final conclusions were summarized in this chapter after the detailed and systematic descriptions of the six chapters of studies presented in the above chapter 3 to 8.

9.1 Conclusions

In Chapter 1 and Chapter 2, the fundamental knowledge framework of the biofunctional composite nanofibers was reviewed and knowledge gaps on the methods fabricating and applying keratin-based nanofibers were identified. The purpose of this research was to fill the knowledge gaps and biofunctional keratin-based antitumor nanofibrous system was explored.

1. To demonstrate the feasibility of transforming wool wastes into the functional protein biomaterials.

This objective has been achieved in Chapter 3. Wool fibers were hydrolyzed and adjusted to predetermined pH value. The dimension of keratin polypeptides were analyzed and determined by SEM investigation. Afterwards, the chemical structure, crystal structure and thermal properties were analyzed by FT-IR spectra, XRD and TGA respectively. The results suggested that keratin polypeptides with different amino acids compositions could be tailored from wool hydrolyzed solution based on isoelectric-point precipitation and had potential application such as biomaterials for

wound healing and drug delivery.

2. To apply keratin polypeptides into biofunctional tissue engineering scaffolds system.

This objective has been achieved in Chapter 4. Biocompatible electrospinning membrane composed of PLLA and keratin is firstly introduced. Ultrafine nanofibrous membranes were successfully prepared by electrospinning the blend of PLLA and keratin suspension. Uniform structure of the composite nanofibers was observed and TEM images indicated keratin was evenly distributed within the composite fibers. The results of FT-IR spectra revealed the composition of keratin/PLLA membrane. The biocompatibility of keratin/PLLA composite membrane was examined by MTT assay. The cells proliferation profile was observed by fluorescent micrographs. The results indicated that with promoting effect on cell adherence and proliferation, this composite material was suitable as a potential materials candidate for tissue engineering.

3. To investigate the degradability of the PLLA/keratin composite nanofibers.

This objective has been achieved in Chapter 5. The evaluation was examined through several aspects. Firstly, the morphology of the membranes was observed by SEM images which indicated that the keratin/PLLA nanofibers kept their basic structures after 120 hours degradation in PBS solution and small pores could be observed on the surface of keratin/PLLA composite nanofibers whereas few pores were observed from pure PLLA nanofibers. The UV spectra further indicated the degradation rate of keratin from the biopolymer nanofibers. The FT-IR spectra demonstrate the same degradation trend by comparing the intensities of keratin

characteristic peaks. The thermal properties of the degraded membranes were tested by TGA thermal analysis. The results indicated that keratin/PLLA composite nanofibers could keep their basic physical structure in long degradation period. The amount of keratin released into the environment was inversely proportional to the amount of keratin maintained in the composite nanofibers.

4. To develop a localized drug delivery nanofibrous membrane system.

This objective has been achieved in Chapter 6. Keratin/PLLA nanofibrous membrane containing hydrophilic drug were synthesized by electrospinning technique and characterized their chemical properties, physical properties and drug release properties. 5-fluorouracil was used as target drug model. The dispersion status of drug in the composite membrane was investigated by several characterization methods. SEM and DSC revealed that individual filament morphology and thermal properties were maintained in the composite filaments. The *in vitro* drug release profiles were examined. Drug release from a composite filament was an additive composite of the drug release profiles obtained from single component filaments, and multi-component filaments could control the release rate of drug through longer period than a mono-component filament. Drug release from a tetra-component filament was calculated based on the individual component drug release profiles and shown to be a good predictor of experimentally determined drug release.

5. To demonstrate the antitumor effect of drug loaded membrane.

This objective has been achieved in Chapter 7. The pH sensitivity was considered as an important property of the drug delivery system. To investigate the optimized factors effect on the controlled release performance of the electrospun composite

membrane in different pH environments, full-factorial design with two factors at two-levels was introduced in this chapter. The factors considered in the present study include: ratio of the two components in the membrane and fabrication electrospun voltage. Then the membranes with different processing parameters were tested in two different pH conditions: pH 7.4 PBS solution and pH 6.0 PBS solution. Results illustrate that the ratio between two components is a main factor to affect the controlled release performance. The result also indicates that this composite electrospun membrane can be used as a potential candidate for the pH sensitivity drug release materials. The antitumor effect was examined by a series of biological evaluations: cell live/dead assay, Fluorescence staining and MTS assay. The biological results indicated 5-Fu/Keratin/PLLA nanofibers has a long-term inhibition effect on tumor cells (HCT-116) compared to 5-FU/PLLA nanofibers. The sustained effect can last from 4 hours observation until 120 hours observation. The 5-FU/Keratin/PLLA kept releasing the antitumor drug in the total 120 hour experiment and proliferation rate of tumor cells were inhibited steadily and sustainably. Adding keratin into the composite membranes can increase the antitumor effect dramatically.

6. Both the anti-tumor drug and antimicrobial peptides was loaded on the nanofibers. The anti-tumor effect of AMPs-loaded nanofibrous system was investigated.

This objective has been achieved in Chapter 8. The experimental results indicated that after adding the antimicrobial peptides into the membrane, the antitumor effect could be observed, especially after 72 hours observation. Unlike the chemical antitumor drug has a short and strong inhibition effect on tumor cells, the biological antimicrobial peptides has a long and sustained inhibition on tumor cells which compensates the short effect of chemical antitumor drugs. After 72 hour observations,

the proliferation of tumor cells was inhibited under the synergistic effect between chemical antitumor drug and antimicrobial peptides. The results indicated the feasibility of combining both chemical antitumor drugs and biological antimicrobial peptides together, which suggested the further direction of applying nanofibers in the realm of antitumor therapy.

9.2 Limitations and future works

Although the objectives of this thesis have been achieved, there are some unavoidable limitations in the current research work that would ideally need further investigations.

The following aspects can be explored deeply:

1. More parameters should be considered to investigate the synergistic effect between antimicrobial peptides and antitumor drugs. The target drug model can be selected from other well-known antitumor drug.
2. The mechanism of synergistic effect between antimicrobial peptides and antitumor drugs could be deeply investigated. The effect of electrospinning process on antimicrobial activity should be considered as a main factor.
3. The biofunctional drug loaded membrane can be applied in animal model to test the antitumor. When considering the animal model experiments, the parameters which were undergone in the *in vivo* experiments should be revised accordingly. For example, the dosage of 5-FU and the proportional between 5-FU and keratin combination. The half-life of 5-FU changed dramatically when applied in biological subject. The shorten half-life of antitumor could be another key issue to be considered in the future study.

REFERENCES

- [1] Griffith LG, Naughton G. Tissue engineering - Current challenges and expanding opportunities. *Science*. 2002;295:1009-+.
- [2] Lee KY, Mooney DJ. Hydrogels for Tissue Engineering. *Chemical Reviews*. 2001;101:1869-80.
- [3] Agrawal CM, Ray RB. Biodegradable polymeric scaffolds for musculoskeletal tissue engineering. *Journal of Biomedical Materials Research*. 2001;55:141-50.
- [4] Chaikof EL, Matthew H, Kohn J, Mikos AG, Prestwich GD, Yip CM. Biomaterials and Scaffolds in Reparative Medicine. *Annals of the New York Academy of Sciences*. 2002;961:96-105.
- [5] Panitch A, Yamaoka T, Fournier MJ, Mason TL, Tirrell DA. Design and Biosynthesis of Elastin-like Artificial Extracellular Matrix Proteins Containing Periodically Spaced Fibronectin CS5 Domains. *Macromolecules*. 1999;32:1701-3.
- [6] Putnam AJ, Mooney DJ. Tissue engineering using synthetic extracellular matrices. *Nature Medicine*. 1996;2:824-6.
- [7] Heath CA. Cells for tissue engineering. *Trends in Biotechnology*. 2000;18:17-9.
- [8] Rabkin E, Schoen FJ. Cardiovascular tissue engineering. *Cardiovascular pathology : the official journal of the Society for Cardiovascular Pathology*. 2002;11:305-17.
- [9] Cortesini R. Stem cells, tissue engineering and organogenesis in transplantation. *Transplant Immunology*. 2005;15:81-9.
- [10] Lin X, Takahashi K, Liu Y, Zamora PO. Enhancement of cell attachment and tissue integration by a IKVAV containing multi-domain peptide. *Biochimica et Biophysica Acta (BBA) - General Subjects*. 2006;1760:1403-10.
- [11] Ghosh K, Ren XD, Shu XZ, Prestwich GD, Clark RAF. Fibronectin functional domains coupled to hyaluronan stimulate adult human dermal fibroblast responses critical for wound healing. *Tissue Engineering*. 2006;12:601-13.
- [12] Kugo K, Okuno M, Masuda K, Nishino J, Masuda H, Iwatsuki M. Fibroblast attachment to Arg-Gly-Asp peptide-immobilized poly(γ -methyl L-glutamate). *Journal of biomaterials science Polymer edition*. 1994;5:325-37.
- [13] Shin H, Jo S, Mikos AG. Biomimetic materials for tissue engineering. *Biomaterials*. 2003;24:4353-64.
- [14] Pierschbacher MD, Ruoslahti E. Influence of stereochemistry of the sequence Arg-Gly-Asp-Xaa on binding specificity in cell adhesion. *Journal of Biological Chemistry*. 1987;262:17294-8.
- [15] Rezwani K, Chen QZ, Blaker JJ, Boccaccini AR. Biodegradable and bioactive porous polymer/inorganic composite scaffolds for bone tissue engineering. *Biomaterials*. 2006;27:3413-31.
- [16] Park KH, Bae YH. Phenotype of hepatocyte spheroids in Arg-Gly-Asp (RGD) containing a thermo-reversible extracellular matrix. *Bioscience Biotechnology and Biochemistry*. 2002;66:1473-8.
- [17] Chen G, Ushida T, Tateishi T. Development of biodegradable porous scaffolds for tissue engineering. *Materials Science and Engineering: C*. 2001;17:63-9.
- [18] Lu L, Peter SJ, Lyman MD, Lai H-L, Leite SM, A. Tamada J, et al. In vitro degradation of porous poly(l-lactic acid) foams. *Biomaterials*. 2000;21:1595-605.
- [19] Yang X, Yuan M, Li W, Zhang G. Synthesis and properties of collagen/polylactic acid blends. *Journal of Applied Polymer Science*. 2004;94:1670-5.
- [20] Kikuchi M, Ikoma T, Itoh S, Matsumoto HN, Koyama Y, Takakuda K, et al. Biomimetic synthesis of bone-like nanocomposites using the self-organization mechanism of hydroxyapatite and collagen. *Composites Science and Technology*. 2004;64:819-25.
- [21] Rodrigues CVM, Serricella P, Linhares ABR, Guerdes RM, Borojevic R, Rossi MA, et al. Characterization of a bovine collagen-hydroxyapatite composite scaffold for bone tissue engineering. *Biomaterials*. 2003;24:4987-97.
- [22] Sachlos E, Reis N, Ainsley C, Derby B, Czernuszka JT. A process to make collagen scaffolds with an artificial circulatory system using rapid prototyping. 2003. p. 187-92.
- [23] Ji W, Yang F, van den Beucken JJJP, Bian Z, Fan M, Chen Z, et al. Fibrous scaffolds loaded with protein prepared by blend or coaxial electrospinning. *Acta Biomaterialia*. 2010;6:4199-207.
- [24] Kim TG, Chung HJ, Park TG. Macroporous and nanofibrous hyaluronic acid/collagen hybrid scaffold fabricated by concurrent electrospinning and deposition/leaching of salt particles. *Acta Biomaterialia*. 2008;4:1611-9.
- [25] Shalumon KT, Binulal NS, Selvamurugan N, Nair SV, Menon D, Furuike T, et al. Electrospinning of carboxymethyl chitin/poly(vinyl alcohol) nanofibrous scaffolds for tissue engineering applications. *Carbohydrate Polymers*. 2009;77:863-9.
- [26] Soliman S, Pagliari S, Rinaldi A, Forte G, Fiaccavento R, Pagliari F, et al. Multiscale

- three-dimensional scaffolds for soft tissue engineering via multimodal electrospinning. *Acta Biomaterialia*. 2010;6:1227-37.
- [27] Liu X, Ma P. Polymeric Scaffolds for Bone Tissue Engineering. *Annals of Biomedical Engineering*. 2004;32:477-86.
- [28] Shen F, Cui YL, Yang LF, Yao KD, Dong XH, Jia WY, et al. A study on the fabrication of porous chitosan/gelatin network scaffold for tissue engineering. *Polymer International*. 2000;49:1596-9.
- [29] Whang K, Thomas CH, Healy KE, Nuber G. A novel method to fabricate bioabsorbable scaffolds. *Polymer*. 1995;36:837-42.
- [30] Kemp P. Tissue Engineering and Cell-Populated Collagen Matrices. In: Streuli C, Grant M, editors. *Extracellular Matrix Protocols: Humana Press*; 2000. p. 287-93.
- [31] O'Brien FJ. Biomaterials & scaffolds for tissue engineering. *Materials Today*. 14:88-95.
- [32] Balasundaram G, Webster TJ. A perspective on nanophase materials for orthopedic implant applications. *Journal of Materials Chemistry*. 2006;16:3737-45.
- [33] Leeuwenburgh SCG, Jansen JA, Malda J, Dhert WA, Rouwkema J, van Blitterswijk CA, et al. Trends in biomaterials research: An analysis of the scientific programme of the World Biomaterials Congress 2008. *Biomaterials*. 2008;29:3047-52.
- [34] Stevens MM, George JH. Exploring and engineering the cell surface interface. *Science*. 2005;310:1135-8.
- [35] Tabata Y, Ikada Y. Protein release from gelatin matrices. *Advanced Drug Delivery Reviews*. 1998;31:287-301.
- [36] Altman GH, Diaz F, Jakuba C, Calabro T, Horan RL, Chen J, et al. Silk-based biomaterials. *Biomaterials*. 2003;24:401-16.
- [37] Khor E, Lim LY. Implantable applications of chitin and chitosan. *Biomaterials*. 2003;24:2339-49.
- [38] George M, Abraham TE. Polyionic hydrocolloids for the intestinal delivery of protein drugs: Alginate and chitosan — a review. *Journal of Controlled Release*. 2006;114:1-14.
- [39] Malafaya PB, Silva GA, Reis RL. Natural-origin polymers as carriers and scaffolds for biomolecules and cell delivery in tissue engineering applications. *Advanced Drug Delivery Reviews*. 2007;59:207-33.
- [40] Badylak SF. The extracellular matrix as a biologic scaffold material. *Biomaterials*. 2007;28:3587-93.
- [41] Lee CH, Singla A, Lee Y. Biomedical applications of collagen. *International Journal of Pharmaceutics*. 2001;221:1-22.
- [42] Hou Y-T, Ijima H, Matsumoto S, Kubo T, Takei T, Sakai S, et al. Effect of a hepatocyte growth factor/heparin-immobilized collagen system on albumin synthesis and spheroid formation by hepatocytes. *Journal of Bioscience and Bioengineering*. 2010;110:208-16.
- [43] Peter M, Binulal NS, Soumya S, Nair SV, Furuike T, Tamura H, et al. Nanocomposite scaffolds of bioactive glass ceramic nanoparticles disseminated chitosan matrix for tissue engineering applications. *Carbohydrate Polymers*. 2010;79:284-9.
- [44] Tachibana A, Kaneko S, Tanabe T, Yamauchi K. Rapid fabrication of keratin hydroxyapatite hybrid sponges toward osteoblast cultivation and differentiation. *Biomaterials*. 2005;26:297-302.
- [45] Seal BL, Otero TC, Panitch A. Polymeric biomaterials for tissue and organ regeneration. *Materials Science and Engineering: R: Reports*. 2001;34:147-230.
- [46] Schrooyen PMM, Dijkstra PJ, Oberthur RC, Bantjes A, Feijen J. Partially Carboxymethylated Feather Keratins. 1. Properties in Aqueous Systems. *Journal of Agricultural and Food Chemistry*. 2000;48:4326-34.
- [47] Schrooyen PMM, Dijkstra PJ, Oberthur RC, Bantjes A, Feijen J. Partially Carboxymethylated Feather Keratins. 2. Thermal and Mechanical Properties of Films. *Journal of Agricultural and Food Chemistry*. 2000;49:221-30.
- [48] SF; T, CR; B, RA. S. Keratin-based tissue engineering scaffold. 2002.
- [49] Yamauchi K, Maniwa M, Mori T. Cultivation of fibroblast cells on keratin-coated substrata. *Journal of Biomaterials Science, Polymer Edition*. 1998;9:259-70.
- [50] Tachibana A, Furuta Y, Takeshima H, Tanabe T, Yamauchi K. Fabrication of wool keratin sponge scaffolds for long-term cell cultivation. *Journal of Biotechnology*. 2002;93:165-70.
- [51] Tanabe T, Okitsu N, Yamauchi K. Fabrication and characterization of chemically crosslinked keratin films. *Materials Science and Engineering: C*. 2004;24:441-6.
- [52] Jones LN, Simon M, Watts NR, Booy FP, Steven AC, Parry DAD. Intermediate filament structure: hard α -keratin. *Biophysical Chemistry*. 1997;68:83-93.
- [53] Coulombe PA, Omary MB. 'Hard' and 'soft' principles defining the structure, function and regulation of keratin intermediate filaments. *Current Opinion in Cell Biology*. 2002;14:110-22.
- [54] Akhtar W, Edwards HGM, Farwell DW, Nutbrown M. Fourier-transform Raman spectroscopic

- study of human hair. *Spectrochimica Acta Part A: Molecular and Biomolecular Spectroscopy*. 1997;53:1021-31.
- [55] Wojciechowska E, Włochowicz A, Weselucha-Birczyńska A. Application of Fourier-transform infrared and Raman spectroscopy to study degradation of the wool fiber keratin. *Journal of Molecular Structure*. 1999;511–512:307-18.
- [56] Fraser RDB, Parry DAD. The structural basis of the filament-matrix texture in the avian/reptilian group of hard β -keratins. *Journal of Structural Biology*. 2011;173:391-405.
- [57] Nelson DL. *Principles of Biochemistry* (4th ed.). New York: W. H. Freeman; 2005.
- [58] Aslaksen MA, Romarheim OH, Storebakken T, Skrede A. Evaluation of content and digestibility of disulfide bonds and free thiols in unextruded and extruded diets containing fish meal and soybean protein sources. *Animal Feed Science and Technology*. 2006;128:320-30.
- [59] Yamauchi K, Yamauchi A, Kusunoki T, Kohda A, Konishi Y. Preparation of stable aqueous solution of keratins, and physicochemical and biodegradational properties of films. *Journal of Biomedical Materials Research*. 1996;31:439-44.
- [60] Yang X, Zhang H, Yuan X, Cui S. Wool keratin: A novel building block for layer-by-layer self-assembly. *Journal of Colloid and Interface Science*. 2009;336:756-60.
- [61] Tonin C, Aluigi A, Vineis C, Varesano A, Montarsolo A, Ferrero F. Thermal and structural characterization of poly(ethylene-oxide)/keratin blend films. *Journal of Thermal Analysis and Calorimetry*. 2007;89:601-8.
- [62] Tanabe T, Okitsu N, Tachibana A, Yamauchi K. Preparation and characterization of keratin–chitosan composite film. *Biomaterials*. 2002;23:817-25.
- [63] Ishaug SL, Yaszemski MJ, Bizios R, Mikos AG. Osteoblast function on synthetic biodegradable polymers. *Journal of Biomedical Materials Research*. 1994;28:1445-53.
- [64] Zeng J, Chen X, Liang Q, Xu X, Jing X. Enzymatic Degradation of Poly(L-lactide) and Poly(ϵ -caprolactone) Electrospun Fibers. *Macromolecular Bioscience*. 2004;4:1118-25.
- [65] Mano JF, Sousa RA, Boesel LF, Neves NM, Reis RL. Bioinert, biodegradable and injectable polymeric matrix composites for hard tissue replacement: state of the art and recent developments. *Composites Science and Technology*. 2004;64:789-817.
- [66] Xu H, Teng C, Yu M. Improvements of thermal property and crystallization behavior of PLLA based multiblock copolymer by forming stereocomplex with PDLA oligomer. *Polymer*. 2006;47:3922-8.
- [67] Liu H-C, Lee IC, Wang J-H, Yang S-H, Young T-H. Preparation of PLLA membranes with different morphologies for culture of MG-63 Cells. *Biomaterials*. 2004;25:4047-56.
- [68] Yang S, Leong KF, Du Z, Chua CK. The design of scaffolds for use in tissue engineering. Part I. Traditional factors. *Tissue Engineering*. 2001;7:679-89.
- [69] Leong KF, Chua CK, Sudarmadji N, Yeong WY. Engineering functionally graded tissue engineering scaffolds. *Journal of the Mechanical Behavior of Biomedical Materials*. 2008;1:140-52.
- [70] Middleton JC, Tipton AJ. Synthetic biodegradable polymers as orthopedic devices. *Biomaterials*. 2000;21:2335-46.
- [71] Mark JE. *Polymer Data Handbook*. Polymer Data Handbook. Oxford: Oxford Press; 1999. p. 527-633.
- [72] Ramakrishna S HZ, Kumar GV, Batchelor AW, Mayer J. *An introduction to biocomposites*. London: Imperial College Press; 2004.
- [73] Lee CH, Singla A, Lee Y. Biomedical applications of collagen. *International Journal of Pharmaceutics*. 2001;221:1-22.
- [74] Bourtoom T, Chinnan MS. Preparation and properties of rice starch-chitosan blend biodegradable film. *LWT - Food Science and Technology*. 2008;41:1633-41.
- [75] Weiler A, Helling HJ, Kirch U, Zirbes TK, Rehm KE. Foreign-body reaction and the course of osteolysis after polyglycolide implants for fracture fixation. Experimental study in sheep. *Journal of Bone and Joint Surgery - Series B*. 1996;78:369-76.
- [76] Martin C, Winet H, Bao JY. Acidity near eroding polylactide-polyglycolide in vitro and in vivo in rabbit tibial bone chambers. *Biomaterials*. 1996;17:2373-80.
- [77] Dunn A, Campbell P, Marra K. The influence of polymer blend composition on the degradation of polymer/hydroxyapatite biomaterials. *Journal of Materials Science: Materials in Medicine*. 2001;12:673-7.
- [78] Heidemann W, Jeschkeit S, Ruffieux K, Fischer JH, Wagner M, Krger G, et al. Degradation of poly(D,L)lactide implants with or without addition of calciumphosphates in vivo. *Biomaterials*. 2001;22:2371-81.
- [79] Hamasaki S, Tachibana A, Tada D, Yamauchi K, Tanabe T. Fabrication of highly porous keratin sponges by freeze-drying in the presence of calcium alginate beads. *Materials Science and Engineering:*

C. 2008;28:1250-4.

[80] Hartgerink JD, Beniash E, Stupp SI. Self-assembly and mineralization of peptide-amphiphile nanofibers. *Science*. 2001;294:1684-8.

[81] Silva GA, Czeisler C, Niece KL, Beniash E, Harrington DA, Kessler JA, et al. Selective Differentiation of Neural Progenitor Cells by High-Epitope Density Nanofibers. *Science*. 2004;303:1352-5.

[82] Zhang S. Fabrication of novel biomaterials through molecular self-assembly. *Nat Biotech*. 2003;21:1171-8.

[83] Hong Y, Legge RL, Zhang S, Chen P. Effect of Amino Acid Sequence and pH on Nanofiber Formation of Self-Assembling Peptides EAK16-II and EAK16-IV. *Biomacromolecules*. 2003;4:1433-42.

[84] Ma PX, Zhang R. Synthetic nano-scale fibrous extracellular matrix. *Journal of Biomedical Materials Research*. 1999;46:60-72.

[85] Ramakrishna S FK, Teo WE, Lim TC, Ma Z. An introduction to electrospinning and nanofibers. Singapore: World Scientific Publishing Company; 2005.

[86] Mi F-L, Lin Y-M, Wu Y-B, Shyu S-S, Tsai Y-H. Chitin/PLGA blend microspheres as a biodegradable drug-delivery system: phase-separation, degradation and release behavior. *Biomaterials*. 2002;23:3257-67.

[87] Selective Delivery of Adiramycin to a Solid Tumor Using a Polymeric Micelle Carrier System. *Journal of Drug Targeting*. 1999;7:171-86.

[88] Luu YK, Kim K, Hsiao BS, Chu B, Hadjiargyrou M. Development of a nanostructured DNA delivery scaffold via electrospinning of PLGA and PLA-PEG block copolymers. *Journal of Controlled Release*. 2003;89:341-53.

[89] Lyons J, Ko F. Melt electrospinning of polymers: A review. *Polymer News*. 2005;30:170-8.

[90] Lyons J, Li C, Ko F. Melt-electrospinning part I: Processing parameters and geometric properties. *Polymer*. 2004;45:7597-603.

[91] Ma Z, Ramakrishna S. Electrospun regenerated cellulose nanofiber affinity membrane functionalized with protein A/G for IgG purification. *Journal of Membrane Science*. 2008;319:23-8.

[92] Ma Z, Kotaki M, Inai R, Ramakrishna S. Potential of nanofiber matrix as tissue-engineering scaffolds. *Tissue Engineering*. 2005;11:101-9.

[93] Ma Z, Kotaki M, Ramakrishna S. Electrospun cellulose nanofiber as affinity membrane. *Journal of Membrane Science*. 2005;265:115-23.

[94] Ma Z, He W, Yong T, Ramakrishna S. Grafting of gelatin on electrospun poly(caprolactone) nanofibers to improve endothelial cell spreading and proliferation and to control cell orientation. *Tissue Engineering*. 2005;11:1149-58.

[95] Liang D, Hsiao BS, Chu B. Functional electrospun nanofibrous scaffolds for biomedical applications. *Advanced Drug Delivery Reviews*. 2007;59:1392-412.

[96] Nam J, Huang Y, Agarwal S, Lannutti J. Improved cellular infiltration in electrospun fiber via engineered porosity. *Tissue Engineering*. 2007;13:2249-57.

[97] Ekaputra AK, Prestwich GD, Cool SM, Hutmacher DW. Combining electrospun scaffolds with electrosprayed hydrogels leads to three-dimensional cellularization of hybrid constructs. *Biomacromolecules*. 2008;9:2097-103.

[98] Bölgen N, Vargel I, Korkusuz P, Menciloğlu YZ, Pişkin E. In vivo performance of antibiotic embedded electrospun PCL membranes for prevention of abdominal adhesions. *Journal of Biomedical Materials Research - Part B Applied Biomaterials*. 2007;81:530-43.

[99] Yoshida M, Langer R, Lendlein A, Lahann J. From advanced biomedical coatings to multi-functionalized biomaterials. *Polymer Reviews*. 2006;46:347-75.

[100] Joung YK, Bae JW, Park KD. Controlled release of heparin-binding growth factors using heparin-containing particulate systems for tissue regeneration. *Expert Opinion on Drug Delivery*. 2008;5:1173-84.

[101] Li LS, Stupp SI. One-dimensional assembly of lipophilic inorganic nanoparticles templated by peptide-based nanofibers with binding functionalities. *Angewandte Chemie - International Edition*. 2005;44:1833-6.

[102] Kalra V, Lee J, Lee JH, Lee SG, Marquez M, Wiesner U, et al. Controlling nanoparticle location via confined assembly in electrospun block copolymer nanofibers. *Small*. 2008;4:2067-73.

[103] Kim BS, Park SW, Hammond PT. Hydrogen-bonding layer-by-layer-assembled biodegradable polymeric micelles as drug delivery vehicles from surfaces. *ACS Nano*. 2008;2:386-92.

[104] Thierry B, Kujawa P, Tkaczyk C, Winnik FM, Bilodeau L, Tabrizian M. Delivery platform for hydrophobic drugs: Prodrug approach combined with self-assembled multilayers. *Journal of the American Chemical Society*. 2005;127:1626-7.

- [105] Na K, Seong Lee E, Bae YH. Adriamycin loaded pullulan acetate/sulfonamide conjugate nanoparticles responding to tumor pH: pH-dependent cell interaction, internalization and cytotoxicity in vitro. *Journal of Controlled Release*. 2003;87:3-13.
- [106] Stubbs M, McSheehy PMJ, Griffiths JR, Bashford CL. Causes and consequences of tumour acidity and implications for treatment. *Molecular Medicine Today*. 2000;6:15-9.
- [107] Bergers G, Benjamin LE. Tumorigenesis and the angiogenic switch. *Nature Reviews Cancer*. 2003;3:401-10.
- [108] Amaravadi RK, Lippincott-Schwartz J, Yin XM, Weiss WA, Takebe N, Timmer W, et al. Principles and current strategies for targeting autophagy for cancer treatment. *Clinical Cancer Research*. 2011;17:654-66.
- [109] Kataoka K, Harada A, Nagasaki Y. Block copolymer micelles for drug delivery: Design, characterization and biological significance. *Advanced Drug Delivery Reviews*. 2001;47:113-31.
- [110] Lavasanifar A, Samuel J, Kwon GS. Poly(ethylene oxide)-block-poly(l-amino acid) micelles for drug delivery. *Advanced Drug Delivery Reviews*. 2002;54:169-90.
- [111] Yokoyama M, Okano T, Sakurai Y, Fukushima S, Okamoto K, Kataoka K. Selective delivery of adriamycin to a solid tumor using a polymeric micelle carrier system. *Journal of Drug Targeting*. 1999;7:171-86.
- [112] Nishiyama N, Okazaki S, Cabral H, Miyamoto M, Kato Y, Sugiyama Y, et al. Novel Cisplatin-Incorporated Polymeric Micelles Can Eradicate Solid Tumors in Mice. *Cancer Research*. 2003;63:8977-83.
- [113] Miyamoto Y, Oda T, Maeda H. Comparison of the Cytotoxic Effects of the High- and Low-Molecular-Weight Anticancer Agents on Multidrug-resistant Chinese Hamster Ovary Cells in Vitro. *Cancer Research*. 1990;50:1571-5.
- [114] Bae Y, Fukushima S, Harada A, Kataoka K. Design of environment-sensitive supramolecular assemblies for intracellular drug delivery: Polymeric micelles that are responsive to intracellular pH change. *Angewandte Chemie - International Edition*. 2003;42:4640-3.
- [115] Bae Y, Nishiyama N, Fukushima S, Koyama H, Yasuhiro M, Kataoka K. Preparation and biological characterization of polymeric micelle drug carriers with intracellular pH-triggered drug release property: Tumor permeability, controlled subcellular drug distribution, and enhanced in vivo antitumor efficacy. *Bioconjugate Chemistry*. 2005;16:122-30.
- [116] Hoffman AS. Applications of thermally reversible polymers and hydrogels in therapeutics and diagnostics. *Journal of Controlled Release*. 1987;6:297-305.
- [117] Firestone BA, Siegel RA. Kinetics and mechanisms of water sorption in hydrophobic, ionizable copolymer gels. *Journal of Applied Polymer Science*. 1991;43:901-14.
- [118] Falamarzian M, Varshosaz J. The effect of structural changes on swelling kinetics of polybasic/hydrophobic pH-sensitive hydrogels. *Drug Development and Industrial Pharmacy*. 1998;24:667-9.
- [119] Diez-Peña E, Quijada-Garrido I, Barrales-Rienda JM. On the water swelling behaviour of poly(N-isopropylacrylamide) [P(N-iPAAm)], poly(methacrylic acid) [P(MAA)], their random copolymers and sequential interpenetrating polymer networks (IPNs). *Polymer*. 2002;43:4341-8.
- [120] Hong SW, Kim KH, Huh J, Ahn C-H, Jo WH. Design and Synthesis of a New pH Sensitive Polymeric Sensor Using Fluorescence Resonance Energy Transfer. *Chemistry of Materials*. 2005;17:6213-5.
- [121] Lee J, Macosko CW, Urry DW. Mechanical properties of cross-linked synthetic elastomeric polypentapeptides. *Macromolecules*. 2001;34:5968-74.
- [122] Boman HG. Antibacterial peptides: basic facts and emerging concepts. *Journal of Internal Medicine*. 2003;254:197-215.
- [123] Kraus D, Peschel A. Molecular Mechanisms of Bacterial Resistance to Antimicrobial Peptides. In: Shafer W, editor. *Antimicrobial Peptides and Human Disease*: Springer Berlin Heidelberg; 2006. p. 231-50.
- [124] Kingsbury WD, Boehm JC, Mehta RJ, Grappel SF, Gilvarg C. A novel peptide delivery system involving peptidase activated prodrugs as antimicrobial agents. Synthesis and biological activity of peptidyl derivatives of 5-fluorouracil. *Journal of Medicinal Chemistry*. 1984;27:1447-51.
- [125] Obeid M. Anticancer activity of targeted proapoptotic peptides and chemotherapy is highly improved by targeted cell surface calreticulin-inducer peptides. *Molecular Cancer Therapeutics*. 2009;8:2693-707.
- [126] Schweizer F. Cationic amphiphilic peptides with cancer-selective toxicity. *European Journal of Pharmacology*. 2009;625:190-4.
- [127] Chen HM, Wang W, Smith D, Chan SC. Effects of the anti-bacterial peptide cecropin B and its analogs, cecropins B-1 and B-2, on liposomes, bacteria, and cancer cells. *Biochimica Et Biophysica*

- Acta-General Subjects. 1997;1336:171-9.
- [128] Hui L, Leung K, Chen HM. The combined effects of antibacterial peptide cecropin A and anti-cancer agents on leukemia cells. *Anticancer Research*. 2002;22:2811-6.
- [129] Papo N, Shai Y. Host defense peptides as new weapons in cancer treatment. *Cellular and Molecular Life Sciences*. 2005;62:784-90.
- [130] Gigliotti JC, Jaczynski J, Tou JC. Determination of the nutritional value, protein quality and safety of krill protein concentrate isolated using an isoelectric solubilization/precipitation technique. *Food Chemistry*. 2008;111:209-14.
- [131] Chen YC, Tou JC, Jaczynski J. Amino acid and mineral composition of protein and other components and their recovery yields from whole antarctic krill (*Euphausia superba*) Using isoelectric solubilization/precipitation. *Journal of Food Science*. 2009;74:H31-H9.
- [132] Po HN, Senozan NM. The Henderson-Hasselbalch equation: its history and limitations. *J Chem Educ*. 2001;78:1499.
- [133] Gillespie JM, Frenkel MJ. The diversity of keratins. *Comparative Biochemistry and Physiology Part B: Comparative Biochemistry*. 1974;47:339-46.
- [134] Xu W, Ke G, Wu J, Wang X. Modification of wool fiber using steam explosion. *European Polymer Journal*. 2006;42:2168-73.
- [135] Tung WS, Daoud WA. Photocatalytic self-cleaning keratins: A feasibility study. *ACTA BIOMATER*. 2009;5:50-6.
- [136] Li J, Li Y, Liu X, Zhang J, Zhang Y. Strategy to introduce an hydroxyapatite-keratin nanocomposite into a fibrous membrane for bone tissue engineering. *Journal of Materials Chemistry B*. 2013.
- [137] Katoh K, Shibayama M, Tanabe T, Yamauchi K. Preparation and physicochemical properties of compression-molded keratin films. *Biomaterials*. 2004;25:2265-72.
- [138] Vasconcelos A, Freddi G, Cavaco-Paulo A. Biodegradable materials based on silk fibroin and keratin. *Biomacromolecules*. 2008;9:1299-305.
- [139] SantaLucia J, Allawi HT, Seneviratne PA. Improved Nearest-Neighbor parameters for predicting DNA duplex stability. *Biochemistry*. 1996;35:3555-62.
- [140] Ramachandran E, Natarajan S. Crystal growth of some urinary stone constituents: III. In- vitro crystallization of L-cystine and its characterization. *Crystal Research and Technology*. 2004;39:308-12.
- [141] Aluigi A, Zoccola M, Vineis C, Tonin C, Ferrero F, Canetti M. Study on the structure and properties of wool keratin regenerated from formic acid. *International Journal of Biological Macromolecules*. 2007;41:266-73.
- [142] Wu W, Liao L, Lien C, Lin J. FTIR study of adsorption, thermal reactions and photochemistry of benzene on powdered TiO₂. *PCCP*. 2001;3:4456-61.
- [143] Li L, Li Y, Li J, Mak AFT, Ko F, Qin L. The effects of PLLA/keratin composite fibrous scaffolds on the proliferation of osteoblasts 2008.
- [144] Cardamone JM. Investigating the microstructure of keratin extracted from wool: Peptide sequence (MALDI-TOF/TOF) and protein conformation (FTIR). *Journal of Molecular Structure*. 2010;969:97-105.
- [145] Goddard DR, Michaelis L. A STUDY ON KERATIN. *Journal of Biological Chemistry*. 1934;106:605-14.
- [146] Larrondo L, St. John Manley R. Electrostatic fiber spinning from polymer melts. I. Experimental observations on fiber formation and properties. *Journal of Polymer Science: Polymer Physics Edition*. 1981;19:909-20.
- [147] Sekaran G, Kumar AG, Swarnalatha S, Gayathri S, Nagesh N. Characterization of an alkaline active thiol forming extracellular serine keratinase by the newly isolated *Bacillus pumilus*. *Journal of Applied Microbiology*. 2008;104:411-9.
- [148] Li J, Li Y, Li L, Mak AFT, Ko F, Qin L. Preparation and biodegradation of electrospun PLLA/keratin nonwoven fibrous membrane. *Polymer Degradation and Stability*. 2009;94:1800-7.
- [149] Zoccola M, Aluigi A, Tonin C. Characterisation of keratin biomass from butchery and wool industry wastes. *Journal of Molecular Structure*. 2009;938:35-40.
- [150] Sionkowska A, Skopinska-Wisniewska J, Planecka A, Kozłowska J. The influence of UV irradiation on the properties of chitosan films containing keratin. *Polymer Degradation and Stability*. 2010;95:2486-91.
- [151] Nistor MT, Chiriac AP, Nita LE, Vasile C. Characterization of the semi-interpenetrated network based on collagen and poly(N-isopropyl acrylamide-co-diethylene glycol diacrylate). *International Journal of Pharmaceutics*. 2013;452:92-101.
- [152] Chen SC, Huang XB, Cai XM, Lu J, Yuan J, Shen J. The Influence of Fiber Diameter of Electrospun Poly(lactic acid) on Drug Delivery. *Fibers and Polymers*. 2012;13:1120-5.

- [153] Zhang J, Li Y, Li J, Zhao Z, Liu X, Zhang Y, et al. Generation of biofunctional and biodegradable electrospun nanofibers composed of poly (L-lactic acid) and wool isoelectric precipitate. *Textile Research Journal*. 2013.
- [154] Cai X, Luan Y, Dong Q, Shao W, Li Z, Zhao Z. Sustained release of 5-fluorouracil by incorporation into sodium carboxymethylcellulose sub-micron fibers. *International Journal of Pharmaceutics*. 2011;419:240-6.
- [155] Park CG, Kim MH, Park M, Lee JE, Lee SH, Park JH, et al. Polymeric nanofiber coated esophageal stent for sustained delivery of an anticancer drug. *Macromolecular Research*. 2011;19:1210-6.
- [156] Basak SC, Kumar KS, Ramalingam M. Design and release characteristics of sustained release tablet containing metformin HCl. *Revista Brasileira De Ciencias Farmaceuticas*. 2008;44:477-83.
- [157] Costa P, Sousa Lobo JM. Modeling and comparison of dissolution profiles. *European Journal of Pharmaceutical Sciences*. 2001;13:123-33.
- [158] Greenwood R. Review of the measurement of zeta potentials in concentrated aqueous suspensions using electroacoustics. *Advances in Colloid and Interface Science*. 2003;106:55-81.
- [159] Bae Y, Jang WD, Nishiyama N, Fukushima S, Kataoka K. Multifunctional polymeric micelles with folate-mediated cancer cell targeting and pH-triggered drug releasing properties for active intracellular drug delivery. *Molecular BioSystems*. 2005;1:242-50.
- [160] Bae Y, Kataoka K. Intelligent polymeric micelles from functional poly(ethylene glycol)-poly(amino acid) block copolymers. *Advanced Drug Delivery Reviews*. 2009;61:768-84.
- [161] Zhang J, Li Y, Li J. pH-Responsive nano-fiber membrane based on PLLA and nano wool protein for controlled release of anti-tumor drugs. *Journal of Controlled Release*. 2013;172:e41-e2.
- [162] *Molecular Mechanisms of Immune Responses in Insects*. New York: Chapman & Hall, London; 1998.
- [163] Arimatsu Y, Kotani E, Sugimura Y, Furusawa T. Molecular characterization of a cDNA encoding extracellular dsRNase and its expression in the silkworm, *Bombyx mori*. *Insect Biochemistry and Molecular Biology*. 2007;37:176-83.
- [164] Taniai K, Ishii T, Sugiyama M, Miyanoshita A, Yamakawa M. Nucleotide sequence of 5'-upstream region and expression of a silkworm gene encoding a new member of the attacin family. *Biochemical and Biophysical Research Communications*. 1996;220:594-9.
- [165] Li Z, Li Y, Liu X, Lan X-Q, Leung PH-M. Expression of a Silkworm Antimicrobial Peptide Gene (*Bmattacin2*) in *Escherichia coli*. In: Li Y, Takatera M, Kajiwara K, Li JS, editors. *Textile Bioengineering and Informatics Symposium Proceedings, Vols 1 and 2* 2012. p. 201-9.
- [166] Parhi P, Mohanty C, Sahoo SK. Nanotechnology-based combinational drug delivery: an emerging approach for cancer therapy. *Drug Discovery Today*. 2012;17:1044-52.
- [167] Karaayvaz M, Zhai H, Ju J. miR-129 promotes apoptosis and enhances chemosensitivity to 5-fluorouracil in colorectal cancer. *Cell Death Dis*. 2013;4.